DFT STUDY OF SOME SELECTED BINARY COMPOUND SEMICONDUCTORS: ELECTRONIC STRUCTURES AND ELASTIC PROPERTIES

A thesis submitted to Assam University, Silchar
in partial fulfilment of the requirement for the degree of
Doctor of Philosophy in Physics

BY
Khoirom Kabita.

Ph. D Regn. No. : Ph.D/2037/2012

DEPARTMENT OF PHYSICS,
SCHOOL OF PHYSICAL SCIENCE
ASSAM UNIVERSITY
SILCHAR-788011, INDIA

2016

DEPARTMENT OF PHYSICS
SCHOOL OF PHYSICAL SCIENCES
ASSAM UNIVERSITY, SILCHAR
(A CENTRAL UNIVERSITY CONSTITUTED UNDER ACT XIII OF 1989)
Silchar-788011, ASSAM, India

Date:

CERTIFICATE

Certified that the thesis entitled **"DFT STUDY OF SOME SELECTED BINARY COMPOUND SEMICONDUCTORS: ELECTRONIC STRUCTURES AND ELASTIC PROPERTIES"** for award of the Degree of Doctor of Philosophy in Department of Physics is a bonafide research work. This work has not been submitted previously for any other degree of this or any other university. It is further certified that the candidate has complied with all the formalities as per the requirements of Assam University. I recommend that the thesis may be placed before the examiners for consideration of award of the degree of this university.

Dr. B. Indrajit Sharma
Associate Professor,
Department of Physics,
Assam University Silchar.

DEPARTMENT OF PHYSICS
SCHOOL OF PHYSICAL SCIENCES
ASSAM UNIVERSITY, SILCHAR
(A CENTRAL UNIVERSITY CONSTITUTED UNDER ACT XIII OF 1989)
Silchar-788011, ASSAM, India

DECLARATION

I, **KHOIROM KABITA** bearing Ph.D. Registration No Ph.D./2037/12 dated 12/09/12, & UNIVERSITY REGISTRATION NO: 24-110033327 of 2011-2012 hereby declare that the subject matter of the thesis entitled "**DFT STUDY OF SOME SELECTED BINARY COMPOUND SEMICONDUCTORS: ELECTRONIC STRUCTURES AND ELASTIC PROPERTIES"** is the record of work done by me and that the contents of this thesis did not form the basis for award of any award to me or to anybody else to the best of my knowledge. The thesis has not been submitted in any other University/Institute.

This thesis is being submitted to Assam University for the degree of Doctor of Philosophy in Physics.

Place:

Date: (Khoirom Kabita)

ACKNOWLEDGEMENT

I take this opportunity to express my deep sense of gratitude and thanks to my mentor and guide, Dr. B Indrajit Sharma, Associate Professor, Department of Physics, Assam University Silchar, whose dedication, keen interest and overwhelming attitude to help his students has been solely and mainly responsible in completion of my thesis work. His timely advice, meticulous scrutiny, scholarly advice and scientific approach has helped me to a very great extent to accomplish my work. I could not have imagined having a better advisor and mentor for my Ph.D study.

I would like to also show my gratitude all the Faculty members, Lab Staffs and Office Staffs of the Department of Physics, for their insightful comments and encouragement which incented me to widen my research from various perspectives.

I also thank my past and present research fellow mates of the Department of Physics and other Departments for sharing their pearls of wisdom with me during the course of my research.

I would like to thank Dean, School of Physical Science for all official logistic support and Assam University Silchar, for providing me with University fellowship as it would have been very difficult to complete my Ph.D work without this financial support.

Lastly but not the least I would like to thank my family: my grandmother, my parents and brothers for supporting me spiritually throughout my Ph.D and my life in general and also pray to God for the time to come.

(Khoirom Kabita)

ABSTRACT

Compound semiconductors which consist of various elements have widely ranging physical properties. It constitutes today's basic building blocks of emitters and receivers in cellular, satellite and fibreglass communication. Semiconductors have attracted much attention in recent years to their great potential for technological importance and have aroused considerably scientific interest. It has therefore become important to understand the electronic structure, elastic properties and the variation of the elastic properties with pressure of binary compound semiconductors. The behavior of a material is predicted by carrying out electronic structure calculations. Elasticity describes the response of a compound to a very small loading which causes reversible deformation. Elastic constant is the fundamental material parameters which characterises the elastic behaviour of a solid. With increase in technology, attempts have also been made to uncover credible alternatives for improving the optoelectronic device performances which has led to the study of III-V alloys. Also the possibility of controlling the physical properties of these alloys in different composition offers immense scope in technological applications studies. Based on these perspectives, the present thesis entitled "**DFT study of some selected Binary Compound Semiconductors: Electronic Structures and Elastic Properties"** have been chosen. This thesis includes a complete study on the structural properties, phase transition, elastic properties and electronic properties of III-V (GaP, GaAs, InP, InAs) and II-VI (ZnS, CdTe and ZnSe) compound semiconductors in both zinc-blende (ZB) and rocksalt (RS) structures under induced pressure in the light of Density Functional Theory (DFT) which is based on electron density rather than the wave function. The effect of InP doped with Ga: $In_xGa_{(1-x)}P$ alloy at different concentration of Ga has also been studied.

The thesis is divided into seven chapters and a detailed layout of these chapters are shown below.

Chapter 1: *Introduction and Review of literature*

This chapter describes the general concepts of compound semiconductors and literature survey on III-V (GaP, GaAs, InP, InAs) and II-VI (ZnS, CdTe and ZnSe) compound semiconductors. It shows the importance of studying the structural properties, phase transition, elastic properties and electronic properties under induced pressure as well as the importance of studying the effect of doping in compound semiconductors.

Chapter 2: *Theoretical methodology*

This chapter describes the theoretical methods used in the present study.

Chapter 3: *Computational tools*

This chapter describes the computational software used in the entire computational calculations of the thesis work.

Chapter 4: *III-V Compound Semiconductors: GaP, GaAs, InP, InAs*

In this chapter, the structural properties of III-V compound semiconductors such as GaP, GaAs, InP and InAs in both zincblende (ZB) and rocksalt (RS) are studied. The structural phase transformation from the ZB to RS structure under induced pressure has also been performed for these compounds and the volume collapse at the transition pressure determined. The elastic constants (C_{11}, C_{12} and C_{44}) of both the ZB and RS phases are found to satisfy the mechanical stability conditions and undergo a linear variation with increase in pressure. The elastic parameters (Zener Anisotropy factor (A), Poisson's ratio (υ), Kleinmann parameter (ζ), B/G ratio, Young's modulus (Y) and Deby's temperature (θ_D)) are also calculated.

The energy band gaps of the ZB and RS structures at zero pressure of GaP, GaAs, InP and InAs are calculated using the LDA, GGA and mBJ-GGA potentials. The implementation of the mBJ-GGA potential in the energy band gap calculation

resolves the underestimation of the band gaps with LDA, GGA and provides better results closer to the experimental value. The corresponding total and partial DOS for the ZB and RS structures at zero pressure are studied within the mBJ-GGA only. The energy band structures as well as the DOS for both ZB and RS structures are studied at different pressures. The energy band gap of ZB phases of GaP, GaAs, InP and InAs are found to be affected by pressure while the energy band gaps of the RS phases are not much affected by pressure.

Chapter 5: *II-VI Compound Semiconductors: ZnS, CdTe, ZnSe*

In this present chapter, we have studied the structural properties of II-VI compound semiconductors, ZnS, CdTe and ZnSe in both ZB and RS structure.

Similar to chapter 4, we have studied the structural phase transition and volume collapse from the zincblende (ZB) to rocksalt (RS) phase of ZnS, CdTe and ZnSe The elastic constants (C_{11}, C_{12} and C_{44}) of both the phases are calculated and found to satisfy the mechanical stability conditions and the corresponding elastic parameters also calculated.

The energy band structures of ZnS, CdTe and ZnSe gaps at zero pressure (in ZB and RS structure) are also calculated using the LDA, GGA and mBJ-GGA methods. The DOS plots for the ZB and RS structures at zero pressure are studied within the mBJ-GGA only and at different pressures. In all the three compounds (ZnS-ZB, CdTe-ZB and ZnSe-ZB) we find that the energy band gap of ZB phases of ZnS, CdTe and ZnSe are affected by pressure while the energy band gaps of the RS phases are not much affected by pressure as in case of the III-V compound semiconductors.

Chapter 6: *Effect of Doping: InP doped with Ga ($In_xGa_{(1-x)}P$)*

In this chapter, the structural phase stability from the zinc-blende (ZB) to rocksalt (RS) structure and electronic structure of $In_{1-x}Ga_{1-x}P$ has been performed to understand the doping effect of Ga in InP compound semiconductor. The lattice parameters of the stable structures of the corresponding doping concentrations are

compared with other available theoretical and experimental results and found to be in good agreement with them. The composition effect on the lattice constant, bulk modulus and the formation energy are studied at different concentration of x (= 0.0, 0.25, 0.5, 0.75, 1) for both B3 and B1 structure. The pressure induce phase transition pressure from B3 to B1 phase in different concentration is found to increase with increase concentration of Ga. For the host binary compounds, the transition pressure is found to be in close agreement with experimental results. The electronic band structure at different concentration of x for both the zinc blende and rock salt structure has been investigated using the total and partial density of states.

Chapter 7: *Overall Conclusion and Outlook*

This chapter presents the overall conclusion of the thesis work (Chapter 4, Chapter 5, Chapter 6) and in future it would be interesting to study the effects of doping in thin films for solar cell studies.

Finally we add an appendix at the end along with the list of publications from the outcome of the results of this dissertation work in referred journal and a list of conference and workshop attended.

CONTENTS

LIST OF FIGURES

LIST OF TABLES

CHAPTER 1: INTRODUCTION AND REVIEW OF LITERATURE

1.1. General Introduction to Compound Semiconductors

A compound semiconductor is a semiconductor composed of elements from two or more different groups of the periodic table. Compound semiconductors which consist of various elements have widely ranging physical properties. They play an important role in the development of science and technology and constitutes today's basic building blocks of emitters and receivers in cellular, satellite and fibreglass communication. Semiconductors have attracted much attention in recent years to their great potential for technological importance and have aroused considerably scientific interest. In the early days Silicon (Si) and Germanium (Ge) were the most important semiconductors which were widely used for developments of various kinds of applications. But the limitations of these semiconductors in high speed devices and devices requiring emission and absorption of light led to the development of other semiconductors like the III-V and the II-VI compound semiconductors since last three decades. The III-V and II-VI compound semiconductors are able to determine the wavelengths of light which it can absorb or emit and because of this property they are widely used in LEDs and construction of lasers with a wide range of visible and infrared portion of the spectrum. They have also been successfully used as sensors, detectors, modulators and in many other scientific applications. Among the III-V and II-VI compound semiconductors, Gallium phosphide (GaP), Gallium Arsenide (GaAs), Indium Arsenide (InAs), Indium Phosphide (InP), Zinc Sulfide (ZnS), Cadmium Telluride (CdTe) and Zinc Selenide (ZnSe) are extensively studied because of their useful physical, electro-optical and other distinctive properties. They are widely used in construction of infrared detectors and diode lasers [1]. They have been utilized in the electronics and telecommunications industries, in the military science and device applications such as top junction solar cells and multi junction solar cell system [2-6].

It has therefore become important to understand the electronic structure, elastic properties and phase transition under induced pressure. The energy band gap is the most important characteristics of semiconductors which distinguish it from metals and insulators. The electronic structure calculation will give the information regarding energy band diagram, total density of states, and partial density of states of the constituent atoms, hence enabling us to understand the contributions of the atomic orbital in the band diagram. Thus one can have the opportunity theoretically to engineer the structure of the material with desire band gap which is an extremely important parameter in technical point of view. It helps in determining the wavelength of light which it can absorb or emit and hence is widely used in many optical and optoelectronic devices. Thus understanding of the basic electronic properties of semiconductors has become important in order to appreciate how semiconductors can be used to create devices.

Understanding of elastic properties of materials is also important as elasticity describes the response of a compound to a very small loading which causes reversible deformation. Elastic constant is the fundamental material parameters which characterises the elastic behaviour of a solid. It gives us important information about the nature of force operation in solids and provides a link between the mechanical and dynamical behaviour of solids. It also provides important information about anisotropic features and structural stability of a material.

Generally compound semiconductors (binary compound) crystallises both in zinc blende (ZB) and rock salt (RS) structure. Therefore, it is interesting to study the structural phase transformation under induced pressure. In view of this, the investigations on band gap, elastic constants under induced pressure and their variation at different pressure can be done and it will provide insight properties under extreme induced pressure.

In recent years, the advancement of compound semiconductors in technological applications has resulted in search for new semiconductor materials and the improvement of existing materials has become an important field of study in materials science. The potential of compound semiconductor to be doped with other atoms that alter its electronic properties in a controllable manner is its important characteristic. The knowledge of the variation of electronic structure with doping for the bulk material is essential to improve the thin film study which is a potential material for solar cell studies. Thus by performing appropriate doping, materials can be engineered with desirable basic properties such as the electronic properties.

1.2. Review of literature

In the early 1960s, Jameson performed the structural phase transition studies in Si and Ge [7] as well as other III-V compound semiconductors [8]. A fist principle electronic structure calculation on III-V and II-VI compound semiconductors was done in 1981 by Wang and Kleein [9]. The phase transition of III-V compound semiconductors was studied by Chelikowsky in 1987 [10]. In 1990 the pressure dependence of the electronic properties of cubic III-V Indium compounds was studied by Van Camp and his co-workers [11]. A. Mujica and R. J. Needs [12] in 1996 found that the simple cubic phase of GaP should be stable between 14.7 GPa and 20.3 GPa. In 2008, A.R. Rashid et al. [13] have studied the structural and electronic properties of GaP and compared the lattice parameters, bulk modulus, and pressure derivative of the bulk modulus with earlier data. The High-pressure properties of the zinc blende structure have been determined by Raman scattering, ultrasonic measurements, fundamental absorption, and refractive-index measurements [14-16]. Froyen and Cohen [17] first reported the structural phase of GaAs in 1983. The structural transformation in GaAs was also investigated by Besson et al [18] and Weir et al [19] using the single-crystal x-ray absorption spectroscopy and elastic neutron scattering. Studies on electronic structures, high-

pressure properties have been reported by various groups [10,20-22]. An ab initio simulation of high pressure phases of GaAs was done by Durandurdu and Drabold in 2002 [21]. The pressure induced phase transition to metallic state of InAs was first reported by Minomura and Drickamer [23] at 8.46 GPa pressure from high pressure resistivity measurements. Pitt and Vyas [4] in 1973 reported the phase transition of InAs from the ZB to RS through resistivity measurements. In 2014, Wang et al. [5] also studied the electronic transport properties of InAs using the non-equilibrium Green's function combined with density functional theory. S. Massidda and his group studied the structural and electronic properties of InAs and InP in 1990 [24]. In 2010, Lukacevic and his co-workers performed a density functional theory study of the phase stability of high pressure phases in InAs and InP [25]. The semiconductor-to-metallic phase transition from ZB to RS structure of InP is found to occur between 8.5 and 13.3 GPa pressure [8, 23, 26,27]. The phase stability of group III phosphide has been studied by Arbouche et al. [28] and reported the phase transition of InP occurring at about 7.35 GPa pressure. Branicio et al. [29] also investigated phase transition of InP at around 10.2 GPa pressure.

The first structural phase transformation of the II-VI compound semiconductors was studied experimentally by Edwards and Drickamer in 1960 [30]. Marino and Warekois in 1963 studied the high pressure phases of II-VI compound semiconductors [31]. Studies on the structures of the high pressure phases of II-VI compound semiconductors were also done in 1963 by Rooymans [32] and Owen and his group [33]. Thermoelectric properties and phase transitions of II-VI compound semiconductors at high pressure was studied by Shchennikov and Ovsyannikov in 2007 [34]. Richard M. Martin in 1970 studied the elastic properties of ZnS [35]. A quasi-particle band structure study of II-VI compound semiconductors was done by Zakharov and his co-workers in 1994 [36]. In 1990 E. Ves and his group studied the effect of pressure on the energy of the direct optical absorption edge and phase transition of cubic ZnS [37]. Desgreniers and his group in 2000 studied the pressure induced structural changes in ZnS [38]. In 2009, M.

Cardona and his group studied the electronic, vibrational and thermodynamic properties of ZnS [39] Energy dispersive X-ray diffraction technique has been used to perform high pressure studies of ZnS by Pan et al. [40]. In 2013, Jun and his co-workers performed XAFS investigation on the zinc belnde structure of ZnS [41]. Lee and Chang in 1995 studied the structural properties of ZnS and ZnSe [42]. In 1993, Mc Mahon and his group found out that with increasing pressure, the ZB structure of CdTe underwent a transition to cinnabar structure which was stable for only a short pressure interval and later changed to RS structure on further increasing pressure [43]. Earlier studies also confirmed the phase transition of CdTe from the ZB to RS structure at 3.8 GPa pressure [44]. In 2000, Kanoun and his co-workers investigated the structural, elastic and electronic properties of cadmium telluride using the molecular dynamic simulation [45]. The structural stability of cadmium chalcogenides under high pressure was studied by Benkhettou and his group in 2006 [46]. In 1998, R. J. Nelmes and Mc Mohan using the X-ray diffraction method confirmed the phase transformation from ZB to RS phase of ZnSe occurring at 13.5 GPa pressure [47]. The ZB to RS phase transition of ZnSe was also found to occur at 18 GPa pressure by Varshney and his co-workers from Slater-Kirkwood variational method [48]. In 2002, M. Jin, Q. Cui, E. Mukhar and D. Ding monitored the structural phase transformation from ZB to RS phase using a second harmonic generation (SHG) measurement [49]. The structural phase transformation of ZnSe under high pressure was also studied by Qteish and Munoz in 2000 using the first principle pseudopotential method [50]. In 2003 Gangadharan and his co-workers studied the structural phase transformation of ZnS and ZnSe compound semiconductors using TB-LMTO method [51]. Bilal and his co-workers in 2014 performed a first principle studies of the structural, elastic electronic and optical properties of Zn-chalcogenides under pressure [52].

1.3 Motivations

The prediction and synthesis of III-V and II-VI compound semiconductors has already been successfully performed by many researchers but still there is great need to exhaustively determine the structural properties, phase transition, elastic properties and electronic structure of these materials under induced pressures. The study of these properties under induced pressure will enable us to understand the behaviour of the materials under extreme conditions of pressures. This kind of information will helps us to understand thermal expansion, atomic bonding and their structural properties at higher pressures. But study of these properties experimentally under high pressure is very difficult. Therefore we can generate the structure of the materials computationally and predict the properties of the desired materials using well established solid state theories. In this thesis we have therefore calculated the structural properties, phase transition, elastic properties and electronic structure of III-V (GaP, GaAs, InP, InAs) and II-VI (ZnS, CdTe, ZnSe) compound semiconductors computationally based on the Density Functional Theory (DFT).

1.4. Research Objectives

The objectives of the thesis work are:

1. To study the structural properties and electronic properties of binary compound semiconductors. This includes the structural studies, Density of states (DOS) and energy band diagram.
2. Investigating the elastic properties of the compound semiconductors such as Elastic constants, Poisson's ratio, Young modulus, and Debye's temperature.
3. To study phase transition and thus study the electronic & elastic properties under induced pressure.
4. To study the effect of doping on the compound semiconductors and thus study its structural phase transformation.

CHAPTER 2: THEORETICAL METHODOLOGY

The electrons and nuclei are the determining factor for understanding the properties of condensed matter and molecules. It provides us information about the electronic, optical, magnetic and bulk properties of the material. An accurate determination of the electronic structure of the molecule is an important factor as it dominates the properties of the whole system. In the last few decades, experimentalist and theoreticians have been studying these properties for various scientific and technological applications. However due to complexity of the condensed matter systems, experimentally studying these properties under extreme conditions of pressures and temperature is tedious and difficult work. Theoretical study often provides a good understanding of the physics of the system under study, and it is often possible to interpolate or extrapolate these models in order to predict the behavior of systems under conditions not yet tested experimentally. Also developments in computational simulation have made it possible to study properties of materials from the first principle calculation with great accuracy. Thus it enables the explanations and prediction of the materials properties which are difficult to study experimentally. Various electronic structure methods have been developed in the past and modern physics is always faced with a challenge to develop computational methods that will accurately treat the interacting system of many electrons and nuclei.

2.1. Many body problem

The behaviour of interacting electrons in a solid is very difficult to understand and is a tremendous task which can only be addressed partially. This is not due to purely theoretical reasons but also to numerical reasons. Computers have become more and more powerful allowing physicists to solve more and more complex problems. However, the interacting-electron problem has been known for more than 80 years and despite the advent of computers and supercomputers, this particular task is still out of reach.

Solving the many-body Schrodinger equation is the starting point for investigating the properties of a material but the number of particles that are involved and the coupling and interactions of the particles cause a problematic issue which can be overcome by using approximation methods.

In a solid system, there are nuclei and electrons. For a solid, the Hamiltonian of the system of nuclei and electrons can be written as

$$\hat{H} = -\frac{1}{2}\sum_{i=1}^{N}\nabla_i^2 - \frac{1}{2}\sum_{A=1}^{M}\frac{1}{M_A}\nabla_A^2 - \sum_{i=1}^{N}\sum_{A=1}^{M}\frac{Z_A}{r_{iA}} + \sum_{i=1}^{N}\sum_{j>i}^{N}\frac{1}{r_{ij}} + \sum_{A=1}^{M}\sum_{B>A}^{M}\frac{Z_A Z_B}{R_{AB}} \qquad (2.1)$$

where, $\hat{H}$ is the Hamiltonian for the system consisting of M nuclei and N electrons. The sum over A and B runs over the M nuclei while the sum over i and j run over the N electrons. M_A and Z_A are the mass and atomic number of A^{th} nucleus, r_{iA} is the distance with A^{th} nucleus and i^{th} electron, r_{ij} represents the distance between i^{th} and j^{th} electrons, R_{AB} is the distance between A^{th} and B^{th} nuclei. Atomic units in which $\hbar = m = e = 1$, are used throughout the thesis work.

The first term is the kinetic energy for the electrons and second term is for the nuclei. The last three terms represents the attractive electrostatic (coulomb) interaction between the electrons and the nuclei and repulsive potential due to the electrons and nucleus-nucleus interaction respectively. Solving this problem is impossible, therefore acceptable approximate eigenstates is found out by making approximations at three levels.

2.2. Born-Oppenheimer approximation

We know that nuclei are much heavier and slower than electrons; we can therefore freeze them at fixed points and assume that only electrons are moving. Now since the nuclei do not move anymore, the kinetic energy becomes zero and the potential energy due to nucleus-nucleus interactions become constant. Thus we are left with three terms: the kinetic energy of the electron, the potential due to

the electron-electron interaction and the potential energy of the electrons in the external potential of the nuclei.

Now the above equation becomes

$$\hat{H} = -\frac{1}{2}\sum_{i=1}^{N}\nabla_i^2 - \sum_{i-1}^{N}\sum_{A=1}^{M}\frac{Z_A}{r_{iA}} + \sum_{i=1}^{N}\sum_{j>i}^{N}\frac{1}{r_{ij}} \tag{2.2}$$

which can be formally written as

$$\hat{H} = \hat{T} + \hat{V}_{ee} + \hat{V}_{ext} \tag{2.3}$$

where

$$\hat{T} = -\frac{1}{2}\sum_{i=1}^{N}\nabla_i^2$$

$$\hat{V}_{ee} = \sum_{i=1}^{N}\sum_{j>i}^{N}\frac{1}{r_{ij}}$$

$$\hat{V}_{ext} = -\sum_{i=1}^{N}\sum_{A=1}^{M}\frac{Z_A}{r_{iA}}$$

The kinetic and the electron-electron terms of the above equation (2.3) depends only on the fact that we are dealing with a many-electron system and are independent of the solid system.

2.3. Density functional theory (DFT)

The Hamiltonian obtained after Born-Oppenheimer approximation is much simpler than the original Hamiltonian. But it is still difficult to solve. There are several methods to reduce equation (2.3) to an approximation but tractable form. One important approximation is the *Density Functional Theory (DFT).*

Density-functional theory (DFT) is one of the most widely used technique in condensed matter physics and quantum chemistry [53,54,55] employed to study the ground state properties calculation of atoms, molecules or solids. It is first principle theory of condensed matter physics for the electron-electron many-body problem through the introduction of an exchange-correlation term in the

functional of the electronic density. It is a very reliable theory for predicting new materials, to confirm experimental discoveries, or to provide explanation of new phenomena observed in experimental work.

DFT is the quantum mechanical approach for solving the many electron system. It is based on the electronic density distribution rather than the many electron wave functions and transforms the many body system into a system of non-interacting fermions in an effective field called Kohn –Sham equation.

The Density Functional Theory concept for atomic spheres was first introduced by Thomas and Fermi around 1927-1928 [56,57] with further improvements by Hartree [58], Dirac [59, 60], Fock [61] and Slater [62] but the formal establishment of DFT was given by Hohenberg and Kohn [63] in 1964.

Hohenberg and Kohn gave two theorems mainly known as the Hohenberg-Kohn theorem. This theorem enables us to establish a unique correspondence between the external potential and ground state density.

2.3.1. Hohenberg and Kohn theorem

Theorem 1: The ground state electron density of a system determines the external potential $V_{ext}(r)$ (within a trivial additive constant). In other words there is one to one correspondence between the ground state density, $\rho(r)$ and the external potential $V_{ext}(r)$.

Theorem 2: The density that minimises the variational energy is the true ground state density for the external potential, V_{ext} i.e. the total energy functional has a minimum equal to the ground state energy at the ground state density of the system.

(The proofs of theorem 1 and theorem 2 are given in appendix B)

2.3.2. Kohn Sham Equation

In 1965 Kohn-Sham gave a proposal which reduced the long task of dealing with many particle Schodinger equation for real system to a relatively easy to solve set of one particle equations of a virtual system [64].

Hohenberg and Kohn proved that the ground state energy can be written as a unique functional of the electron density.

Therefore the total energy of an interacting system is

$$E[\rho] = T[\rho] + E_{ee}[\rho] + E_{ext}[\rho] \tag{2.4}$$

Now we can consider a virtual system of non-interacting electron system of same density ρ having the same energy functional $E[\rho]$ with the original system, then rearranging the terms, we can write as

$$E[\rho] = T_S[\rho] + E_{Hartree}[\rho] + E_{ext}[\rho] + \{T[\rho] - T_S[\rho] + E_{ee}[\rho] - E_{Hartree}[\rho]\} \tag{2.5}$$

where $T_s[\rho]$ is the non-interacting kinetic energy corresponding to density ρ. The kinetic energy functional *T[ρ]* has been replaced by the non-interacting kinetic energy term $T_s[\rho]$.

$E_{Hatree}[\rho]$ is the Hatree energy which is the usual classical coulomb interaction as a functional of density ρ. Therefore the energy functional remains the same. The first three terms in the above expression are the major terms quantitatively and can be treated exactly.

The last term,

$$\{T[\rho] - T_S[\rho]\} = E_C[\rho] \; ; \{E_{ee}[\rho] - E_{Hatree}[\rho]\} = E_X[\rho]$$

$$\{T[\rho] - T_S[\rho] + E_{ee}[\rho] - E_{Hartree}[\rho]\} = E_C[\rho] + E_X[\rho] = E_{XC}[\rho]$$

is called exchange correlation energy.

It is about 10% of the total energy. Therefore an approximation of reasonable accuracy is acceptable for this part as far as energy calculation is concerned. It is this part which draws most of the attention of DFT researchers.

Now the kinetic energy functional of the non-interacting electron system $T_s[\rho]$ is expressed as,

$$T_S[\rho] = -\frac{1}{2}\left\langle \psi_S[\rho] \middle| \nabla^2 \middle| \psi_S[\rho] \right\rangle \tag{2.6}$$

where ψ_S is Slater determinant formed from single particle orbitals $\phi_i's$. It is given as,

$$\psi_s = \frac{1}{\sqrt{N!}} \begin{vmatrix} \phi_1(x_1) & \phi_1(x_2) & \cdots & \phi_1(x_{N-1}) & \phi_1(x_N) \\ \phi_2(x_1) & \phi_2(x_2) & \cdots & \phi_2(x_{N-1}) & \phi_2(x_N) \\ \vdots & \vdots & \cdots & \vdots & \vdots \\ \phi_{N-1}(x_1) & \phi_{N-1}(x_2) & \cdots & \phi_{N-1}(x_{N-1}) & \phi_{N-1}(x_N) \\ \phi_N(x_1) & \phi_N(x_N) & \cdots & \phi_N(x_{N-1}) & \phi_N(x_N) \end{vmatrix} \tag{2.7}$$

The ground state electron density is then given by

$$\rho(r) = \sum_i |\phi_i(r)|^2 \tag{2.8}$$

Thus,

$$E[\rho] = -\frac{1}{2}\sum_i \left\langle \phi_i[\rho] \middle| \nabla^2 \middle| \phi_i[\rho] \right\rangle + \frac{1}{2}\iint \frac{\rho(r)\rho(r')}{|r-r'|} dr dr' + \int v_{ext}\rho dr + E_{XC}[\rho] \tag{2.9}$$

Minimising the above expression for energy with respect to the orbital's and using the condition $\int |\phi_k(r)|^2 dr = 1$ we get,

$$\left[-\frac{1}{2}\nabla^2 + \int \frac{\rho(r')}{|r-r'|} dr' + v_{ext}(r) + v_{XC}(r) \right] \phi_k = \varepsilon_k \phi_k \tag{2.10}$$

This equation is DFT counterpart of Schrodinger equation and is known as the Kohn-Sham equation. Here ϕ_k's are the Kohn-Sham orbital's and ε_k's enter into the equation as Lagrange undetermined multiplier and are the Kohn-Sham orbital energies. v_{ext} and v_{XC} are respectively, external potential and the exchange correlation potential.

Total energy of the system is also expressed as,

$$E[\rho] = \sum_{k=1}^{N} \varepsilon_k - \frac{1}{2} \iint \frac{\rho(r)\rho(r')}{|r-r'|} dr dr' - \int v_{ext}\rho(r) dr + E_{XC}[\rho] \tag{2.11}$$

The Kohn-Sham calculation proceeds as follows. At first we start with an initial density ρ(r) and solve the Kohn-Sham equation self-consistently to generate a set of Kohn-Sham orbitals from which then we calculate ground state total energy as a functional of ground state density.

(Detailed mathematical steps of this calculation is given in appendix C)

2.4. Approximations to exchange correlation potential

Exchange correlation potential is obtained as the functional derivative of the exchange correlation energy as,

$$v_{xc}(r) = \frac{\delta E_{xc}[\rho]}{\delta \rho(r)} \tag{2.12}$$

In practice, exchange correlation energy is split into exchange and correlation part separately. Therefore we have,

$$E_{xc}[\rho] = E_x[\rho] + E_c[\rho] \tag{2.13}$$

Corresponding potentials are also defined separately as, $v_x(r) = \frac{\delta E_x[\rho]}{\delta\rho(r)}$ and $v_c(r) = \frac{\delta E_c[\rho]}{\delta\rho}$. Exchange part constitutes about 10% of the total energy while correlation part constitutes less than one percent of the total energy for the majority systems. Correlation effects, although small become important in certain cases such as information of negative ions. Therefore it is very important that accurate exchange and correlation energy functional be available for density functional calculations.

There are different types of approximations involved in DFT calculation for the unknown exchange-correlation density functional $E_{XC}[\rho]$ which make DFT practically implementable. The approximations are Local Density Approximation (LDA), Generalised Gradient Approximation (GGA) and Generalised Density Approximation with modified Becke Johnson (GGA+mbJ).

2.4.1. Localised Density Approximation (LDA)

The Local Density Approximation (LDA) also known as the local functional proposed by Kohn and Sham in 1965 and is the basis of all approximate exchange-correlation function. In LDA one assumes that the exchange correlation energy leads to an exchange correlation potential depending on the value of density in 'r' and not on its gradient.

$$E_{XC} = \int \rho(r)\varepsilon_{xc}[\rho(r)]dr \tag{2.14}$$

where ε_{xc} is the exchange-correlation energy density of the uniform electron gas of density $\rho(r)$[65]. It is exact for a homogenous electron gas so it works well for systems in which the electron density does not vary too rapidly. The LDA

functional reproduces the ground state properties of many systems very accurately. They are also known to predict inaccurately the energy band gap of semiconductor materials [66,67,68].

2.4.2. Generalised Density Approximation (GGA)

Besides the local density approximation (LDA), a number of non-local approximations have been suggested. The reason for that is a high value of density gradient in some materials. But even when the gradient is not small the LDA gives good results. The approximation which accounts for spatial variation of density is usually termed as the Generalised Gradient Approximation (GGA). In GGA the gradient of the charge density is included in the exchange-correlation functional in order to account for the non-homogeneity of the true electron density i.e. the exchange correlation potential is a function of both the charge density at a given point and the first order gradient of the charge density at the same point.

$$E_{XC}[\rho] = \int \rho(r)\varepsilon_{xc}(\rho(r)\nabla\rho(r))d^3r \qquad (2.15)$$

Generally, GGA has the following advantages over LDA [69, 70, 71]:

1. GGA improves ground state properties for light atoms, molecules and clusters.

2. GGA predicts the correct magnetic properties of 3d transition metals such as body centred iron.

There are different types of GGA functional and detailed discussions on the different types of GGA functionals are present in the reference [72].

2.4.3. Generalised Density Approximation with modified Becke Johnson (GGA+mBJ)

The Generalised Density Approximation with modified Becke Johnson (GGA+mBJ) overcomes the underestimation in the calculation of energy band

gaps within the LDA and GGA and competes in accuracy with the expensive hybrid and GW methods. The modified Becke Johnson potential was proposed by Tran and Blah in 2009 [73]. It is a semi local approximation to an atomic "exact-exchange" potential and a screening term. In the modified Becke Johnson potential,

$$\upsilon_{x,\sigma}^{mBJ}(r) = c\,\upsilon_{x,\sigma}^{BR}(r) + (3c-2)\frac{1}{\pi}\sqrt{\frac{5}{6}}\sqrt{\frac{t_\sigma(r)}{\rho_\sigma(r)}} \tag{2.16}$$

where $\rho_\sigma = \sum_{i=1}^{N_\sigma}\left|\psi_{i,\sigma}\right|^2$ is the electron density, $t_\sigma = \left(\frac{1}{2}\right)\sum_{i=1}^{N_\sigma}\nabla\psi_{i,\sigma}^{*}.\nabla\psi_{i,\sigma}$ is the kinetic energy density, $\upsilon_{x,\sigma}^{BR}(r) = -\frac{1}{b_\sigma(r)}\left(1-e^{-x_\sigma(r)}-\frac{1}{2}x_\sigma(r)e^{-x_\sigma(r)}\right)$ is the Becke-Roussel (BR) exchange potential [74] which was proposed to model the coulomb potential created by the exchange hole and $\sqrt{\frac{t_\sigma(r)}{\rho_\sigma(r)}}$ is the screening term. In equation (2.16),

$c = \alpha + \beta\left(\frac{1}{V_{cell}}\int_{cell}\frac{\left|\nabla\rho(r')\right|}{\rho(r')}d^3r\right)^{1/2}$ i.e. for any value of c, the exchange potential is obtained for constant electron density. Here V_{cell} is the unit cell volume and α = -0.012 and β = 1.023 $bohr^{1/2}$ are the two free parameters.

This semi local exchange potential, which recovers the local-density approximation (LDA) for a constant electron density, mimics very well the behaviour of orbital-dependent potentials and leads to calculations which are

barely more expensive than LDA calculations and can be applied to very large systems in an efficient way.

2.5. Concepts of Phase Transition.

During a phase transition, certain properties of a given medium often discontinuously changes due to some external conditions such as temperature, pressure and others. These changes of phase are called phase transitions and the phenomena are very important not only in natural processes, but also in industry. In early years the rate at which the transition occurred were observed in attempting the classification of phase transition in solid states. Based on different characteristics of transition, three types of approaches are used for describing phase transition namely the kinetic approach, the thermodynamic approach and the structural approach.

Kinetic approach gives in consideration the transition rate and the activation energy between polymorphs of a given compound. In the thermodynamic approach the changes in the Gibbs free energy as a function of external parameters like temperature, pressure, magnetic field, or electric field are investigated. Lastly in structural approach the structures of the polymorphic phases before and after the transformation are compared. In general, the distinction between transformation types is open to more than one definition and is related to a phenomenological rather than an atomistic understanding of the transition.

In nature, structural phase transitions are common phenomena that can be induced by pressure or temperature. It plays an important role in the discovery of new phases with different chemical and physical properties in solid states. Transformations on increasing pressure often lead to crystalline polymorphs with a defined symmetry because of volume restriction. The basic problems about phase transformations, crystal structure and the nature of atomic bonding can be answered using high-pressure techniques. Also the use of high pressure to

synthesize new materials, to study the behaviour of existing materials and to tune materials physical properties provides tremendous potential for advancement in applied materials research.

There are various observable which characterize the energy aspect of a system. The internal energy U which is the total energy of the system is conserved. The enthalpy $H(=U+PV)$ is the energy needed for creation or destruction of the system with volume V in an environment at a fixed pressure P. As the enthalpy can be used to characterize the heat, the aspects of work can be characterized by the free energy.

The Gibb's free energy is defined as

$$G = U + PV - TS \tag{2.17}$$

In the present study the structural phase transformation from the zinc blende to the rock salt phase is studied. The structural phase transition from ZB to RS (B3→B1) phase is determined by calculating the Gibbs free energy G. Since our calculation is done at zero temperature we have ignored the entropy contribution. Therefore the structural phase transition has been calculated from the condition of equal enthalpies i.e. H=E+PV.

2.6. Theory of Elastic Constants.

The elastic constant of solids provides a link between the mechanical and dynamical behaviours of a crustal and also gives significant information concerning the nature of forces in solids.

Solids are not perfectly rigid and therefore when proper forces are applied, there is change in the shape and size of the material. After the removal of the forces if the changes are not too large, the bodies regain their original shape and size. This property of solid by virtue of which they regain their original shape and size is called elasticity. When an external force is applied to a body in which one part

exerts a force on the neighbouring parts it is known as stress. The elastic constant of a material can represent the deformation of materials under any small stress. According to the linear theory of elasticity strain (relative elongations and distortion) are linearly proportional to the applied stress within the elastic limit of the body. Outside this elastic limit a non linear effects break the proportionality between the stress and strain and for large stresses the deformation becomes irreversible.

The stress and strain of a material are linearly connected by the generalised Hooke's law,

$$\sigma_{mn} = C_{mnpr}\varepsilon_{pr} \tag{2.18}$$

where σ_{mn} is the stress tensor along with the individual elements which are called the stress components, C_{mnpr} are the elastic constants or the stiffness tensor popularly known as the stiffness matrix and ε_{pr} is the strain tensor with its individual elements known as the strain components. Here, m, n, p, r = 1,2, 3.

The stiffness coefficients for this linear stress-strain relationship are the individual elements and therefore the stress and strain tensor has 3×3 = 9 components each while the stiffness tensor has 3^4 = 81 independent elements. These individual elements are referred by various names as elastic constants, elastic moduli and stiffness coefficients and they are the fundamental parameters providing detailed information on the materials mechanical properties. A proper knowledge of these parameters enables us in understanding various mechanical behaviour of the material at different conditions. The number of these elastic constants can be reduced from different symmetries.

Under the stress symmetry, the stress components are symmetric. i.e. $\sigma_{mn} = \sigma_{nm}$ and therefore the nine stress components is reduced to six components only.

Thus equation (2.18) can be written as

$$\sigma_{nm} = C_{nm\,pr}\varepsilon_{pr} \tag{2.19}$$

Now, subtracting equation (2.19) from (2.18) we get,

$$\sigma_{mn} - \sigma_{nm} = \varepsilon_{pr}\left(C_{mnpr} - C_{nmpr}\right)$$

i.e. $C_{mnpr} = C_{nmpr}$ (2.20)

There are six independent ways to express m and n taken together and still nine independent ways to express p and r taken together. Thus with this symmetry the number of independent elastic constants reduces to (6×9=) 54 from 81.

Under the strain symmetry the strain components are symmetric. i.e. $\varepsilon_{pr} = \varepsilon_{rp}$. Therefore from equation (2.18),

$$\sigma_{mn} = C_{mnrp}\varepsilon_{rp} \tag{2.21}$$

Again, subtracting equation (2.20) from (2.19) we get,

$$C_{mnpr} = C_{mnrp} \tag{2.22}$$

Thus we find from equation (2.20) and equation (2.21) that there are six independent ways of expressing m and n when p and r are fixed and six independent ways of expressing p and r when m and n are fixed. Hence there are 6×6=36 independent constants with stress and strain symmetry.

Thus in matrix format the stress-strain relation showing the 36 independent components of stiffness can be represented as

$$\begin{pmatrix} \sigma_1 \\ \sigma_2 \\ \sigma_3 \\ \sigma_4 \\ \sigma_5 \\ \sigma_6 \end{pmatrix} = \begin{pmatrix} C_{11} & C_{12} & C_{13} & C_{14} & C_{15} & C_{16} \\ C_{21} & C_{22} & C_{23} & C_{24} & C_{25} & C_{26} \\ C_{31} & C_{32} & C_{33} & C_{34} & C_{35} & C_{36} \\ C_{41} & C_{42} & C_{43} & C_{44} & C_{45} & C_{46} \\ C_{51} & C_{52} & C_{53} & C_{54} & C_{55} & C_{56} \\ C_{61} & C_{62} & C_{63} & C_{64} & C_{65} & C_{66} \end{pmatrix} \begin{pmatrix} \varepsilon_1 \\ \varepsilon_2 \\ \varepsilon_3 \\ \varepsilon_4 \\ \varepsilon_5 \\ \varepsilon_6 \end{pmatrix} \tag{2.23}$$

$$\sigma_m = C_{mn}\varepsilon_n \quad \text{(m, n=1, 2, …, 6)} \tag{2.24}$$

Now, if we consider the Strain energy density function W, then

$$W = \frac{1}{2} C_{mn}\varepsilon_m\varepsilon_n \tag{2.25}$$

$$\text{where } \sigma_i = \frac{\partial W}{\partial \varepsilon_i} \tag{2.26}$$

We see that W is quadratic function of strain and thus can be also written as

$$W = \frac{1}{2} C_{nm}\varepsilon_n\varepsilon_m \tag{2.27}$$

Now, subtracting equation (2.27) from equation (2.25) we get

$$C_{mn} = C_{nm} \tag{2.28}$$

Thus stiffness is symmetric and has 21 independent elastic constants. These 21 independent elastic constants can further be reduced by considering the symmetry conditions found in different crystals.

In particular for a cubic lattice due to higher symmetry there are only three independent elastic constants C_{11}, C_{12} and C_{44}.

$$\text{i.e. } C_{cubic} = \begin{pmatrix} C_{11} & C_{12} & C_{12} & 0 & 0 & 0 \\ C_{12} & C_{11} & C_{12} & 0 & 0 & 0 \\ C_{12} & C_{12} & C_{11} & 0 & 0 & 0 \\ 0 & 0 & 0 & C_{44} & 0 & 0 \\ 0 & 0 & 0 & 0 & C_{44} & 0 \\ 0 & 0 & 0 & 0 & 0 & C_{44} \end{pmatrix} \tag{2.29}$$

Explicit form of other lattice symmetries can be found in ref [79].

In principle there are two ways of calculating the elastic constants of a material from the ab initio methods, the stress theorem [76] and the energy approach [77]. The stress theorem relies on the ab initio approach to directly calculate the stress tensor. And once the stress tensor has been computed by ab initio method, the elastic constants are directly derived from the generalised Hook's law in equation (2.18). In our calculations of elastic constant we have used the energy approach. The energy approach is based on the computed total energy of properly selected strained states of crystal and is given in detail in Chapter 3, Computational Tools.

CHAPTER 3: COMPUTATIONAL TOOLS

3.1. The WIEN2K code

All the calculations presented in this work are performed using the WIEN2k software package developed by P. Blaha and K. Schwarz *et al*. [78] based on Full Potential Linearized Augmented Plane wave (FP-LAPW) method [79] for computation of the electronic structures of crystals (solids) within the Density Functional Theory (DFT). This method is one of the most accurate methods for estimation of the ground state properties of solids.

The main advantages of this package (code) are that it is an all-electron and full-potential method and performs investigation of properties which are sensitive to core electrons. Using this code, the simulation of a wide range of material's properties, such as structural, electronic, optical properties (elastic constants, NMR spectroscopy, X-Ray, XPS, EELS...) are also possible. Also a web interface is present which provides a clear guidance at each calculation levels.

The basis set used in the WIEN2k code is the Linearized Augmented Plane Wave (LAPW). In this method the lattice is divided into non-overlapping spheres (called an atomic or muffin tin (MT) sphere) surrounding each atomic site and an interstitial region. Therefore two different types of basis sets are chosen for expressing the single particle wave functions. Inside the MT region, the basis function is a product of radial function and spherical harmonics $Y_{lm}(r)$

$$\text{i.e. } \phi_{k_n} = \sum_{lm} [A_{lm,k_n} u_l(r, E_l) + B_{lm,k_n} \dot{u}_l(r, E_l)] Y_{lm}(\hat{r}) \tag{3.1}$$

where $u_l(r, E_l)$ is the regular solution of the radial Schroedinger equation for energy E_l and the spherical part of the potential inside sphere t; $\dot{u}_l(r, E_l)$ is the energy derivative of u_l evaluated at the same energy E_l. A linear combination of

these two functions constitute the linearization of the radial functions; the coefficients A_{lm} and B_{lm} are functions of k_n determined by requiring that this basis matches each plane wave the corresponding basis function of the interstitial region; u_l and $\dot{u}_l$ are obtained by numerical integration of the radial Schroedinger equation on a radial mesh inside the sphere.

For the interstitial regions that are outside the MT sphere, the basis functions are expanded in plane waves.

i.e. $$\phi_{k_n} = \frac{1}{\sqrt{\omega}} e^{ik_n \cdot r} \tag{3.2}$$

where $k_n = k + K_n$; K_n are the reciprocal lattice vectors and k is the wave vector inside the first Brillouin zone. Each plane wave is augmented by an atomic-like function in every atomic sphere.

The solutions to the Kohn-Sham equations are expanded in this combined basis set of LAPW's according to the linear variation method.

$$\psi_k = \sum_n c_n \phi_{k_n} \tag{3.3}$$

And the coefficients c_n are determined by the Rayleigh-Ritz variational principal. The convergence of this basis set is controlled by a cut off parameter $R_{mt}K_{max}$=6-9, where R_{mt} is the smallest atomic sphere radius in the unit cell and K_{max} is the magnitude of the largest K vector in equation (3.3).

Two major parts are present in the program: the initialization, and the main self-consistent field (SCF) cycle. Many analytical tools like band structure, density of states, charge densities, volume optimization, optical properties etc are implemented.

In the initialisation part the nearest neighbours are calculated up to a specified distance and the atomic sphere radii. Overlapping spheres, coordination numbers and nearest neighbour distances are also checked. It is also checked whether the equivalent atoms are really crystallographically equivalent and then calculates the point and space groups for the given structure. The space group symmetry operation is generated. The point group of the individual atomic sites are determined and generated for the lattice harmonics and local rotation matrices. The symmetry operations and the point groupsymmetry of the atoms (to compare them with the "International Tables for X-Ray Crystallography") are then checked. The atomic valance densities are then generated. The k-mesh is generated in the Brillouin zone (BZ). Thus in the initialisation part an initial crystal density is obtained by superposition of atomic densities for the SCF cycle.

The second part i.e. SCF cycle consists of five steps:

1. LAPW0 which generates the potential from the density and construct the effective potential.

2. LAPW1 which calculates the valance band i.e. the eigenvalues and eigenvectors by solving the Kohn Sham equation of valance electrons.

3. LAPW2 which computes new valance densities from the eigenvectors.

4. LCORE which computes the potential and the charge density of the core electrons, and

5. LMIXER which mixes the electron densities of core, semi-core and valance states and generate new input density for the next iterations.

In all the calculations, the number of k-points used for the integration part for both zinc blende and rock salt structure of III-V and II-VI compound semiconductors is 8000 k-points with 20*20*20 k mesh which is reduced to 256 irreducible k-points inside the Brillion zone including five high symmetry points

W, L, Γ, X and K. Convergence of the basis set is obtained at $R_{MT}K_{max}$ = 9.0 where K_{max} gives us the plane wave cut-off. The position of the of the first and second atom in ZB structure is taken to be (0,0,0) and (0.25,0.25,0.25) and in RS structure it is (0,0,0) and (0.5,0.5,0.5) respectively.

3.2. Elastic constant code: Cubic Elastic

The elastic constant calculations have been performed using the energy approach. In this method elastic constants were calculated by applying small strains to the unstrained lattice.

For a cubic system only three independent elastic constants namely C_{11}, C_{12} and C_{44} are present. Hence, a set of three sets of distortions are used to determine the three elastic constants. For determining the C_{11} and C_{12} we use two types of distortion D_1 and D_2

The first distortion is the orthorhombic distortion,

$$D_1 = \begin{bmatrix} 1+\delta & 0 & 0 \\ 0 & 1-\delta & 0 \\ 0 & 0 & \dfrac{1}{(1-\delta)^2} \end{bmatrix} \tag{3.4}$$

which gives us the energy,

$$E(V,\delta) = E_0 + V_0\{(C_{11}-C_{12})\delta^2 + O(\delta^4)\} \tag{3.5}$$

The second distortion or strain is the volume cubic distortion,

$$D_2 = \begin{bmatrix} 1+\delta & 0 & 0 \\ \delta & 1+\delta & 0 \\ 0 & 0 & 1+\delta \end{bmatrix}$$

The volume is expanded giving the energy,

$$E(V,\delta) = E_0 + V_0\delta(\sigma_1 + \sigma_2 + \sigma_3) + V_0\left\{\frac{3}{2}(C_{11} + 2C_{12})\delta^2 + O(\delta^3)\right\} \quad (3.6)$$

The third distortion is the distortional monoclinic deformation which determines the C_{44},

$$D_3 = \begin{bmatrix} 1 & \delta & 0 \\ \delta & 1 & 0 \\ 0 & 0 & \frac{1}{(1+\delta^2)} \end{bmatrix}$$

which give us the energy,

$$E(V,\delta) = E_0 + V_0\{(2C_{44})\delta^2 + O(\delta^4)\} \quad (3.7)$$

The elastic constants are thus determined from the above three equations (3.5, 3.6, 3.7).

The elastic constants are calculated with the elastic package interfaced with WIEN2k as developed by Morteza Jamal [80]. The cubic elastic package is a set of programs and scripts that can calculate elastic tensor calculations for cubic phases (primitive, body-centred, or face centred) by using WIEN code. To run this program a valid cubic structure file should exist. This package generates WIEN input files simulating strained structures. It also generates scripts to make WIEN calculate these structures and analyse the results, plot them, and derive their elastic parameters.

CHAPTER 4: III-V COMPOUND SEMICONDUCTORS

Till date there have been many studies on the structural and electronic properties of group III-V compound semiconductors. The detailed literatures available on these semiconductors have been discussed in chapter 1 (Introduction), sub section 1.2 (Review of literatures). But the high-pressure study on the electronic structures and elastic properties is still very rare. The experimental study of these quantities at high pressure is very difficult and therefore, many theoretical calculations are usually used.The main aim of the study in the present chapter is to have a detailed understanding of the structural, electronic, phase transition as well as the effects of pressure on the electronic and elastic properties of the group III-V compound semiconductors: GaP, GaAs, InP and InAs.

4.1. STRUCTURAL STABILITY AND PHASE TRANSITION

The static equilibrium properties of the crystal structure of zincblende (ZB) and rocksalt (RS) of GaP, GaAs, InP and InAs are obtained by minimization of the total energy with respect to the unit cell volumes per molecule and fitting it to the Birch–Murnaghan equation [81]. The phase with the lowest Gibbs energy at a given pressure and temperature determines the Enthalpy of the phase. Since our calculation is done at zero temperature we have ignored the entropy contribution. Therefore the structural phase transition has been calculated from the condition of equal enthalpies i.e. $H = E + PV$.

The structural properties and Phase transition of III-V compound semiconductors: GaP, GaAs, InP and InAs are discussed in this section. In all calculations, we have used LDA and GGA exchange correlations to see the comparative results.

(a) Gallium Phosphide (GaP)

The total energy as a function of volume of GaP for both the ZB and RS structure that are calculated with LDA and GGA for structure optimization are shown in

figure 4.1. From the figure, it is observed that GaP-ZB structure has lower total energy at the equilibrium volume in both LDA and GGA methods thus indicating that GaP in ZB structure is more stable than the RS structure.

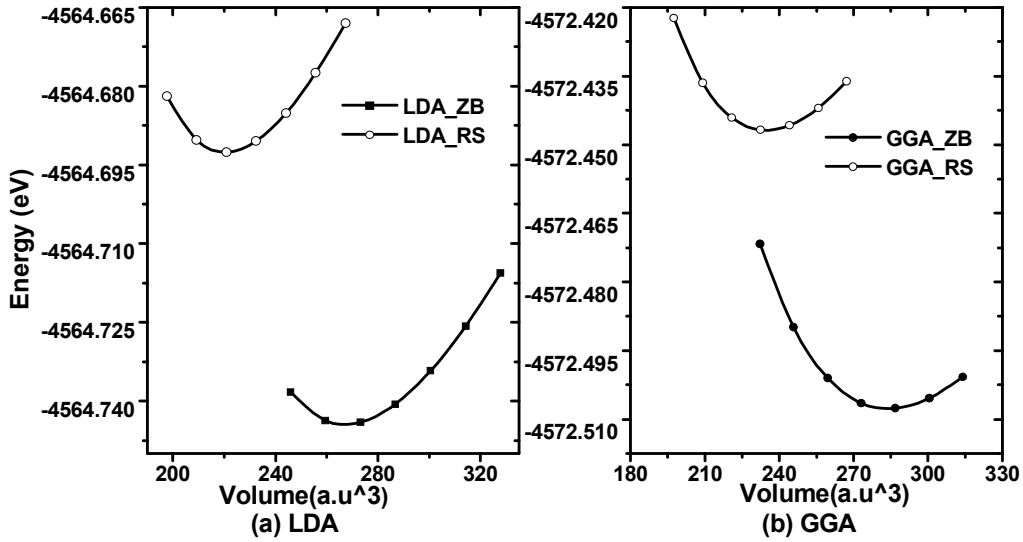

Figure 4.1.Total energy as a function of primitive cell volume of GaP-ZB and GaP-RS with (a) LDA method and (b) GGA method

Table 4.1. Experimental and calculated ground state structural parameters of GaP in ZB and RS structure

		Zinc Blende (ZB) Strucutre			**Rock Salt (RS) Structure**		
		a_0 (A^0)	B_0 (GPa)	$B^/$	a_0 (A^0)	B_0 (GPa)	$B^/$
Present work	LDA	5.41	91.19	4.72	5.07	105.80	4.83
	GGA	5.52	77.71	4.34	5.18	88.34	4.84
Expt. work		5.47[a], 5.50[b], 5.45[c]	77.2[b],	4.88[b],	-	-	-
Other Theo. calculation		5.41[d], 5.54[e], 5.51[f]	90.0[d], 76.0[f],	4.50[d], 4.59[f]	5.165[g], 5.160[f]	87.3[g], 87.59[f]	3.78[g], 4.54[f]

[a]Ref[82], [b]Ref[83], [c]Ref[84], [d]Ref[12], [e]Ref[85] , [f]Ref[13], [g]Ref[86]

The results of present study of GaP-ZB and GaP-RS are compared with other available experimental and theoretical data and are given in table 4.1. For the GaP-ZB phase for which the experimental values are available for comparison, the lattice parameter calculated with LDA method shows a difference of only 0.9% while that of GGA shows a difference of 0.36% which is quite acceptable under the 2% difference. Thus our results are in good agreement with other studies and used for further calculation of phase transition and energy band structure.

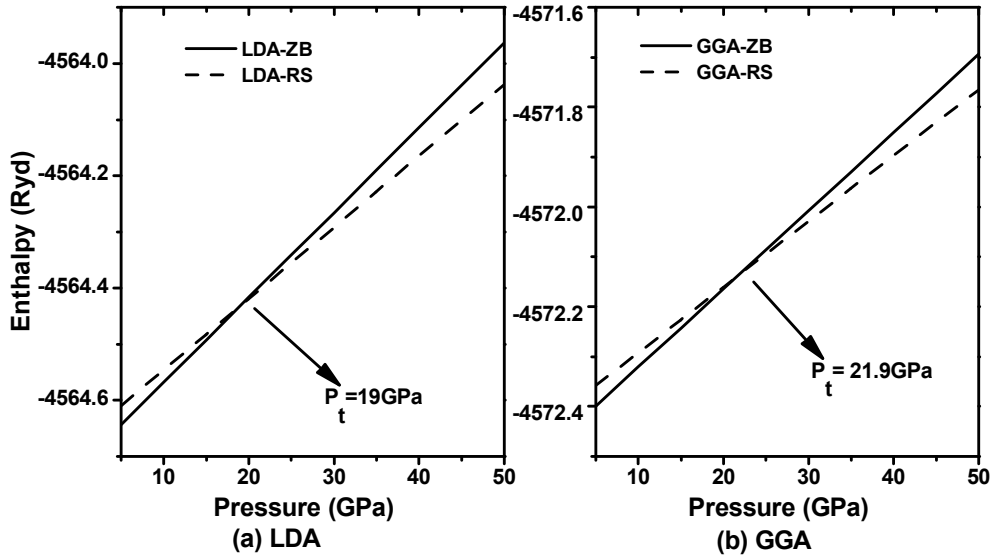

Figure 4.2. Enthalpy as a function of pressure for ZB and RS phase of GaP within (a) LDA method and (b) GGA method

Table 4.2. Phase transition pressure 'P_t(GPa)' and volume collapse of GaP

	Present calculation	**Expt. results**	**Theoretical results**
Transition pressure (P_t)(GPa)	19 (LDA) 21.9 (GGA)	22[a],24±0.3[b], 21.5±0.8 [c]	21.7[d], 18.8[e], 16.8[f],
Volume collapse (%)	14.11		14[g], 16[h]

[a]Ref[87], [b]Ref[88], [c]Ref[89], [d]Ref[90], [e]Ref[91], [f]Ref[92], [g]Ref[93], [h]Ref[94]

Under the induced pressure, GaP in ZB structure transforms to RS structure. When the phase transition takes place, the Enthalpy of both the phases are same. Thus the

pressure at equal Enthalpy determines the phase transition pressure. Figure 4.2 shows the variation of Enthalpy with pressure for both the methods i.e. LDA and GGA. The transition pressure with LDA method shows a phase transition of 19 GPa pressure while within GGA method the phase transformation takes place at 21.9 GPa pressure which is more nearer to experimental result as shown in table 4.2. Since GGA gives us better calculation of the phase transition we have calculated the volume collapse of GaP within the GGA only. The normalised volume as a function of pressure is also shown in figure 4.3. During the phase transition the normalised volume of the ZB and RS phase is 0.829 and 0.688 respectively with a volume decrease of 14.11% indicating that ZB phase is more compressible than the RS phase.

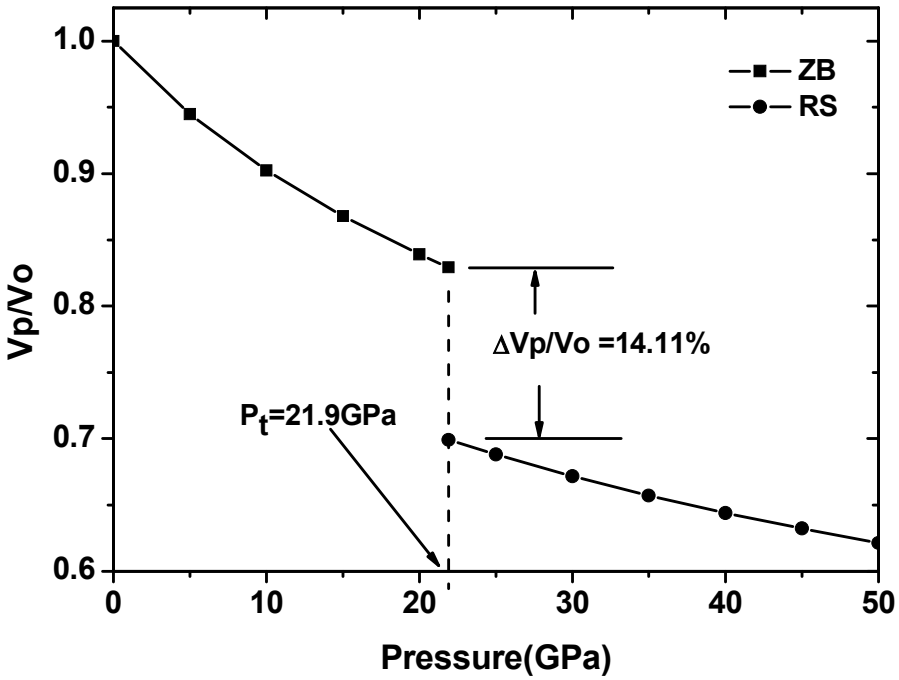

Figure 4.3. Normalized volume as a function of pressure of GaP-ZB and GaP-RS

(b) Gallium Arsenide (GaAs)

The results of structural properties and phase transition of GaAs are discussed in this sub section following the same methods of calculations as before.

In Figure 4.4, the total energy as a function of volume of GaAs shows that the GaAs in ZB structure is more stable than the RS structure. The present calculated parameters are compared with other experimental and theoretical data in table 4.3. The present results are in good agreement with other studies and thus used for phase transition and energy band structure study.

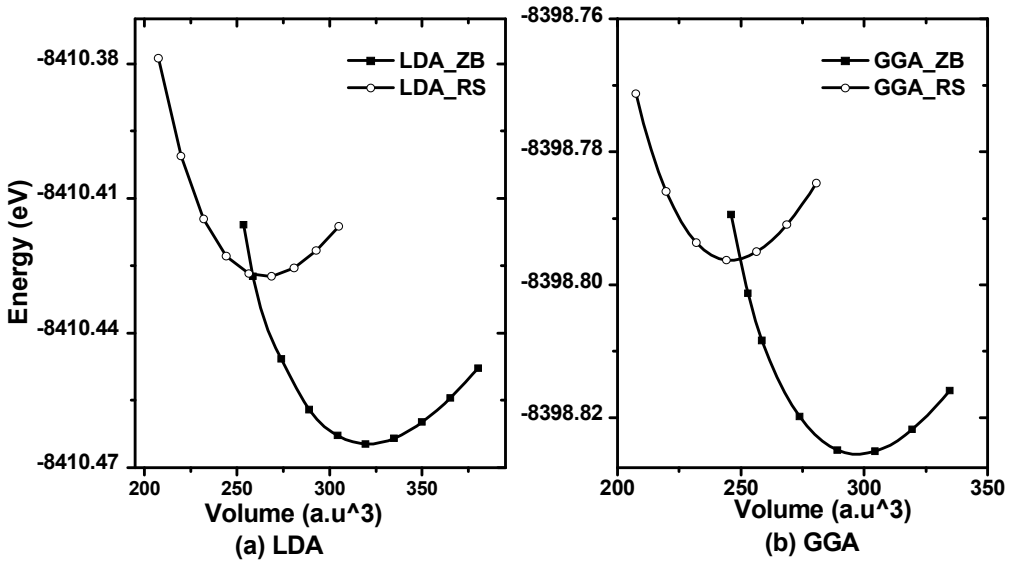

Figure 4.4. Total energy as a function of primitive cell volume for GaAs-ZB and GaAs-RS with (a) LDA method and (b) GGA method

Table 4.3. Experimental and calculated ground state structural parameters of GaAs in ZB and RS structure

		Zinc Blende (ZB) Structure			**Rock Salt (RS) Structure**		
		a_0 (A^0)	B_0 (GPa)	$B^/$	a_0 (A^0)	B_0 (GPa)	$B^/$
Present work	LDA	5.61	75.46	4.93	5.26	88.73	4.95
	GGA	5.74	61.08	4.80	5.37	71.10	4.90
Expt. work		5.65[a]	75.7[b], 74.8[c]	4.00[b], 4.56[c]	-	-	-
Other Theo. calculation		5.74[d], 5.64[e], 5.65[f]	75.76[e], 73.4[f]	4.71[e], 4.50[f]	5.29[e], 5.32[f]	73.54[b], 83.68[e]	5.10[e], 4.77[f]

[a]Ref[95], [b]Ref[96], [c]Ref[97], [d]Ref[98], [e]Ref[99], [f]Ref[100]

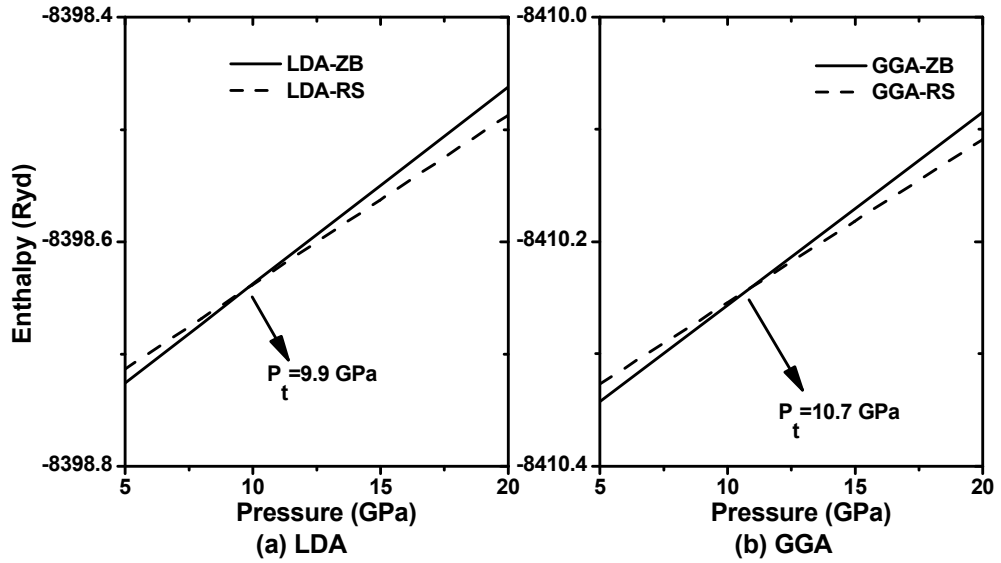

Figure. 4.5. Enthalpy as a function of pressure for ZB and RS phase of GaAs with (a) LDA method and (b) GGA method

Table 4.4. Phase transition pressure 'P_t(GPa)' and volume collapse of GaAs

	Present calculation	**Expt. results**	**Theoretical results**
Transition pressure (P_t)(GPa)	9.9 (LDA) 10.7 (GGA)	12±1.5[a]	12.0[b], 16.3[c], 17.3[d],10.5[e]
Volume collapse (%)	14.2	-	-

[a]Ref[101], [b]Ref[102], [c]Ref[96], [d]Ref[99], [e]Ref[103]

The Enthalpy graph as shown in figure 4.5 shows a transition pressure of 9.9 GPa pressure with LDA method while the transition pressure with GGA method is 10.7 GPa pressure. The normalised volume (with GGA method in figure 4.6) of ZB and RS phase is 0.876 and 0.734 respectively. Thus there is a volume decrease of 14.2% during the phase transition. It concludes that ZB phase is more compressible than the RS phase. The results of phase transition and volume collapse are compared with other experimental and theoretical studies in table 4.4.

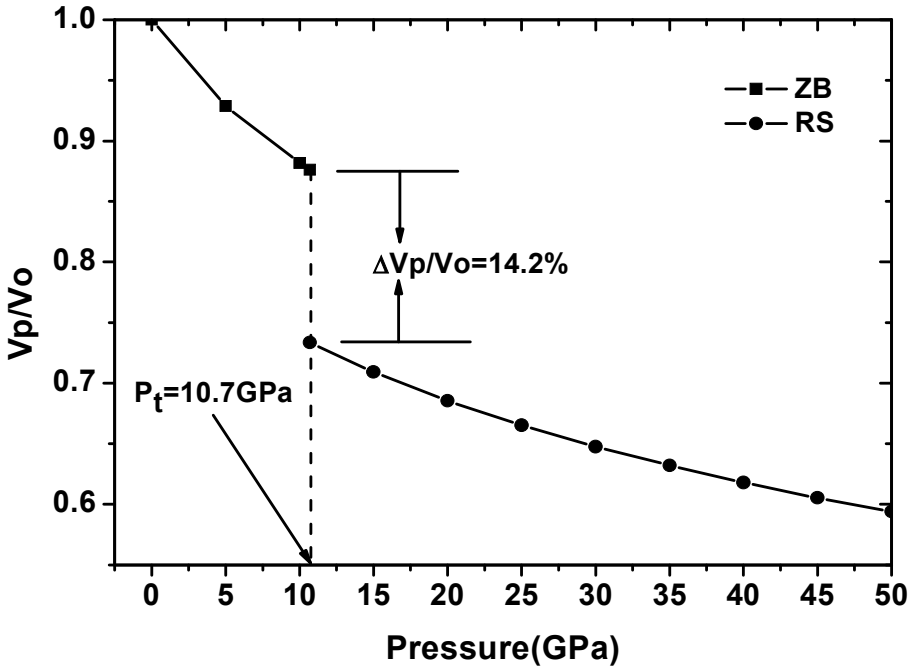

Figure 4.6. Normalized volume as a function of pressure for GsAs-ZB and GaAs-RS

(c) Indium Phosphide (InP)

In this subsection, the structural parameters and phase transition of InP are studied. The total energy as a function of volume of InP are shown in figure 4.7 and the ZB structure of InP is found to be more stable than the RS structure. In table 4.5, the results of present calculated parameters of InP-ZB and InP-RS are compared with other experimental and theoretical data.

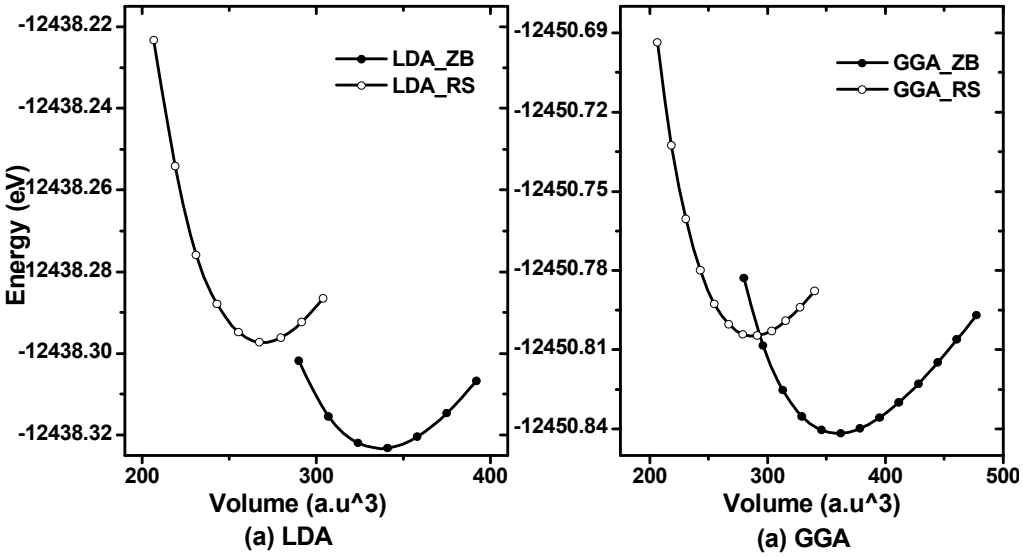

Figure 4.7.Total energy as a function of primitive cell volume for InP-ZB and InP-RS with (a) LDA method and (b) GGA method

Table 4.5. Lattice constant 'a(A^0)', bulk modulus 'B(GPa)' and pressure derivative of bulk modulus ($B^/$) of ZB and RS structure of InP at zero pressure

		Zinc Blende (ZB) Structure			**Rock Salt (RS) Structure**		
		a_0 (A^0)	B_0 (GPa)	$B^/$	a_0 (A^0)	B_0 (GPa)	$B^/$
Present work	LDA	5.84	71.93	4.79	5.42	88.61	5.04
	GGA	5.97	60.5	4.64	5.54	74.78	4.76
Expt. work		5.90[a], 5.87[b]	65.5[d], 72[e]	4.59[c]	-	-	-
Other Theo. calculation		5.94[b], 5.95[c]	68[b],71[f], 60[g]	4.9[b], 4.41[g], 4.67[h]	5.71[b], 5.24[b]	-	-

[a]Ref[104], [b]Ref[105], [c]Ref[106], [d]Ref[107],[e]Ref[108], [f]Ref[109], [g]Ref[110], [h]Ref[111]

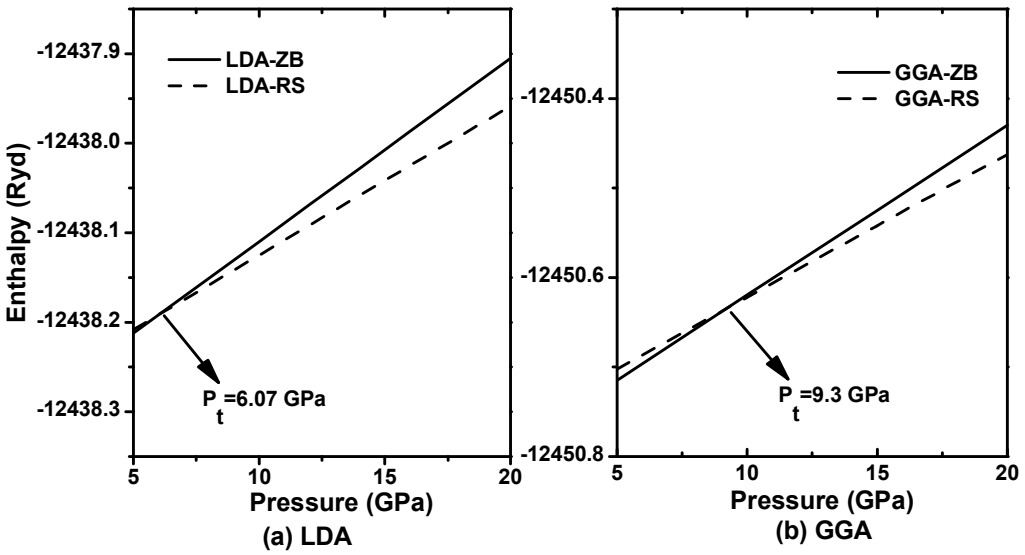

Figure. 4.8. Enthalpy as a function of pressure for ZB and RS phase of InP with (a) LDA method and (b) GGA method

Table 4.6. Phase transition pressure 'P_t(GPa)' and volume collapse of InP

	Present calculation	**Expt. results**	**Theoretical results**
Transition pressure (P_t)(GPa)	6.07 (LDA) 9 .3 (GGA)	9.5[a],10.3±0.2[b], 9.8[c]	7.3[d], 7.5[e], 8.5[f],11.0[g]
Volume collapse (%)	16.45	14.9[b]	18[f], 15[g],17[h]

[a]Ref[27], [b]Ref[28], [c]Ref[105], [d]Ref[25], [e]Ref[112], [f]Ref[93], [g]Ref[94], [h]Ref[113]

The enthalpy curve in figure 4.8 indicates the structural transition pressure of InP in ZB to RS structure at 6.07 GPa pressure with LDA method and at 9.3GPa pressure with GGA method. The volume collapse of InP (within GGA) is shown in figure 4.9 with a volume decrease of 16.45% indicating that the ZB phase is more compressible than the RS phase. A comparison of results is shown in table 4.6.

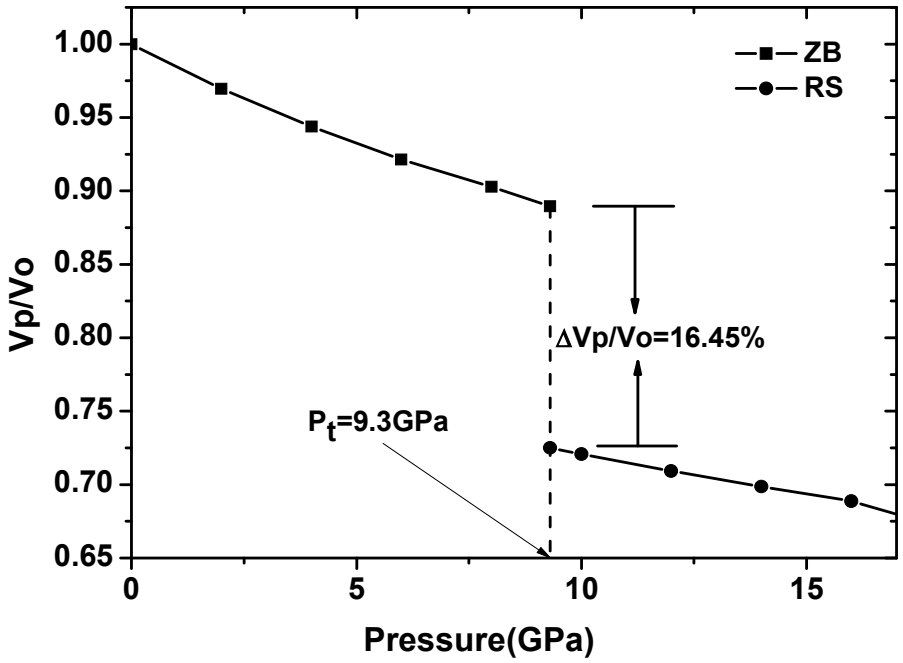

Figure 4.9. Normalized volume as a function of pressure for InP-ZB and InP-RS

(d) Indium Arsenide (InAs)

The structural stability and phase transition of InAs are studied in this subsection. The structural optimization curve of InAs is shown in figure 4.10 and shows more stability in ZB structure as compared to RS structure. The structural parameters for the present study and available experimental results are given in table 4.7. The transformation of ZB structure to RS structure of InAs under induced pressure takes place at 3.9GPa pressure and at 4.7GPa pressure with LDA, GGA method respectively as shown in the Enthalpy curve in figure 4.11. The volume collapse (in figure 4.12) in the phase transformation is found to have a volume decrease of 17.2% and implies that ZB phase is more compressible than the RS phase. Our calculated results of phase transition and volume collapse are compared with other experimental and theoretical results as shown in table 4.8.

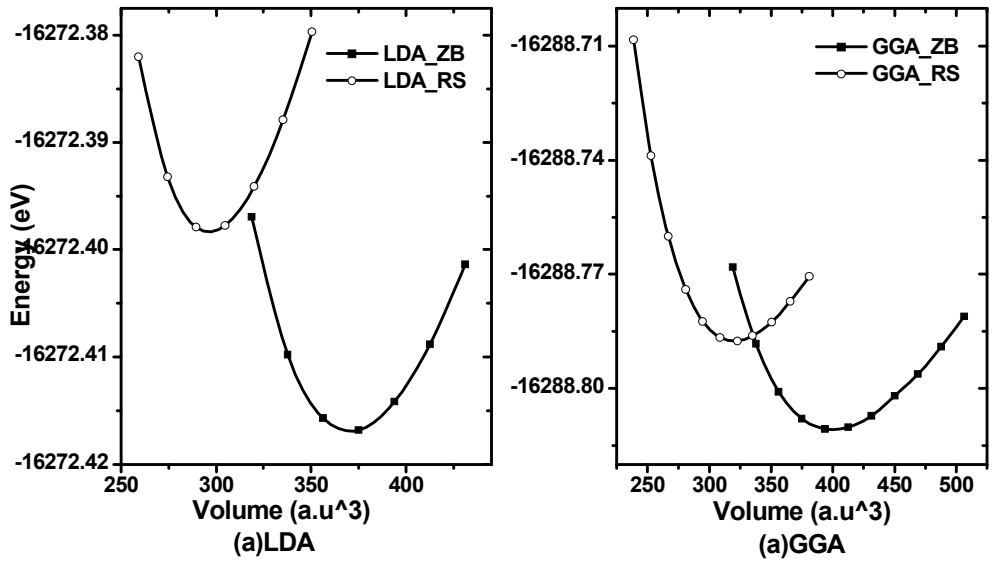

Figure 4.10. Total energy as a function of primitive cell volume for InAs-ZB and InAs-RS with (a) LDA method and (b) GGA method

Table 4.7. Experimental and calculated ground state structural parameters of InAS in ZB and RS structure

		Zinc Blende (ZB) Structure			**Rock Salt (RS) Structure**		
		a_0 (A^0)	B_0 (GPa)	$B^/$	a_0 (A^0)	B_0 (GPa)	$B^/$
Present work	LDA	6.03	61.3	4.86	5.60	77.604	4.96
	GGA	6.18	49.48	4.78	5.74	62.98,	4.84
Expt. work		6.10[a]	59.2±5[e]	6.8±2[e]	5.5005[e], 5.514[f]	40.6±14[e]	7.3±1[e]
Other Theo. calculation		6.10[b], 6.08[c]	55.51[c], 50.4[d]	-	5.65[c]	-	-

[a]Ref[81],[b]Ref[114],[c]Ref[115],[d]Ref[116],[e]Ref[117],[f]Ref[118].

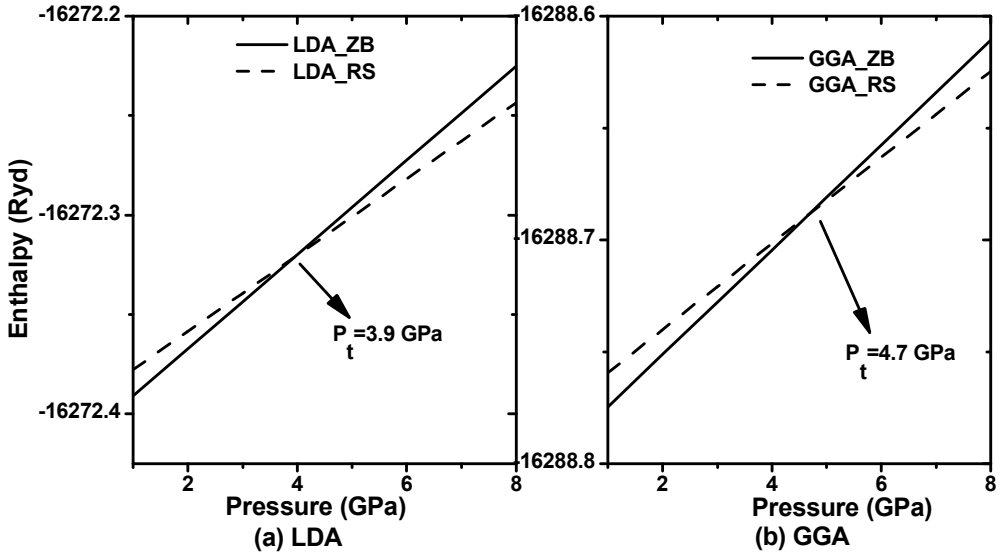

Figure. 4.11. Enthalpy as a function of pressure for ZB and RS phase of InAs with (a) LDA method and (b) GGA method

Table 4.8. Phase transition pressure 'P_t(GPa)' and volume collapse of InAs

	Present calculation	**Expt. results**	**Theo. results**
Transition pressure (P_t) (GPa)	3.9 (LDA) 4.7 (GGA)	7[a] , 6.9±0.2[b]	3.9[c], 4.0[d]
Volume collapse (%)	17.2	17.0±0.2[a], 18.8[b]	17.0[d]

[a]Ref[4], [b]Ref[117],[c]Ref[119],[d]Ref[120]

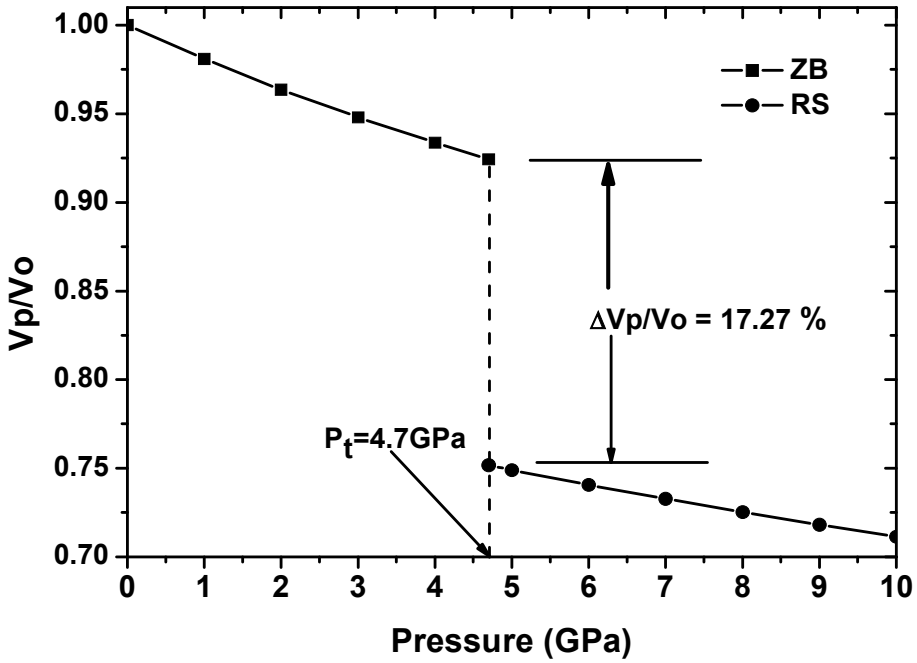

Figure 4.12. Normalized volume as a function of pressure for InAs-ZB and InAs-RS

4.3. ELASTIC PROPERTIES

The elastic constants play an important role in the study of relationship between crystal structures and bonding of a material. They give us important information about the nature of force operating in the solids and are basic parameters that are used for studying the elastic properties of a material. The mechanical stability condition of a crystal at high pressure can be understood from the pressure

dependence of the elastic constant. For a cubic crystal, the Born mechanical stability conditions are as follows: $(C_{11}+2C_{12}) > 0$; $C_{11}-C_{12} > 0$; $C_{11} > 0$; $C_{12} > 0$.

The Zener anisotropy factor (A), Poisson's ratio (υ), Kleinmann parameter (ξ), B/G ratio, Young's modulus (Y) and Debye's temperature (θ_D) are important parameters which determine the mechanical and thermal properties of a material. The elastic isotropy of a material is determined by the Zener Anisotropy factor (A). For A = 1, the material is elastically isotropic and deform uniformly along all directions of the body. If A > 1, it is stiffest along <111> plane body diagonals and when A < 1, it is stiffest along <100> cube axes. It is expressed as:

$$A = \frac{2C_{44}}{C_{11} - C_{12}} \tag{4.1}$$

The Poisson's ratio (υ), provides a sharp criterion for differentiating the brittleness and ductility in solids and give us information about the characteristics of bonding forces. For covalent materials υ=0.1 whereas for ionic materials, υ= 0.25 [121]. The upper and the lower limits of υ in central force solids have been reported to be 0.25 and 0.5 respectively [122]. It is calculated using the relation,

$$\upsilon = \frac{1}{2}\left(\frac{B - (2/3)G}{B + (1/3)G}\right) \tag{4.2}$$

where B is the Bulk modulus and G is the isotropic shear modulus as given by

$$G = \frac{G_V + G_R}{2} \tag{4.3}$$

G_v is the Voigt's shear modulus corresponding to the upper bound of G values, and G_R is the Reuss's shear modulus corresponding to the lower bound of G values. G_v and G_R can be expressed as:

$$G_V = \frac{C_{11} - C_{12} + 3C_{44}}{5} \tag{4.4}$$

$$G_R = \frac{5(C_{11} - C_{12})C_{44}}{4C_{44} + 3(C_{11} - C_{12})} \tag{4.5}$$

Kleinmann parameter (ζ) describes the relative position of the cation and anion sub-lattices and is given by the relation

$$\zeta = \frac{C_{11} + 8C_{12}}{7C_{11} + 2C_{12}} \tag{4.6}$$

It also implies resistance against bond bending or bond angle distortion. In a system, minimising bond bending leads to ζ=0 and minimising bond stretching leads to ζ=1.

The ductile and brittle behaviour of a material can be understood from the ratio of the bulk and shear modulus (B/G) [123]. If the shear modulus (G) is low we know that it has a low resistance to shear and hence is ductile while if a material has low bulk modulus, it means the resistance fracture is low and hence brittle. We know that the critical value which separates the ductility and brittleness of a material is 1.75. A material is said to be ductile if B/G > 1.75 and brittle if B/G < 1.75.

The Young's modulus is determined to measure the stiffness of the solid and is given by:

$$Y = \frac{9GB}{G + 3B} \tag{4.7}$$

Debye's temperature gives us explicit information about lattice vibrations and is also an important parameter determining the thermal characteristics of a material. It is calculated using the average sound velocity (υ_m) given by the relation [124]:

$$\theta_D = \frac{h}{k}\left[\frac{3n}{4\pi}\left(\frac{N_A\rho}{M}\right)\right]^{1/3}\upsilon_m \tag{4.8}$$

where h is the Plank's constant, k is the Boltzmann constant, N_A is the Avogadro's number, n is the number of atoms per formula unit, M is the molecular mass per formula unit, ρ is the density and υ_m is given by [125]:

$$\upsilon_m = \left[\frac{1}{3}\left(\frac{2}{\upsilon_t^3}+\frac{1}{\upsilon_l^3}\right)\right]^{-(1/3)} \tag{4.9}$$

where υ_t and υ_l are the transverse and longitudinal velocities respectively, which are obtained from Navier's equation as [126]:

$$\upsilon_l = \sqrt{\frac{3B+4G}{3\rho}} \tag{4.10}$$

$$\upsilon_t = \sqrt{\frac{G}{\rho}} \tag{4.11}$$

In the present study, the elastic constants, C_{11}, C_{12} and C_{44} at different pressures are calculated within the GGA only.

(a) Gallium Phosphide (GaP)

In the previous subsection, we have observed a phase transformation from zincblende (ZB) to rocksalt (RS) phase of GaP under induced pressure at 21.9 GPa pressure. Thus the elastic constants of GaP are calculated for the lattice corresponding to pressure ranging from 0 GPa to 20 GPa pressure for ZB structure and from 23 GPa to 37 GPa pressure for RS structure. We find that the present calculated results as shown in figure 4.13 satisfy the mechanical stability conditions: $(C_{11}+2C_{12}) > 0$; $C_{11}C_{12} > 0$; $C_{44} > 0$; $C_{11} > 0$ for the ZB and RS phases.

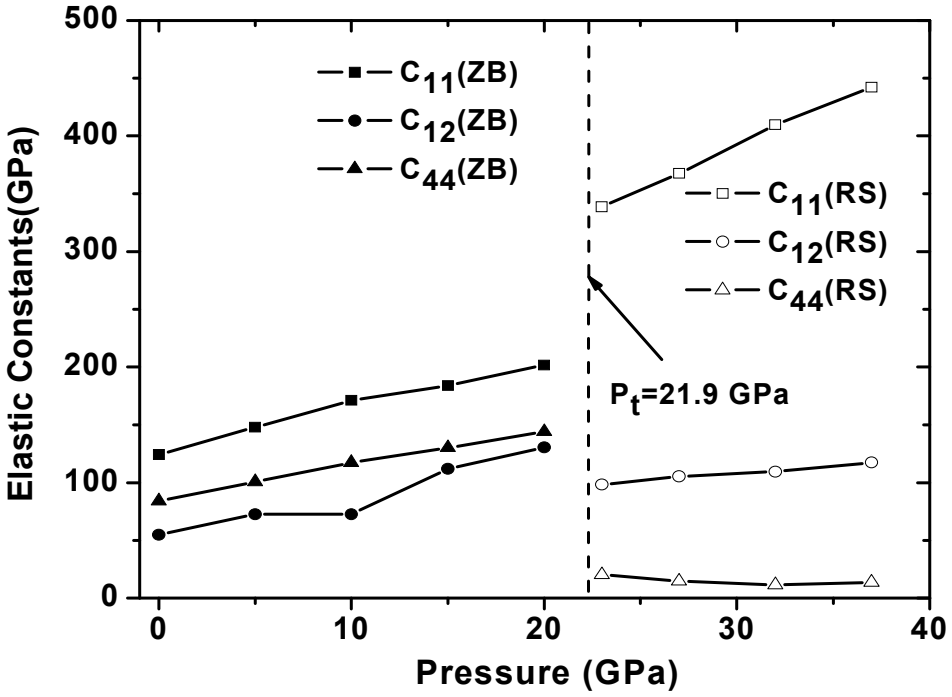

Figure 4.13. Elastic constants (C_{11}, C_{12}, C_{44}) as a function of pressure of GaP-ZB and GaP-RS phase

The elastic parameters such as Zener Anisotropy factor (A), Poisson's ratio (υ), kleinmann's parameter (ζ), B/G ratio, Young's modulus (Y) and Deby's temperature (θ_D) are calculated for both GaP-ZB and GaP-RS phases at different pressures to study mechanical and thermal behavior of GaP at high pressures.

In figure 4.14 the elastic parameters (Zener Anisotropy factor (A), Poisson's ratio (υ), kleinmann's parameter (ζ) and B/G ratio) as a function of pressure are given.

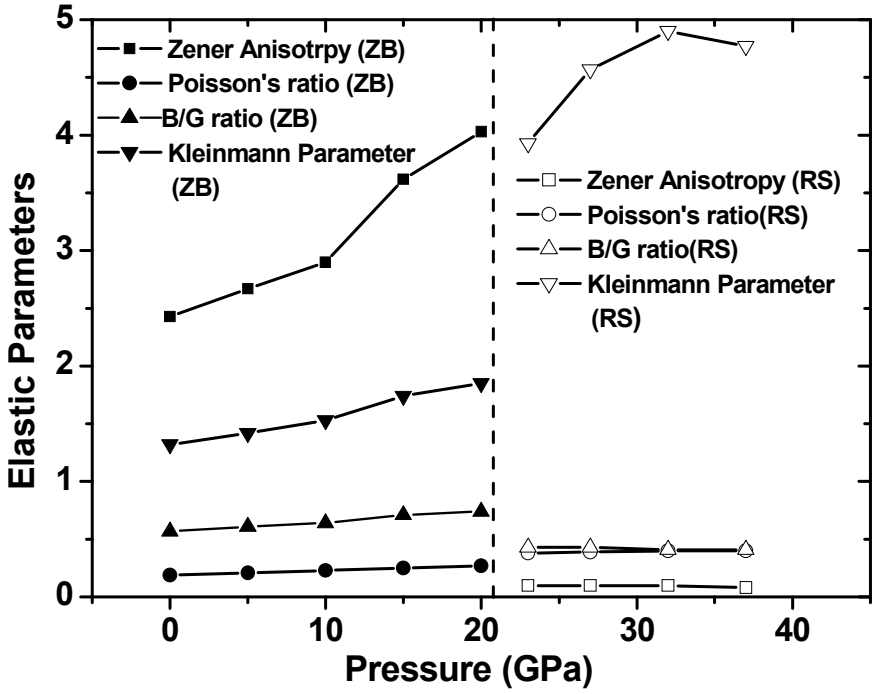

Figure 4.14. Elastic parameters (Zener Anisotropy factor, Poisson's ratio, Kleinmann parameter and B/G ratio) as a function of pressure for ZB and RS phases of GaP

Our calculation of the Zener Anisotropy factor (A) shows a variation from 2.43 to 4.03 in the ZB phase while in the RS phase it decreases from 0.16 to 0.08 with pressure. Thus we find that A is stiffest along <111> body diagonal in ZB phase and after transition to RS phase it becomes stiffest along <100> cube axes. Our results of Poisson's ratio (υ) shows that as pressure increases, the value of υ increases from 0.19 to 0.27 in ZB phase while it increases from 0.38 to 0.40 in RS phase indicating higher ionic contribution in the inter atomic bonding with increasing pressure. It also indicates with increasing pressure inter atomic forces tend to be more central. In the present study, the Kleinmann parameter (ζ) of the ZB phase is found to vary from 0.57 to 0.74 with pressure while in RS phase it is found to decrease from 0.43 to 0.41 showing shrinkage in bond stretching in the ZB phase and shrinkage in bond bending in the RS phase. We also find that with

increase in pressure the B/G ratio of GaP-ZB phase increases from 1.32 to 1.86 while the GaP-RS phase shows an increase from 3.93 to 4.77. Hence we conclude that the brittle nature of ZB phase of InAs becomes ductile as pressure increases and retains its ductility even after it undergoes a structural phase transition to RS phase.

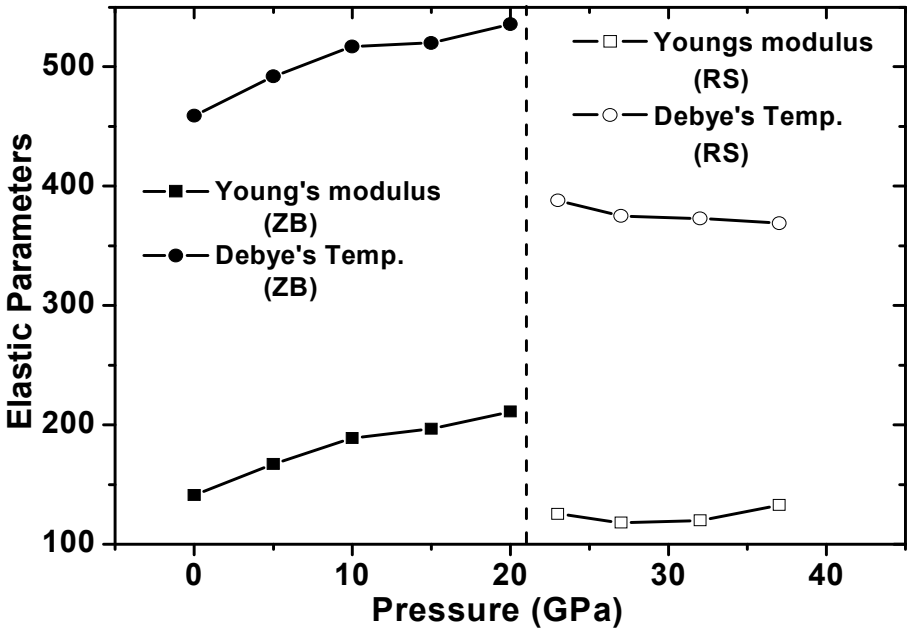

Figure 4.15. Elastic parameters (Young's modulus and Debye's temperature) as a function of pressure of GaP in ZB phase and RS phase

The elastic parameters (Young's modulus and Debye's temperature) as a function of pressure of both GaP-ZB and GaP-RS phases are shown in figure 4.15. From the figure it is observed that with increase in pressure the value of Y increases from 141.06 GPa to 210 GPa in ZB phase while in RS phase the value of Y at first decreases from 125.29 GPa to 117. 86 GPa and then increases to 132.61 GPa. Thus GaP becomes more rigid with increase in pressure in ZB phase but after it undergoes a structural transformation to RS phase, the rigidity of GaP slightly decreases at certain pressure but soon attains its rigidity again as pressure goes on increasing. As the pressure increases, the value of Debye's temperature also

increases from 459 K to 536 K for ZB phase indicating stiffer lattice and better thermal conductivity but after undergoing structural transformation to RS phase the temperature decreases from 388 K to 369 K indicating weaker lattice and decrease in thermal conductivity.

(b) Gallium Arsenide (GaAs)

The transition pressure of GaAs for ZB to RS phase is found as 10.7 GPa pressure as shown in the previous subsection. Figure 4.16 shows the elastic constants (C_{11}, C_{12}, C_{44}) of Gallium Arsenide (GaAs) under pressure 0 GPa to 10 GPa pressure for ZB structure and 12 GPa to 20 GPa pressure for RS structure. It is noted that the mechanical stability conditions are found to satisfy for the ZB phase only and not for the RS phase. In the figure 4.16, there is a linear variation of elastic constants with pressure up to 10 GPa pressure in ZB phase while in the RS phase the value of C_{44} are found less than 0 GPa which indicates the instability of the RS phase at higher pressures. Therefore the elastic parameters at higher pressures are studied only for the ZB phase.

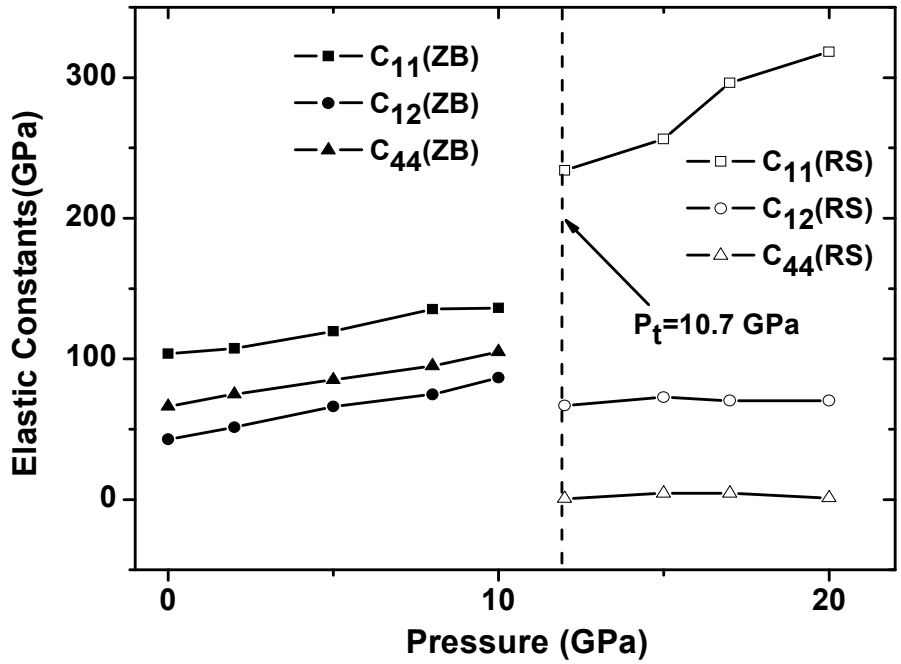

Figure 4.16. Elastic constants (C_{11}, C_{12}, C_{44}) as a function of pressure of GaAs-ZB and GaAs-RS phase

Figure 4.17 shows the elastic parameters (Zener Anisotropy factor, Poisson's ratio, Kleinmann parameter and B/G ratio) as a function of pressure of GaAs in ZB phase. The Zener Anisotropy factor (A) shows a variation from 2.17 to 4.22 in the ZB phase thus A is stiffest along <111> body diagonal in the ZB structure. The Poisson's ratio (υ) shows that the value of υ increases from 0.18 to 0.25 indicating higher ionic contribution in inter atomic bonding with increasing pressure. It also indicates that with increasing pressure inter atomic forces tend to be more central. The Kleinmann parameter (ζ) of the ZB phase is found to vary from 0.55 to 0.73 with pressure showing bond stretching in the ZB phase. The B/G ratio of ZnS-ZB phase increases from 1.26 to 1.73. Hence we conclude that the brittle nature of GaAs in ZB structure becomes ductile as the pressure increases.

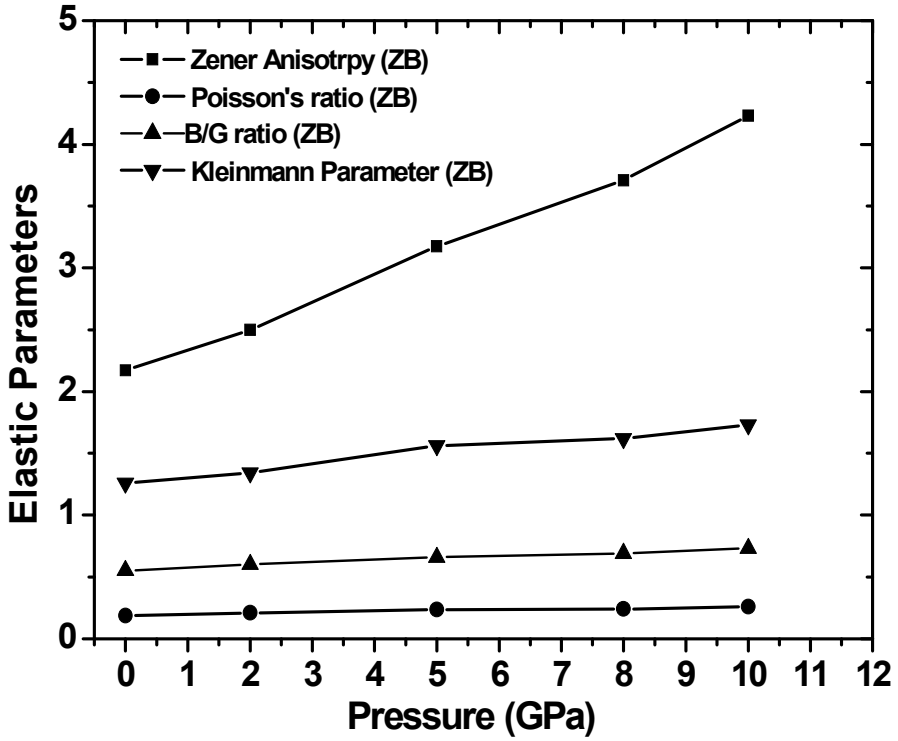

Figure 4.17. Elastic parameters (Zener Anisotropy factor, Poisson's ratio, Kleinmann parameter and B/G ratio) as a function of pressure of GaAs in ZB phase

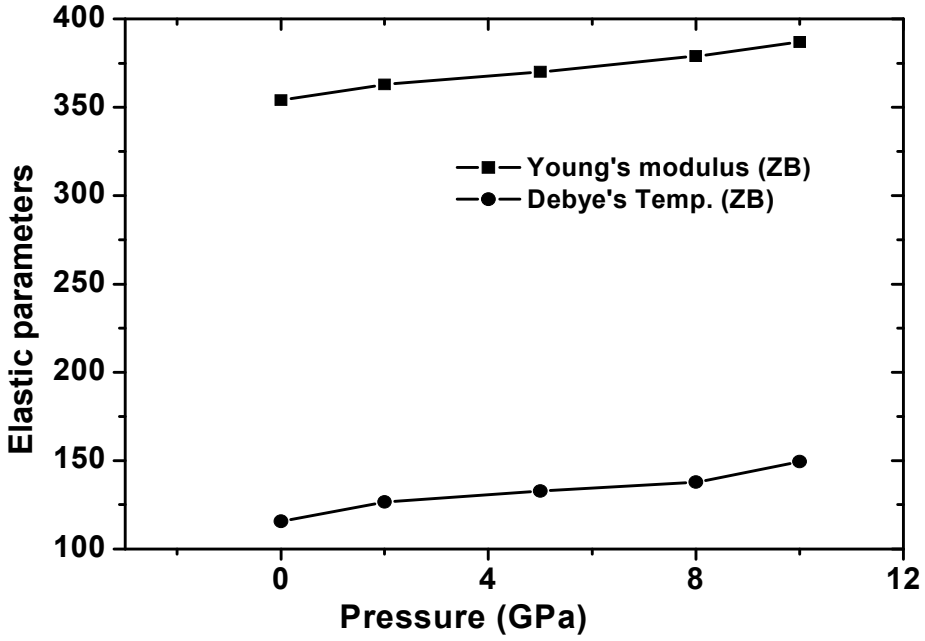

Figure 4.18. Elastic parameters (Young's modulus and Debye's temperature) as a function of pressure of GaAs in ZB phase

The elastic parameters (Young's modulus and Debye's temperature) as a function of pressure of ZnS-ZB are shown in figure 4.18. From the figure it is seen that with increase in pressure the value of Y increases from 115.73 GPa to 149.45 GPa in ZB phase. Thus in ZB phase, GaAs becomes more rigid with increase in pressure. As the pressure increases, the value of Debye's temperature also increases from 354 K to 387 K indicating stiffer lattice and better thermal conductivity of GaAs-ZB phase.

(c) Indium Phosphide (InP)

As calculated above the transition pressure of InP-ZB to InP-RS structure is 9.3 GPa, therefore the elastic constants are calculated for Indium phosphide (InP) ranging from 0 GPa to 8 GPa pressure for ZB and from 10 GPa to 16 GPa pressure for RS (figure 4.19). The obtained results are found to be satisfying the mechanical stability conditions for both the phases. Hence the elastic parameters of InP under

high pressure are calculated for both ZB and RS phases. The elastic parameters (Zener Anisotropy factor (A), Poisson's ratio (υ), kleinmann's parameter (ζ) and B/G ratio) are shown in figure 4.20.

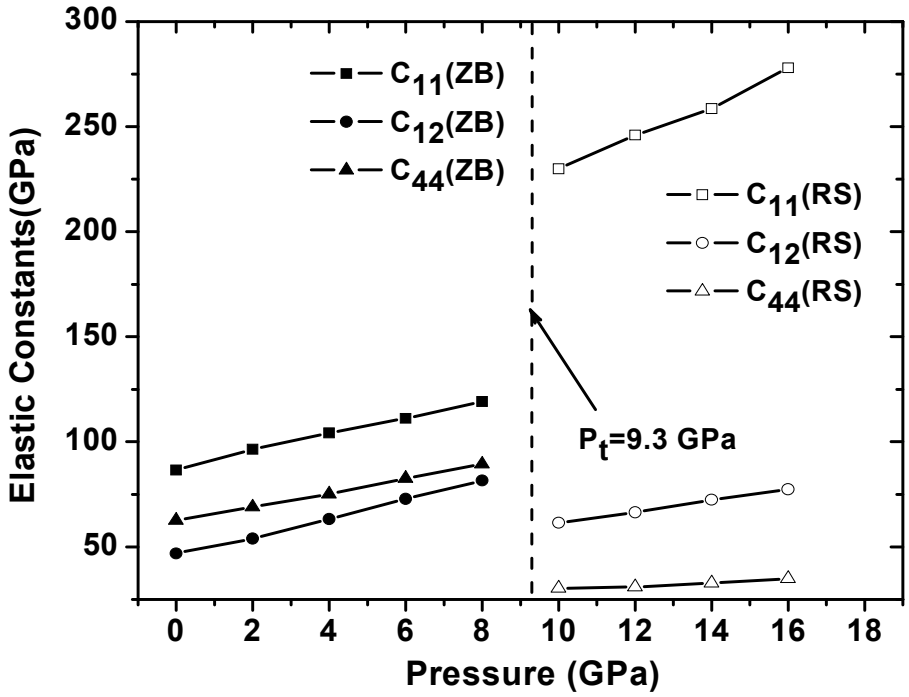

Figure 4.19. Elastic constants (C_{11}, C_{12}, C_{44}) as a function of pressure of InP-ZB and InP-RS phase

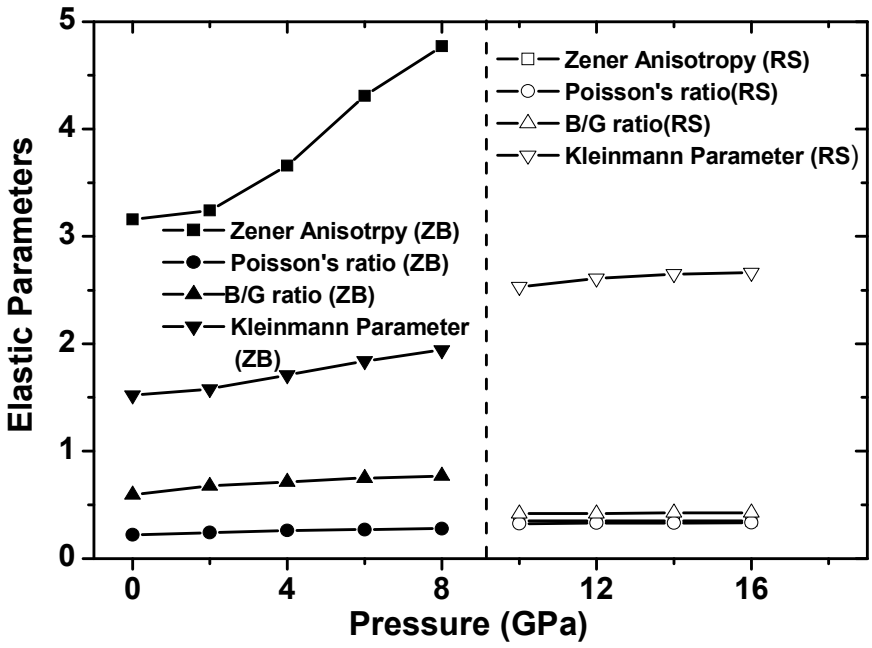

Figure 4.20. Elastic parameters (Zener Anisotropy factor, Poisson's ratio, Kleinmann parameter and B/G ratio) as a function of pressure of InP-ZB phase and InP-RS phase

Zener Anisotropy factor (A) shows a variation from 3.16 to 4.77 and 0.35 to 0.36 with increase in pressure of ZB and RS phase respectively and thus showing the degree of elastic anisotropy. Thus A is stiffest along <111> body diagonal in the ZB phase and after transition to RS phase it becomes stiffest along <100> cube axes. As pressure increases, the value of Poisson's ratio (υ) increases from 0.22 to 0.28 in ZB phase while it increases from 0.32 to 0.33 in RS phase indicating higher ionic contribution in the inter atomic bonding with increasing pressure and also indicates that with increasing pressure inter atomic forces tend to be more central. The Kleinmann parameter (ζ) of t ZB phase is found to increase from 0.59 to 0.77 with pressure while in RS phase it is found to increase from 0.41 to 0.42 showing shrinkage in bond stretching in both ZB and RS phases. As pressure increases the B/G ratio of InP-ZB phase increases from 1.52 to 1.94 while in InP-RS phase it increases from 2.5 to 2.6. Hence we conclude that the brittle nature of the ZB phase

of InP becomes ductile as the pressure increases and retains its ductility even after it undergoes a structural phase transition to RS phase.

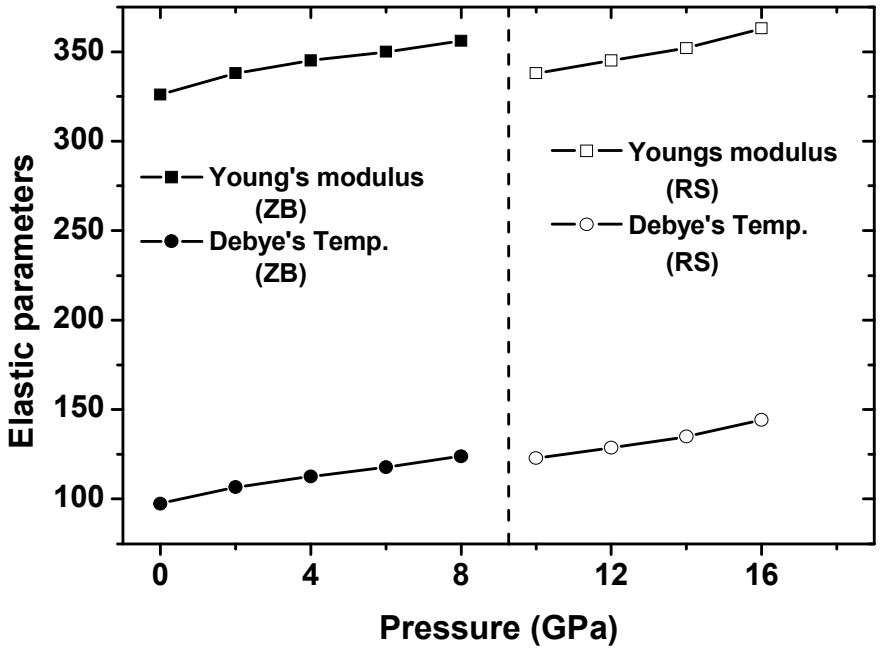

Figure 4.21. Elastic parameters (Young's modulus and Debye's temperature) as a function of pressure of InP in ZB phase and RS phase

It is seen in figure 4.21, with increase in pressure the value of Y increases from 97.48 GPa to 123 GPa in the ZB phase while in the RS phase the value of Y increases from 122.85 GPa to 144.36 GPa. Thus it is interesting to note that InP becomes more rigid with increase in pressure in ZB phase and even after it undergoes a structural transformation to RS phase the rigidity of InP is maintained. The increase in Debye's temperature with increasing pressure in figure 4.21, indicates stiffer lattice and better thermal conductivity under pressure in both the phases.

(d) Indium Arsenide (InAs)

Similarly as in above subsections, the elastic constants have been calculated for 0 GPa to 4 GPa pressure of InAs-ZB and from 5 GPa to 9 GPa pressure of InAs-RS as the structural phase transition of InAs from the zincblende to rocksalt occurs at 4.7 GPa pressure. The calculated elastic constants in figure 4.23 satisfy the mechanical stability conditions and are shown in figure 4.22. In figure 4.23, the elastic parameters (Zener Anisotropy factor (A), Poisson's ratio (υ), Kleinmann's parameter (ζ) and B/G ratio) are given.

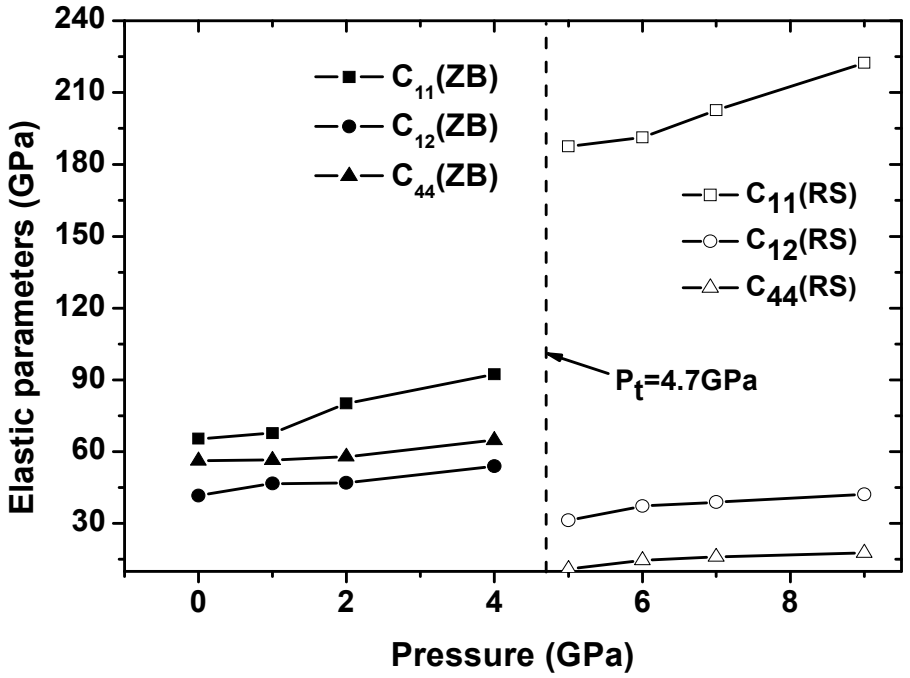

Figure 4.22. Elastic constants (C_{11}, C_{12}, C_{44}) as a function of pressure of InAs-ZB and InAs-RS phase

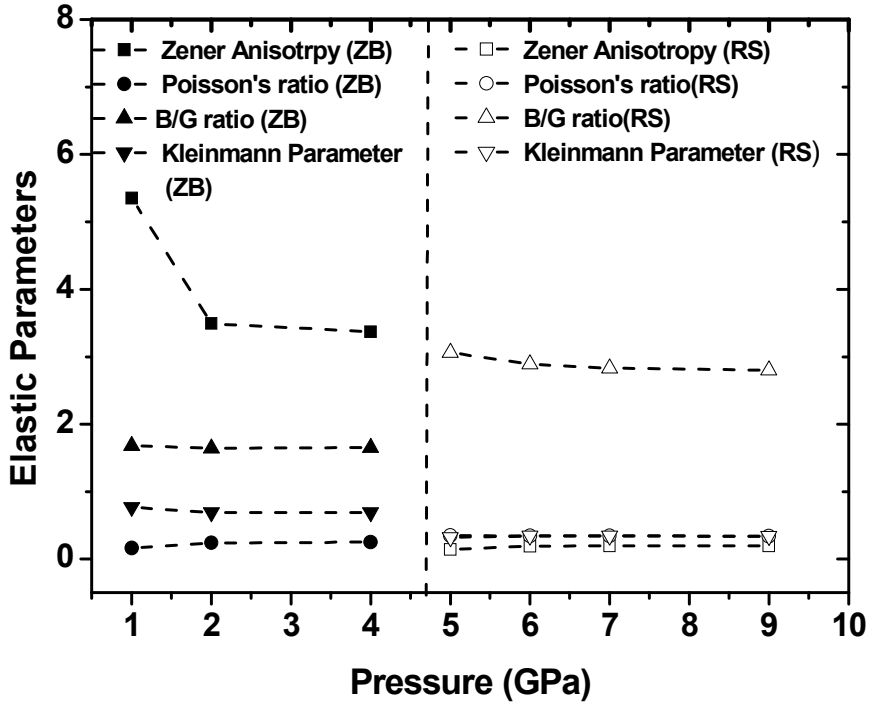

Figure 4.23. Elastic parameters (Zener Anisotropy factor, Poisson's ratio, Kleinmann parameter and B/G ratio) as a function of pressure of InAs in ZB phase and RS phase

It is seen that Zener Anisotropy factor (A) varies from 5.35 to 3.37 in the ZB phase while in the RS phase it is found to increase from 0.18 to 0.2. Thus A is stiffest along <111> body diagonal in the ZB phase and after transition to RS phase it becomes stiffest along <100> cube axes. There is an increase in the value of υ from 0.16 to 0.25 in ZB phase while it remains unchanged around 0.34 in the RS phase indicating dominant nature in the ionic contribution to the inter atomic bonding. The Kleinmann parameter (ζ) of ZB phase is found to vary from 0.77 to 0.69 with pressure while in RS phase it is found to increase from 0.31 to 0.34 showing shrinkage in bond stretching in the ZB phase and shrinkage in bond bending in the RS phase. With increase in pressure, the B/G ratio of InAs-ZB remains around 0.64 while in InAs-RS phase it is greater than 1.75 and then decreases.

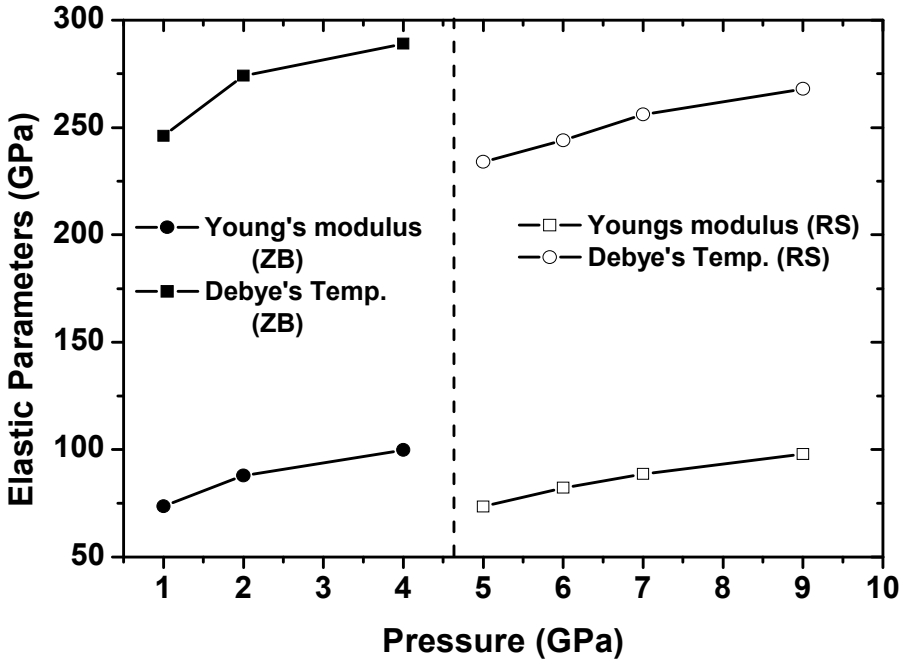

Figure 4.24. Elastic parameters (Young's modulus and Debye's temperature) as a function of pressure of InAs in ZB phase and RS phase

In figure 4.24, Young's modulus (Y) and Debye's temperature (θ_D) as a function of pressure are shown. As the pressure increases, the value of Y increases from 73.62 GPa to 99.72 GPa in the ZB phase while in the RS phase also the value of Y increases from 73.53 GPa to 97.84 GPa. Thus InAs becomes more rigid with increase in pressure in both the ZB and RS. As the pressure increases, the value of Debye's temperature also increases from 246 K to 290 K for the ZB phase and from 243K to 268 K in the RS phase indicating stiffer lattice and better thermal conductivity in both phases.

4.4. ELECTRONIC PROPERTIES

(a) Gallium Phosphide (GaP)

The electronic band structure calculation of GaP-ZB phase and GaP-RS phase at zero pressure (0 GPa) are performed with the methods (a) LDA, (b) GGA and (c)

mBJ-GGA and are shownin figure 4.25 and figure 4.26 respectively. In figure 4.25(a), (b) and (c) it is clearly seen that in all the three calculations within LDA, GGA and mBJ-GGA methods, the valence band maximum occurs at the Γ point while the minimum conduction band occurs at L point confirming an indirect band gap. One interesting point is the shifting of the conduction band towards higher energy and wide opening of the band gaps. The band gap calculated with LDA and GGA methods show a band gap of 1.46eV and 1.49eV respectively while calculation with mBJ-GGA method gives a band gap of 2.33eV which is very close to the experimental values of 2.32eV [101]. The order of the energy band gaps of GaP is LDA < GGA < mBJ-GGA. Thus the implementation of the mBJ-GGA potential resolves the underestimation of the band gaps and provides better results closer to the experimental value. Again in figure 24.6(a), (b) and (c), there is crossing over of the conduction band at the Fermi energy towards the valence band indicating metallic nature of GaP-RS phase. The metallic nature of GaP-RS structure is due to broadening of the band with increase in pressure and overlapping of the filled valence band and conduction band.

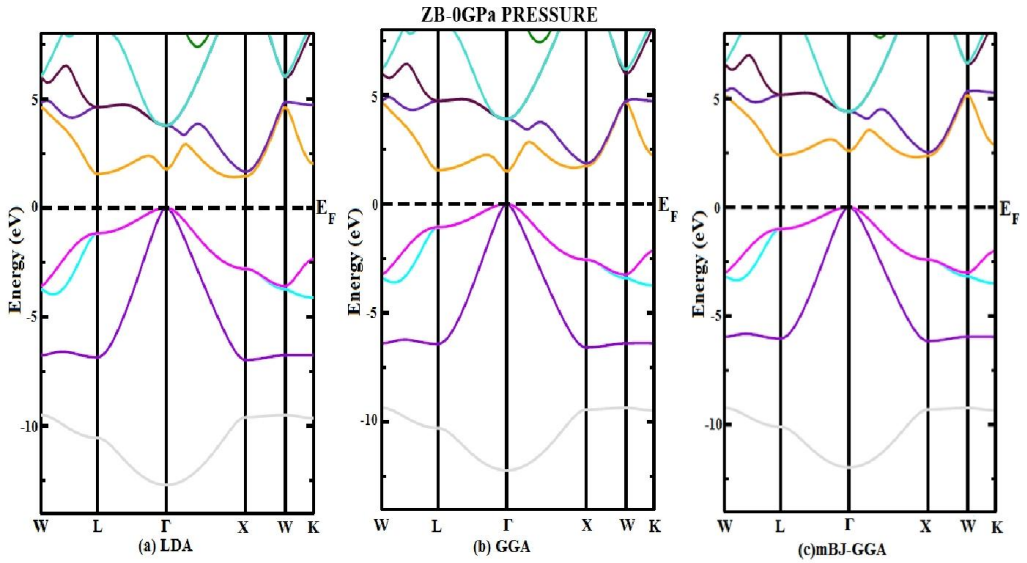

Figure 4.25. Energy band diagram of GaP-ZB phase at 0 GPa pressure within (a) LDA, (b) GGA and (c) mBJ-GGA

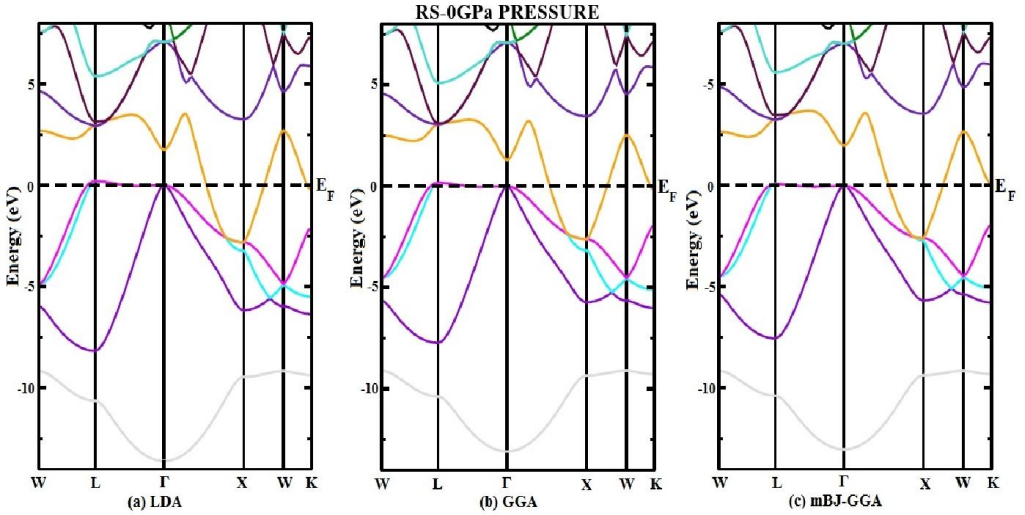

Figure 4.26. Energy band diagram of GaP-RS phase at 0 GPa pressure within (a) LDA, (b) GGA and (c) mBJ-GGA

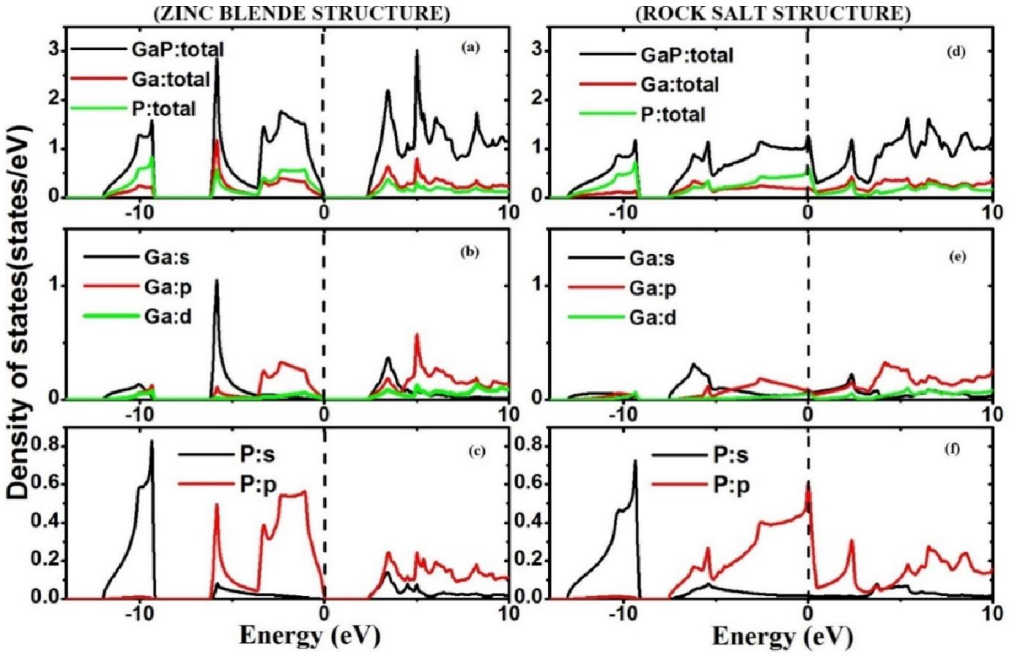

Figure 4.27. Total and Partial DOS of GaAS-ZB and GaAs-RS phase within mBJ-GGA

The nature of the energy band structure of a compound is related to the corresponding density of states. Therefore for better understanding of band gaps the total and partial density of states (DOS) are studied. But as we observed, the

calculations within the mBJ-GGA (as compare to LDA, GGA methods) gives us better results close to experimental value, we have calculated the total DOS and partial DOS with mBJ-GGA only. In figure 4.27, the total and partial DOS of GaP-ZB and GaP-RS are shown. Figure 4.27(a), (b) and (c) clearly show that the lowest band appears in energy band diagram (figure 4.26) is mainly contributed from s-non metal (P atom) orbital with little contribution from the p-metal (Ga atom) orbital and d-metal of (Ga atom) orbital while the valance band is mainly contributed by the s-metal (Ga-atom) orbital along with p-metal (Ga-atom) orbital and s-non metal (P atom) orbital with little contribution from the s-non metal (P-atom) orbital. Further the lowest band is mainly contributed by the s-non metal (P atom) orbital with little contribution from the p-metal (Ga-atom) orbital and d-metal (Ga-atom) orbital while the valance band is mainly contributed by the p-non metal (P-atom) orbital along with s-metal (Ga-atom) orbital and p-metal (Ga-atom) orbital. Other than the band structure at zero pressure, it is interesting to study how the band diagram changes under variation of pressures. In the following, we study the variation of band diagram under induce pressure of GaP-ZB phase and GaP-RS phase separately.

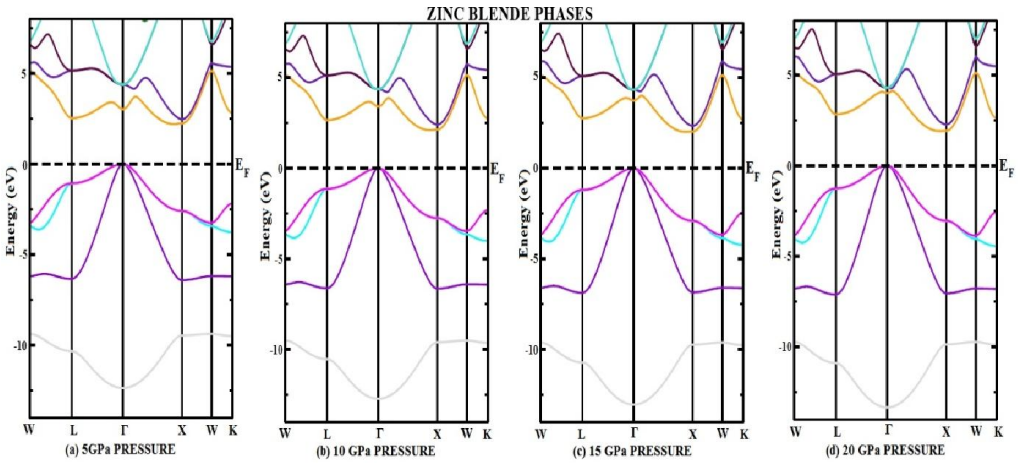

Figure 4.28. Energy band diagram of GaP-ZB phase at (a) 5 GPa pressure (b) 10 GPa pressure (c) 15 GPa pressure and (d) 20 GPa pressure

Figure 4.28 (a),(b),(c) and (d) show the energy band diagram of GaP-ZB at different pressures 5 GPa, 10 GPa, 15 GPa and 20 GPa. In figure 4.28 (a-d), it is observed that as the pressure increases to 5 GPa, 10 GPa 15 GPa and 20 GPa, the gap between the Γ-L increases but if we closely study the energy band diagram we find that the gap between Γ-X decreases towards the Fermi level indicating possibilities of crossing over of the conduction band towards the valance band at higher pressure confirming the metallic nature at higher pressure. The variation in the energy band gap with pressure is also shown in figure 4.29 for clear analysis of changes between Γ-X and Γ-L with pressure.

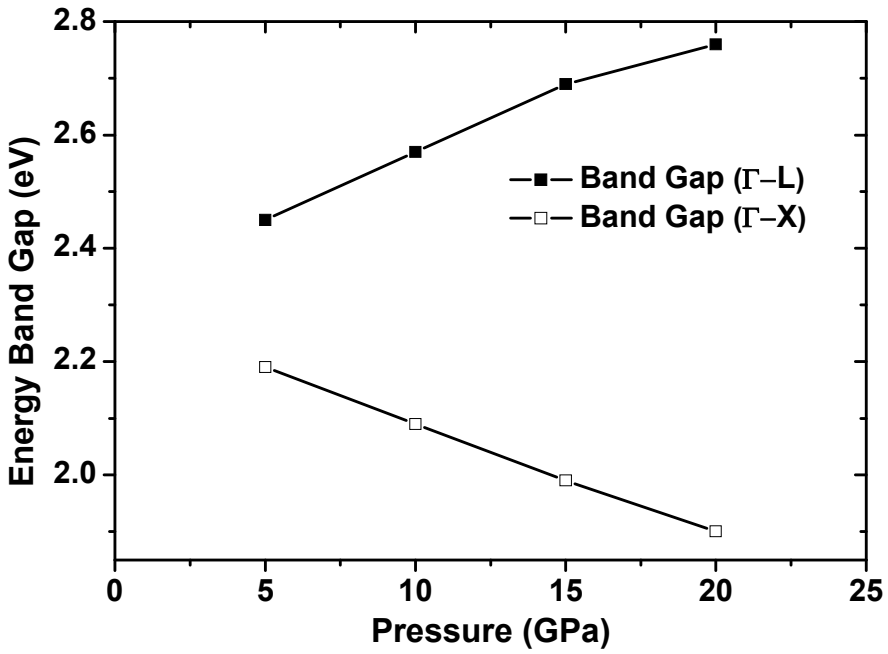

Figure 4.29. Variation of Energy band gaps of GaP-ZB phase with pressure

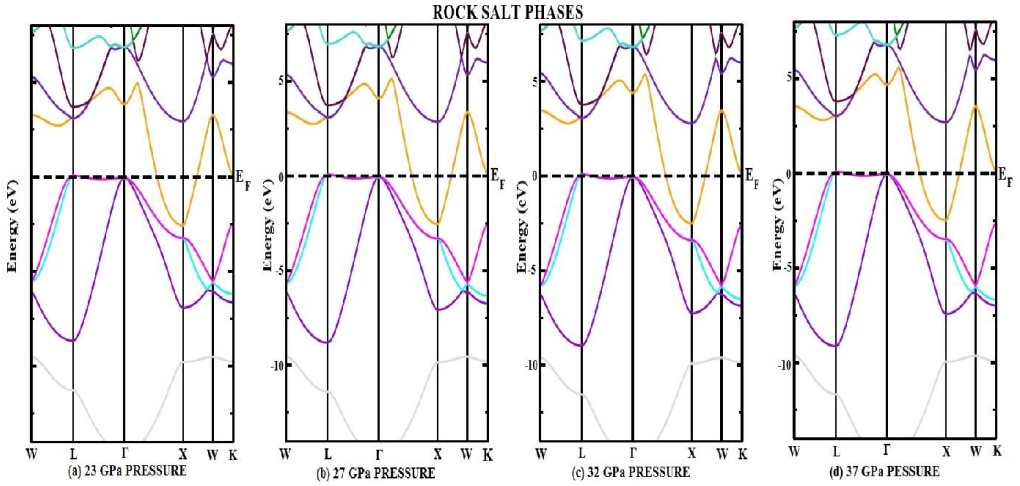

Figure 4.30. Energy band diagram of GaP-RS phase at (a) 23 GPa pressure (b) 27 GPa pressure (c) 32 GPa pressure and (d) 37 GPa pressure

In the similar way, we study the variation of band structure with pressure of GaP-RS phase. Figure 4.30 (a), (b), (c) and (d) show the energy band diagram of GaP-RS phase at 23 GPa, 27 GPa, 32 GPa and 37 GPa pressure respectively. From the figures, it is clearly seen that the metallic nature is retained even at high pressure. Hence we conclude that the energy band gap of GaP-ZB phase is affected by pressure while the energy band gaps of GaP-RS phase is not much affected by pressure.

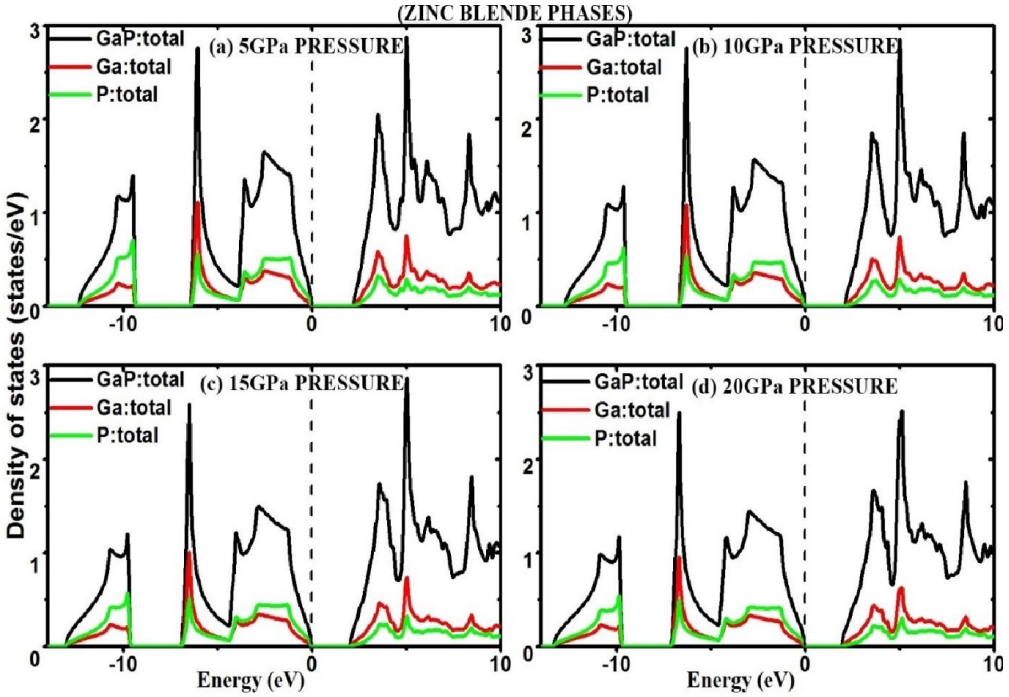

Figure 4.31. Total DOS of GaP-ZB at (a) 23 GPa pressure (b) 27 GPa pressure (c) 32 GPa pressure and (d) 37 GPa pressure

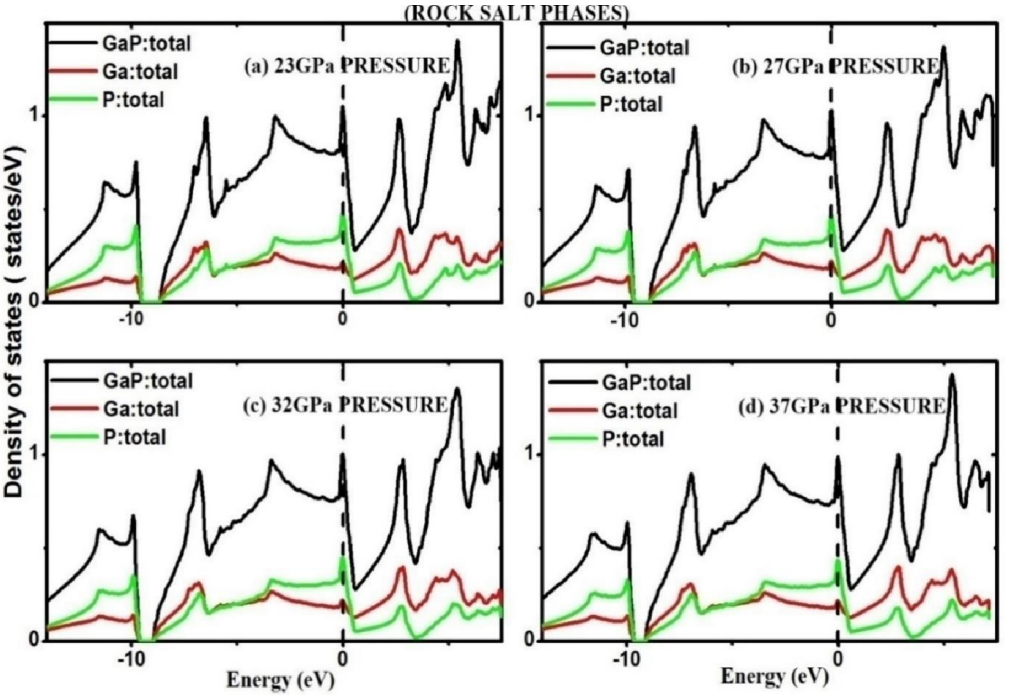

Figure 4.32. Total DOS of GaP-RS at (a) 23 GPa pressure (b) 27 GPa pressure (c) 32 GPa pressure and (d) 37 GPa pressure

To understand the effect of pressure in the band structures, we study the total DOS of GaP-ZB and GaP-RS at different pressure. Figure 4.31 shows the total DOS of GaP-ZB at (a) 5 GPa pressure (b) 10 GPa pressure (c) 15 GPa pressure and (d) 20 GPa pressure. From the DOS figures, we could clearly observe the gap (between Γ-X in band diagram figure 4.30) between the valence band and conduction band around the Fermi line (vertical dotted lines at 0 eV on the X-axis). Further it clearly also shows a slight increase of the wide of gap with increase in pressure.

In figure 4.32, the total DOS of GaP-RS at (a) 23 GPa pressure (b) 27 GPa pressure (c) 32 GPa pressure and (d) 37 GPa pressure are shown. The characteristic feature of metallic nature in the band diagram (figure 4.30), is clearly also reflected in DOS plot. Figure 4.32 shows orbital crossing the Fermi level and hence there is crossover of valence and conduction band. Thus GaP-RS phase retains its metallic nature under induced pressures.

4.4.2. Gallium Arsenide (GaAs)

Following the same methodology of band structure calculation as done for GaP in the previous subsection, Figure 4.33 show the electronic band structure of GaAs-ZB and GaAs-RS at 0 GPa pressure. In figure 4.33 of GaAs-ZB phase, calculations with the three methods: LDA, GGA and mBJ-GGA, show a direct band gap. The band gap calculated with LDA and GGA show a band gap of 0.17eV and 0.45 eV respectively while calculation within mBJ-GGA gives a band gap of 1.3eV which is very close to the experimental values of 1.5eV [101]. In figure 4.34 of GaAs-RS phase, the crossing over of the conduction band at the Fermi energy towards the valance band predicts the metallic nature of GaP-RS phase. The metallic nature of GaAs-RS is due to broadening of the band and overlapping of the filled valance band and conduction band.

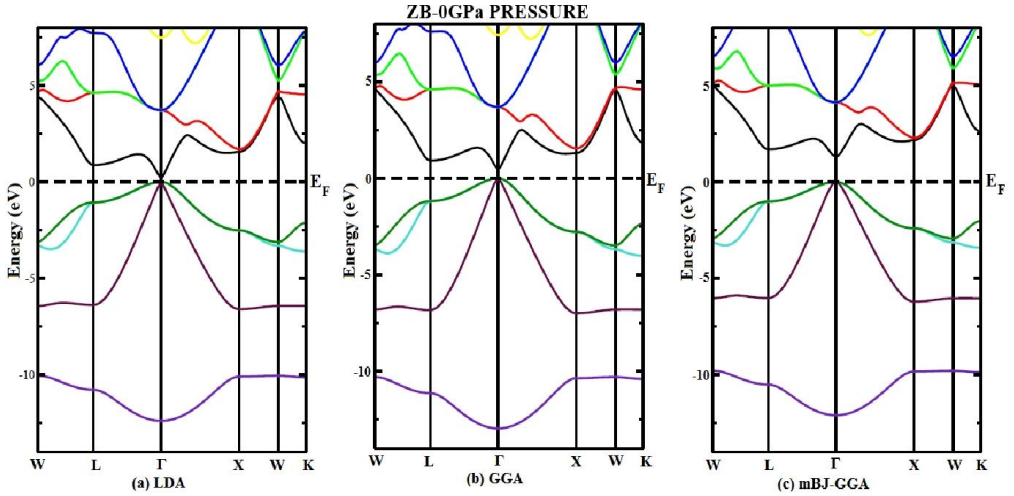

Figure 4.33.Band structure of GaAs-ZB at 0 GPa pressure within (a) LDA, (b) GGA and(c) mBJ-GGA

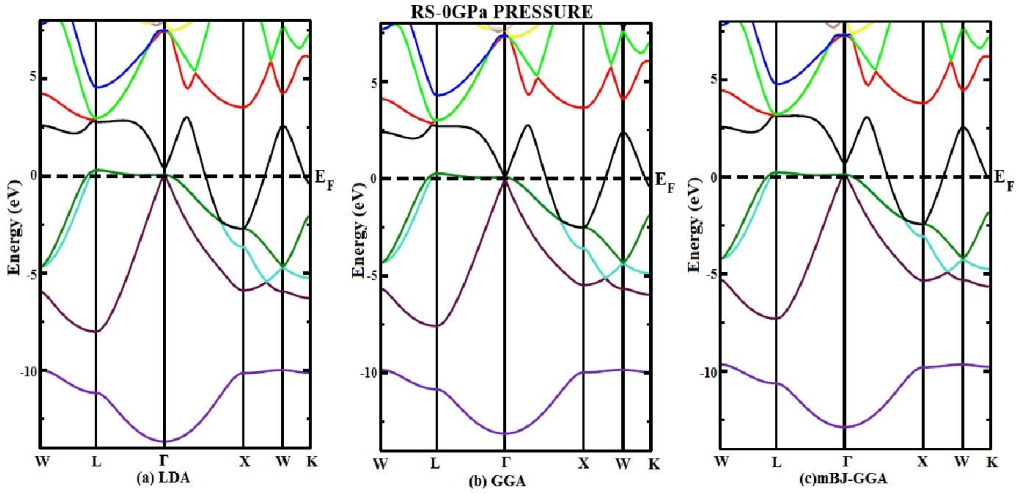

Figure 4.34. Band structure of GaAs-RS at 0 GPa pressure within (a) LDA, (b) GGA and (c) mBJ-GGA

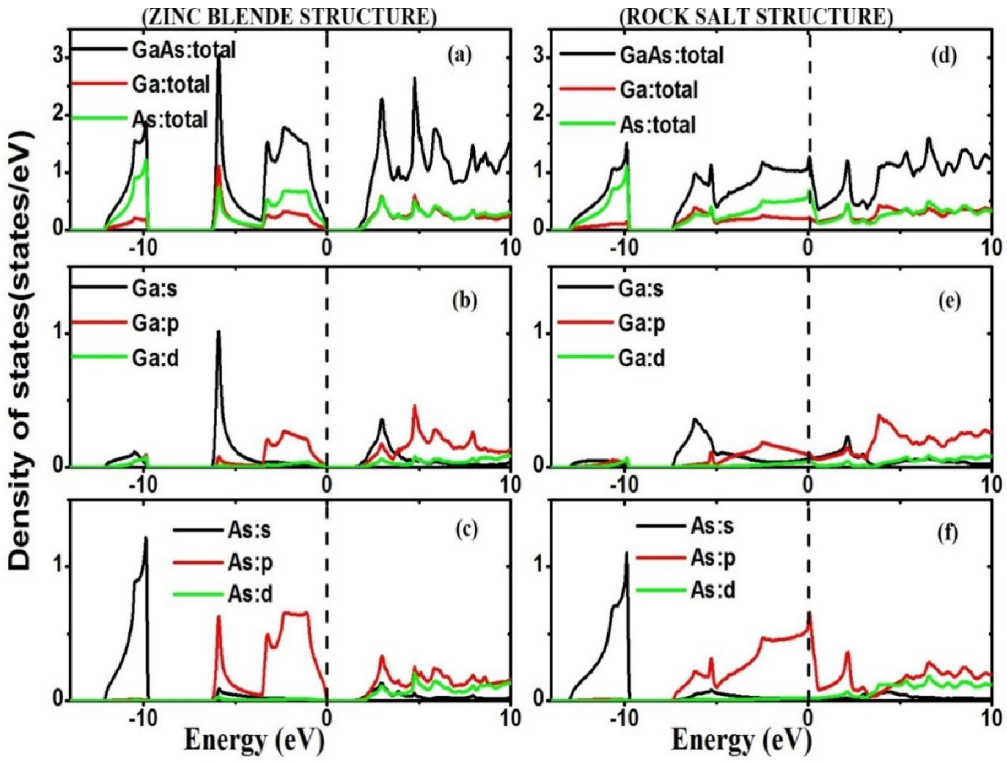

Figure.4.35. Total and Partial DOS of GaAS-ZB and GaAs-RS within mBJ-GGA

As mentioned above, the origin of the energy band structure of a compound is related to the corresponding density of states. In figure 4.35, the total and partial DOS of GaAs-ZB and GaAs-RS are shown. From figure 4.35(a), (b) and (c), for GaAs-ZB, we find that the lowest band is mainly contributed by the s-non metal (As atom) orbital while the valance band is mainly contributed by the s-metal (Ga atom) orbital with little contribution from the p-metal (Ga-atom) orbital. Again from figure 4.35(d),(e) and (f) for GaAs-RS we find that the lowest band is mainly contributed by the s-non metal (As atom) orbital with little contribution from the p-metal (Ga-atom) orbital and d-metal (Ga-atom) orbital while the valance band is mainly contributed by the p-non metal (As-atom) orbital and s-metal (Ga-atom) orbital with little contribution from the p-metal (Ga-atom) and d-metal (Ga-atom) orbital.

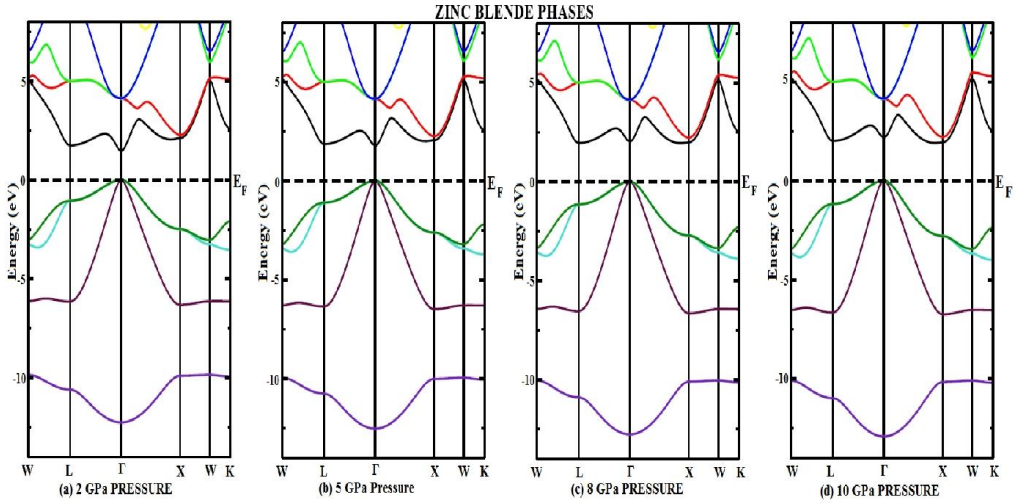

Figure 4.36. Energy band diagram of ZB phase of GaAs at (a) 2 GPa pressure (b) 5 GPa pressure (c) 8 GPa pressure and (d) 10 GPa pressure

Variation of band diagrams at various pressures of GaP-ZB structure are shown in figure 4.36(a),(b),(c) and (d). As the pressure increases to 2GPa, 5GPa, 8GPa and 10 GPa, the gap between the Γ- Γ point increases but if we closely study the energy band diagram we find that there is an increases in the gap between Γ-L point while the gap between Γ-X decreases. It predicts the possibility of crossing over Fermi level at higher pressure and phase transformation may take place to RS structure. The variation in the energy band gap with pressure for GaAs-ZB is also shown in figure 4.37 for clear analysis of the changes in the gap between Γ- Γ point, Γ-X point and Γ-L point.

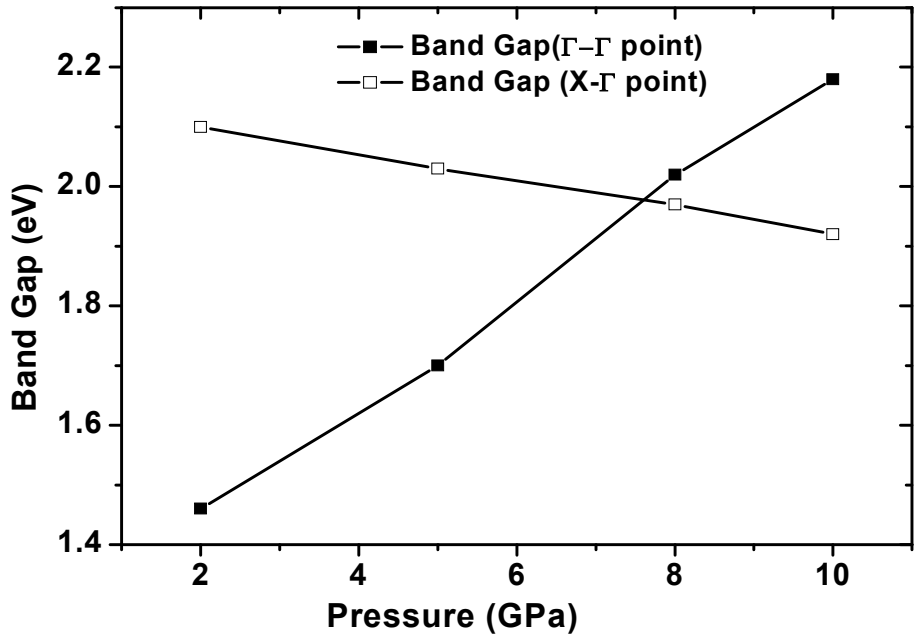

Figure 4.37. Variation of Energy band gaps of GaAs-ZB phase with pressure

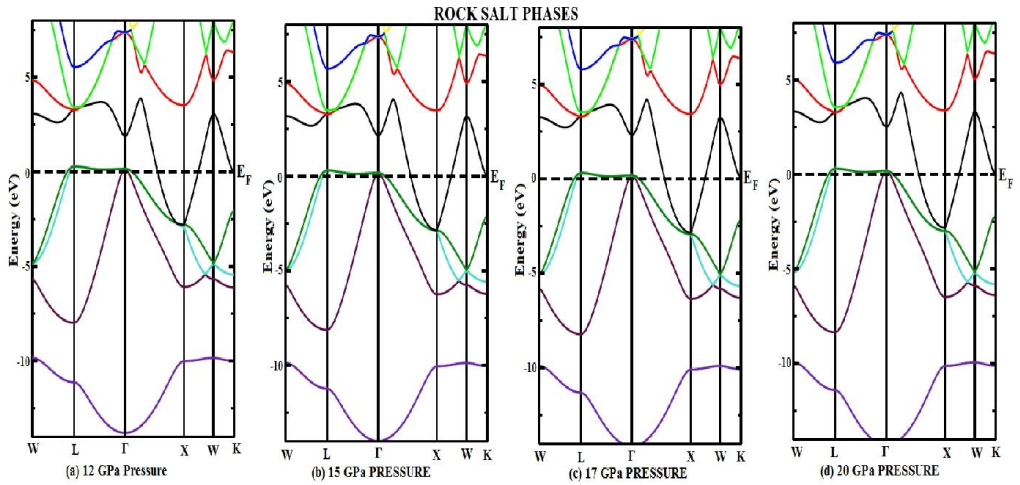

Figure 4.38. Energy band diagram GaAs-RS at (a) 12 GPa pressure (b) 15 GPa pressure (c) 17 GPa pressure and (d) 20 GPa pressure

For GaAs-RS phase, the energy band diagrams of GaAs-RS phase at different pressures are given in figure 4.38(a), (b), (c) and (d). From the figures we find that the metallic nature is retained even at high pressure without much variation.

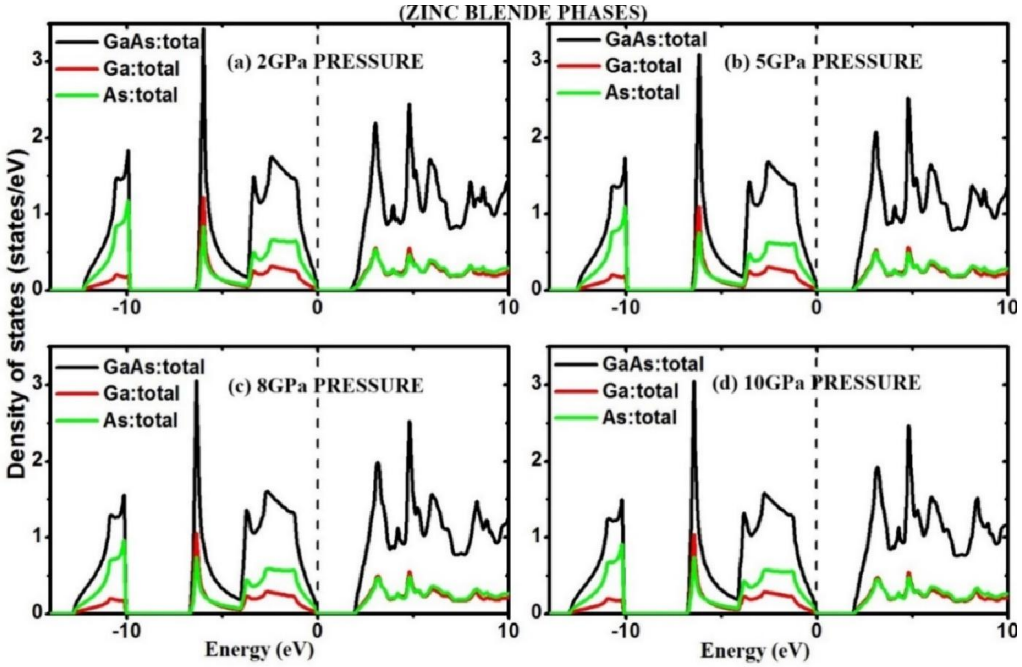

Figure 4.39. Total DOS of GaAs-ZB at (a) 2 GPa pressure (b) 5 GPa pressure (c) 8 GPa pressure and (d) 10 GPa pressure.

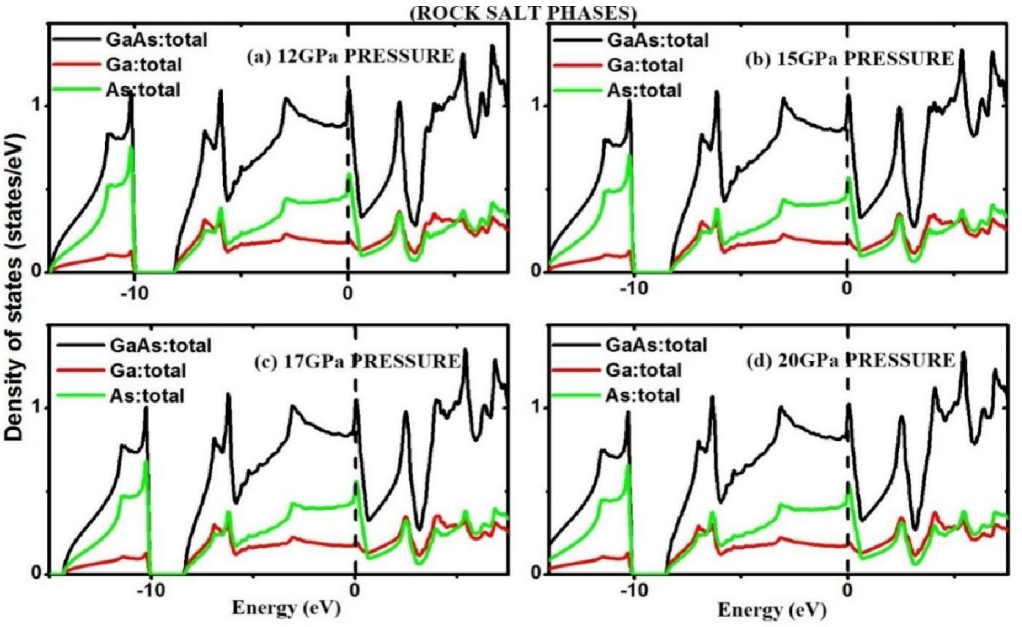

Figure 4.40. Total DOS of GaAs-RS at (a) 12 GPa pressure (b) 15 GPa pressure (c) 17 GPa pressure and (d) 20 GPa pressure.

To further understand the effect of pressure in the band structures, we study the total DOS of GaAs-ZB and GaAs-RS at different pressures. Figure 4.39 shows total DOS of GAaS-ZB at (a) 2 GPa (b) 5 GPa (c) 8 GPa and (d) 10 GPa pressure. In the DOS plot, it is clearly seen the lowest band, valence band and conduction band. The wide of the band between valence band and conduction band give the band gaps under the induced pressure. We also observe a mere variation of this gap under different pressures. This DOS plots support the real understanding of band structure as discussed above (figure 4.36). In figure 4.40, the total DOS of GaAs-RS at (a) 12GPa pressure (b) 15 GPa pressure (c) 17 GPa pressure and (d) 20 GPa pressure are given. In DOS plots, around the Fermi line, crossing over of valence band towards conduction band is clearly observed. Thus the DOS plots confirm the metallic nature as observed in the band diagram (figure 4.38).

4.4.3. Indium Phosphide (InP)

Figure 4.41 and 4.42 show the energy band structure of InP-ZB and InP-RS at zero pressure calculated with (a) LDA, (b) GGA and (c) mBJ-GGA methods. In short, from the band diagrams it concludes that InP-ZB is a direct band gap semiconductor and InP-RS shows metallic nature. As discussed above, the band gap of InP-ZB as obtained with mBJ-GGA is of 1.31eV which is very close to the experimental value of 1.27eV [101].

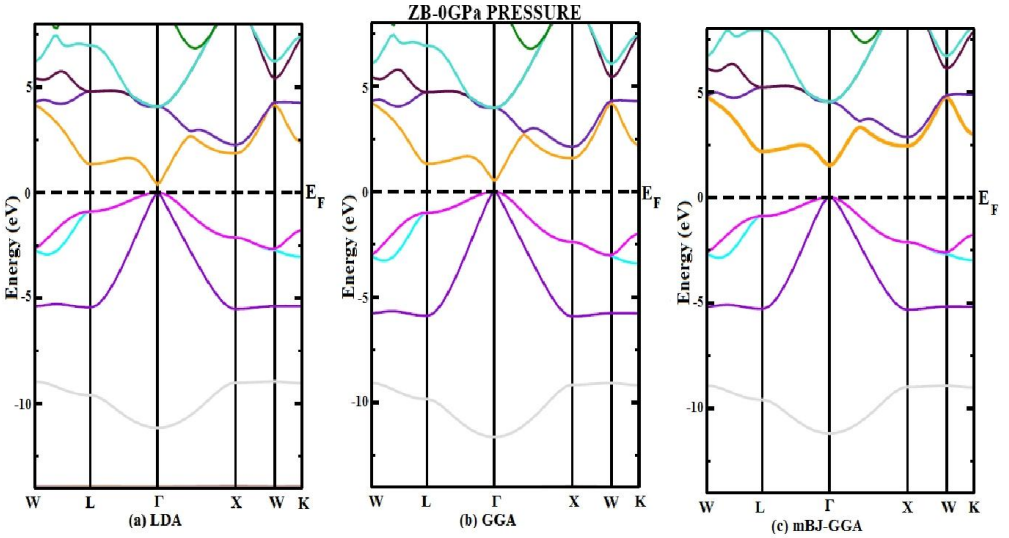

Figure 4.41. Band structure of InP-ZB at 0 GPa pressure within (a) LDA, (b) GGA and (c) mBJ-GGA

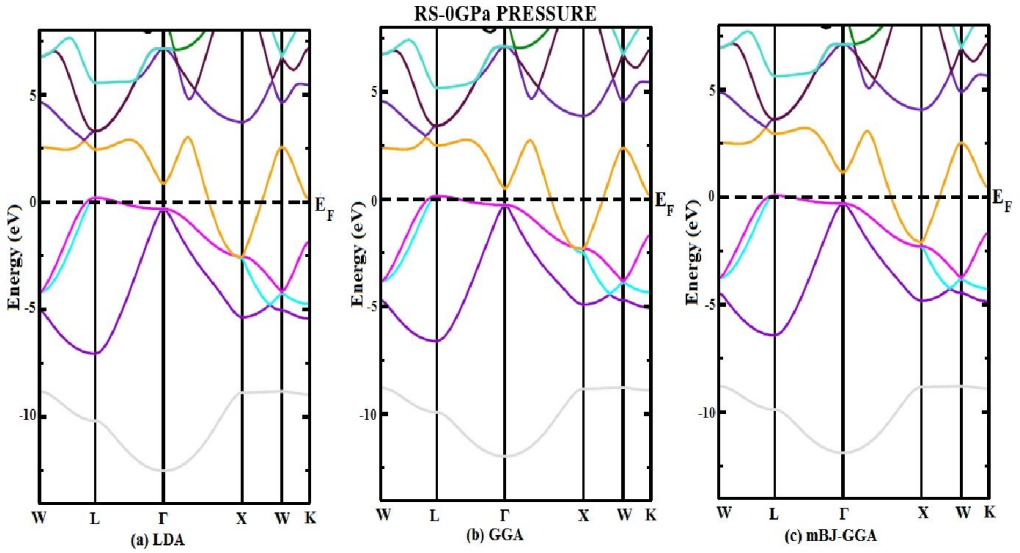

Figure 4.42. Band structure of InP-RS at 0 GPa pressure within (a) LDA, (b) GGA and (c) mBJ-GGA

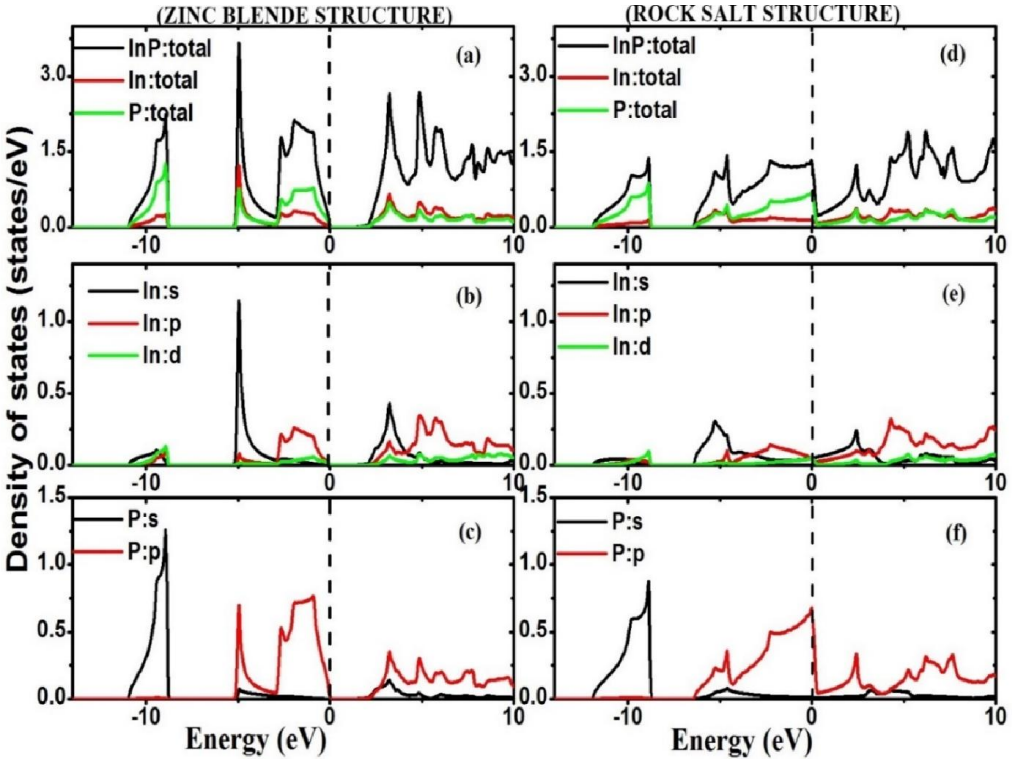

Figure 4.43 Total and Partial DOS of InP-ZB and InP-RS within mBJ-GGA

In figure 4.43 the total and partial DOS of InP-ZB and InP-RS are shown. From figure 4.43(a), (b) and (c) of InP-ZB we observe that the lowest band is mainly contributed by the s-non metal (P atom) orbital with little contribution from the s-metal (In atom) orbital, p-metal (In atom) orbital and d-metal (In atom) orbital and while the valance band is mainly contributed by the s-metal (In atom) orbital with significant contribution from p-metal (In atom) orbital, p-non metal (P atom) and small contribution from p-metal (In atom) orbital and d-metal (In atom) orbital. Again from figure 4.43(d), (e) and (f) for InP-RS we observe that the lowest band is mainly contributed by the s-non metal (P atom) orbital with little contribution from the d-metal (In atom) orbital and s-metal (In atom) orbital while the valance band is mainly contributed by the p-non metal (P atom) orbital along with s-metal (In atom) orbital and s-non metal (P atom) orbital with little contribution from the p-metal (In atom) orbital.

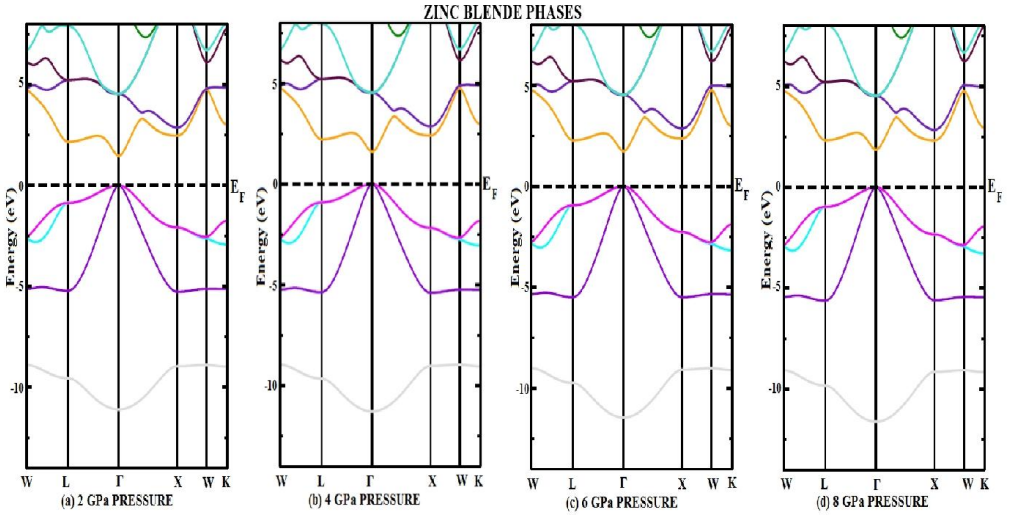

Figure 4.44. Energy band diagram InP-ZB at (a) 2 GPa pressure (b) 4 GPa pressure (c) 6 GPa pressure and (d) 8 GPa pressure

In figure 4.44(a), (b), (c) and (d), the energy band diagrams of InP-ZB phase at different pressures are given. One interesting thing, we see from the band structure diagrams in figure 4.44 is that as the pressure increases to 2 GPa, 4 GPa, 6 GPa and 8 GPa, the gap between the Γ- Γ point increases but if we closely study the energy band diagram we find that the gap at the Γ-L point increases while the gap at the Γ-X point decreases indicating possibility of crossing over at higher pressure. The variation of gap at the Γ- Γ, Γ-L and Γ- X point of InP-ZB with increase in pressure is given in figure 45 for clear analysis.

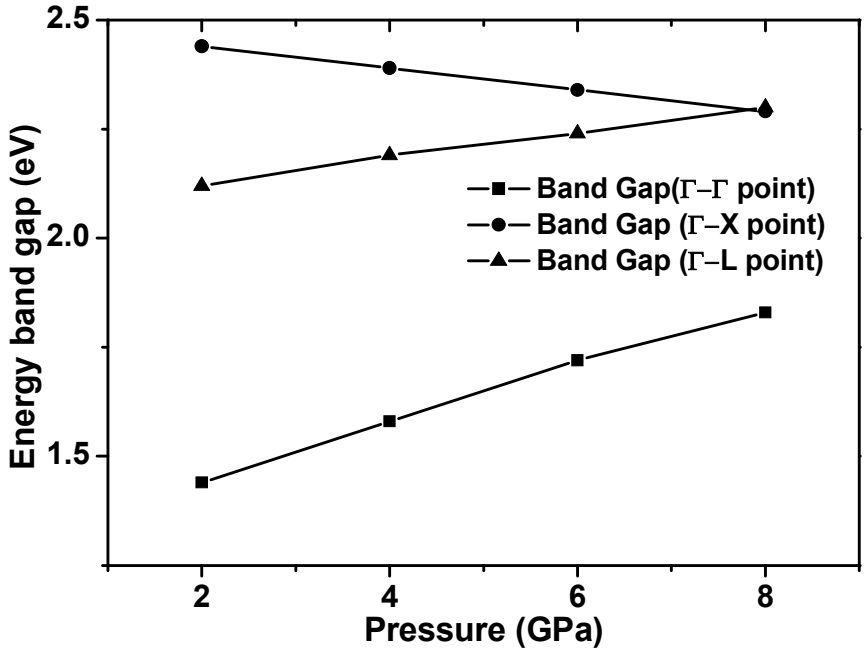

Figure 4.45. Variation of Energy band gaps of InP-ZB phase with pressure

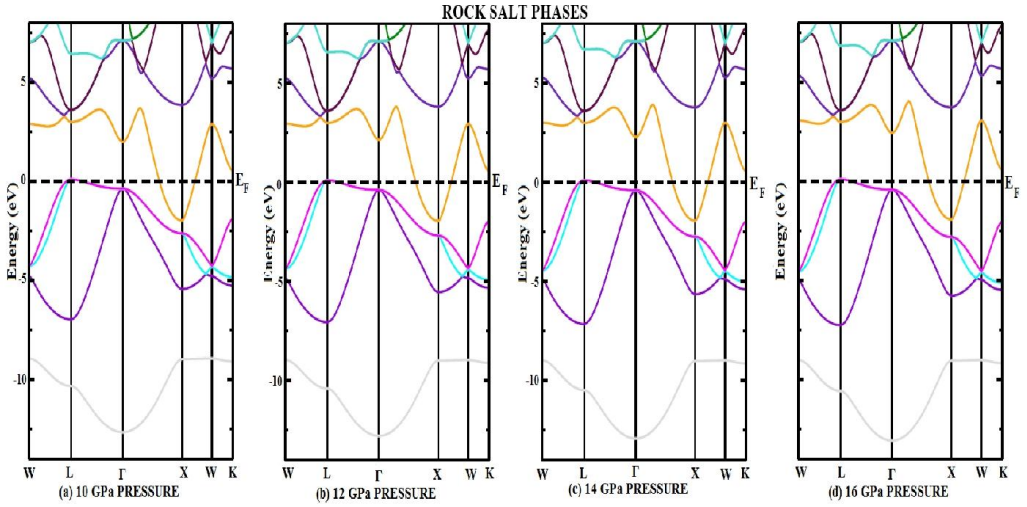

Figure 4.46. Energy band diagram InP-RS in (a) 10 GPa pressure (b) 12 GPa pressure (c) 14 GPa pressure and (d) 16 GPa pressure

In figure 4.46(a), (b), (c) and (d) the energy band diagram of InP-RS phase at different pressures are given. From the figures, we can see that the metallic nature is retained even at high pressure without much variation. Hence we conclude that

the energy band gap of InP-ZB phase is affected by pressure while the energy band gaps of InP-RS phase is not much affected by pressure.

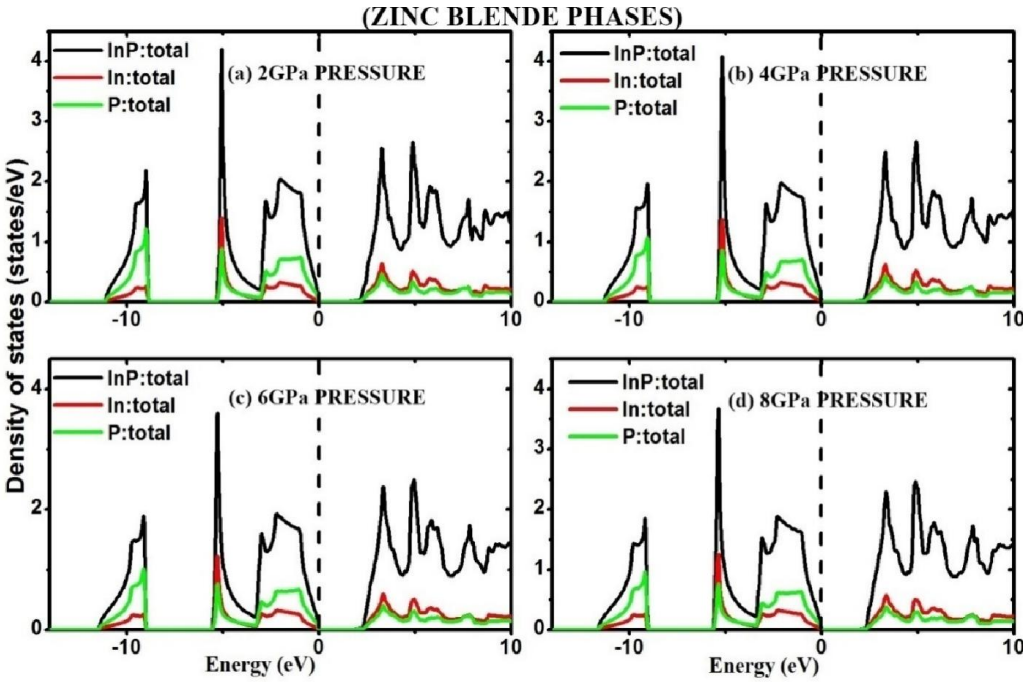

Figure 4.47. Total DOS of InP-ZB at (a) 2 GPa pressure (b) 4 GPa pressure (c) 6 GPa pressure and (d) 8 GPa pressure

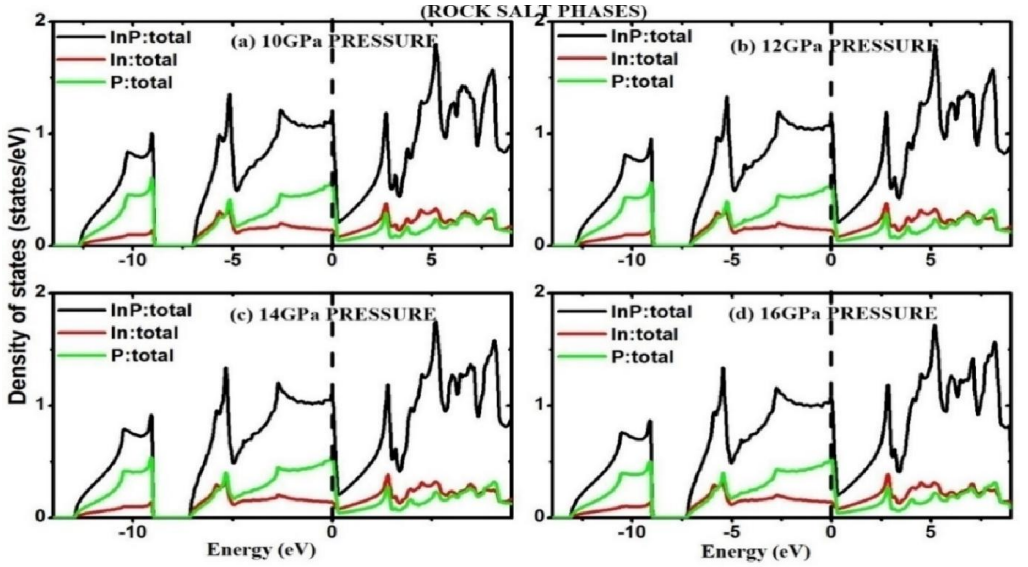

Figure 4.48. Total DOS of InP-RS at (a) 10 GPa pressure (b) 12 GPa pressure (c) 14 GPa pressure and (d) 16 GPa pressure

To further understand the effect of pressure in the band structures we also study the total DOS of InP-ZB and InP-RS at different pressures. In figure 4.47 the total DOS of InP-ZB at (a) 2 GPa pressure (b) 4 GPa pressure (c) 6 GPa pressure and (d) 8 GPa pressure are shown. From the figures, the increase of band gap under induced pressure (as observed in band diagrams in figure 4.44a-d)) is clearly observed in the DOS plots as separation of valence band and conduction band near Fermi line marked on the X-axis. Further, DOS plots of InP-RS as given in figure 4.48 at (a) 10 GPa (b) 12 GPa (c) 14 GPa and (d) 16 GPa pressure show crossing over of valence and conduction band towards Fermi line confirming the metallic nature as concluded before in the band diagrams of figure 4.46.

4.4.4. Indium Arsenide (InAs)

In the above, we have discussed electronic structure of Group III-Vcompound semiconductors in detailed with interpretation. Generally, we observed common characteristics of direct band gap in zincblende structure and metallic nature in rocksalt structure. In short, we have discussed here the electronic structure of InAs. The band structure of InAs-ZB and InAs-RS at zero pressure are shown in figure 4.49 and figure 4.50 respectively. As seen in Figure 4.49 (c) of InAs-ZB with mBJ-GGA, we see a direct band gap of 0.35 eV which is in good agreement to the experimental value of 0.36eV [101] in comparison to LDA, GGA methods. Also figure 4.50 (a-c) of InAs-RS shows metallic nature as indicated due to crossing over of valence and conduction band.

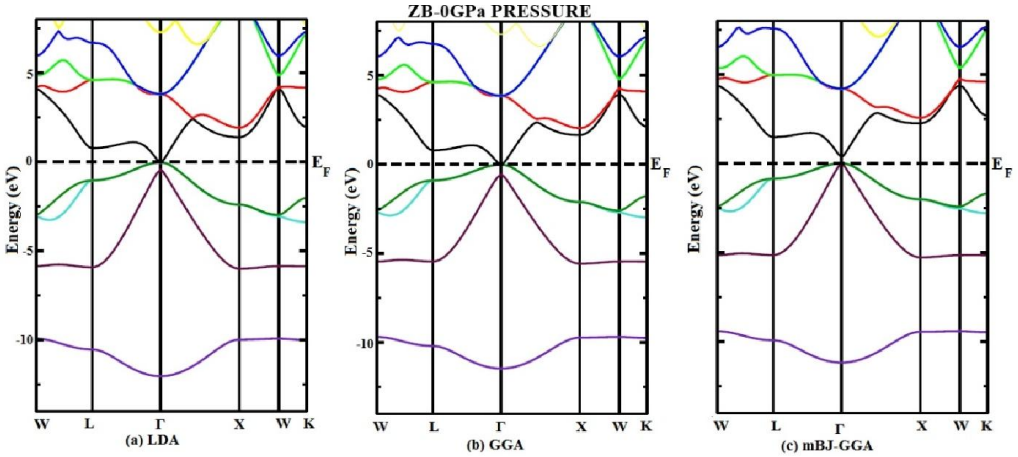

Figure 4.49. Band structure of InAs-ZB at 0 GPa pressure within (a) LDA, (b) GGA and (c) mBJ-GGA

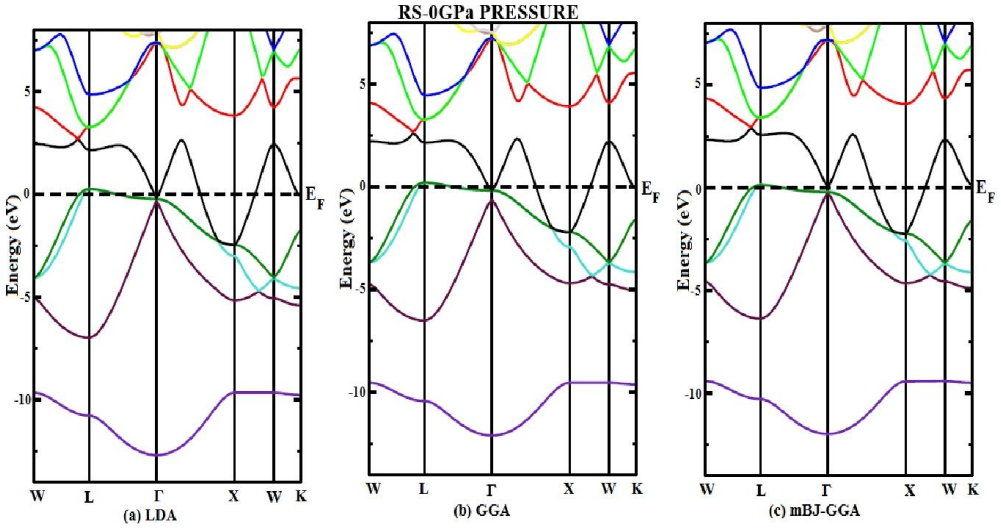

Figure 4.50. Band structures of InAs-RS at 0 GPa pressure within (a) LDA, (b) GGA and (c) mBJ-GGA

In figure 4.51, the total and partial DOS of InAs-ZB and InAs-RS are shown. From figure 4.51(a, b, c), of InAs-ZB, we find that the lowest band is mainly contributed by the As-s state and valance band is contributed by the In-s state with significant contribution from the As-p state and In-p state with little contribution from In-d state. A strong hybridisation is found to occur between the In and As atoms. Again figure 4.51(d, e, f) of InAs-RS, the lowest band is mainly dominated by the As-s state and the valance band is dominated by As-p orbital and In-p orbital.

The band structures of InAs-ZB at 1 GPa, 2 GPa, 3 GPa and 4 GPa pressure are shown in figure 4.52(a, b, c, d). If we closely study the energy band diagrams, it can be observed that the gap at the Γ-L point increases while the gap at the Γ-X point decreases indicating possibility of crossing over at higher pressure. The variation of gap at the Γ- Γ point, Γ-L point and Γ- X point with increase in pressure is given in figure 4.53 for further clear analysis.

In figure 4.54(a, b, c, d) show the energy band diagram of InAs-RS phase at (a) 5 GPa (b) 6 GPa (c) 7 GPa and (d) 9 GPa pressure. Figures show the metallic nature is retained even at high pressure without much variation.

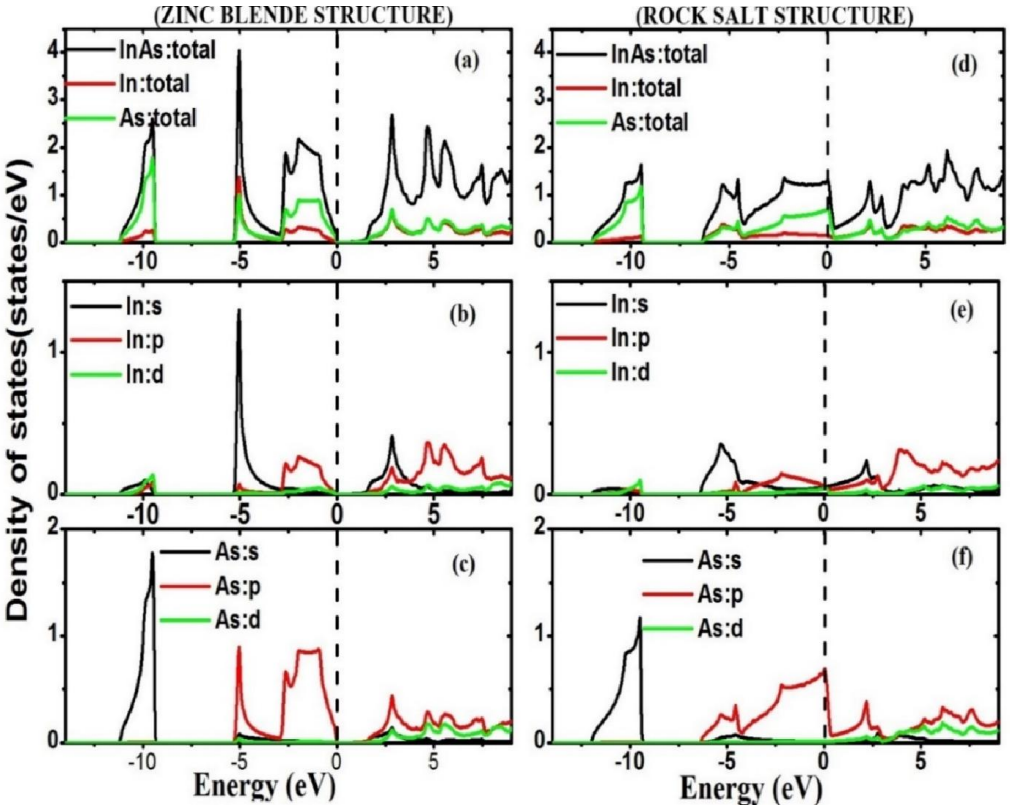

Figure 4.51. Total and Partial DOS of InAs-ZB and InAs-RS within mBJ-GGA

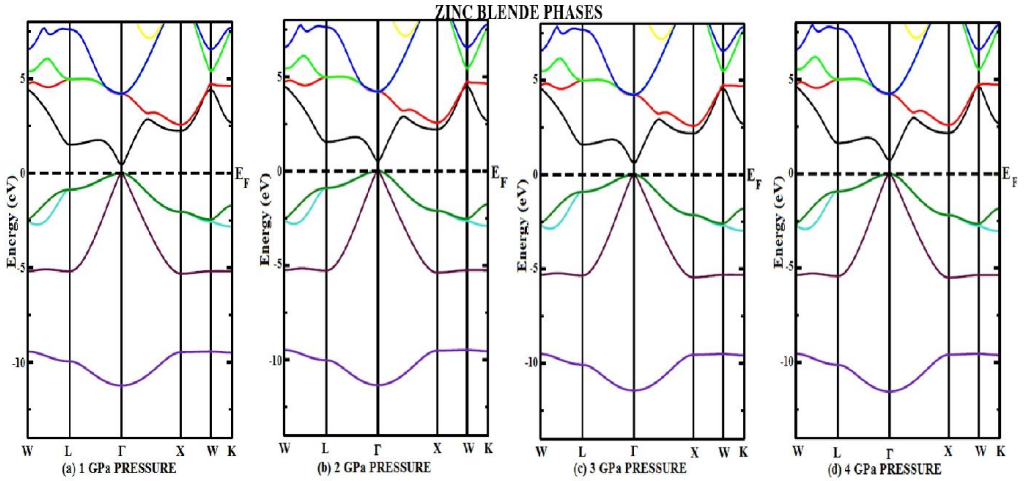

Figure 4.52. Energy band diagram InAs-ZB in (a) 1 GPa pressure (b) 2 GPa pressure (c) 3 GPa pressure and (d) 4 GPa pressure

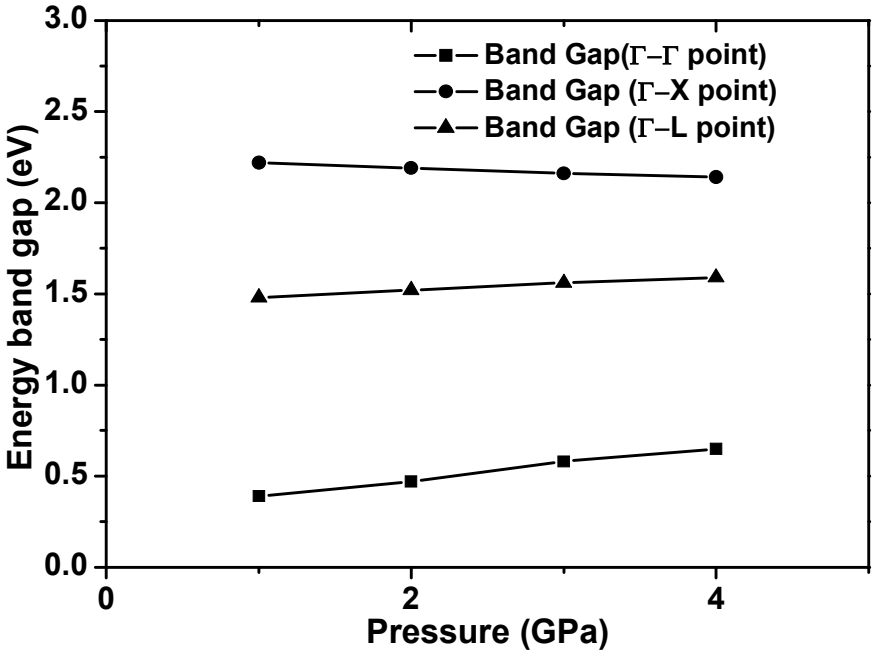

Figure 4.53. Variation of Energy band gaps of InAs-ZB phase with pressure

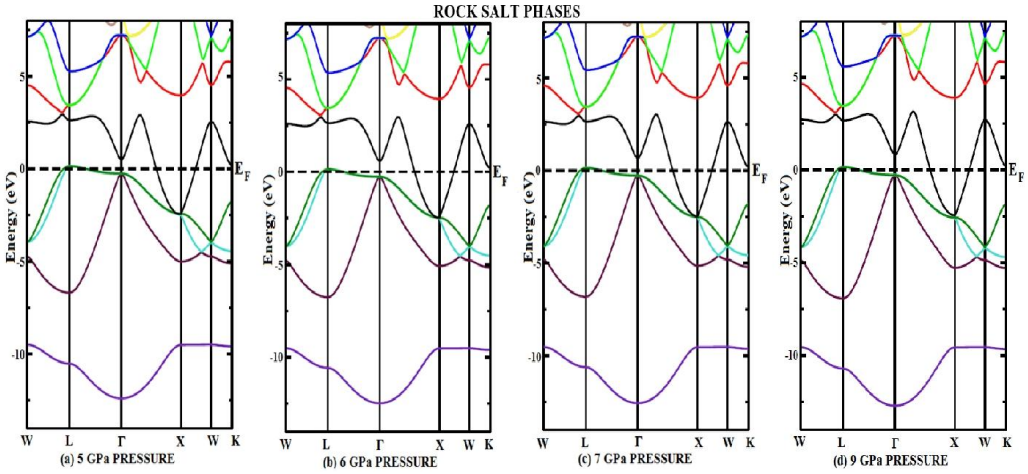

Figure 4.54. Energy band diagram InAs-RS at (a) 5 GPa pressure (b) 6 GPa pressure (c) 7 GPa pressure and (d) 9 GPa pressure

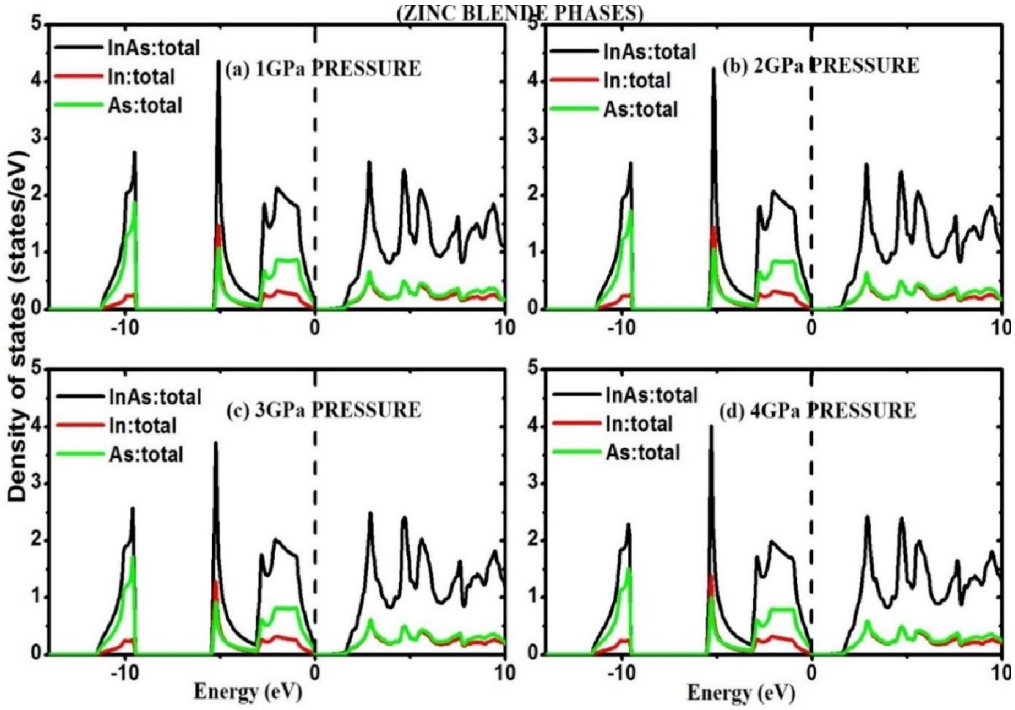

Figure 4.55. Total DOS of InAs-ZB at (a) 1 GPa pressure (b) 2 GPa pressure (c) 3 GPa pressure and (d) 4 GPa pressure

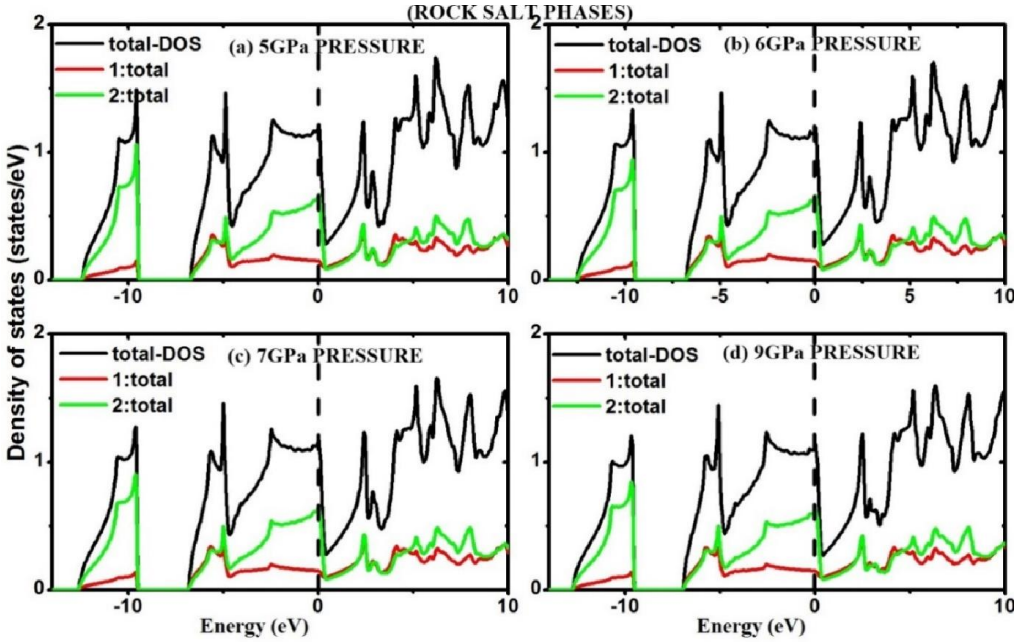

Figure 4.56. Total DOS of InAs-RS at (a) 5 GPa pressure (b) 6 GPa pressure (c) 7 GPa pressure and (d) 9 GPa pressure

In figure 4.55 show the total DOS of InAs-ZB at (a) 1 GPa pressure (b) 2 GPa pressure (c) 3 GPa pressure and (d) 4 GPa pressure. As concluded in the above discussion, the increase of band gap (of InAs-ZB) with increase of pressure is clearly confirmed as the wide of gap between valence band and conduction band around Fermi line in the DOS plots at different pressures (figure 4.55). Figure 4.56(a-e) shows the DOS plots of InAs-RS at 5 GPa 6 GPa, 7 GPa, 9 GPa pressure. Also, the metallic nature of InAs-RS as oberved in the band diagrams (in figure 4.54) is clearly confirmed in the DOS plots (figure 4.55) as crossing over of valence and conduction band around Fermi line.

4.5. CONCLUSION

The structural properties of group III-V compound semiconductors such as GaP, GaAs, InP and InAs in both zincblende (ZB) and rocksalt (RS) are studied and found to be in good agreement with the experimental and theoretical results. The structural phase transformation from the ZB to RS structure under induced pressure

has also been performed for these compounds and the volume collapse at the transition pressure determined.

i. The structural parameters of GaP, GaAs, InP and InAs are calculated with both the LDA and GGA methods as given in table 4.1, table 4.4, table 4.7 and table 4.10.

ii. The structural phase transition from the ZB to RS of

- GaP are found to occur at 21.9 GPa pressure with a volume collapse of 14.11% at the transition pressure
- GaAs at 10.7 GPa pressure with a volume collapse of 14.2% at the transition pressure,
- InP at 9.3 GPa pressure with a volume collapse of 16.45% at the transition pressure,and
- InAs at 4.7 GPa pressure for InAs with a volume collapse of 17.2% at the transition pressure,

iii. The elastic constants (C_{11}, C_{12} and C_{44}) of both the ZB nad RS phases are found to satisfy the mechanical stability conditions and undergo a linear variation with increase in pressure. The elastic parameters (Zener Anisotropy factor (A), Poisson's ratio (υ), Kleinmann parameter (ζ), B/G ratio, Young's modulus (Y) and Deby's temperature (θ_D)) are also calculated.

iv. The energy band gaps of the ZB and RS structures at zero pressure of GaP, GaAs, InP and InAs are calculated using the LDA, GGA and mBJ-GGA potentials. The implementation of the mBJ-GGA potential in the energy band gap calculation resolves the underestimation of the band gaps with

LDA, GGA and provides better results closer to the experimental value. In the energy band diagram it is observed that

- GaP is an indirect band gap semiconductor and energy band gap calculated with mBJ-GGA method is of 2.33eV.
- GaAs, is a direct band gap semiconductor within mBJ-GGA method with a gap of 1.3eV.
- InP is a also direct band gap semiconductor of 1.31eV within mBJ-GGA method.
- Lastly in case of InAs, calculation of the energy band structure within the mBJ-GGA method shows a direct band gap of 0.35 eV

v. The corresponding total and partial DOS for the ZB and RS structures at zero pressure are studied within the mBJ-GGA method only. The energy band structures as well as the DOS for both ZB and RS structures are studied at different pressures. For all the four compounds (GaP, GaAs, InP and InAs) in ZB phase, as the pressure increases the energy band gap between the Γ-L increases but the gap between Γ-X are found to decrease towards the fermi level indicating possibilities of crossing over of the conduction band towards the valance band and confirming the metallic nature of the RS phases of these compounds at higher pressure. But in the RS phases of these compounds (GaP, GaAs, InP and InAs) the metallic nature is retained even at high pressure without much variation. Hence we conclude that the energy band gap of ZB phases of GaP, GaAs, InP and InAs are affected by pressure while the energy band gaps of the RS phases are not much affected by pressure.

CHAPTER 5: II-VI COMPOUND SEMICONDUCTORS

The II-VI compound semiconductors are materials exhibiting various interesting solid-state phenomenon of great significance because of its developments in the field of optoelectronics and scientific applications. Zinc sulphide (ZnS), Cadmium Telluride (CdTe) and Zinc Selenide (ZnSe) are II-VI compound semiconductor having wide band gap. They are found to crystallize in zinc-blende (ZB) and wurzite (WZ) structure under ambient pressure conditions. In various studies, a phase transition from four-fold co-ordinated zinc-blende (ZB) to six-fold co-ordinated rock-salt (RS) has been reported at elevated pressure.

Detail literature review on the available research papers have been discussed in chapter 2.

The primary aim of the work in this chapter is to perform a detailed study on the structural stability and phase transition from zincblende (ZB) to rocksalt (RS) phase of ZnS, CdTe and ZnSe as well as the effects of pressure in the elastic properties and electronic structures of these compounds.

5.1. Structural Properties and Phase transition

The static equilibrium properties of the crystal structure of ZB and RS of ZnS, CdTe and ZnSe are obtained by minimization of the total energy with respect to the unit cell volumes per molecule and fitting it to the Birch–Murnaghan equation [81]. As discussed in III-V compounds, the structural phase transition has been calculated from the condition of equal enthalpies, H=E+PV. Since our calculation is done at zero temperature we have ignored the entropy contribution.

In the following, the structural properties and phase transition of II-VI compound semiconductors: ZnS, CdTe and ZnSe are discussed. In all calculations, we have used LDA and GGA exchange correlations to see the comparative results.

(a) Zinc Sulfide (ZnS)

For the structural optimization of ZnS (in ZB and RS structure), the total energy as a function of volume with LDA and GGA as exchange correlation are shown in figure 5.1(a-b). From the figures, it is observed that ZnS in ZB structure has lower total energy at the equilibrium volume in both the methods thus indicating that the ZnS-ZB structure is more stable than the ZnS-RS structure.

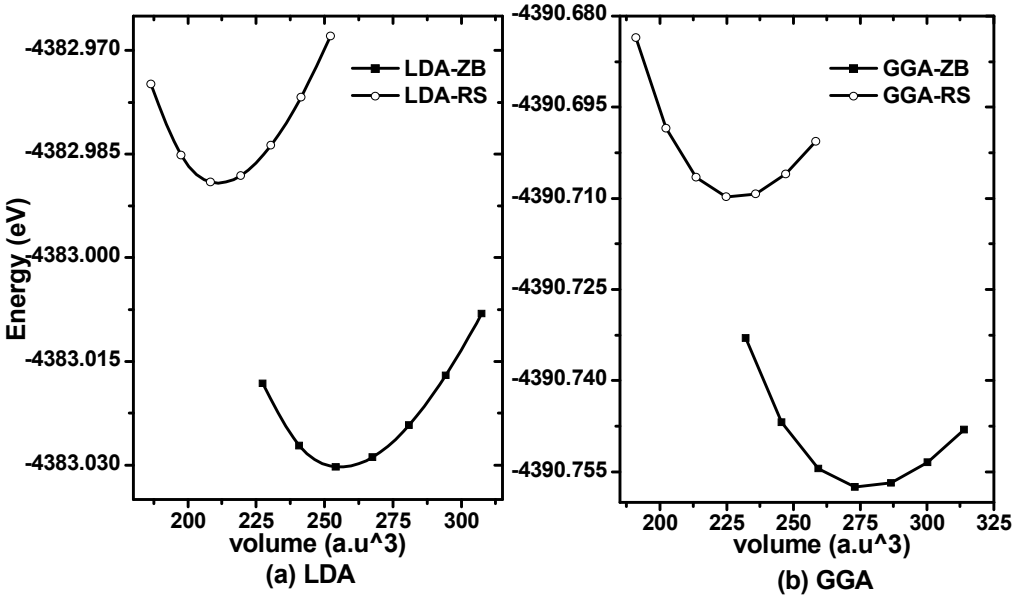

Figure 5.1. Total energy as a function of primitive cell volume for ZnS-ZB and ZnS-RS with (a) LDA and (b) GGA

Table 5. 1. Experimental and calculated ground state structural parameters of ZnS in ZB and RS structure

		Zinc Blende (ZB) Strucutre			**Rock Salt (RS) Structure**		
		a_0 (A^0)	B_0 (GPa)	$B^/$	a_0 (A^0)	B_0 (GPa)	$B^/$
Present work	LDA	5.336	88.88	4.62	5.004	111.75	4.83
	GGA	5.475	71.75	4.51	5.135	88.73	4.83
Expt. work		5.412[a], 5.410[k]	75[a], 76.9[k],	4.4[f], 4.9[k]	5.06[h], 5.13[j]	103.6[h], 85.01[j]	4.00[h]
Other theo. calculation		5.328[b], 5.335[c], 5.342[d]	83.8[b], 83.70[c], 89.67[d], 77.1[e]	4.48[g], 4.05[h],	5.066[i]	100.1[h]	4.05[h] ,

[a]Ref[127], [b]Ref[128], [c]Ref[129], [d]Ref[130], [e]Ref[131], [f]Ref[132], [g]Ref[39], [h]Ref[37], [i]Ref[42], [j]Ref[133], [k]Ref[134]

The calculated ground state structural parameters of ZnS-ZB and ZnS-RS are given in table 5.1 and compared with other available experimental and theoretical data.

For the stable ZnS-ZB phase, the experimental lattice parameter within the LDA shows a difference of 1.40% while that of GGA shows a difference of 1.16% which is quite acceptable within 2% difference. Thus our results are in good agreement with other studies and are used for further calculation of phase transition and energy band structure.

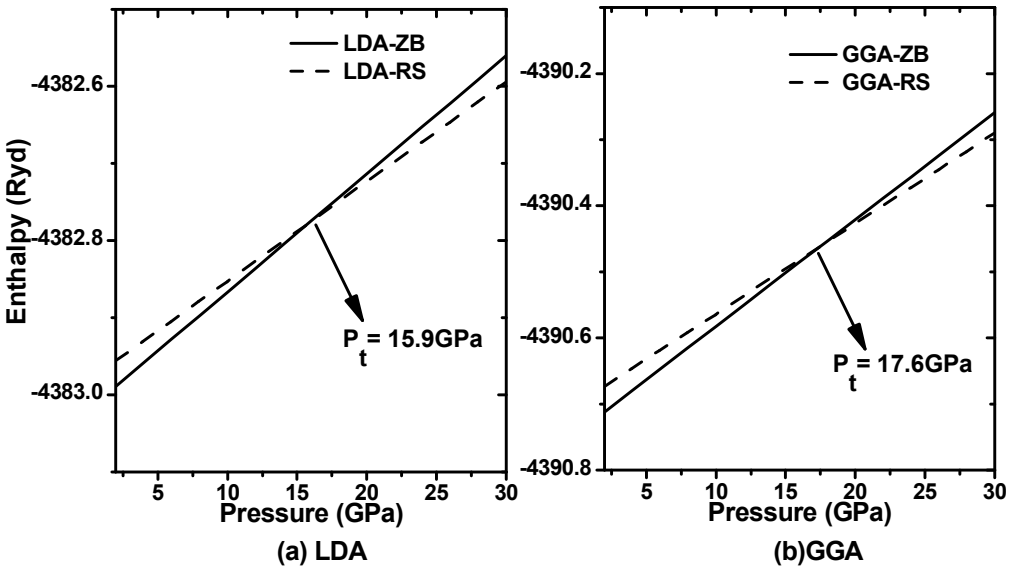

Figure 5.2. Enthalpy as a function of pressure of ZnS-ZB and ZnS-RS phase within (a) LDA and (b) GGA

Table 5.2. Phase transition pressure 'P_t(GPa)' and volume collapse of ZnS.

	Present calculation	**Expt. Results**	**Theoretical results**
Transition pressure (P_t)(GPa)	15.9 (LDA) 17.6 (GGA)	18.1[a],16.9[b],	14.35[c], 14.5[d], 17.4[e], 17.5[f]
Volume collapse (%)	12.86		-

[a]Ref[135], [b]Ref[41], [c]Ref[50], [d]Ref[136], [e]Ref[137], [f]Ref[138],

The phase transition under induced pressure is the pressure at which both the phases have equal Enthalpy. The plot of Enthalpy as a function of various pressures of both the phases is shown in figure 5.2. From the figure we see the transformation from ZnS-ZB to ZnS-RS within the LDA calculation occurs at 15.9 GPa pressure while the transition within the GGA calculation is at 17.6 GPa pressure. As GGA gives us better result of phase transition, we have calculated the volume collapse of ZnS within the GGA only as shown in figure 5.3. Figure 5.3 shows normalised volume (Vp/Vo) as a function of pressure. During the phase transition, the normalised volume of ZB and RS phase is 0.845 and 0.716 respectively with a volume decrease of 12.86% indicating that the ZB phase is more compressible than the RS phase. The

phase transition parameters of the present work are compared with other experimental and theoretical results in table 5.2.

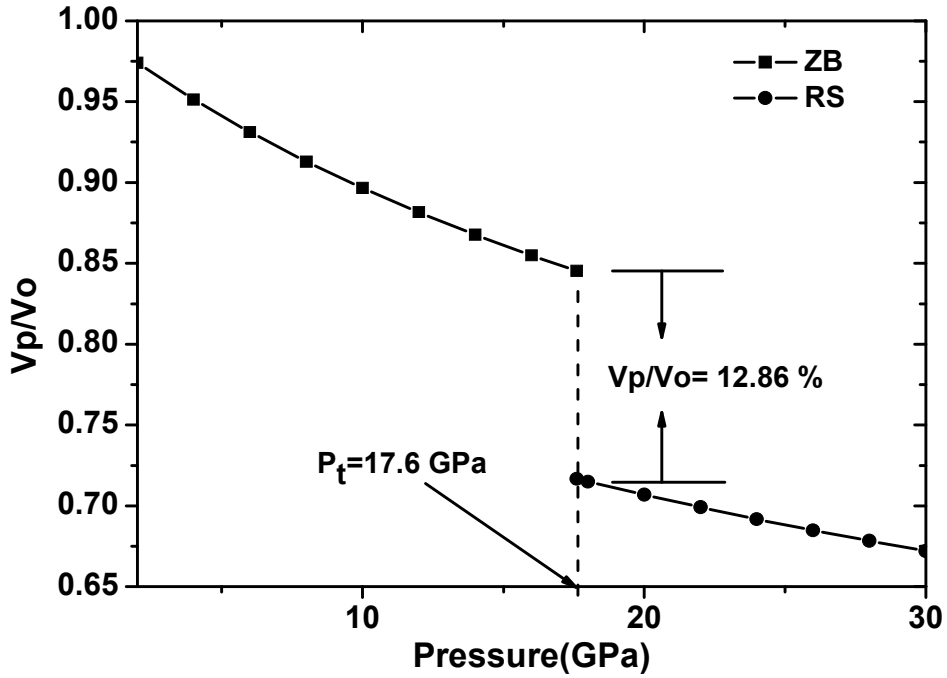

Figure 5.3. Normalized volume as a function of pressure for ZnS-ZB and ZnS-RS

(b) Cadmium Telluride (CdTe)

Following the same methods of calculations as before, the results of structural properties and phase transition of CdTe are discussed in this sub section.

For structure optimization, the total energy as a function of volume of CdTe of both the ZB and RS phase within LDA and GGA are shown in figure 5.4. The lower total energy at the equilibrium volume in both LDA and GGA method indicates the CdTe-ZB structure is more stable than the RS structure. The structural parameters of present work and the experimental data along with other calculations available in the relevant literatures are given in table 5.3

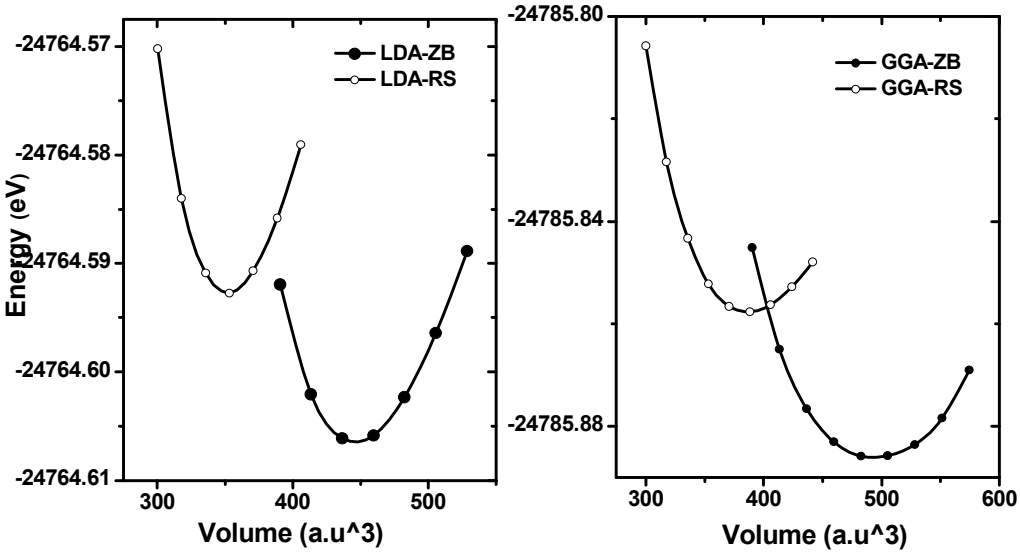

Figure 5.4. Total energy as a function of volume of CdTe- ZB and CdTe-RS structure with LDA and GGA methods

Table 5.3. Experimental and calculated ground state structural parameters of CdTe

		Zinc Blende (ZB) Strucutre			**Rock Salt (RS) Structure**		
		a_0 (A^0)	B_0 (GPa)	$B^/$	a_0 (A^0)	B_0 (GPa)	$B^/$
Present work	LDA	6.42	47.67	5.05	5.92	63.82	5.01
	GGA	6.65	25.28	8.35	6.11	48.24	4.99
Expt. work		6.53[a], 6.49[b]	42[g], 45[h]	6.4[g]	-	-	-
Other Theo. Calculation		6.63[c], 6.62[d], 6.58[e]	33.8[c], 39.0[d], 36.6[e]	5.26[c], 5.14[c], 4.6[d]	6.11[d], 5.94[d], 5.9[f]	56.0[d], 66.4[f]	4.3[d], 5.1[d], 4.67[i]

[a]Ref[139], [b]Ref[140], [c]Ref[141], [d]Ref[142], [e]Ref[143], [f]Ref[144], [g]Ref[145], [h]Ref[146], [i]Ref[147].

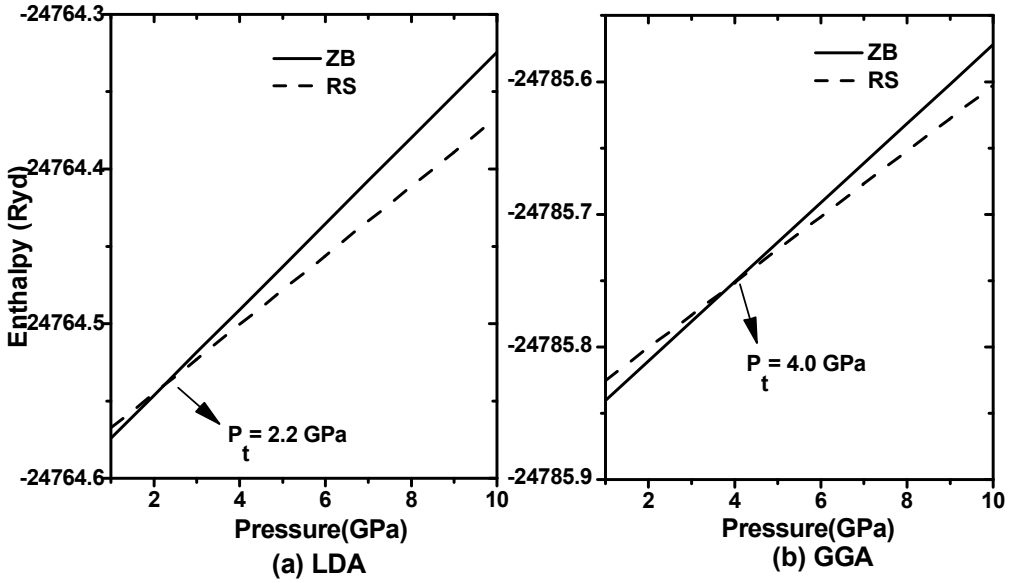

Figure 5.5. Enthalpy as a function of pressure for ZB and RS phase of CdTe with (a) LDA method and (b) GGA method

Table 5. 4. Phase transition pressure and volume collapse of CdTe.

	Present calculation	**Expt. results**	**Theoretical results**
Phase Transition pressure(P_t) (GPa)	2.2 (LDA) 4.0 (GGA)	3.9[a],3.8[b], 3.8[c],3.8[d]	4.0[e], 3.9[f]
Volume collapse (%)	20.9	-	19.0[b], 19.0[e]

[a]Ref[137], [b]Ref[148], [c]Ref[149], [d]Ref[150], [e]Ref[151], [f]Ref[152].

Figure 5.5 shows the phase transition of CdTe-ZB to CdTe-RS at 2.2 GPa with LDA method and at 4.0 GPa pressure with GGA calculation. Table 5.4 shows that the transition pressure obtained with GGA method is more accurate as compare to the available experimental data and hence volume collapse is calculated using GGA method as given in figure 5.6. During the phase transition the normalised volume of the CdTe-ZB and Cd-Te-RS phase is 0.90 and 0.69 respectively with a volume reduction of 20.9% indicating that the ZB phase is more compressible than the RS phase.

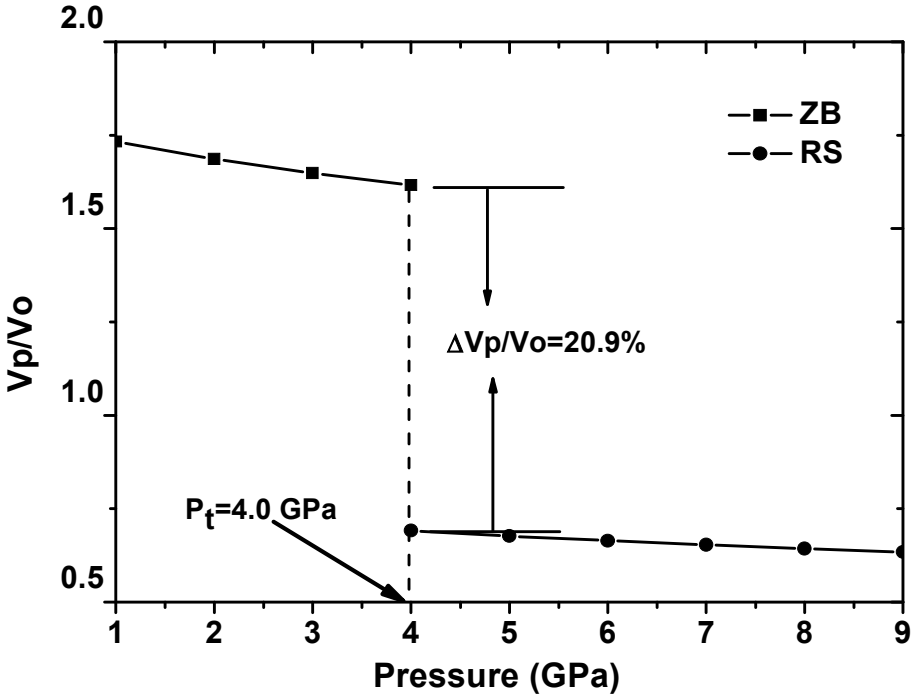

Figure 5.6. Normalised volume versus pressure of CdTe-ZB and CdTe-RS structure within GGA

(c) Zinc Selenide (ZnSe)

The results of the structural properties and the phase transition of ZnSe as obtained in the same methodology as discussed above are explained in brief in this subsection.

In case of ZnSe also, the ZnSe-ZB structure is found to be more stable than ZnSe-RS structure as observed the lower total energy at the equilibrium volume in both LDA and GGA methods as shown in figure 5.7. The structural parameters of ZnSe-ZB and ZnSe-RS of present work are compared with other experimental and theoretical data in table 5.5.

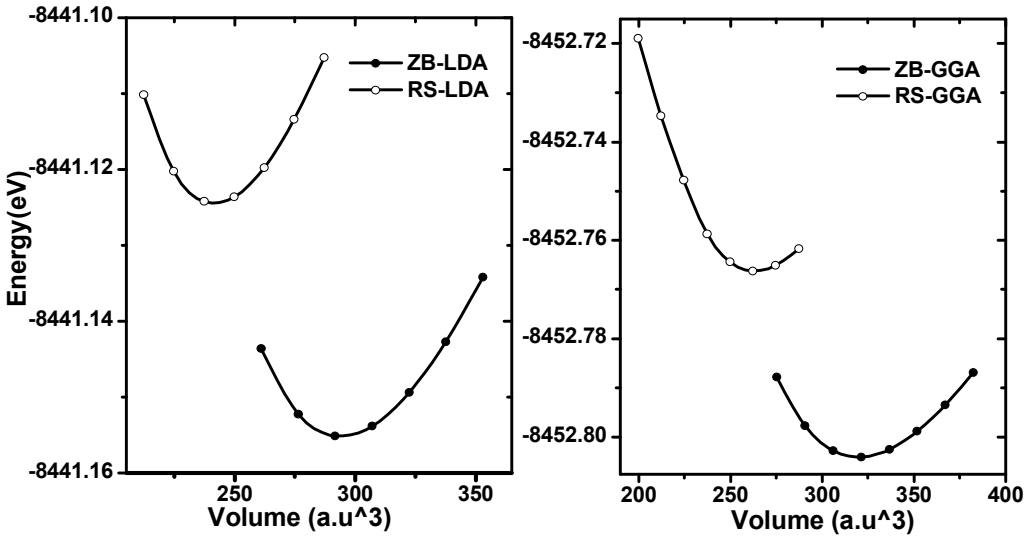

Figure 5.7. Total energy as a function of volume of ZnSe -ZB and ZnSe-RS structure within LDA and GGA methods.

Table 5.5. Experimental and calculated ground state structural parameters of ZnSe in ZB and RS structure

		Zinc Blende (ZB) Strucutre			**Rock Salt (RS) Structure**		
		a_0 (A^0)	B_0 (GPa)	$B^/$	a_0 (A^0)	B_0 (GPa)	$B^/$
Present work	LDA	5.58	73.40	4.70	5.23	91.84	4.87
	GGA	5.74	57.89	4.48	5.38	71.27	4.78
Expt. work		5.66[a],	64.7[a]	4.77[a]	5.66[b]	104[b]	4.0 [b]
Other Theo. Calculation		5.75 [c], 5.63[d]	57.30[c], 68.9 [d]	4.56 [c], 4.36 [d]	5.38[c], 5.26[d]	75.59[c], 88.5[d]	3.60[c], 4.28[d]

[a]Ref[153], [b]Ref[154], [c]Ref[155], [d]Ref[50]

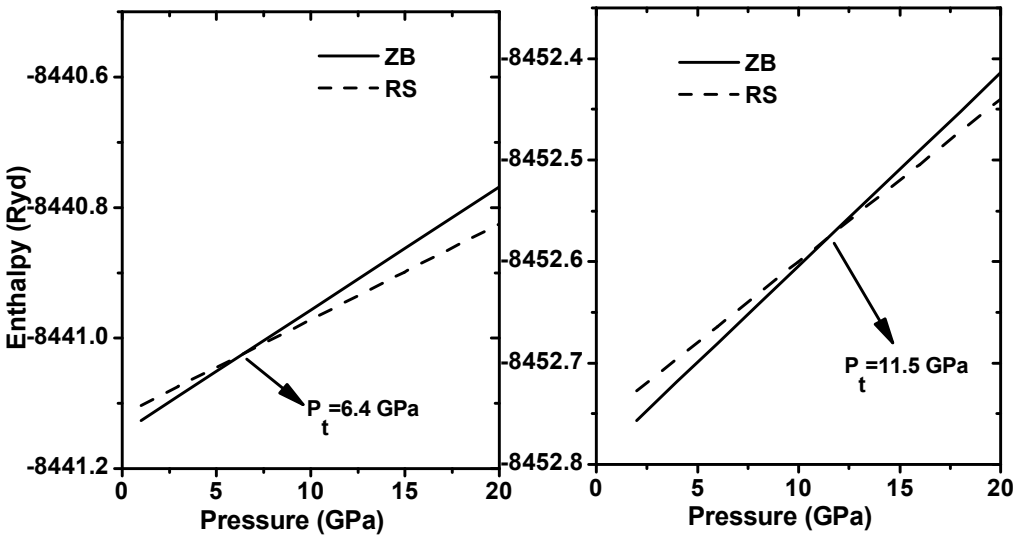

Figure 5.8. Enthalpy as a function of pressure for ZB and RS phase of ZnSe with (a) LDA method and (b) GGA method

Table 5.6. Phase transition pressure 'P_t(GPa)' and volume collapse of ZnSe

	Present calculation	**Expt. results**	**Theoretical results**
Transition pressure (P_t)(GPa)	6.4 (LDA) 11.5 (GGA)	13.0±0.5[a],11.8±0.5[b], 13.0[c]	9.95[d], 15[e], 13.7[f],
Volume collapse (%)	13.74	15.2[c]	-

[a]Ref[156], [b]Ref[157], [c]Ref[158], [d]Ref[10], [e]Ref[159], [f]Ref[52]

The structural phase transition pressure of ZnSe-ZB to ZnSe-RS is obtained at equal enthapy from the plot of enthalpy versus pressure in figure 5.7. The phase transition pressures as obtained with LDA and GGA are given in table 5.6. As the transition pressure obtained with GGA is more accurate to LDA as compare to experimental results, we calculate volume collapse with GGA method. As shown in figure 5.9, during the phase transition, the normalised volume of ZnSe-ZB are found to be 0.866 and that of ZnSe-RS phase is 0.728 with a volume decrease of 13.74%. It means that ZB phase is more compressible than the RS phase. The present results of the calculated volume collapse are compared with other experimental and theoretical results in table 5.6.

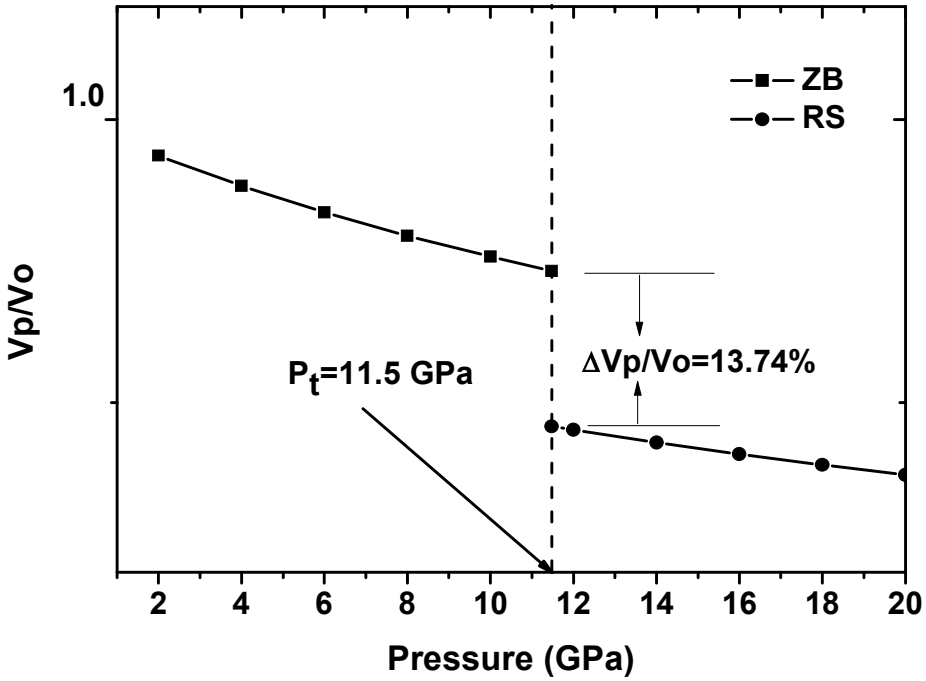

Figure 5.9. Normalized volume as a function of pressure of ZnSe-ZB and ZnSe-RS

5.3. ELASTIC PROPERTIES

(a) Zinc Sulfide (ZnS)

In the present study of Zinc Sulfide (ZnS), the elastic constants are calculated within the GGA only as it has already been shown in previous calculations that the structural phase transition within the GGA gives us better results than LDA. The structural phase transition of ZnS from the zincblende to rocksalt structure with the GGA method has been calculated in figure 5.2 which is occurred at 17.6 GPa pressure. Therefore the elastic constants for ZnS-ZB are calculated corresponding to pressure ranging from 0 GPa to 16 GPa pressure and from 18 GPa to 30 GPa pressure for ZnS-RS. The values of elastic constants of the present work satisfy the mechanical stability conditions: $(C_{11}+2C_{12}) > 0$; $C_{11}-C_{12} > 0$; $C_{44} > 0$; $C_{11} > 0$ for the both the phases.The figure 5.10 shows the variation of elastic constants with pressure. There is a linear variation of elastic constants with pressure up to 16GPa of the ZB phase and 18GPa to 30 GPa of RS phase after the transition pressure of 17.6 GPa.

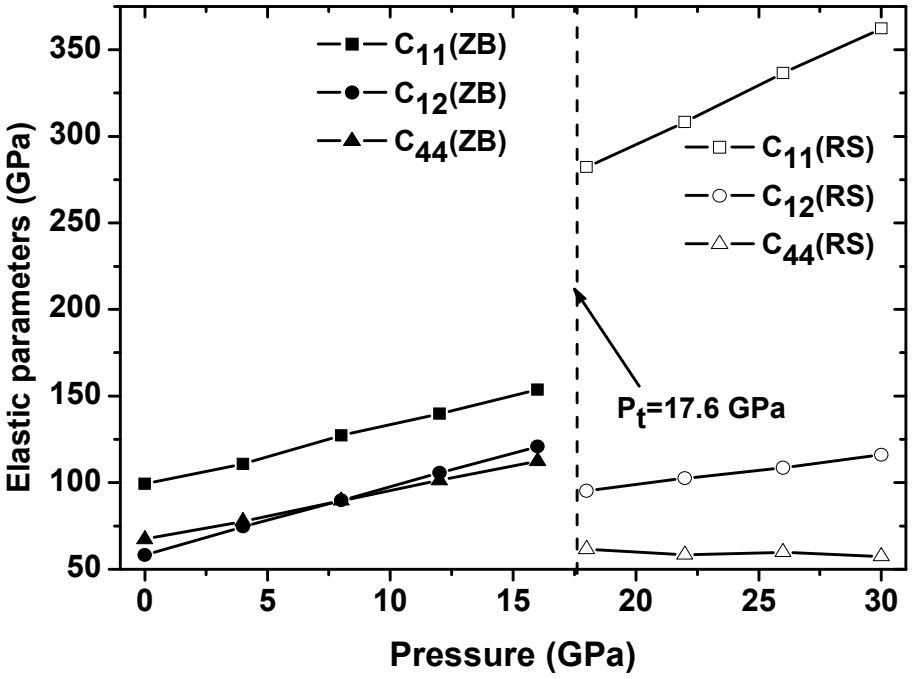

Figure 5.10. Elastic constants (C_{11}, C_{12}, C_{44}) as a function of pressure for ZnS-ZB and ZnS-RS structure

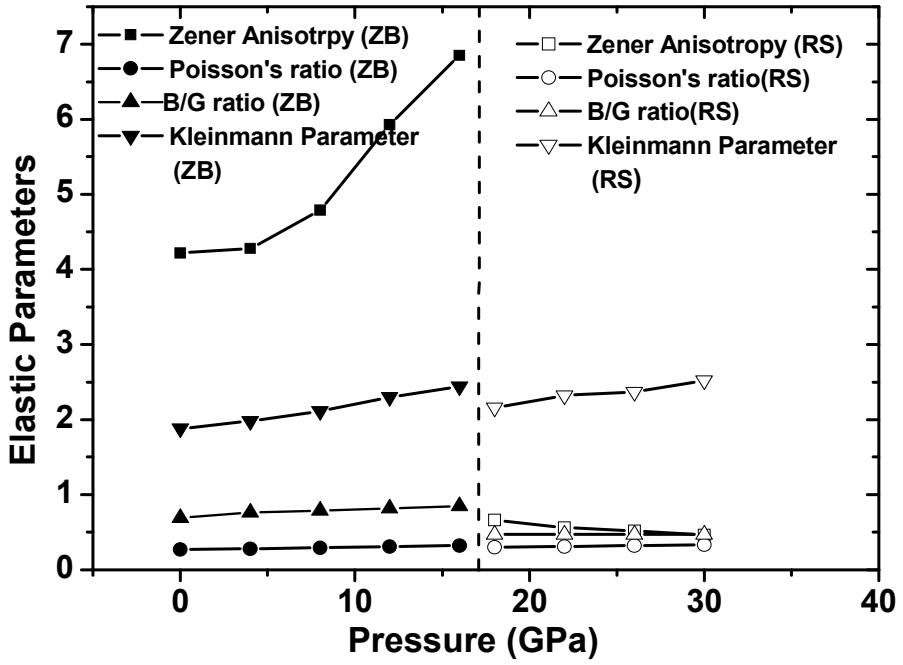

Figure 5.11. Elastic parameters (Zener Anisotropy factor, Poisson's ratio, Kleinmann parameter and B/G ratio) as a function of pressure for ZB and RS phase of ZnS

In the light of these observations, the elastic parameters such as Zener Anisotropy factor (A), Poisson's ratio (υ), Kleinmann's parameter (ζ), B/G ratio, Young's modulus (Y) and Deby's temperature (θ_D) are calculated for both ZnS-ZB and ZnS-RS phases at different pressures as shown in figure 5.11. These elastic parameters are used to determine the mechanical and thermal behavior of ZnS at high pressures.

In figure 5.11, a consistent pattern of linear variation in the elastic parameters with increase in pressure is observed. The Zener Anisotropy factor (A) shows a variation from 4.22 to 6.85 in the ZB phase while it decreases from 0.66 to 0.46 with pressure in case of RS phase. In the present study, the Kleinmann parameter (ζ) of the ZB phase is found to vary from 0.69 to 0.85 with pressure showing bond stretching in the ZB phase while it is found to be 0.48 to 0.46 showing shrinkage in bond bending in the RS phase. The B/G ratio of ZnS-ZB phase increases from 1.88 to 2.44 while the ZnS-RS phase shows an increase from 2.16 to 2.52. Hence we conclude that the brittle nature of the ZB phase of ZnS becomes ductile as the pressure increases and retains its ductility even after it undergoes a structural phase transition to RS phase.

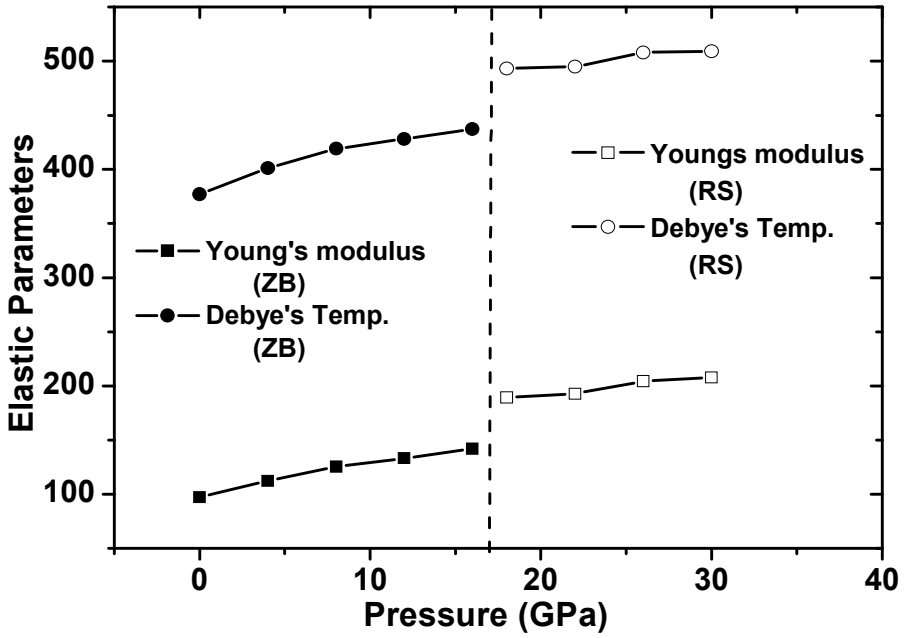

Figure 5.12. Elastic parameters (Young's modulus and Debye's temperature) as a function of pressure of ZnS in ZB phase and RS phase

The elastic parameters (Young's modulus and Debye's temperature) as a function of pressure for both ZnS-ZB and ZnS-RS phases are shown in figure 5.12. From the figure it is seen that with increase in pressure the value of Y increases from 97.18 GPa to 142.08 GPa in the ZB phase while in case of RS phase the value of Y increases from 189.43 GPa to 207.86 GPa. Thus ZnS becomes more rigid with increase in pressure in both the ZB phase and RS phase. As the pressure increases, the value of Debye's temperature also increases from 377 K to 438 K for the ZB phase and from 493 K to 509 K for the RS phase indicating stiffer lattice and better thermal conductivity in both the phases.

(c) Cadmium Telluride (CdTe)

In this sub section, the elastic constants of Cadmium Telluride (CdTe) are calculated at various pressure ranging from 0 GPa to 3 GPa pressure of CdTe-ZB and from 5 GPa to 7 GPa pressure of CdTe-RS as the structural phase transition from ZB to RS occurred at 4 GPa pressure as shown above. The present results are found to satisfy the mechanical stability conditions for both

the phases and shown in figure 5.13. It is observed that under pressure there is a linear variation in the elastic constants up to 2 GPa pressure in ZB phase and 5 GPa to 7 GPa pressure in the RS phase. Around 3 GPa pressure, the stability condition of CdTe-ZB phase is not satisfied indicating that the structural transformation from ZB to RS starts at around 3 GPa pressure and completes at 4 GPa pressure. The elastic parameters like Zener anisotropic factor (A), Poisson's ratio (υ), Kleinmann parameter (ζ), B/G ratio, Young's modulus (Y), and Debye's temperature (θ_D) to determine the mechanical and thermal behaviour of both the phases as shown in figure 5.14.

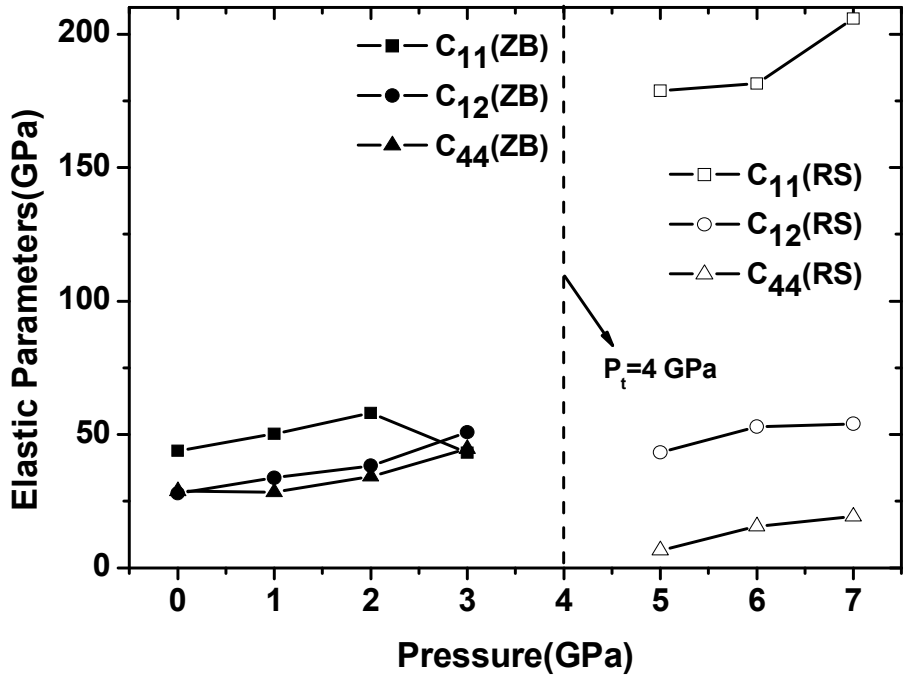

Figure 5.13. Elastic parameters versus pressure for ZB and RS phase of CdTe

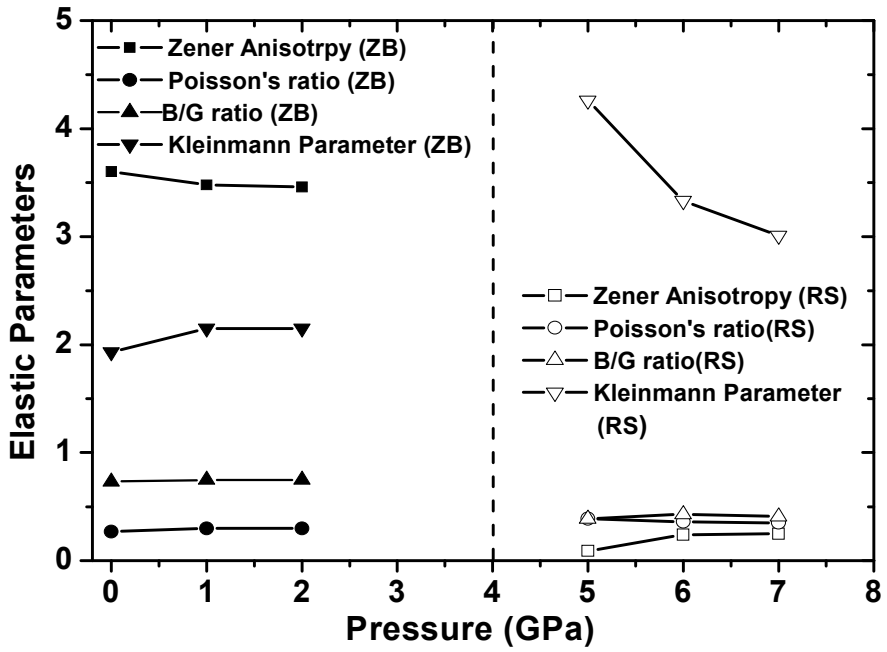

Figure 5.14. Elastic parameters (Zener Anisotropy factor, Poisson's ratio, Kleinmann parameter and B/G ratio) as a function of pressure for ZB and RS phases of CdTe

As the pressure increases, the Zener Anisotropy factor (A) for CdTe-ZB phase decreases from 3.60 to 3.46 while for CdTe-RS, it increases from 0.09 to 0.25 indicating that CdTe is not an elastically isotropic material. There is increase in Poisson's ratio (υ) from 0.27 to 0.30 in the ZB phase and decrease from 0.39 to 0.35 in the RS phase indicating higher ionic contribution in intra-atomic bonding with increasing pressure in both the phases. The present result also indicates that inter atomic forces tends to be more central with pressure. As the pressure increases, Kleinmann parameter does not vary much and remains around 0.75 for CdTe-ZB and 0.41 for CdTe-RS indicating shrinkage in bond-stretching in both phases. The B/G ratio for CdTe-ZB ranges from 1.93 to 2.15 with increase in pressure indicating ductile nature at high pressure. For CdTe-RS, B/G ratio decreases from 4.26 to 3.01 with increase in pressure but is greater than 1.75. Hence we can conclude that both CdTe-ZB and CdTe-RS retains its ductile nature even at higher pressures.

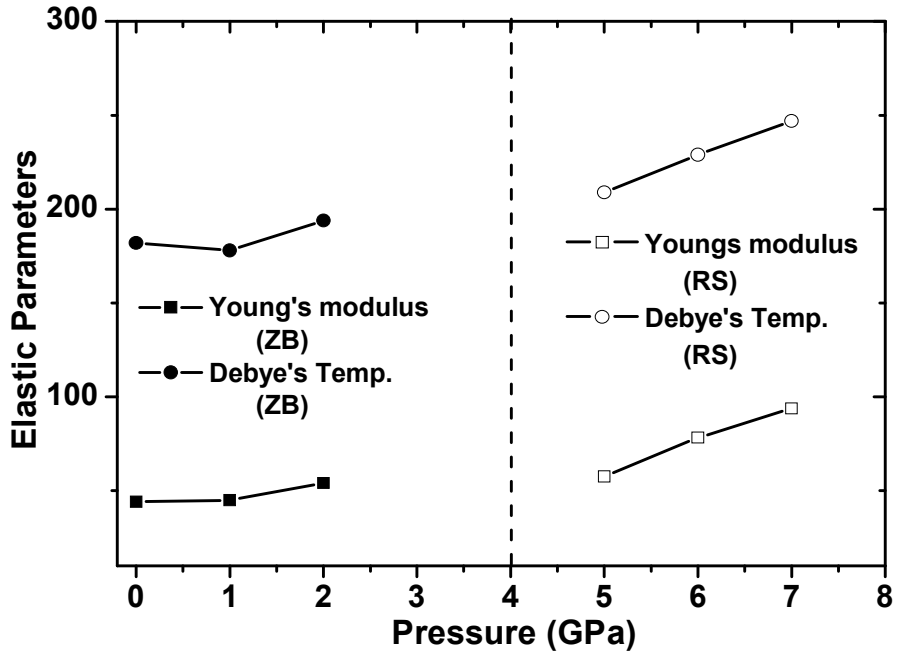

Figure 5.15. Elastic parameters (Young's modulus and Debye's temperature) as a function of pressure of CdTe in ZB phase and RS phase

In figure 5.15, the elastic parameters (Young's modulus and Debye's temperature) as a function of pressure for both CdTe-ZB and CdTe-RS phases are shown. With increase in pressure the value of Y increases from 44.08 GPa to 54.15 GPa in CdTe-ZB while in CdTe-RS it increases from 57.65 GPa to 93.84 GPa. Hence CdTe becomes stiffer with increase in pressure in both phases. The Debye's temperature calculated also shows an increase from 181 K to 194 K for CdTe-ZB and from 209 K to 247 K in CdTe-RS phase indicating better thermal conductivity under pressure.

c) Zinc Selenide (ZnSe)

As mentioned above, phase transition of Zinc Selenide (ZnSe) under pressure occurs at 11.5 GPa and thus figure 5.16 shows the elastic constants of ZnSe-ZB structure at various pressure from 0 GPa to 8 GPa pressure and from 12 GPa to 18 GPa pressure in rocksalt structure and found to satisfy the mechanical stability conditions for both phases.

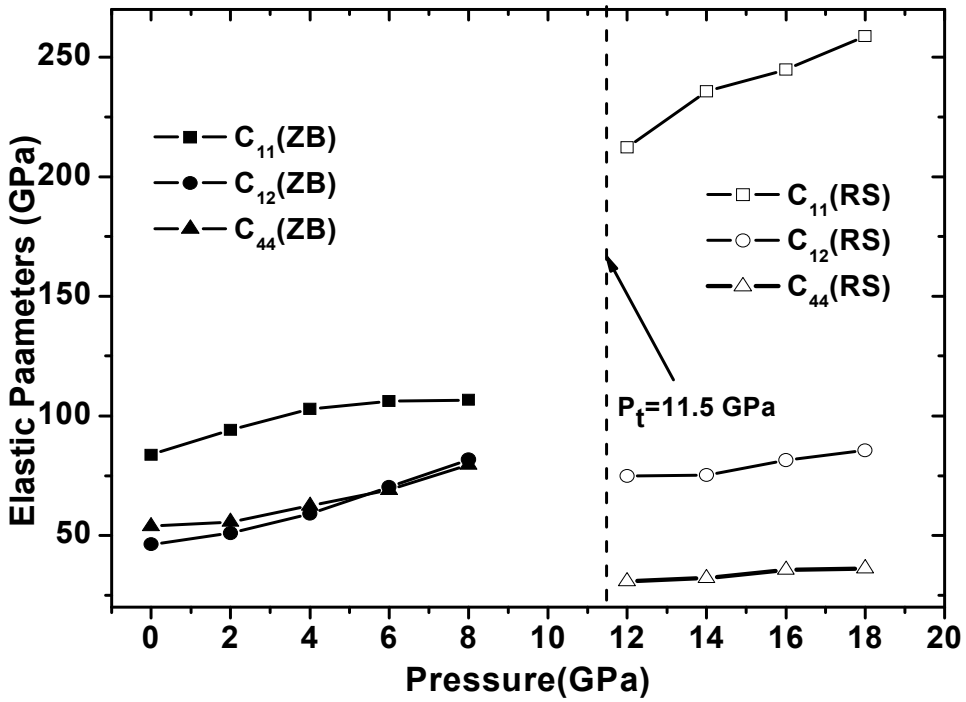

Figure 5.16. Elastic constants (C_{11}, C_{12}, C_{44}) as a function of pressure of ZnSe-ZB and ZnSe-RS phase

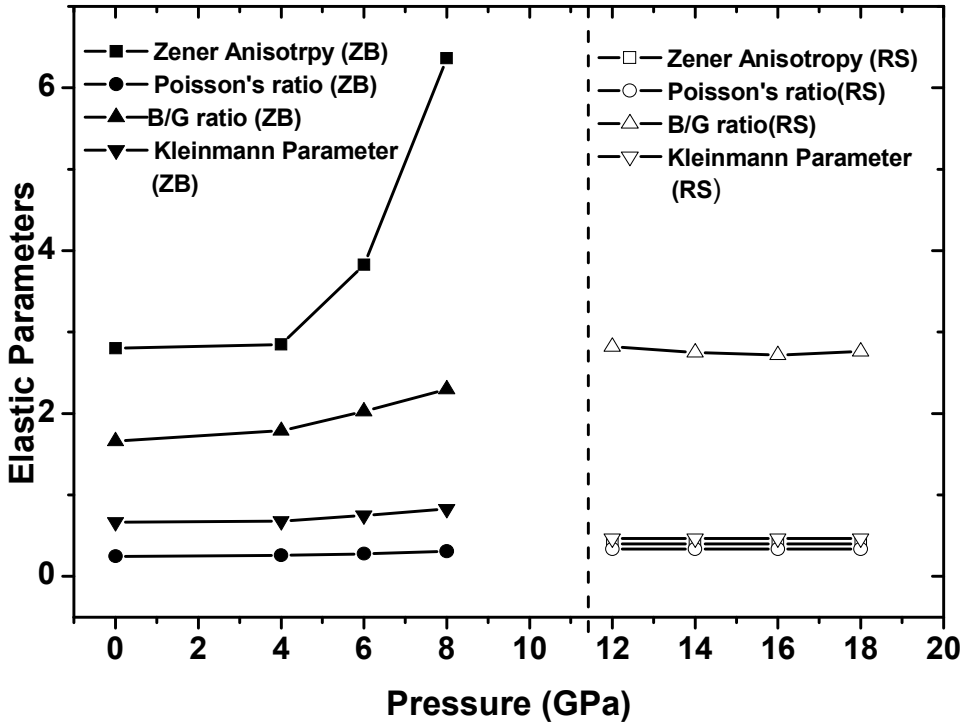

Figure 5.17. Elastic parameters (Zener Anisotropy factor, Poisson's ratio, Kleinmann parameter and B/G ratio) as a function of pressure for ZnSe-ZB and ZnSe-RS

In figure 5.17 our calculated elastic parameters (Zener Anisotropy factor (A), Poisson's ratio (υ), kleinmann's parameter (ζ) and B/G ratio) as a function of pressure are shown.

The Zener Anisotropy factor, A shows a variation from 2.88 to 6.36 in the ZB phase while in the RS phase it decreases from 0.44 to 0.41with increasing pressure. The value of Poisson's ratio, υ increases from 0.25 to 0.35 in ZB phase indicating higher ionic contribution in the inter atomic bonding with increasing pressure while in the RS phase it remains around 0.34. In the present study, the Kleinmann parameter,ζ is found to vary from 0.67 to 0.83 with pressure of the ZB phase while it is found to decrease from 0.49 to 0.47 in the RS phase showing shrinkage in bond stretching in the ZB phase and shrinkage in bond bending in the RS phase. With increasing pressure, the B/G ratio of ZnSe-ZB phase increases from 1.66 to 2.30 while ZnSe-RS phase shows a decrease from 2.82 to 2.76. Hence the ZB phase is brittle in nature but as the pressure increases it tends to becomes ductile and retains its ductility even after it undergoes a structural phase transition to RS phase.

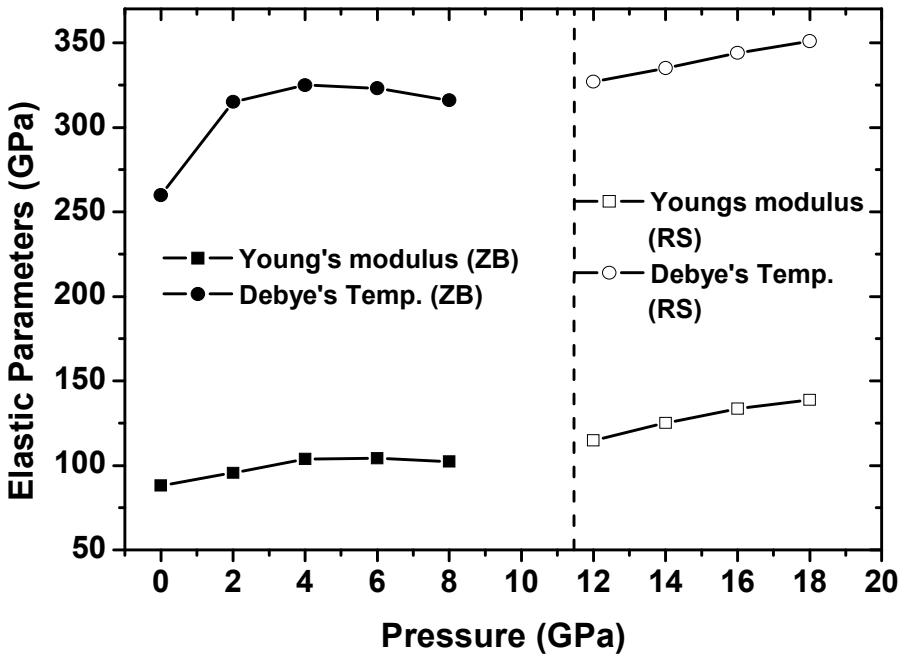

Figure 5.18. Elastic parameters (Young's modulus and Debye's temperature) as a function of pressure of ZnSe in ZB phase and RS phase

The elastic parameters (Young's modulus and Debye's temperature) as a function of pressure for both ZnSe-ZB and ZnSe-RS phases are shown in figure 5.18. The value of Y increases from 88.09 GPa to 102 GPa in the ZB phase while in the RS phase the value of Y increases at first from 114.78 GPa to 104.24 GPa and then decreases to 102.32 GPa as it comes nearer to the transition pressure. Thus ZnSe-ZB becomes more rigid with increase in pressure but certain deformation is found to occur just before it undergoes a structural transformation to the RS phase and after completion of the transition it attains its rigidity again as pressure goes on increasing. Similarly the value of Debye's temperature also increases from 260 K to 323 K for the ZB phase indicating stiffer lattice and better thermal conductivity but slightly decreases just before it undergoes structural transformation to the RS phase and after transition to the RS phase it again increase from 327K to 351 K showing better thermal conductivity.

5.4. ELECTRONIC PROPERTIES

(a) Zinc Sulfide (ZnS)

The electronic band structure calculation of ZnS-ZB and ZnS-RS at 0 GPa pressure are performed within (a) LDA, (b) GGA and (c) mBJ-GGA methods and are shown in figure 5.19 and figure 5.20 respectively. For ZnS-ZB, figure 5.1 (a, b and c) shows that the valance band maximum and conduction band minimum occurs at the Γ point confirming a direct band gap. The band gap with LDA and GGA calculation shows a band gap of 1.89 eV and 1.99 eV respectively while with mBJ-GGA calculation gives a band gap of 3.5 eV which is very close to the experimental values of 3.6 eV [101]. Again the band structures of ZnS-RS are shown in figure 5.20 (a, b and c). In figure 5.20 (a) and 5.20 (b) with the LDA and GGA calculation, there is a crossing over of the conduction band at the Fermi energy towards the valance band. However electronic band structure calculation with the mBJ-GGA as shown in figure 5.20 (c) shows that the valance band maximum occurs at the Γ point while the conduction band minimum occurs at L point confirming an indirect band gap.

Thus the implementation of the mBJ-GGA potential resolves the underestimation of the band gaps.

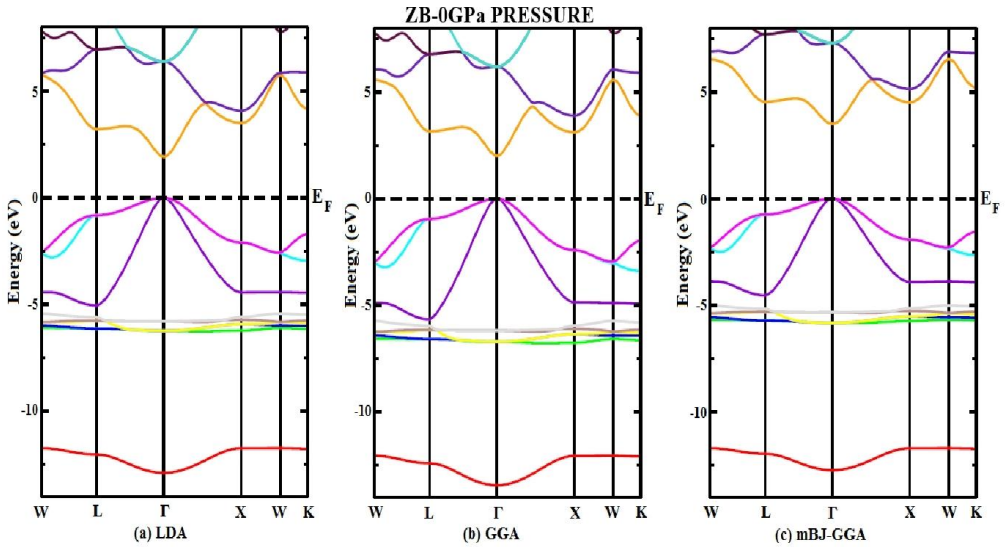

Figure 5.19. Band structure of ZnS-ZB at 0 GPa pressure within (a) LDA, (b) GGA and (c) mBJ-GGA

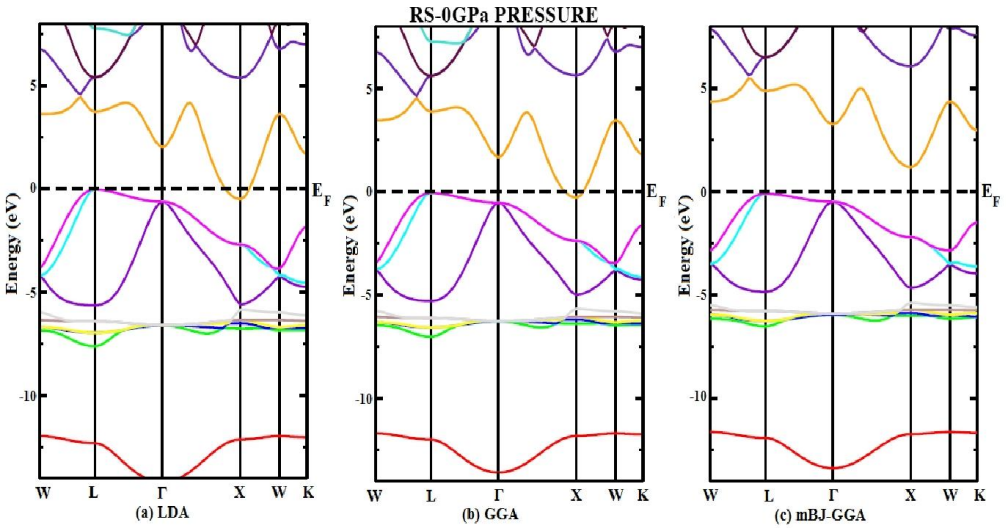

Figure 5.20. Band structure of ZnS-RS at 0 GPa pressure within (a) LDA, (b) GGA and (c) mBJ-GGA

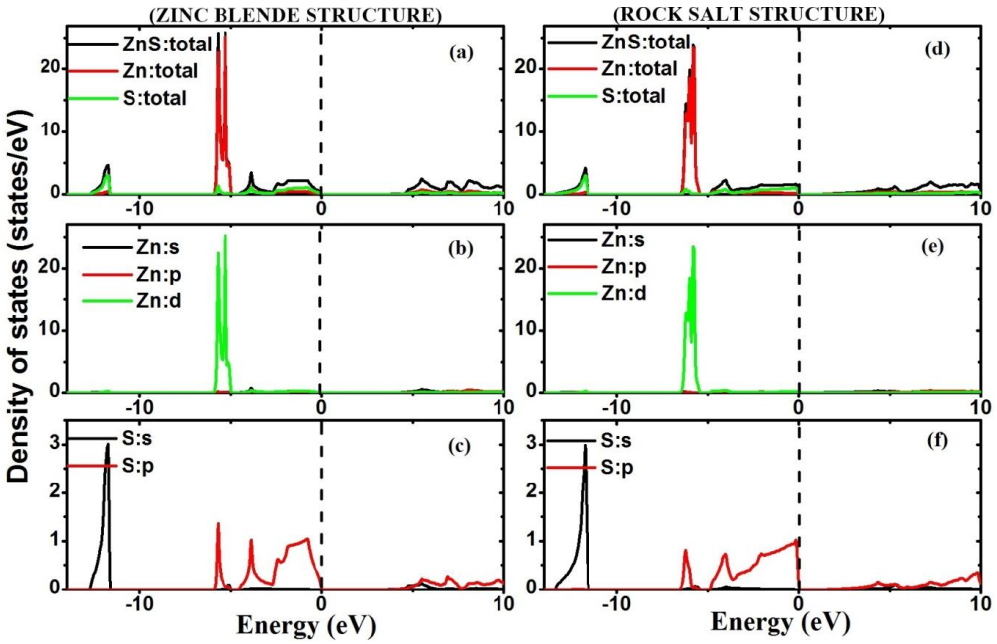

Figure 5.21. Total and Partial DOS of ZnS-ZB and ZnS-RS within mBJ-GGA.

The origin of the energy band structure of a compound is related to the corresponding density of states. Therefore for better understanding of band gaps the total and partial density of states (DOS) are studied. But since we find that calculations within the mBJ-GGA gives us better results than within LDA and GGA, we have therefore studied the total DOS and partial DOS within the mBJ-GGA only. In figure 5.21, the total and partial DOS of ZnS-ZB and ZnS-RS are shown. From figure 5.21(a), (b) and (c), for ZnS-ZB phase, we find that the lowest band appearing in energy band diagram is mainly contributed from s-non metal (S atom) orbital while the valance band is mainly contributed by the d-metal (Zn- atom) orbital. Again from figure 5.21(d), (e) and (f) for ZnS-RS, the lowest band is mainly contributed by the s-non metal (S atom) orbital while the valance band is mainly contributed by the d-metal (Zn-atom) orbital with little contribution from the p (S-atom) orbital.

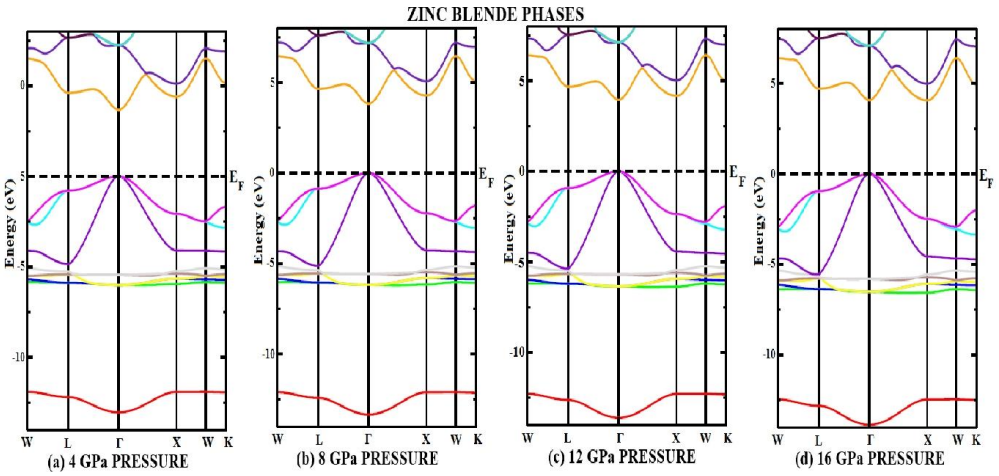

Figure 5.22. Energy band diagram ZnS-ZB at (a) 4 GPa pressure (b) 8 GPa pressure (c) 12 GPa pressure and (d) 16 GPa pressure.

Next we are interested to study the variation of band diagram with pressure. Figure 5.22 (a, b, c) and d) shows the energy band diagram of ZnS-ZB structure at different pressures. we observe from the band structure diagrams (in figure 5.22) that as the pressure increases to 5 GPa, 10 GPa 15 GPa and 20 GPa, there is an increase in the gap between Γ-L point while the gap between Γ-X decreases towards the Fermi level indicating possibilities of crossing over of the conduction band towards the valance band at higher pressure indicating to be metallic nature of ZnS-RS. The variation in the energy band gap with pressure for ZnS-ZB is also shown in figure 5.23 for clear analysis of the changes in the gap between Γ- Γ point, Γ-X point and Γ-L point with pressure.

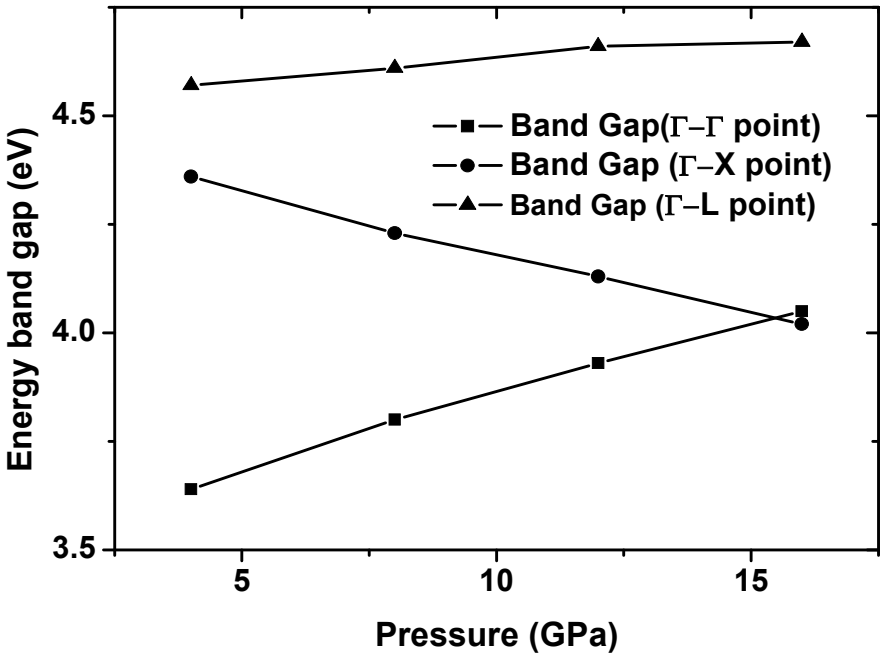

Figure 5.23. Variation in Energy band gaps of ZnS-ZB phase with pressure.

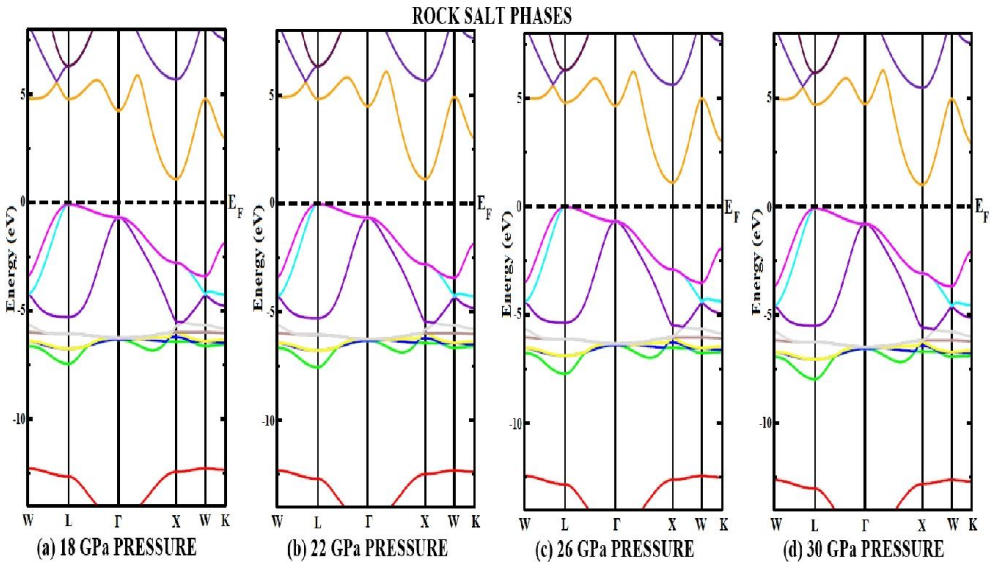

Figure 5.24. Energy band diagram ZnS-RS phase at (a) 18 GPa pressure (b) 22 GPa pressure (c) 26 GPa pressure and (d) 30 GPa pressure

In figure 5.24(a, b, c and d) the energy band diagrams of ZnS-RS phase at different pressures are given. From the figure we find that the indirect band gap nature of ZnS-RS is retained even at high pressure without much variation. Hence we conclude that the energy band gap of ZnS-ZB phase is

affected by pressure while the energy band gap of ZnS-RS phase is not much affected by pressure.

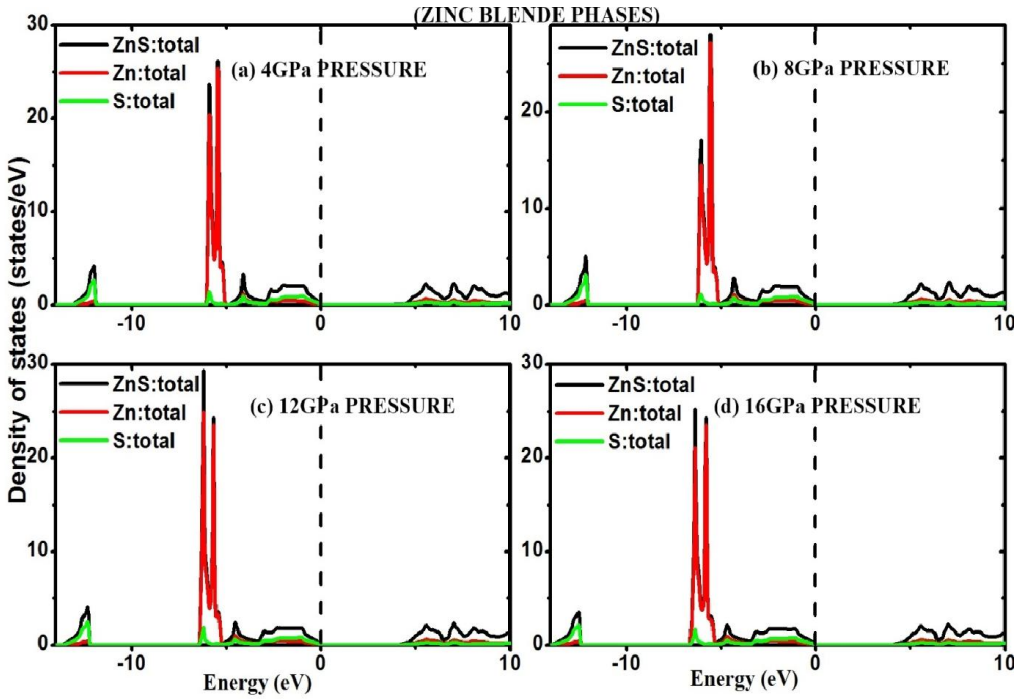

Figure 5.25. Total DOS of ZnS-ZB structure at (a) 4 GPa pressure (b) 8 GPa pressure (c) 12 GPa pressure and (d) 16 GPa pressure.

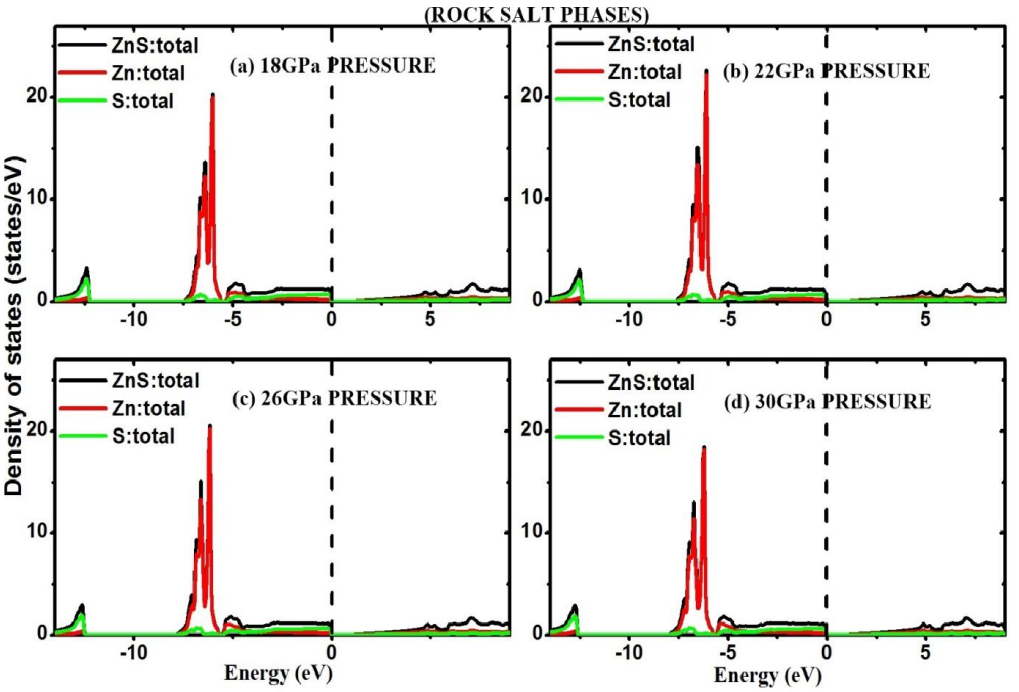

Figure 5.26. Total DOS of ZnS-RS structure at (a) 18 GPa pressure (b) 22 GPa pressure (c) 26 GPa pressure and (d) 30 GPa pressure

Further, the total DOS of ZnS-ZB at (a) 4 GPa pressure (b) 8 GPa pressure (c) 12 GPa pressure and (d) 16 GPa pressure are given in figure 5.25. From the figure we find that in the lowest band the contribution of the S atom merely increases with increase in pressure while the contribution of the Zn atom decreases with increasing pressure. Again in the valance band as the pressure increases the contribution of Zn atom increases up to 12 GPa and its contribution starts to decrease at 16 GPa which is expected near to phase transition pressure (around17GPa) while there is no change in the contribution of S atom. In figure 5.26, the total DOS of ZnS-RS at (a) 18 GPa pressure (b) 22 GPa pressure (c) 26 GPa pressure and (d) 30 GPa pressure are shown. From the figure we see that in the lowest band, with increase in pressure, the contribution of the S atom does not change. In the valance band, the contribution of the Zn-atom increases and then decreases as the pressure goes on increasing. Hence for ZnS-ZB phase the change in pressure affects both the Zn atom as well as the S atom but in case of ZnS-RS phase the change in pressure mainly affects the Zn atom.

(b) Cadmium Telluride (CdTe):

Figure 5.27(a, b and c) and 5.28(a, b and c) show the electronic band structure of CdTe-ZB and CdTe-RS at zero pressure within (a) LDA, (b) GGA and (c) mBJ-GGA methods. Energy band diagrams in figure 5.27 (c) of CdTe-ZB reveals a direct band gap of 1.46 eV with mBJ-GGA which is close to the experimental values of 1.44eV [101]. In figures 5.28 (a), (b) and (c), there is crossing over of the conduction band at the Fermi energy towards the valance band indicating metallic nature of CdTe-RS.

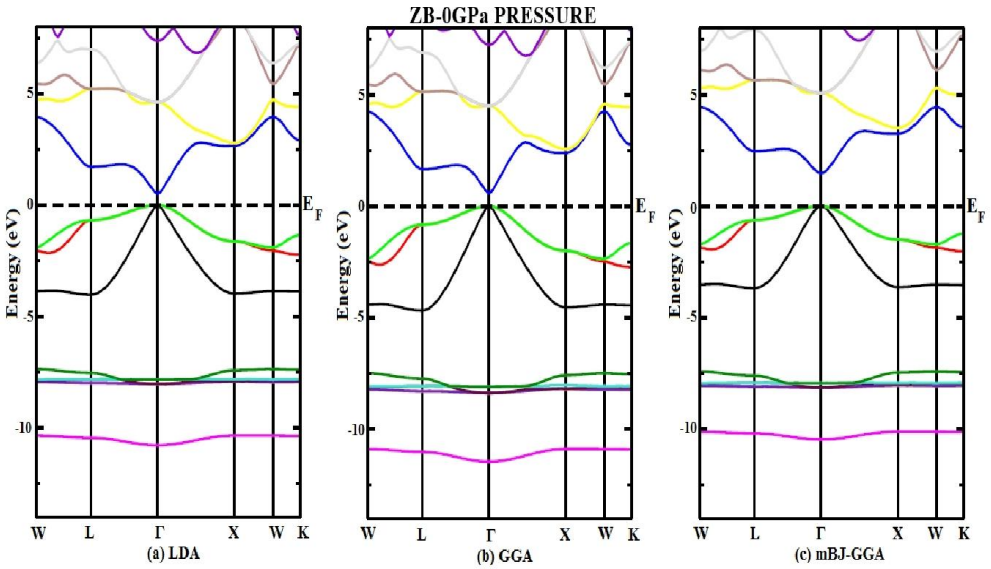

Figure 5.27. Band structure of CdTe-ZB at 0 GPa pressure within (a) LDA, (b) GGA and (c) mBJ-GGA methods

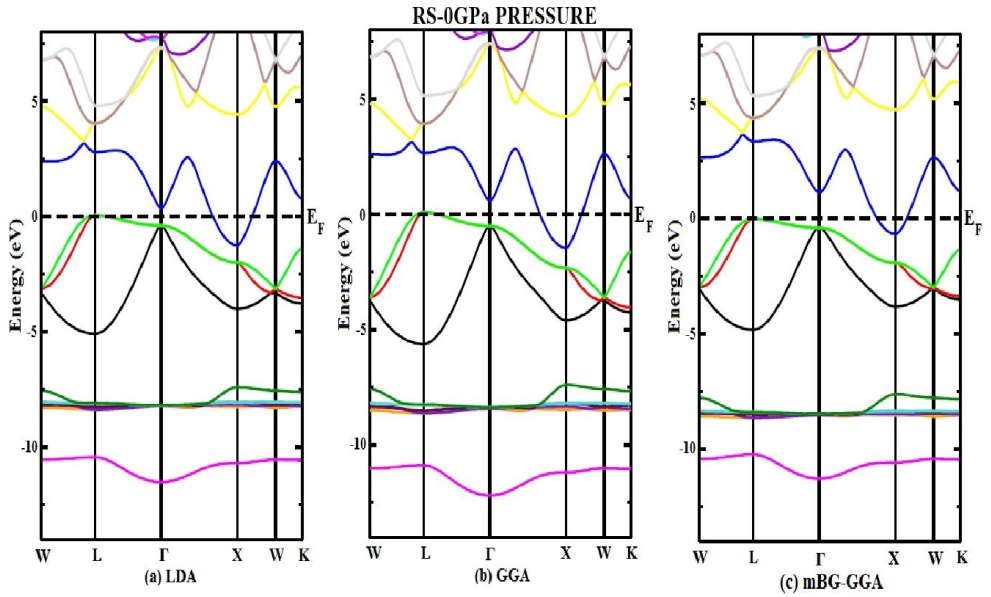

Figure 5.28. Band structure of CdTe-RS at 0 GPa pressure within (a) LDA, (b) GGA and (c) mBJ-GGA methods

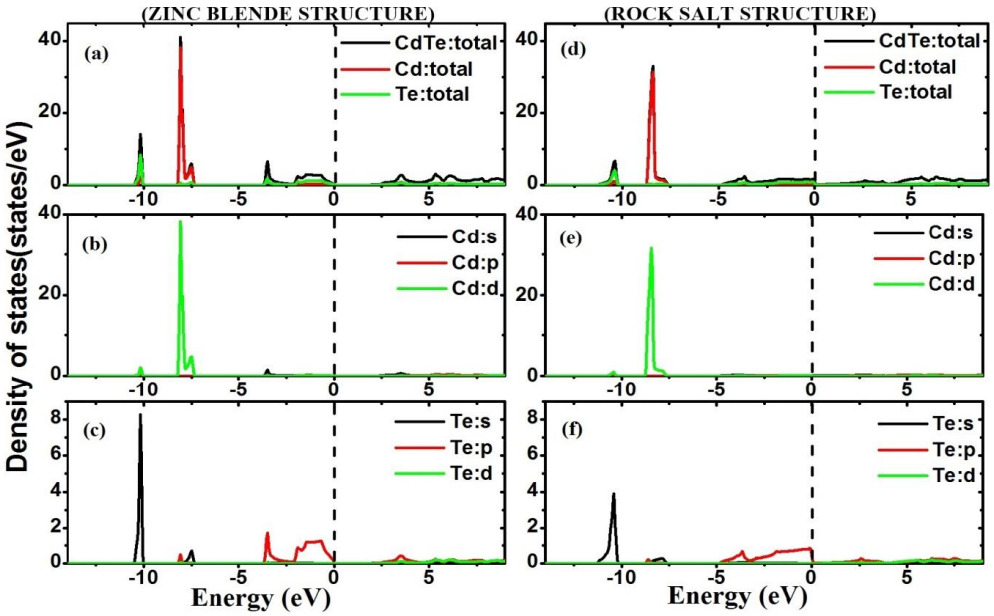

Figure 5.29. Total and Partial DOS of CdTe-ZB and CdTe-RS within mBJ-GGA method

From the DOS plot of CdTe-ZB in figure 5.29(a, b and c) it is observed that first lowest band in the band structure is mainly contributed by the s-non metal (Te-atom) orbital with little contribution from the d-metal (Cd-atom) orbital while the second lowest band shows higher contribution of the d-metal (Cd atom) orbital. The valance band is mainly contributed by the s-metal (Cd-atom) orbital and s-non metal (Te-atom) orbital. Also in figure 5.29(d, e and f) of CdTe-RS, the lowest band is mainly contributed by the s-non metal (Te atom) orbital with little contribution from the p-metal (Cd-atom) orbital and d-metal (Cd-atom) orbital while the valance band is mainly contributed by the d-metal (Cd-atom) orbital with little contribution from the p-non metal (Te-atom) orbital.

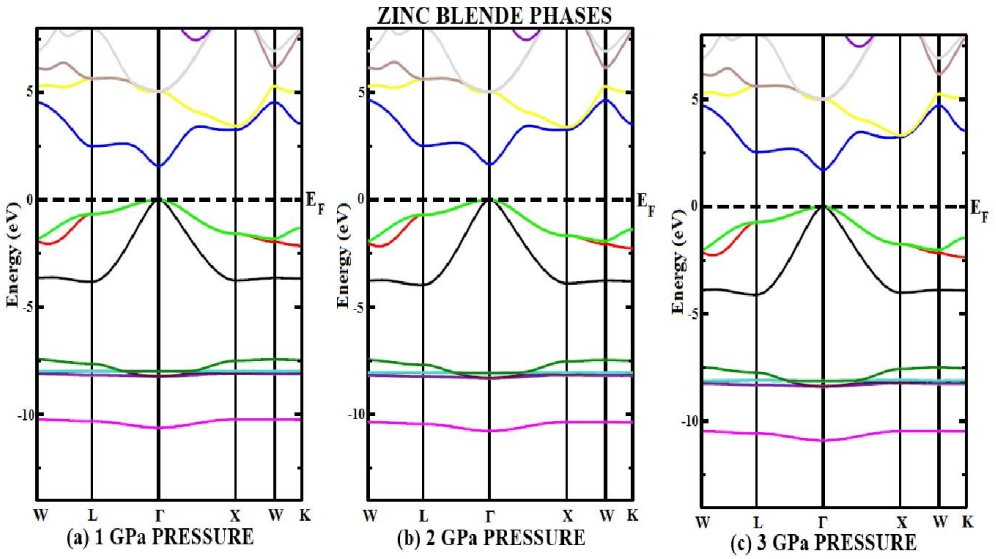

Figure 5.30. Energy band diagram CdTe-ZB at (a) 1 GPa pressure (b) 2 GPa pressure and (c) 3 GPa pressure.

Figure 5.31(a, b, c and d) shows the energy band diagrams of CdTe-ZB phase at different pressures. In figure 5.31, as the pressure increases to 1 GPa, 2 GPa and 3 GPa pressure, the gap between the Γ- Γ point increases. The variations of gaps at Γ- Γ point, Γ-L point and Γ- X point with increase in pressure are given in figure 5.31. Also Figure 5.32 (a, b and c) shows energy band diagrams of CdTe-RS phase at different pressures showing metallic nature is retained even at high pressure without much variation.

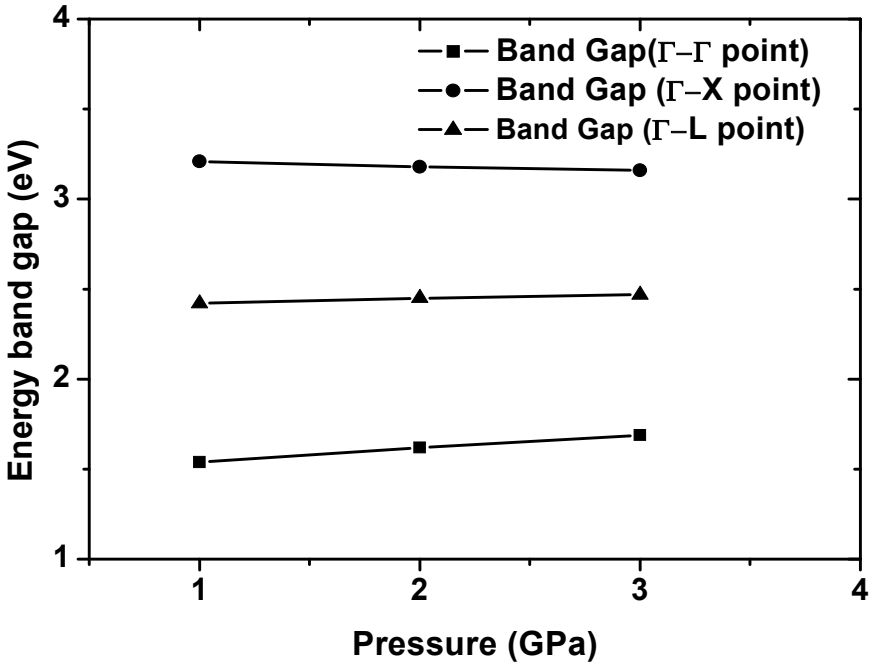

Figure 5.31. Variation of Energy band gaps of CdTe-ZB phase with pressure

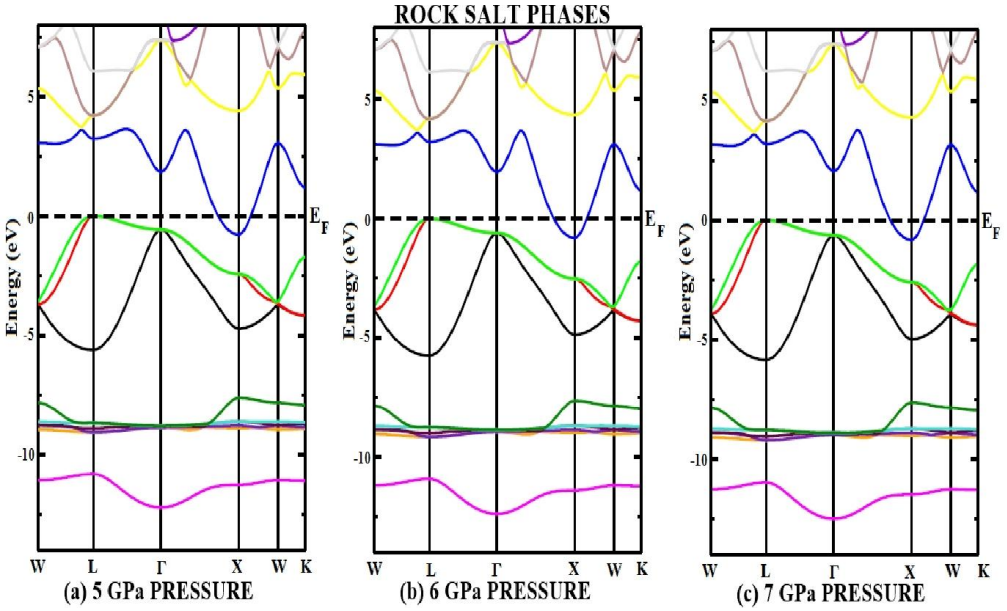

Figure 5.32. Energy band diagram CdTe-RS at (a) 5 GPa pressure (b) 6 GPa pressure and (c) 7 GPa pressure

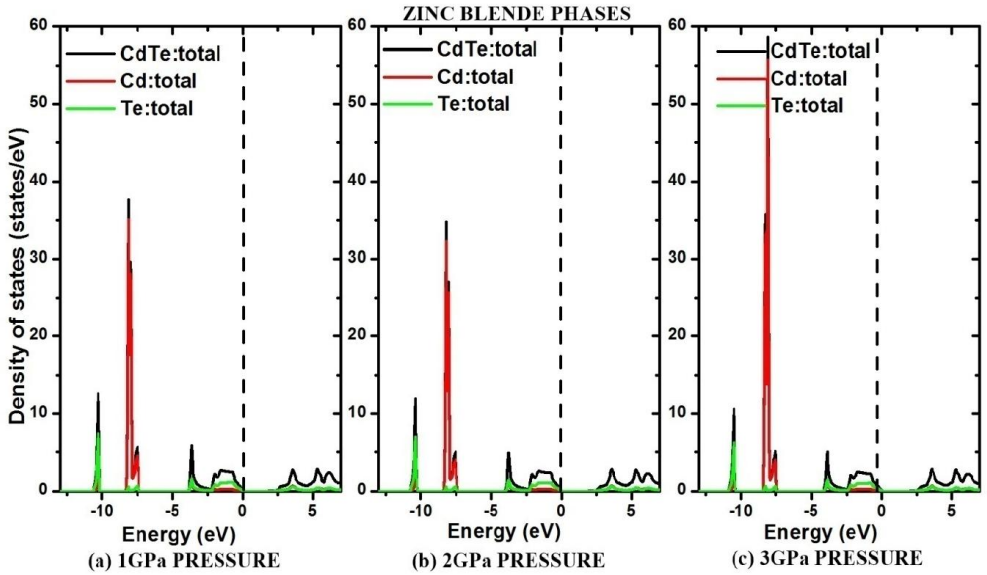

Figure 5.33. Total DOS of CdTe-ZB structure at (a) 1 GPa pressure, (b) 2 GPa pressure and (c) 3 GPa pressure

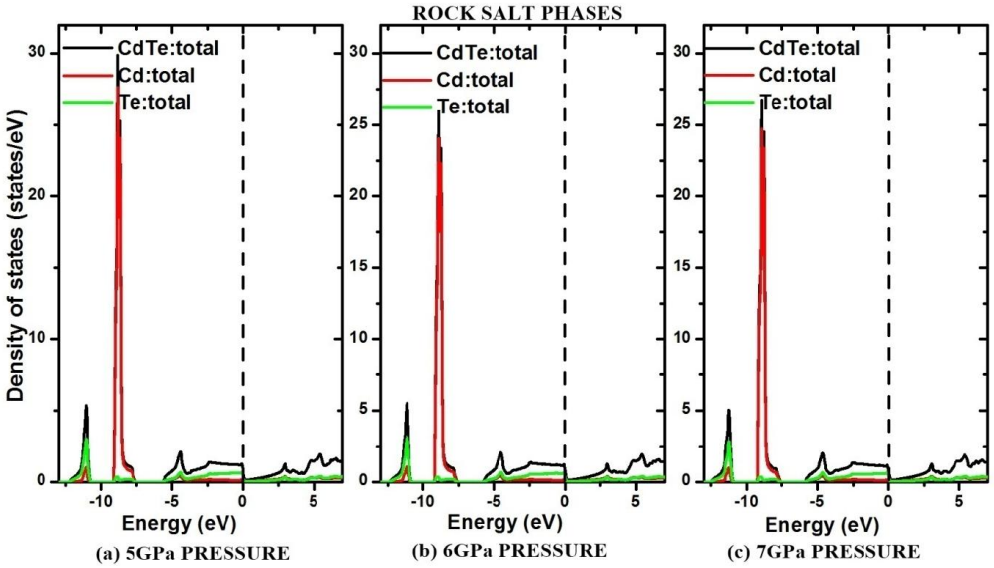

Figure 5.34. Total DOS of CdTe-RS structure at (a) 5 GPa pressure, (b) 6 GPa pressure and (c) 7 GPa pressure

The total DOS of CdTe-ZB at (a) 1 GPa pressure (b) 2 GPa pressure and (c) 3 GPa pressure are given in figure 5.33. The variation of gap between valence and conduction band observed in the DOS plot clearly reflects the increase of band gap with pressure in the band diagram as discussed above. Also figure 5.34 shows the total DOS of CdTe-RS at (a) 5 GPa pressure (b) 6 GPa pressure and (c) 7 GPa pressure. In this plot, it is clearly observed the crossing

of orbitals towards valence and conduction band around Fermi line. It confirms the metallic nature of CdTe-RS structure as observed in band diagram as mentioned above.

(c) Zinc Selenide (ZnSe)

In the same way as discussed, the electronic band structure of ZnSe in zincblende and rocksalt structure at 0 GPa pressure calculated with the three methods (LDA, GGA, mBJ-GGA) are shown in figure 5.35 and figure 5.36. Figure 5.35 (c) shows ZnSe-ZB is a direct band gap compound semiconductor of 1.46eV. As we see crossing over of orbital in figure 5.36 at the Fermi line indicates metallic nature of ZnSe-RS.

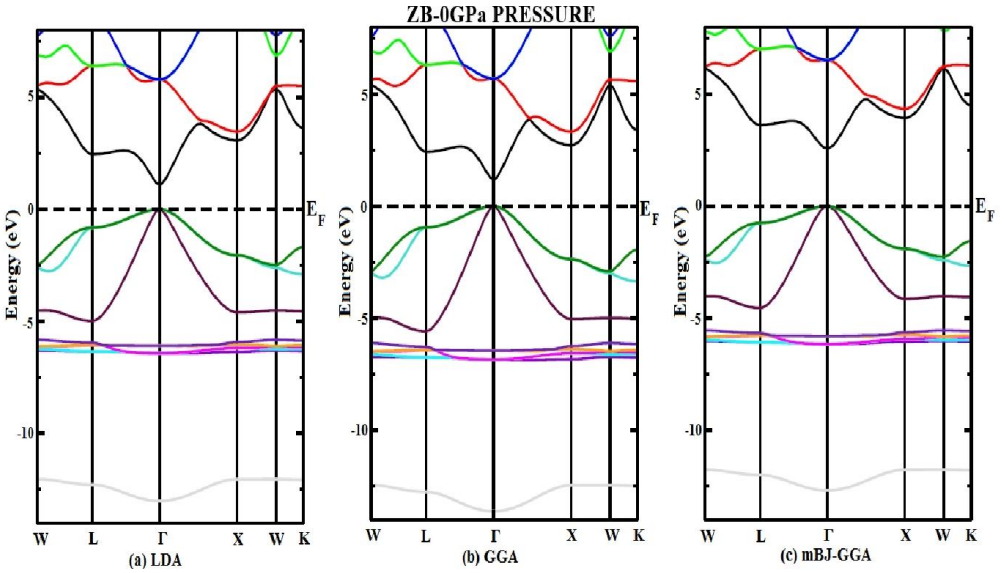

Figure 5.35. Band structure of ZnSe-ZB at 0 GPa pressure within (a) LDA, (b) GGA and (c) mBJ-GGA

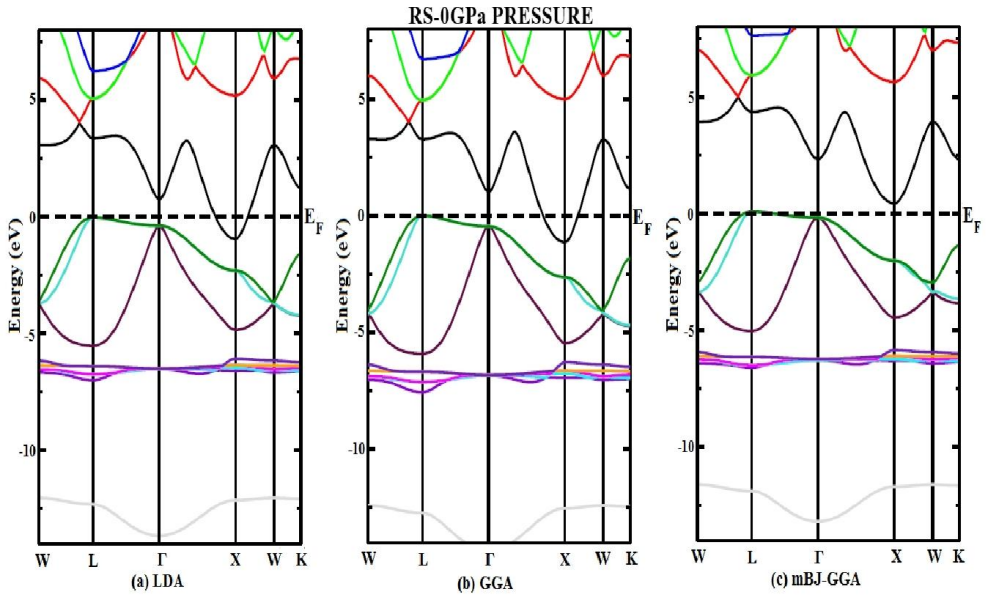

Figure 5.36. Band structure of ZnSe-RS at 0 GPa pressure within (a) LDA, (b) GGA and (c) mBJ-GGA

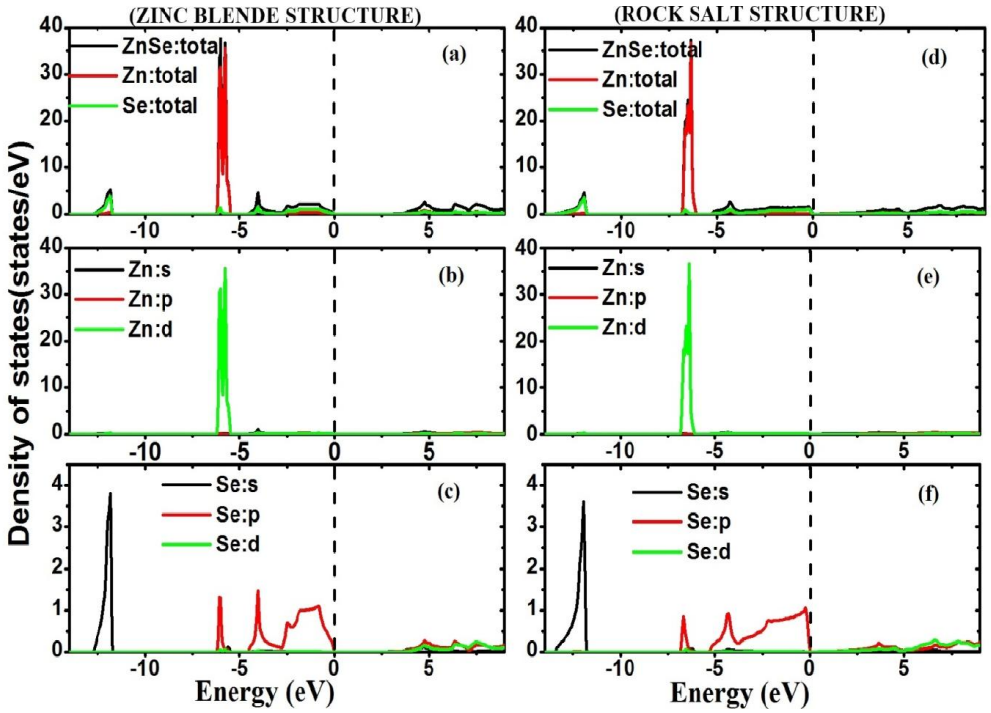

Figure 5.37. Total and Partial DOS of ZnSe-ZB and ZnSe-RS within mBJ-GGA

The total and partial DOS of ZnSe for both the phases within mBJ-GGA are shown in figure 5.37 (a-f). For the ZB phase, in figure 5.37(a), (b) and (c), we see that the lowest band is mainly contributed from s-non metal (Se atom) orbital with little contribution from the p-metal (Zn atom) orbital and d-metal (Zn atom) orbital while the valance band is mainly contributed by the d-metal

(Zn atom) orbital along with little contribution from the p-non metal (Se-atom) orbital. Again from figure 5.37(d), (e) and (f) for RS phase we find that the lowest band is mainly contributed by the s-non metal (Se atom) orbital while the valance band is mainly contributed by the d-metal (Zn-atom) and a small contribution from p-metal orbital with p-non metal (Se-atom) orbital.

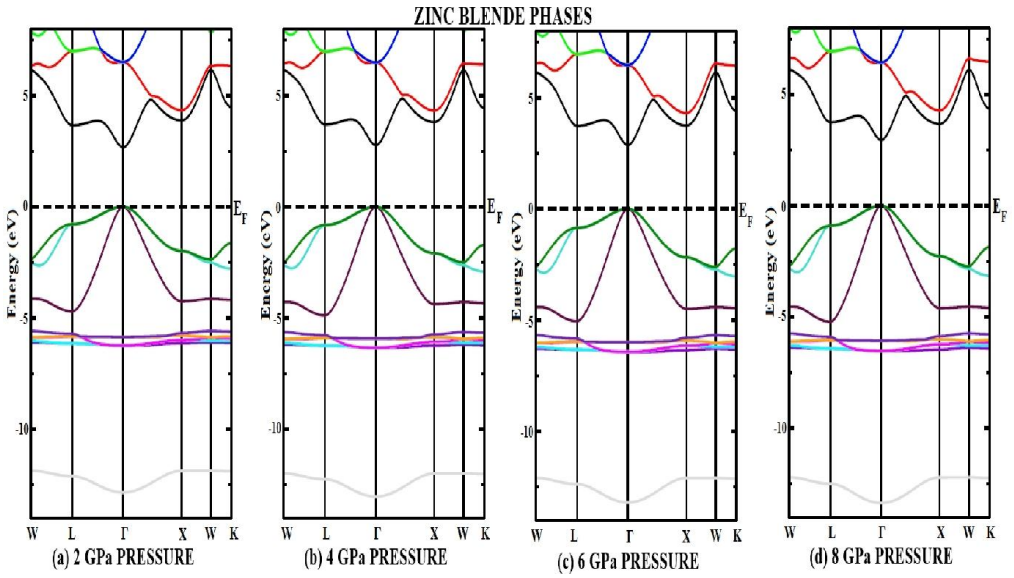

Figure 5.38. Energy band diagram ZnSe-ZB at (a) 2 GPa pressure (b) 4 GPa pressure, (c) 6 GPa pressure and (d) 8 GPa pressure

In figure 5.38 (a, b, c and d), the energy band diagrams of ZnSe-ZB at different pressures show the increase of gap at Γ- Γ point as pressure increases. Figure 5.39 shows the variation in the energy band gap between Γ-Γ point, Γ-X point and Γ-L with pressure for better understanding of the changes in the energy band gap. In figure 5.40 (a, b, c and d), the energy band diagram of ZnSe-RS phase at different pressures show the metallic nature and is observed to be retained metallic even at high pressure without much variation.

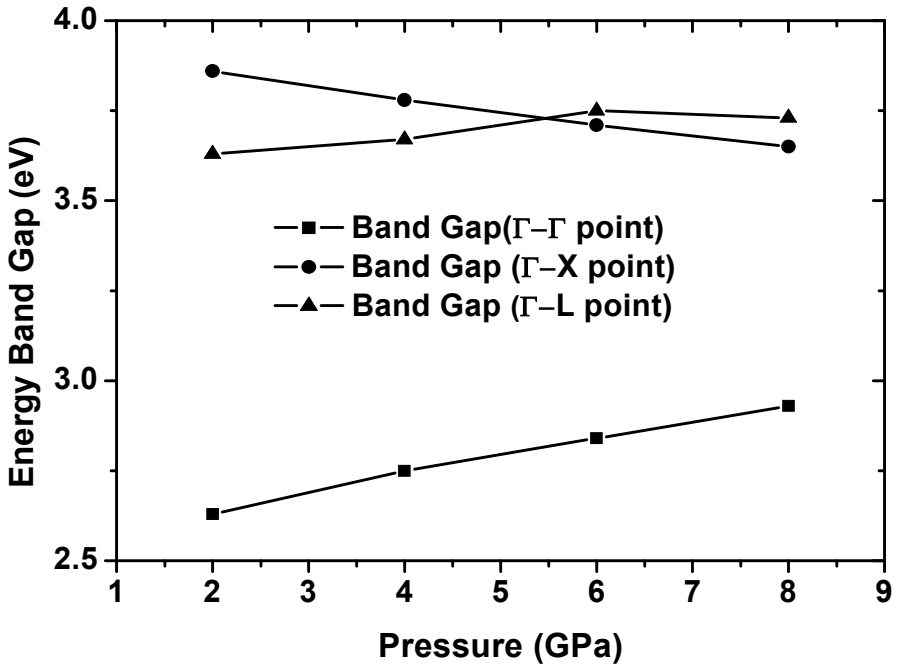

Figure 5.39. Variation of Energy band gaps of ZnSe-ZB phase with pressure.

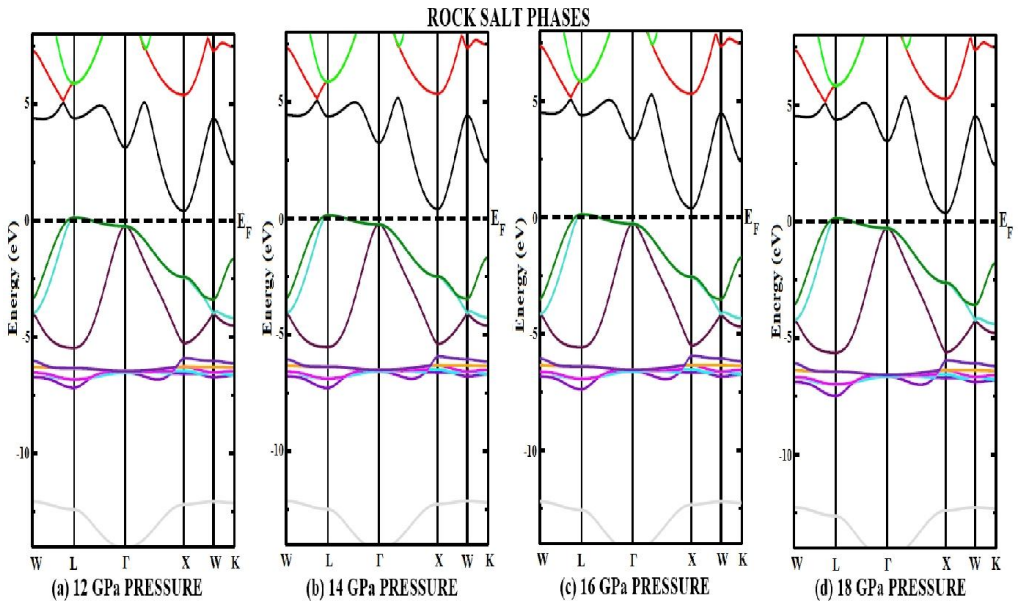

Figure 5.40. Energy band diagram ZnSe-RS at (a) 12 GPa pressure (b) 14 GPa pressure, (c) 16 GPa pressure and (d) 18 GPa pressure.

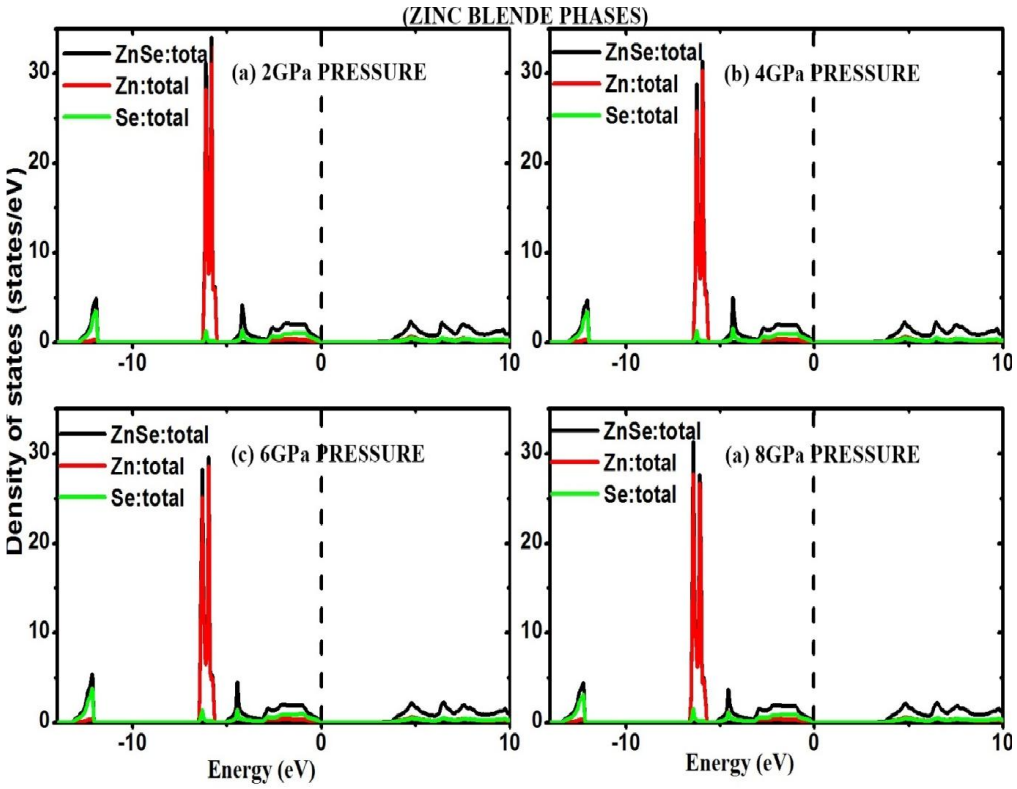

Figure 5.41. Total DOS of ZnSe-ZB at (a) 2 GPa pressure (b) 4 GPa pressure (c) 6 GPa pressure and (d) 8 GPa pressure.

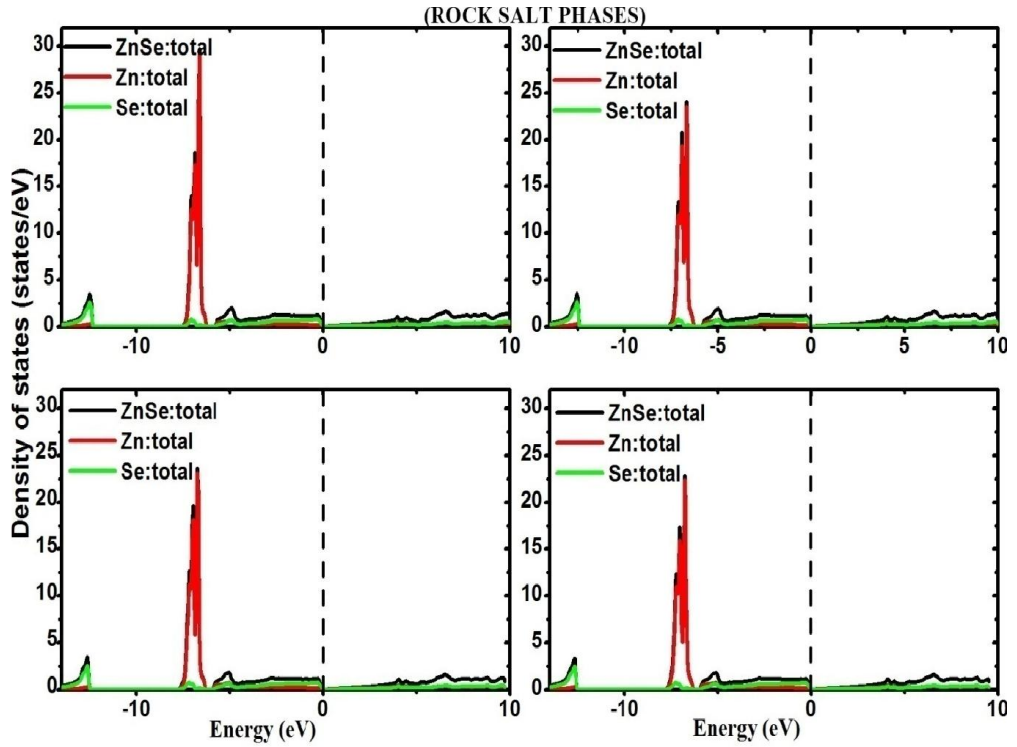

Figure 5.42. Total DOS of ZnSe-RS at (a) 12 GPa pressure (b) 14 GPa pressure (c) 16 GPa pressure and (d) 18 GPa pressure.

The total DOS of ZnSe-ZB at (a) 2 GPa pressure (b) 4 GPa pressure (c) 6 GPa pressure and (d) 8 GPa pressure (in figure 5.41) show the variation of the wide of the valence and conduction band with increase in pressure. Also the DOS plots of ZnSe-RS at (a) 12 GPa (b) 14 GPa (c) 16 GPa and (d) 18 GPa pressure (in figure 5.42) show the crossover of band at Fermi line that supports the retention of metallic nature of ZnSe-RS as observed in band diagram under pressure discussed above.

5.5. CONCLUSION

In this chapter, we have studied the structural properties of group II-VI compound semiconductors (ZnS, CdTe and ZnSe) in both ZB and RS structures. Our results are found to be in good agreement with the experimental and theoretical results.

i. The structural parameters of ZnS, CdTe and ZnSe are calculated within both the LDA and GGA as shown in table 5.1, table 5.4 and table 5.7.
ii. The structural phase transition from the zincblende (ZB) to rocksalt (RS) phase of ZnS, CdTe and ZnSe are found to occur at 17.6 GPa pressure with a volume collapse of 12.86%, 4.0 GPa pressure with a volume collapse of 20.9% and 11.5 GPa pressure with a volume collapse and 13.74% respectively.
iii. The elastic constants (C_{11}, C_{12} and C_{44}) of both the phases are calculated and found to satisfy the mechanical stability conditions The corresponding elastic parameters (Zener Anisotropy factor (A), Poisson's ratio (υ), Kleinmann parameter (ζ), B/G ratio, Young's modulus (Y) and Deby's temperature (θ_D)) are also calculated.
iv. The energy band structures of ZnS, CdTe and ZnSe at zero pressure (in ZB and RS structure) are calculated using the LDA, GGA and mBJ-GGA methods.
    - ZnS-ZB structure is a direct band gap semiconductor and energy band gap calculation with LDA and GGA shows a band gap of 1.89 eV and 1.99 eV respectively while calculation within mBJ-GGA gives a band gap of 3.5 eV which is close to experimental

result. In case of ZnS-RS, it is found to be an indirect band gap compound semiconductor of 1.1eV (within mBJ-GGA).

- CdTe in ZB phase is a direct band gap semiconductor of 1.46eV (within mBJ-GGA method) and CdTe-RS show metallic character.
- Similarly, ZnSe-ZB is found to be a direct band gap semiconductor of 2.5 eV (within mBJ-GGA method) while ZnSe-RS is metallic.

v. The DOS plots for the ZB and RS structures at zero pressure are studied within the mBJ-GGA only and at different pressures.

- In all the three compounds (ZnS-ZB, CdTe-ZB and ZnSe-ZB) we find that with increasing pressure the energy band gap between the Γ- Γ point and Γ-L increases but the gap between Γ-X are found to decrease.
- But for the RS phases, we find that the indirect band gap of ZnS and metallic nature of CdTe and ZnSe are retained even at high pressure without much variation.

Hence we conclude that the energy band gap of ZB phases of ZnS, CdTe and ZnSe are affected by pressure while the energy band gaps of the RS phases are not much affected by pressure.

CHAPTER 6: EFFECT OF DOPING: InP doped with Ga ($In_xGa_{(1-x)}P$)

The increase in technology has resulted in attempts to uncover credible alternatives for improving the optoelectronic device performances which has led to the study of Group III-V alloys. Also the possibility of controlling the physical properties of these alloys in different composition offers immense scope and advantage resulting in a number of theoretical and experimental studies. Among the III-V semiconductors, InP and GaP have attracted special attention on technological studies. In this chapter, we study the Structural properties, Phase transition and Electronic structure of InP doped with Ga that is $In_xGa_{(1-x)}P$ alloys for the composition x =0, 0.25, 0.5, 0.75, 1.

6.1. Structural properties and Phase transition

As discussed above in chapter 4, DFT based ab-initio method is used for investigating structural phase transition under induce pressure and electronic structure of InP alloys ($In_{1-x}Ga_xP$: x = 0, 0.25, 0.5, 0.75, 1). The alloys are modeled at some selected compositions (x = 0.0, 0.25, 0.50, 0.75, 1.0) with structures described in terms of periodically repeated supercells. The minimization of the total energy with respect to the cell parameters give optimized structure, the equilibrium lattice parameter and bulk modulus are obtained fitting to the Birch-Murnaghan equation of states [85]. The energy versus volume curve for both zinc blende (B3) and rock salt (B1) structures at different composition are shown in figure 6.1. The calculated equilibrium parameters are summarized in table 6.1. It is observed that InP for x=0.0 and GaP for x=1.0 whose comparison data are available and our results are in good agreement.

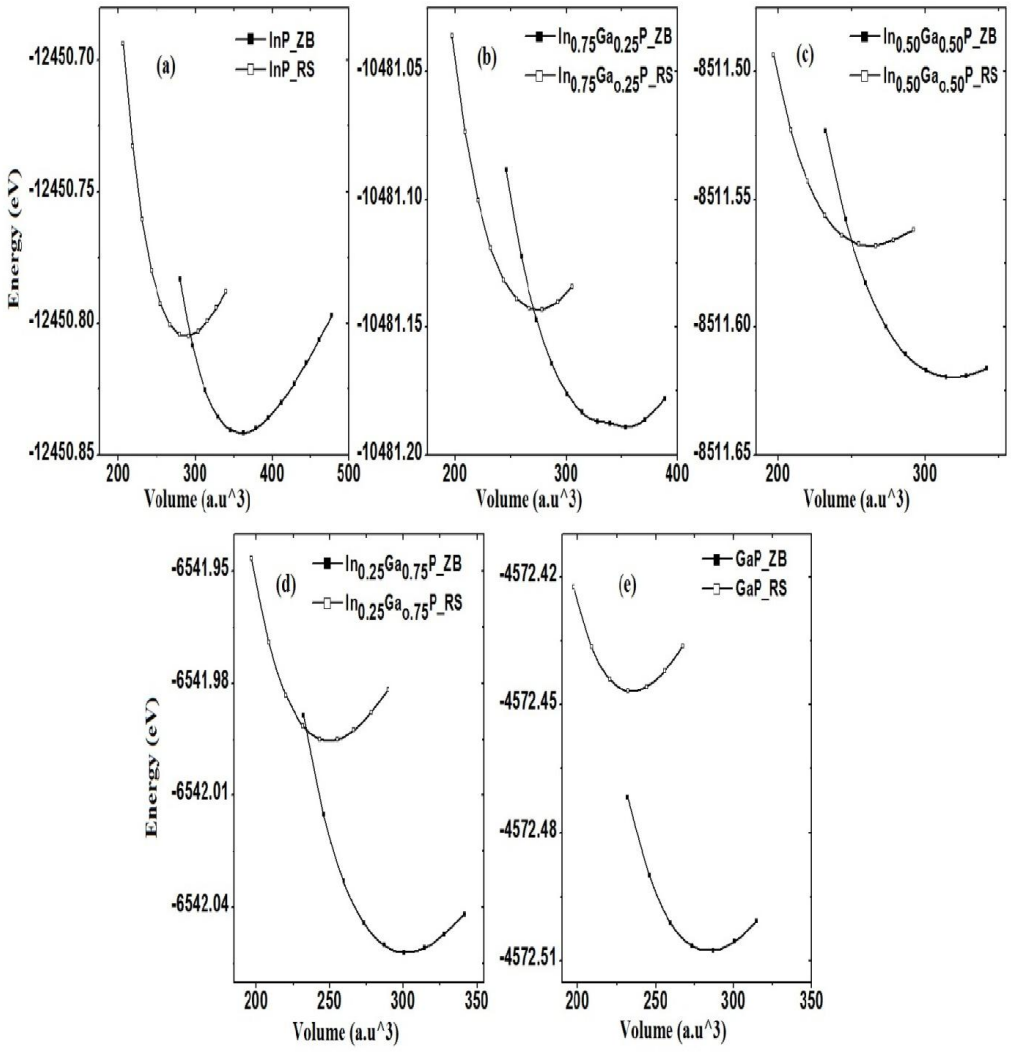

Figure 6.1. Energy versus volume curve of $In_{1-x}Ga_xP$ alloy within GGA in ZB and RS structure at different concentration of x

Table 6.1. Lattice parameters of $In_{1-x}Ga_xP$ alloy (in ZB and RS structure) at different concentration of x.

		Zinc Blende			Rock Salt		
		a_0	B_0	$B^/$	a_0	B_0	$B^/$
InP	Present work	5.9	60.5	4.64	5.54	74.78	4.76
	Expt. results	5.90[a], 5.87[b]	65.5[d], 72[e]	4.59[c]	5.71[b], 5.24[b]	-	-
	Other Theo. results	5.94[b], 5.95[c]	68[b], 71[f]	4.9[b], 4.67[g]	-	-	-
$In_{0.75}Ga_{0.25}P$	Present work	5.851	65.161	4.424	5.461	76.753	4.600
$In_{0.5}Ga_{0.5}P$	Present work	5.738	67.722	4.468	5.377	78.496	4.703
$In_{0.25}Ga_{0.75}P$	Present work	5.633	72.017	4.566	5.288	82.653	4.741
GaP	Present work	5.523	77.70	4.347	5.181	88.303	4.840
	Expt. results	5.47[h], 5.50[i], 5.45[j]	77.2[i]	4.88[i],	-	-	-
	Other Theo. results	5.41[k], 5.54[l], 5.51[m]	90.0[k], 76.0[m]	4.50[k], 4.59[m]	5.165[n], 5.160[o]	87.3[n], 87.59[o]	3.78, 4.54[o]

[a]Ref[104], [b]Ref[105], [c]Ref[106], [d]Ref[107], [e]Ref[108], [f]Ref[110], [g]Ref[111], [h]Ref[82], [i]Ref[84], [j]Ref[83], [k]Ref 12], [l]Ref[85], [m]Ref[13], [n]Ref[86], [o]Ref[13]

According to Vegard's law [160,161] there is a linear relation between crystal lattice constant of an alloy and composition 'x' at constant temperature.

$$a_{(A_{1-X}B_XC)} = x(a_{AC}) + (1-x)(a_{BC}) \tag{6.1}$$

where a_{AC} and a_{BC} are the equilibrium lattice constants of the binary compounds AC and BC respectively and $a_{(A_{1-x}B_xC)}$ is the lattice constant of the alloy.

For the $In_{1-x}Ga_xP$ alloy, we can write

$$a_{(In_{1-X}Ga_XP)} = x(a_{InP}) + (1-x)(a_{GaP}) \tag{6.2}$$

where a_{InP} and a_{GaF} are the equilibrium lattice constants of the binary compounds AC and BC respectively and $a_{(In_{1-x}Ga_xP)}$ is the lattice constant of the alloy. But deviation in the semiconductor alloys from Vegard's law in experimental [162] and theoretical [163,164,165,166.167] studies resulted in the description of the lattice constant as:

$$a_{(In_{(1-x)}Ga_xP)} = xa_{InP} + (1-x)a_{GaP} - x(1-x)b \tag{6.3}$$

where the quadratic term 'b' is the bowing parameter.

The Composition dependence of the calculated lattice parameter (A^0) and Bulk modulus (B) within GGA in (a) ZB and (b) RS structure as compared with Vegard's prediction is given in figure 6.2 and figure 6.3 respectively. Our results of the calculated lattice parameter in figure 6.2 shows an almost linear variation with a marginal downward bowing parameter of 0.02823 A^0 for ZB structure and an upward bowing parameter of -0.07189A^0 for the RS structure.

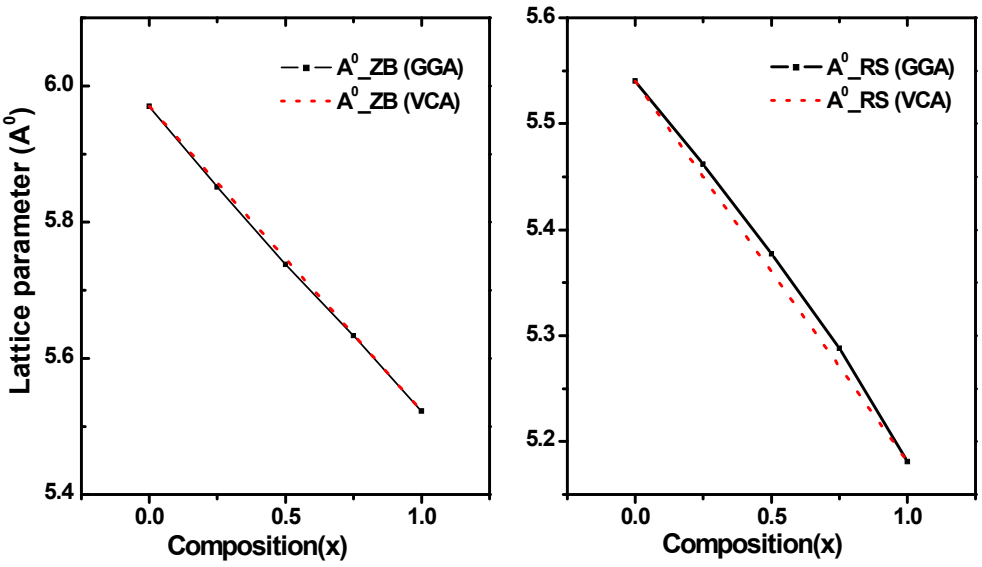

Figure 6.2. Composition dependence of lattice parameter (A^0) within GGA in (a) ZB and (b) RS structure of $In_{1-x}Ga_xP$ alloy as compared with Vegard's prediction.

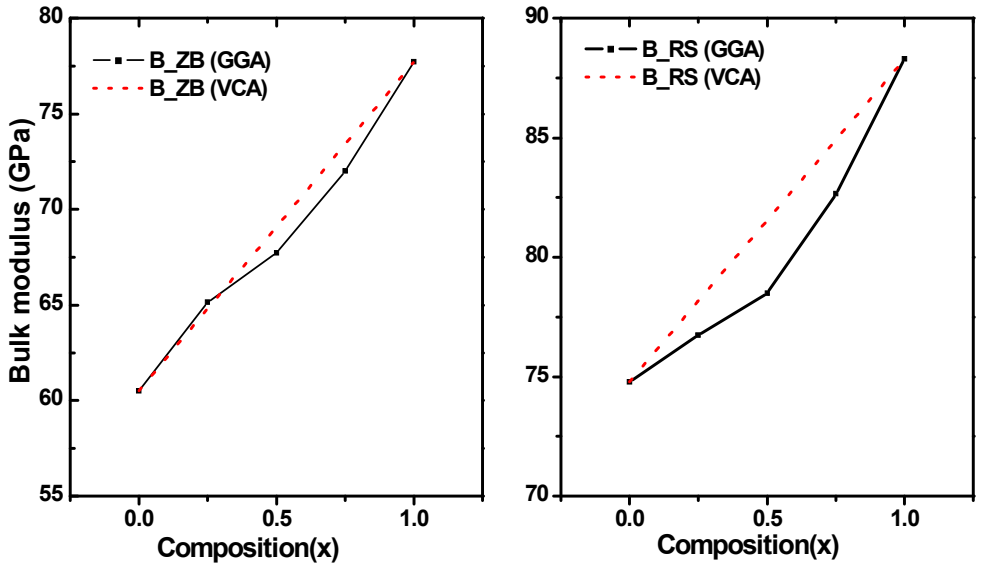

Figure 6.3. Composition dependence of bulk modulus within GGA in (a) ZB and (b) RS structure of $In_{1-x}Ga_xP$ alloy as compared with Vegard's prediction

For the bulk modulus in figure 6.3 we find that for both ZB and RS structure there is a deviation from the linear concentration dependence with a downward bowing parameter of 4.33704 GPa and 11.1624 GPa respectively. This deviation is mainly due to the bulk modulus mismatch between InP and GaP.

It is clearly seen that the lattice constant of In_{1-x} Ga_xP alloy linearly decreases while the bulk modulus increases as the concentration of 'x' increases representing the bond weakening or strengthening effects induced by changing the Ga composition in InP. In other sense, the compressibility decreases as the concentration 'x' (of doping Ga atom) increases in InP. Thus it concludes that compressibility from high to low is: InP > $In_{0.75}$ $Ga_{0.25}$ P > $In_{0.5}$ $Ga_{0.5}$ P >$In_{0.25}$ $Ga_{0.75}$ P > GaP. Thus from InP (x=0.0) to GaP (x=1.0), it generally becomes less compressible resulting harder InP as compare to GaP. This may be due to lower mass of Ga atom than In atom in the alloy.

The formation energy (E_f) for $In_{1-x}Ga_xP$ has also been calculated by using the following relationship:

$$E_f = E_{In_{(1-x)}Ga_xP} - [(1-x)E_{InP} + xE_{GaP}] \quad (6.4)$$

at different concentrations. The calculated formation energies of $In_{1-x}Ga_xP$ alloy as a function of Ga for zinc blende and rock salt phase are given in table 6.2 suggesting that a phase separation is preferable for this system.

Table 6.2. Formation energies of $In_{1-x}Ga_xP$ (for zinc blende and rock salt phase) alloy at different concentration of x

	Composition	**E_f (ZB)**	**E_f (RS)**
$In_{0.75}Ga_{0.25}P$	0.25	0.070	0.072
$In_{0.5}Ga_{0.5}P$	0.50	0.055	0.057
$In_{0.25}Ga_{0.75}P$	0.75	0.039	0.015

The structural phase transition from ZB to RS phase at different composition of x (0.0, 0.25, 0.5, 0.75, 1.0) for $In_{1-x}Ga_xP$ alloys are determined by calculating the Gibbs free energy G. The phase with the lowest Gibbs energy at a given pressure and temperature determines the enthalpy of the phase. As mentioned above (chapter 4 and chapter 5), our calculation is done at zero temperature we e ignored the entropy contribution. Therefore the structural phase transition is calculated from the condition of equal enthalpies i.e. $H = E + PV$. Figure 6.4 shows the variation of Enthalpy with pressure for both the LDA and GGA methods. The enthalpy as a function of pressure at different composition are shown in figure 6.4. The obtained results of transition pressure for different concentration of $In_{1-x}Ga_xP$ alloy is given in table 6.3.

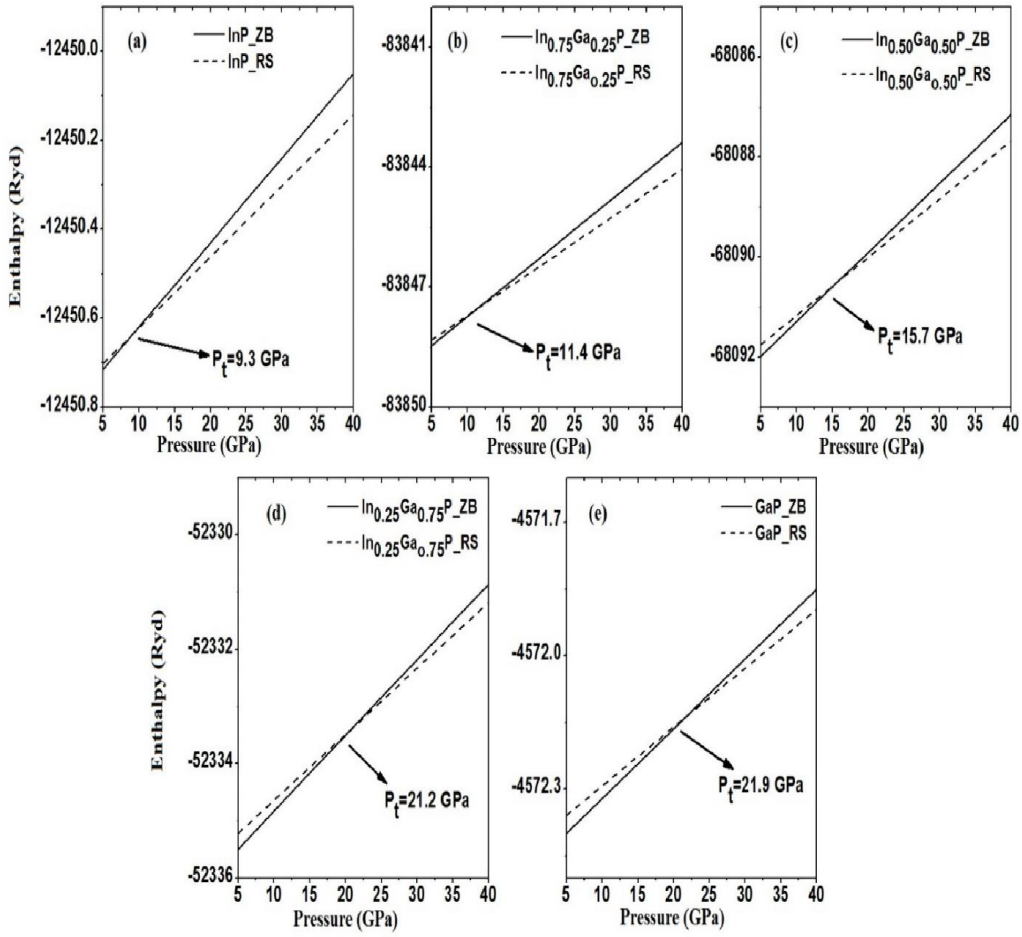

Figure 6.4. Enthalpy versus Pressure of $In_{1-x}Ga_xP$ alloy at different concentration of x

Table 6.3. Transition pressure of $In_{1-x}Ga_xP$ alloy at different concentration of x

	Phase transition (P_t) GPa		
	Present work	**Expt. Results**	**Theo. results**
InP	9.3	9.5[a],10.3±0.2[b], 9.8[c]	7.3[d], 7.5[e], 8.5[f],11.0[g]
$In_{0.75}Ga_{0.25}P$	11.4	-	-
$In_{0.5}Ga_{0.5}P$	15.7	-	-
$In_{0.25}Ga_{0.75}P$	21.2	-	
GaP	21.9	22[h],24±0.3[i], 21.5±0.8 [j]	21.7[k], 18.8[l], 16.8[m],

[a]Ref[27], [b]Ref[28], [c]Ref[105], [d]Ref[25], [e]Ref[112], [f]Ref[93], [g]Ref[94], [h]Ref[87], [i]Ref [88], [j]Ref [89], [k]Ref [90], [l]Ref [91], [m]Ref [92]

The present study of transition pressure of InP and GaP are found to be in close agreement with other experimental and theoretical results. In cases where the experimental and theoretical data are not available at concentrations (x= 0.25, 0.50 and 0.75), the present result may serve as a reference. In figure 6.4 the phase transition of $In_{1-x}Ga_xP$ alloys at different concentration of x (0.0, 0.25, 0.50, 1.0) are shown. From the figure, we can clearly see that introduction of Ga at the site of InP increases the transition pressure.

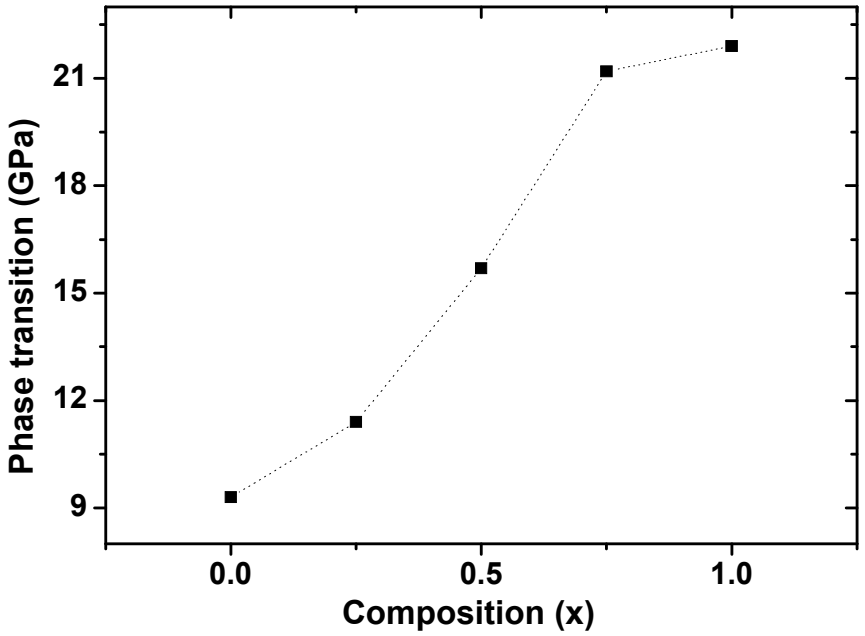

Figure 6.5. Phase transition of $In_{1-x}Ga_xP$ alloy at different concentration of x

6.2. Electronic Properties

Energy band diagram of $In_{1-x}Ga_xP$ alloy (in both zinc blende and rock salt structure) are calculated at different concentrations using the obtained equilibrium lattice constant and are shown in figure 6.6 and figure 6.7 respectively.

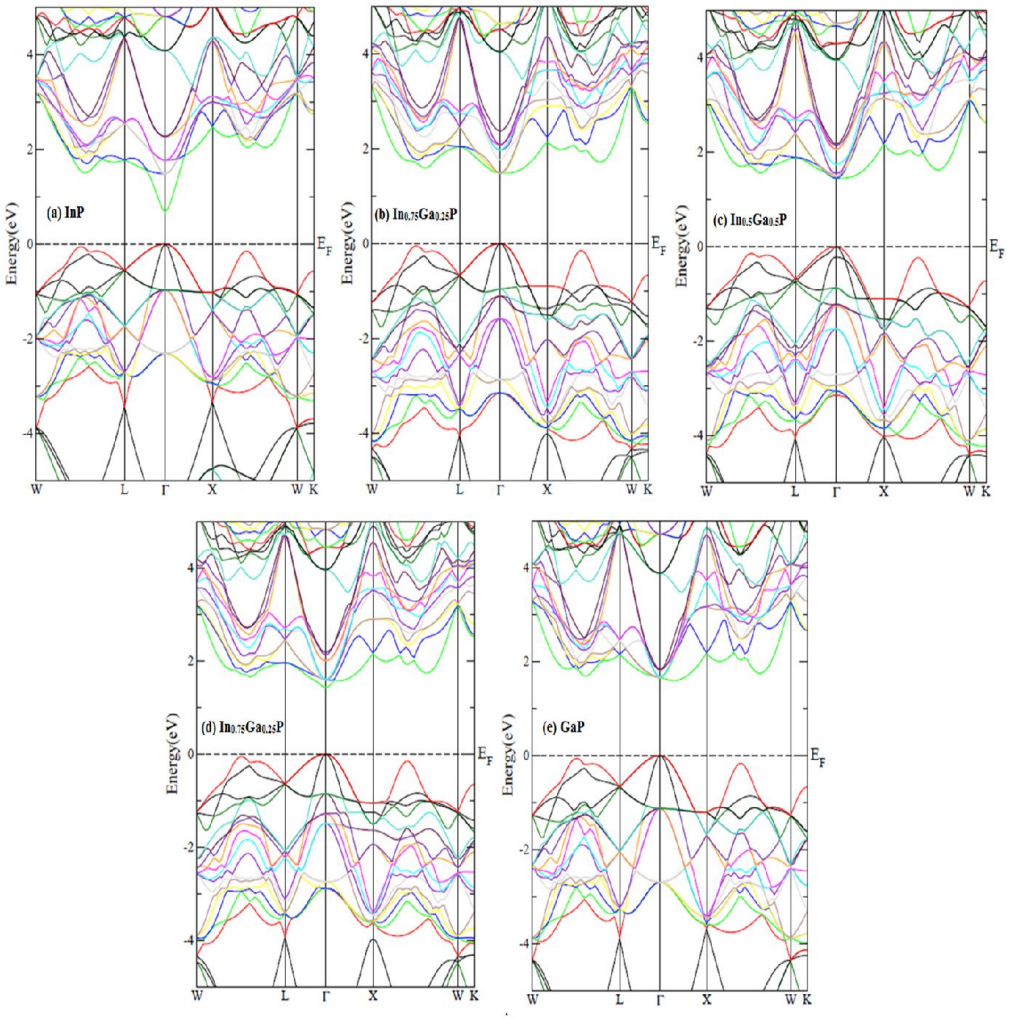

Figure 6.6. Energy band diagram of $In_{1-x}Ga_xP$ (zincblende phase) alloy at different concentration of x

From figure 6.6, we observe that for InP (x=0.0) is a direct band gap of 0.58 eV while in case of GaP (x=1.0), is an indirect band gap of 1.56 eV. This has also been discussed earlier in chapter 4 [25,88,107,116]. It is noted that with increase

in concentration of x (0.25, 0.5, 0.75) in $In_{1-x}Ga_xP$ alloy, the direct band gap is found to increase upto a concentration of 0.25 but as the composition of 'x' increases it starts decreasing. The band gap of present study of $In_{1-x}Ga_xP$ (zinc blende phase) alloy at different concentration of 'x' are compared with other available experimental, theoretical data and are shown in table 6.4. Our results are found to be smaller than the experimental results which are expected as GGA calculation within DFT generally underestimates the energy band gaps. This decrease in the band gap may be due to structural relaxation of the alloy and charge exchange that are respectively proportional to the difference in the atomic orbital sizes. Finally at a concentration of x=1.0, $In_{1-x}Ga_xP$ alloy becomes in its pure form of GaP that becomes indirect as discussed above. This transition from the direct to indirect band gap is due to strong hybridization of the Ga and In with P which results in the splitting off of the conduction band at the Γ point producing another conduction band minimum between the Γ-X points resulting in an indirect band gap. The transition from the direct to indirect energy band gap may also be explained in terms of the ordering induced evolution of band states at high symmetry points and their consequent folding into the same symmetry states in the ordered ternary alloys [168]. In Figure 6.7, the energy band diagrams of $In_{1-x}Ga_xP$ (rock salt phase) alloy at different concentration of 'x' show crossing over of the conduction band and the valance band at the Fermi energy thus indicating metallic character of the $In_{1-x}Ga_xP$ alloy (in rock salt structure) at all concentrations of x.

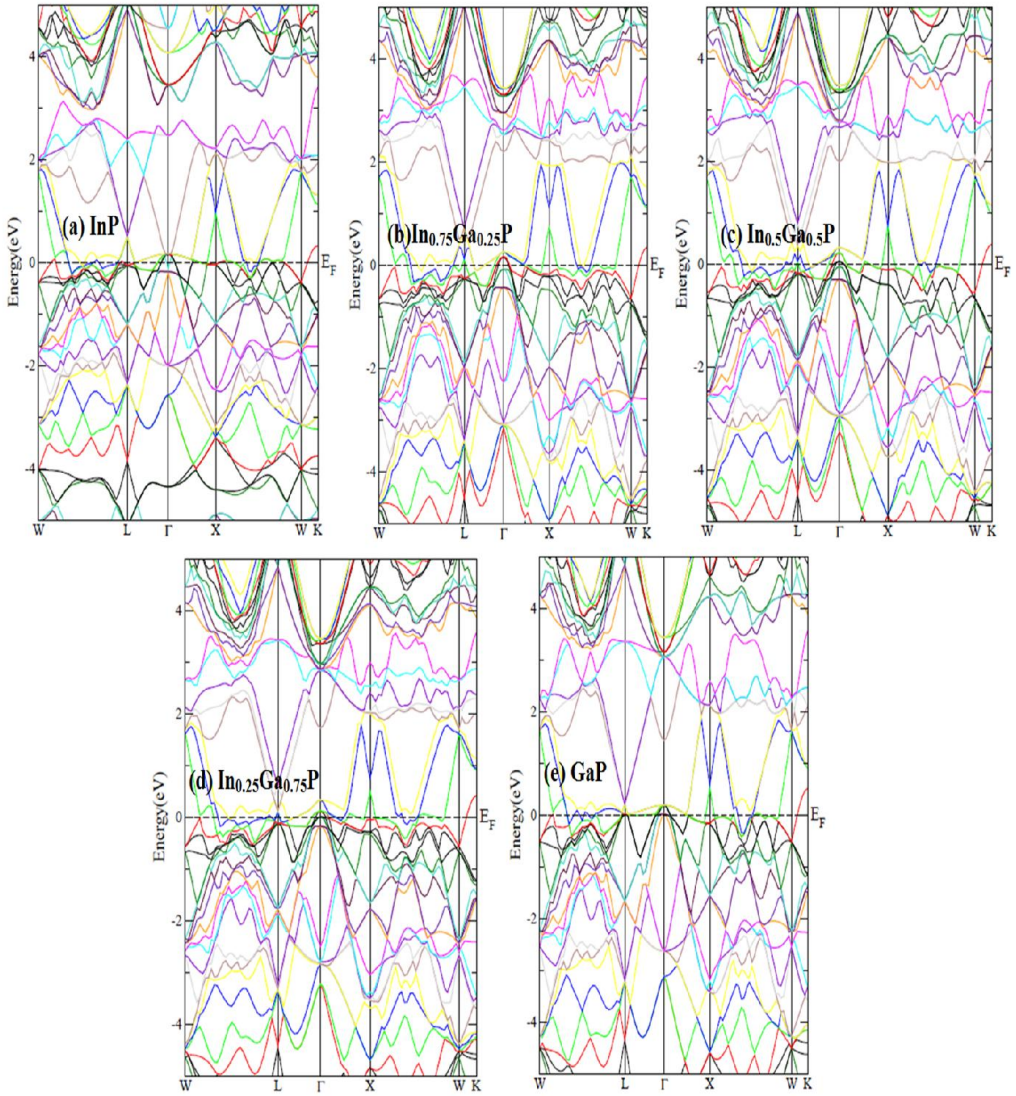

Figure 6.7. Energy band diagram of $In_{1-x}Ga_xP$ (rocksalt phase) alloy at different concentration of x.

Table 6.4. Calculated energy band gap of $In_{(1-x)}Ga_xP$:

	Concentration (x)		**Energy Band Gap**
InP	0.0	Γ-Γ	0.58 (direct)
$In_{0.75}Ga_{0.25}P$	0.25	Γ-Γ	1.46 (direct)
$In_{0.5}Ga_{0.5}P$	0.50	Γ-Γ	1.44 (direct)
$In_{0.25}Ga_{0.75}P$	0.75	Γ-Γ	1.37 (direct)
GaP	1.0	between Γ-X	1.56 (Indirect)

To further understand the effects of atomic relaxation on the electronic band structure of $In_{1-x}Ga_xP$ (zinc blende phase) alloy, the total density of states (TDOS) and partial density of states (PDOS) are calculated and shown in figure 6.8(a, b, d, e). For the compound InP (x=0.0) we see that p state (of P atom) is concentrated at the valance band minimum (VBM) while the conduction band minimum (CBM) is mainly formed by the s state (of In atom) and p state (of P atom). When the concentration x=0.25 of Ga atom is doped in InP, we find a presence of p state (of Ga atom) along with the p state (of P atom) in the VBM, while in the CBM there is an equal contribution of the s state (of Ga atom) and s state (of In atom) but replacement of the Ga atom in the In atom causes shifting of the states towards higher energy resulting an increase in the energy band gap. As the concentration of Ga (x=0.5) increases there is a push in the s orbital (of Ga atom) in the CBM towards the Fermi energy causing reduction in the energy band gap with the VBM fixed. More increase in the concentration of Ga (x=0.75) causes all s state (of Ga atom) and s state (of In atom) to push towards the Fermi energy further reducing the energy band gap to 1.37 eV. We also see that as the concentration of 'x' increases, the contribution of the s state (of Ga atom) in the CBM increases while the p state (of P atom), p state (of Ga atom) and p state (of In atom) becomes more concentrated towards the VBM. Finally when all the In atoms are replaced by the Ga atom, we find that in the CBM the s state (of Ga atom) and p state (of P atom) increases along with the p state (of Ga atom).

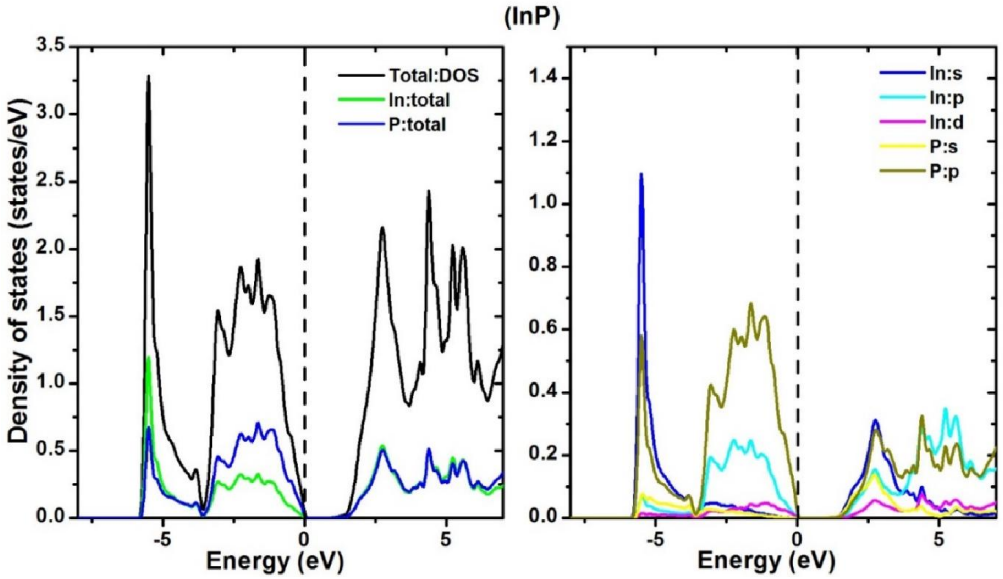

Figure 6.8(a). Total and partial DOS of InP-zinc blende phase

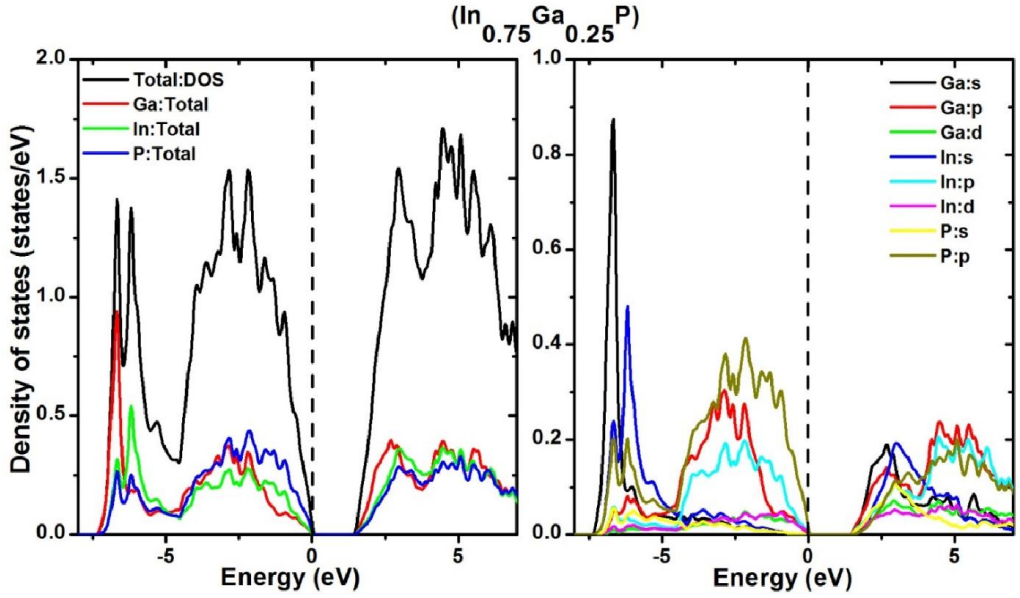

Figure 6.8(b). Total and partial DOS of $In_{0.75}Ga_{0.5}P$-zinc blende phase

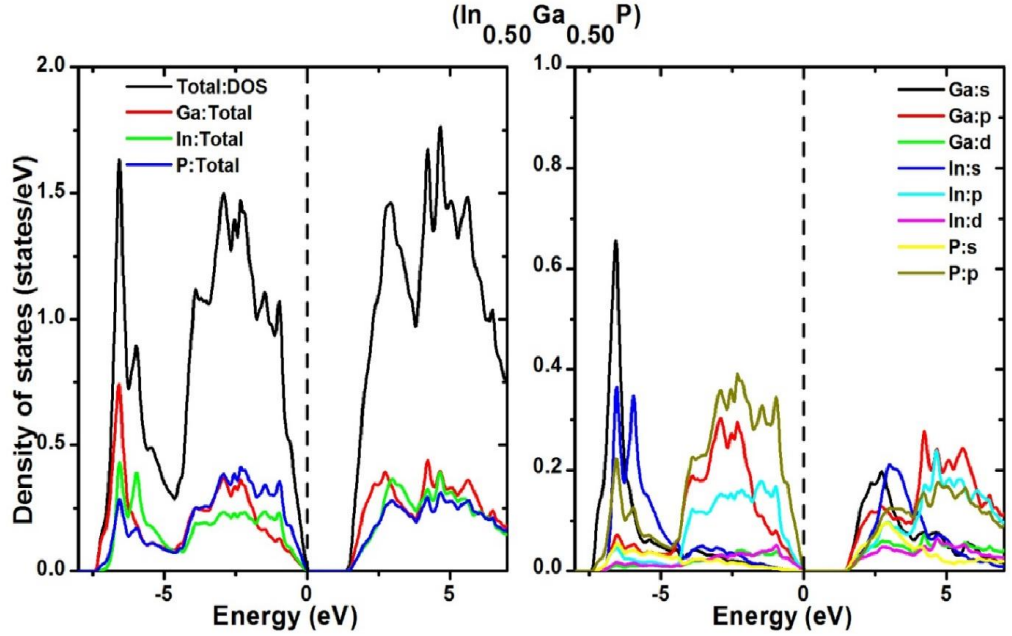

Figure 6.8(c). Total and partial DOS of $In_{0.50}Ga_{0.5}P$-zincblende phase

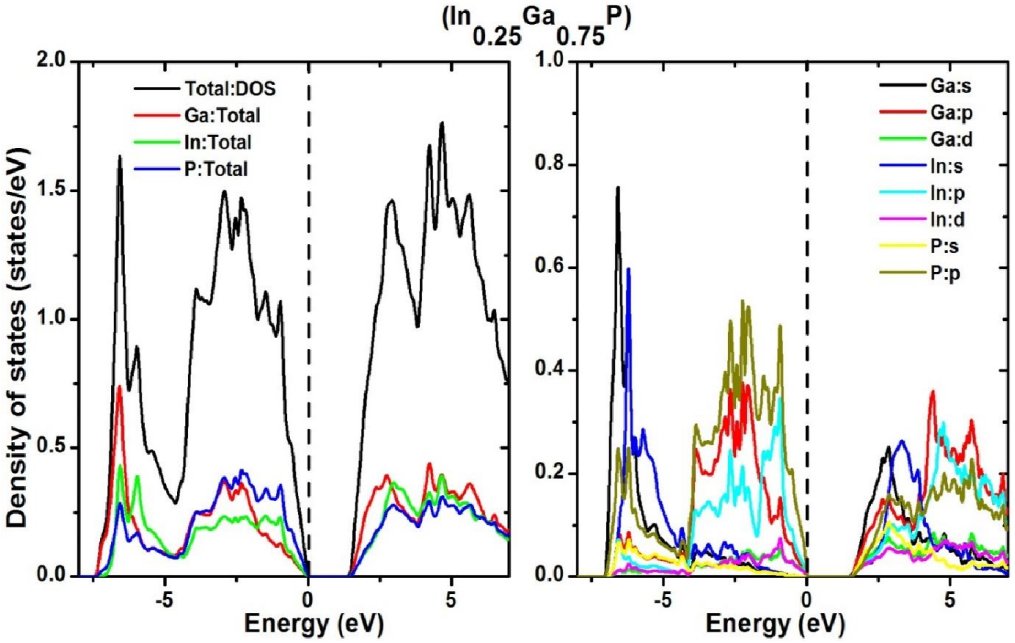

Figure 6.8(d). Total and partial DOS of $In_{0.25}Ga_{0.75}P$-zinc blende phase

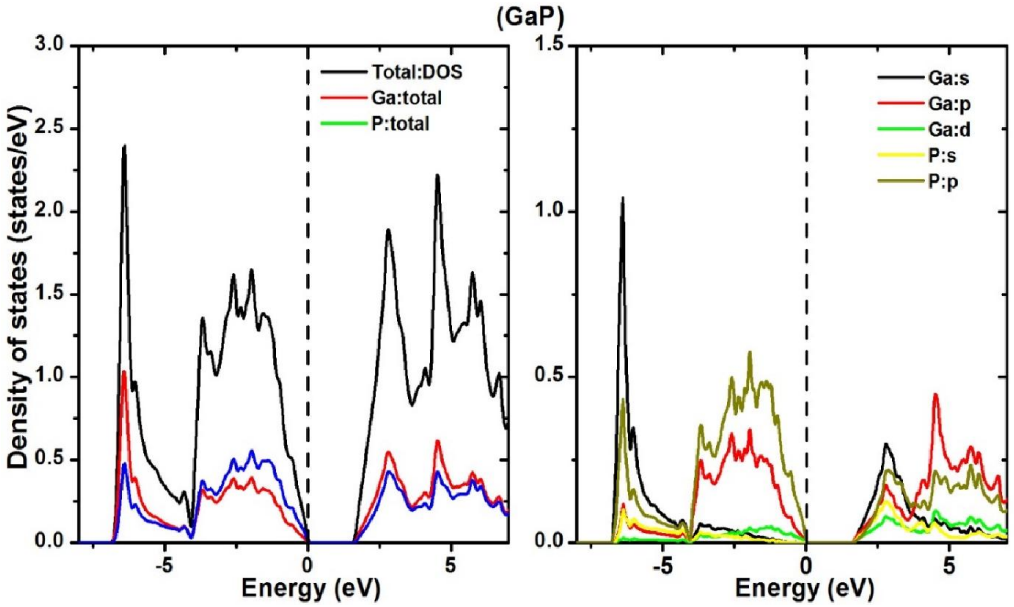

Figure 6.8(e). Total and partial DOS of GaP-zinc blende phase

6.3. Conclusion

The structural and electronic properties of $In_{1-x}Ga_xP$ alloy (in both zincblende and rocksalt structures) are studied at different concentration of Ga atom (x = 0.0, 0.25, 0.50, 1.0).

i. The composition dependence of the lattice constant and bulk modulus in both the phases are calculated and found to have a linear dependence obeying Vegard's law.

ii. The bulk modulus of $In_{1-x}Ga_xP$ alloy increases with increasing concentration of Ga atom which indicates larger in the strength of the alloy and thus makes it less compressible.

iii. The formation energy at different concentrations of 'x' for both the phases are also calculated. The phase transition from zincblende to rocksalt phase for the alloy with different doping concentrations of Ga are also studied and transition pressure is found to increase with increasing concentration.

iv. The study on the energy band gap of $In_{1-x}Ga_xP$ (zincblende phase) alloy shows a non linear behavior with concentration. We find that the direct energy band gap of InP increases as the concentration of Ga atom increases upto 0.25. After that it starts decreasing with concentration (x=0.5, 0.75) and finally it becomes indirect band gap of GaP at x=1.0.

v. The DOS study confirms that doping of Ga atom increases the energy band gap with respect to InP compound as predicted in energy band diagrams.

vi. For $In_{1-x}Ga_xP$ (rocksalt phase) alloy at different concentration of 'x' shows crossing over of conduction band and valance band at Fermi level thus showing metallic character of the $In_{1-x}Ga_xP$ (rocksalt phase) alloy at all the concentrations of 'x'.

CHAPTER 7: OVERALL CONCLUSION AND OUTLOOK

In this thesis, we have reported a complete study on the structural phase transition, elastic properties and electronic properties of Group III-V (GaP, GaAs, InP, InAs) and Group II-VI (ZnS, CdTe and ZnSe) compound semiconductors in both zinc blende (ZB) and rock salt (RS) structures. We have also studied the effect of InP doped with Ga: $In_xGa_{(1-x)}P$ alloy at different concentration of Ga. The major outcome of this wok can be summarized as

A. Group III-V Compound semiconductors

The structural properties of GaP, GaAs, InP and InAs has been studied in both zinc blende (ZB) and rock salt (RS) structures. The structural phase transformation from ZB to RS phase under induce pressure for GaP, GaAs, InP and InAs are found to occur at 21.9 GPa pressure with a volume collapse of 14.11%, 10.7 GPa pressure with a volume collapse of 14.2%, 9.3 GPa pressure with a volume collapse of 16.45% and 4.7 GPa pressure with a volume collapse of 17.2% respectively.

The elastic constants (C_{11}, C_{12} and C_{44}) of both the ZB and RS phases of these compounds are found to satisfy the mechanical stability conditions and undergo a linear variation with increase in pressure. The elastic parameters (Zener Anisotropy factor (A), Poisson's ratio (υ), Kleinmann parameter (ζ), B/G ratio, Young's modulus (Y) and Deby's temperature (θ_D) are also calculated.

The energy band structures for GaP, GaAs, InP and InAs (in both the phases) at zero pressure as well as under induced pressures are studied within the LDA, GGA and mBJ-GGA. At zero GPa pressure, we find that calculation within the mBJ-GGA gives us better results (energy band gaps) than the LDA and GGA methods. The ZB structures of GaP is found to be an indirect band gap semiconductor with band gap of 2.33 eV while GaAs, InP, InAs show a direct

energy band gap of 1.3 eV, 1.31 eV and 0.35 eV respectively. The RS structures of the above semiconductor compounds are found to be metallic without much variation under induced pressure.

Further analysis in the band structure of the ZB phase of these semiconductor compound shows an increase in the energy band gap between the Γ-L point and a decrease between Γ-X point towards the Fermi level with increasing pressure indicating possibilities of shifting of the energy bands and crossing over of the conduction band towards the valance band confirming the metallic nature of GaP, GaAs, InP and InAs after structural transformation to the RS phase.

B. Group II-VI compound semiconductors

Following similar trend as in chapter 4, the structural properties, elastic properties and phase transformation from the ZB to RS structure under induced pressure for ZnS, CdTe and ZnSe are studied. We find that the above semiconductor compounds undergo a phase transition from ZB to RS at 17.6 GPa pressure with a volume collapse of 12.86%, 4.0 GPa pressure with a volume collapse of 20.9% and 11.5 GPa pressure with a volume collapse and 13.74% respectively.

The energy band structures study of the ZB phase shows a direct band gap of 1.46 eV, 3.5 eV and 2.5 eV in case of ZnS, CdTe and ZnSe respectively. RS phase for CdTe and ZnSe show a metallic character while ZnS (RS phase) shows an indirect band gap.

We find that implementation of the mBJ-GGA potential in the energy band gap calculation resolves the underestimation of the band gaps with LDA, GGA and provides better results closer to the experimental value while study of the energy band gap under induced pressures reveals that the energy band gap of ZB phases are affected by pressure while the energy band gaps of the RS phases are not much affected by pressure.

C. Effect of Doping: InP doped with Ga ($In_xGa_{(1-x)}P$)

Understanding the doping effect in the compound semiconductors is very important to see the possibility of tailoring physical properties and electronic structure. The structural phase stability from the zinc blende to rock salt structure and electronic structure of $In_{1-x}Ga_{1-x}P$ has been performed to understand the doping effect of Ga in InP compound semiconductor. The lattice parameters of the stable structures of the corresponding doping concentrations are compared with other available theoretical and experimental results and found to be in good agreement with them. The composition effect on the lattice constant, bulk modulus and the formation energy are studied at different concentration of x (= 0.0, 0.25, 0.5, 0.75, 1) for both zinc blende and rock salt structure. The phase transition pressure from zinc blende to rock salt phase in different concentration is found to increase with increase in concentration of Ga. The electronic band structure at different concentration of 'x' has been investigated using the total and partial density of states. The study on the energy band gap of zinc blende phase of $In_{1-x}Ga_xP$ alloy shows a non-linear behaviour with concentration. The direct energy band gap of InP increases as the concentration of Ga atom increases upto 0.25. After that it starts decreasing with concentration (x=0.5, 0.75) and finally change to an indirect band gap of GaP at x=1.0. The DOS study shows an increase in energy band gap in lower concentration of Ga while increase concentration of Ga atom leads to a decrease in the energy band gap. The rock salt phase of $In_{1-x}Ga_xP$ alloy at different concentration of 'x' shows crossing over of the conduction band and the valance band at the Fermi energy thus showing metallic character of the $In_{1-x}Ga_xP$ alloy at all the concentrations of 'x'.

Hence our study constitute a preliminary step to future work dealing with super lattices, complex system semiconductors. It will stimulate experimental studies of high pressures and shed new light on high pressure application of optoelectronic devices.

BIBILOGRAPHY

1. Lide, D.R. (1998). Handbook of chemistry and Physics. CRC Press, Boca Raton, Fla. 87th ed.

2. Robinson, A.L. (1983). GaAs Readied for High-Speed Microcircuits. *Science (New York, NY)*, Vol. 219 No. 4582, pp. 275-277.

3. Harrison, R.J. (1985) Gallium arsenide. *Occupational medicine (Philadelphia, Pa.)*, Vol.1, No. 1, pp. 49-58.

4. Pitt, G.D.; Vyas, M.K.R. (1973). Electrical properties of InAs to very high pressures. *Journal of Physics C: Solid State Physics*, Vol. 6, No. 2, pp.274-284.

5. Wang, Q.; Zhang, J.; Li, R.; Xu, Y.; Miao, X.; Zhang, D. (2014). Metallic behavior and negative differential resistance properties of (InAs) n (n= 2− 4) molecule cluster junctions via a combined non–equilibrium Green's function and density functional theory study. *Journal of Applied Physics*, Vol. 115, No. 23, pp. 233712(1-6)

6. Fawcett, W.; Hilsum, C.; Rees, H.D.; (1969). Effects of non-parabolicity on non-ohmic transport in InAs. *Solid State Communications*, Vol. 7, No. 17, pp. 1257-1259.

7. Jamieson, J.C. (1963). Crystal structures at high pressures of metallic modifications of silicon and germanium. *Science*, Vol. 139, No. 3556, pp. 762-764

8. Jamieson, J.C. (1963). Crystal structures at high pressures of metallic modifications of compounds of indium, gallium, and aluminum. *Science*, Vol. 139, No. 3557, pp. 845-847.

9. Wang, C.S. and Klein, B.M., 1981. First-principles electronic structure of Si, Ge, GaP, GaAs, ZnS, and ZnSe. I. Self-consistent energy bands, charge

densities, and effective masses. *Physical Review B*, Vol. 24, No. 6, pp.3393-3216.

10. Chelikowsky, J.R. (1987). High-pressure phase transitions in diamond and zinc-blende semiconductors. *Physical review B*, Vol. 35, No. 3, pp.1174-1180.

11. Van Camp, P.E., Van Doren, V.E. and Devreese, J.T. (1990). Pressure dependence of the electronic properties of cubic III-V In compounds. *Physical Review B*, Vol. 41, No. 3, pp.1598-1602.

12. Mujica, A.;Needs, R.J. (1997). Theoretical study of the high-pressure phase stability of GaP, InP, and InAs. *Physical Review B*, Vol. 55, No. 15, pp.9659-9670.

13. Ahmed, R.; Hashemifar, S.J.; Akbarzadeh, H. (2008). First-principles study of the structural and electronic properties of III-phosphides. *Physica B: Condensed Matter*, Vol. 403, No.10, pp.1876-1881.

14. Itie, J.P.; Polian, A.; Jauberthie-Carillon, C.; Dartyge, E.; Fontaine, A.; Tolentino, H.; Tourillon, G. (1989). High-pressure phase transition in gallium phosphide: An x-ray-absorption spectroscopy study. *Physical Review B*, Vol. 40, No.14, pp.9709-9714.

15. Weinstein, B.A.; Piermarini, G.J. (1975). Raman scattering and phonon dispersion in Si and GaP at very high pressure. *Physical Review B*, Vol. 12, No. 4, pp.1172-1186.

16. Miller, A.J.; Saunders, G.A.; Yo [Gbar] urtçu, Y.K.; Abey, A.E. (1981). The pressure dependence of elastic constants and bond bending in HgTe. *Philosophical Magazine A*, Vol. 43, No. 6, pp.1447-1471.

17. Froyen, S.; Cohen M. L. (1983). Structural properties of III-V zinc-blende semiconductors under pressure. *Phys. Rev. B*, Vol. 28, No. 6, pp. 3258-3265.

18. Besson, J.M.; Itie, J.P.; Polian, A.; Weill, G.; Mansot, J.L.; Gonzalez, J. (1991). High-pressure phase transition and phase diagram of gallium arsenide. *Physical Review B*, Vol. 44, No. 9, pp. 4214-4234.

19. Weir, S.T.; Vohra, Y.K.; Vanderborgh, C.A.; Ruoff, A.L. (1989). Structural phase transitions in GaAs to 108 GPa. *Physical Review B*, Vol. 39, No. 2, pp. 1280-1285.

20. Venkateswaran, U.; Chandrasekhar, M.; Chandrasekhar, H.R.; Vojak, B.A.; Chambers, F.A.; Meese, J.M. (1986). High-pressure studies of GaAs-Ga 1− x Al x As quantum wells of widths 26 to 150 Å. *Physical Review B*, Vol. 33, No. 12, pp. 8416-8423.

21. Durandurdu, M.; Drabold, D.A. (2002). Ab initio simulation of high-pressure phases of GaAs. *Physical Review B*, Vol. 66, No. 4, pp. 045209(1-5).

22. Mujica A.; Needs, R.J. (1996). The Cmcm structure as a stable phase of binary compounds: application to GaAs-II. *J. Phys. Condens. Matter*, Vol. 8, No. 15, pp. L237 –L243.

23. Minomura, S.; Drickamer, H.G. (1962). Pressure induced phase transitions in silicon, germanium and some III–V compounds. *Journal of Physics and Chemistry of Solids*, Vol. 23, No. 5, pp.451-456.

24. Massidda, S.; Continenza, A.; Freeman, A.J.; De Pascale, T.M.; Meloni, F.; Serra, M. (1990). Structural and electronic properties of narrow-band-gap semiconductors: InP, InAs, and InSb. *Physical Review B*, Vol. 41, No. 17, pp. 12079-12085.

25. Lukacevic, I.; Kirin, D.; Jha, P.K.; Gupta, S.K. (2010). Density functional study of stability of high pressure phases in InP and InAs crystals. *Physica status solidi (b)*, Vol. 247, No. 2, pp. 273-277.

26. Soma, T.; Satoh, J.; Matsuo, H. (1982). Thermal expansion coefficient of GaAs and InP. *Solid State Communications*, Vol. 42, No. 12, pp. 889-892.

27. Menoni, C.S.; Spain, I.L. (1987). Equation of state of InP to 19 GPa. *Physical Review B*, Vol. 35, No. 14, pp. 7520-7525.

28. Arbouche, O.; Belgoumène, B.; Soudini, B.; Azzaz, Y.; Bendaoud, H.; Amara, K. (2010). First-principles study on structural properties and phase stability of III-phosphide (BP, GaP, AlP and InP). *Computational Materials Science*, Vol. 47, No. 3, pp.685-692.

29. Branicio, P.S.; Rino, J.P.; Shimojo, F. (2006). High-pressure phases of InP: An ab initio and molecular-dynamics study. *Applied physics letters*, Vol. 88, No. 16, pp. 161919(1-3).

30. Edwards, A.L.; Drickamer, H.G. (1961). Effect of pressure on the absorption edges of some III-V, II-VI, and I-VII compounds. *Physical Review*, Vol. 122, No.4, pp. 1149-1157.

31. Mariano, A.N.; Warekois, E.P. (1963). High pressure phases of some compounds of groups II-VI. *Science*, Vol. 142, No. 3593, pp.672-673.

32. Rooymans, C.J.M. (1963). Structure of the high pressure phase of CdS, CdSe and InSb. *Physics Letters*, Vol. 4, No. 3, pp. 186-187.

33. Owen, N.B.; Smith, P.L.; Martin, J.E.; Wright, A.J. (1963). X-ray diffraction at ultra-high pressures. *Journal of Physics and Chemistry of Solids*, Vol. 24, No.12, pp. 1519-1520.

34. Shchennikov, V.V.; Ovsyannikov, S.V. (2007). Thermoelectric properties and phase transitions of II–VI semiconductors at high pressure. *physica status solidi (b)*, Vol. 244, No. 1, pp.437-442.

35. Martin, R.M. (1970). Elastic properties of ZnS structure semiconductors. *Physical Review B*, Vol. 1, No. 10, pp. 4005-4011.

36. Zakharov, O.; Rubio, A.; Blase, X.; Cohen, M.L.; Louie, S.G. (1994). Quasiparticle band structures of six II-VI compounds: ZnS, ZnSe, ZnTe, CdS, CdSe, and CdTe. *Physical Review B*, Vol. 50, No. 15, pp. 10780-10787.

37. Ves, S.; Schwarz, U.; Christensen, N.E.; Syassen, K.; Cardona, M. (1990). Cubic ZnS under pressure: Optical-absorption edge, phase transition, and calculated equation of state. *Physical Review B*, Vol. 42, No. 14, pp. 9113-9118.

38. Desgreniers, S.; Beaulieu, L.; Lepage, I. (2000). Pressure-induced structural changes in ZnS. *Physical Review B*, Vol. 61, No. 13, pp. 8726-8733.

39. Cardona, M.; Kremer, R.K.; Lauck, R.; Siegle, G.; Muñoz, A.; Romero, A.H.; Schindler, A. (2010). Electronic, vibrational, and thermodynamic properties of ZnS with zinc-blende and rocksalt structure. *Physical Review B*, Vol. 81, No.7, pp. 075207(1-13).

40. Pan, Y.; Qu, S.; Dong, S.; Cui, Q.; Zhang, W.; Liu, X.; Liu, J.; Liu, B.; Gao, C.; Zou, G. (2002). An investigation on the pressure-induced phase transition of nanocrystalline ZnS. *Journal of Physics: Condensed Matter*, Vol. 14, No.44, pp. 10487-10490.

41. Jun, Y.; Feng, Z.; Qian, Z.; Ye, W.; Xiang, W.; Shan, Q.; Jun-Cai, D.; Dong-Liang, C. (2013). In situ XAFS investigation on zincblende ZnS up to 31.7 GPa. *Chinese Physics Letters*, Vol. 30, No. 4, pp. 046101(1-4).

42. Lee, S.G. and Chang, K.J., 1995. First-principles study of the structural properties of MgS-, MgSe-, ZnS-, and ZnSe-based superlattices. *Physical Review B*, Vol. 52, No. 3, pp. 1918-1925.

43. McMahon, M.I.; Nelmes, R.J.; Wright, N.G.; Allan, D.R. (1993). Phase transitions in CdTe to 5 GPa. *Physical Review B*, Vol. 48, No. 22, pp. 16246-16251.

44. Nelmes, R.J.; McMahon, M.I.; Wright, N.G.; Allan, D.R. (1993). Observation of a high-pressure cinnabar phase in CdTe. *Physical Review B*, Vol. 48, No. 2, pp. 1314-1317.

45. Kanoun, M.B.; Sekkal, W.; Aourag, H.; Merad, G. (2000). Molecular-dynamics study of the structural, elastic and thermodynamic properties of cadmium telluride. *Physics Letters A*, Vol. 272, No. 1, pp.113-118.

46. Benkhettou, N.; Rached, D.; Rabah, M. (2006). Ab-initio calculation of stability and structural properties of cadmium chalcogenides CdS, CdSe, and CdTe under high pressure. *Czechoslovak Journal of Physics*, Vol. 56, No. 4, pp. 409-418.

47. Nelmes, R.J. and McMahon, M.I. (1998). High Pressure in semiconductor Physics. *Semiconductors and Semimetals*, 54, p.145

48. Varshney, D.; Kaurav, N.; Sharma, P.; Shah, S.; Singh, R.K. (2004). Structural phase transition and elastic properties of ZnSe at high pressure. *Phase Transitions*, Vol. 77, No. 12, pp. 1075-1091.

49. Jin, M.; Cui, Q.; Mukhtar, E.; Ding, D. (2002). Second-harmonic-generation measurements on ZnSe under high pressure. *Journal of Physics: Condensed Matter*, Vol. 14, No. 44, pp. 11037-11040.

50. Qteish, A.; Munoz, A. (2000). Ab initio study of the phase transformations of ZnSe under high pressure: stability of the cinnabar and SC16 phases. *Journal of Physics: Condensed Matter*, Vol. 12, No. 8, pp. 1705-1713.

51. Gangadharan, R.; Jayalakshmi, V.; Kalaiselvi, J.; Mohan, S.; Murugan, R.; Palanivel, B. (2003). Electronic and structural properties of zinc chalcogenides ZnX (X= S, Se, Te). *Journal of alloys and compounds*, Vol. 359, No. 1, pp.22-26.

52. Bilal, M.; Shafiq, M.; Ahmad, I.; Khan, I.; (2014). First principle studies of structural, elastic, electronic and optical properties of Zn-chalcogenides under pressure. *Journal of Semiconductors*, Vol. 35, No. 7, pp. 072001(1-9).

53. Seminario, J.M. ed. (1996). *Recent developments and applications of modern density functional theory* (Vol. 4). Elsevier.

54. Singh, R.; Deb, B.M., (1999). Developments in excited-state density functional theory. *Physics reports*, Vol. 311, No. 2, pp. 47-94.

55. Kamal, C.; Ghanty, T.K.; Banerjee, A.; Chakrabarti, A. (2009). The van der Waals coefficients between carbon nanostructures and small molecules: A time-dependent density functional theory study. *The Journal of chemical physics*, Vol. 131, No.16, pp. 164708(1-11).

56. Thomas, L.H. (1927). The calculation of atomic fields. In *Mathematical Proceedings of the Cambridge Philosophical Society*, Cambridge University Press, Vol. 23, No. 05, pp. 542-548.

57. Fermi, E. (1927). Statistical method to determine some properties of atoms. *Rend. Accad. Naz. Lincei*, Vol. 6, pp. 602-607.

58. Hartree, D.R. (1928). The wave mechanics of an atom with a non-Coulomb central field. Part I. Theory and methods. In *Mathematical Proceedings of the Cambridge Philosophical Society* Cambridge University Press. Vol. 24, No. 01, pp. 89-110.

59. Dirac, P.A. (1928), The quantum theory of the electron. In *Proceedings of the Royal Society of London A: Mathematical, Physical and Engineering Sciences.* The Royal Society. Vol. 117, No. 778, pp. 610-624.

60. Dirac, P.A. (1930). Note on exchange phenomena in the Thomas atom. In *Mathematical Proceedings of the Cambridge Philosophical Society*. Cambridge University Press. Vol. 26, No. 03, pp. 376-385.

61. Fock, V. (1930). Approximation method for solving the quantum mechanical many-body problem. *Journal of Physics*, Vol. 61 No. (1-2), pp.126-148.

62. Slater, J.C. (1951). A simplification of the Hartree-Fock method. *Physical Review*, Vol. 81, No. 3, pp. 385-390; Slater, J.C., 1951. Magnetic effects and the Hartree-Fock equation. *Physical Review*, Vol. 82, No. 4, pp. 538-541.
63. Kohn, W.; Becke, A.D.; Parr, R.G. (1996). Density functional theory of electronic structure. *The Journal of Physical Chemistry*, Vol. 100, No. 31, pp. 12974-12980.
64. Kohn, W.; Sham, L.J. (1965). Self-consistent equations including exchange and correlation effects. *Physical review*, Vol. 140, No. 4A, pp. A1133-A1138.
65. Koch, W.; Holthausen, M.C. (2001). Hydrogen bonds and weakly bound systems. *A Chemist's Guide to Density Functional Theory, Second Edition*, pp. 217-238.
66. Grüning, M., Marini, A. and Rubio, A., 2006. Density functionals from many-body perturbation theory: The band gap for semiconductors and insulators. *The Journal of chemical physics*, Vol. 124, No. 15, pp. 154108(1-9).
67. Lebegue, S.; Klintenberg, M.; Eriksson, O.; Katsnelson, M.I. (2009). Accurate electronic band gap of pure and functionalized graphane from GW calculations. *Physical Review B*, Vol. 79, No. 24, pp. 245117(1-5).
68. Rinke, P.; Qteish, A.; Neugebauer, J.; Freysoldt, C.; Scheffler, M. (2005). Combining GW calculations with exact-exchange density-functional theory: an analysis of valence-band photoemission for compound semiconductors. *New Journal of Physics*, Vol. 7, No. 1, p.126(1-35).
69. Langreth, D.C.; Mehl, M.J. (1983). Beyond the local-density approximation in calculations of ground-state electronic properties. *Physical Review B*, Vol. 28, No. 4, pp. 1809-1834.
70. Becke, A.D. (1988). Density-functional exchange-energy approximation with correct asymptotic behavior. *Physical review A*, Vol. 38, No. 6, pp. 3098-3100.

71. Perdew, J.P.; Chevary, J.A.; Vosko, S.H. (1992). Atoms, molecules, solids and surfaces: Applications of generalized gradient approximation for exchange and correlation. *Phys. Rev. B*, Vol. 46, p. 6671.
72. Haas, P.; Tran, F.; Blaha, P.; Schwarz, K.; Laskowski, R. (2009). Insight into the performance of GGA functionals for solid-state calculations. *Physical Review B*, Vol. 80, No. 19, p. 195109 (1-13).
73. Tran, F.; Blaha, P. (2009). Accurate band gaps of semiconductors and insulators with a semilocal exchange-correlation potential. *Physical review letters*, Vol. 102, No. 22, pp. 226401(1-4).
74. Becke, A.D.; Roussel, M.R. (1989). Exchange holes in inhomogeneous systems: A coordinate-space model. *Physical Review A*, Vol. 39, No. 8, pp. 3761-3767.
75. Nye, J.F. (1985). *Physical properties of crystals: their representation by tensors and matrices*. Oxford university press.
76. Nielsen, O.H.; Martin, R.M. (1983). First-principles calculation of stress. *Physical Review Letters*, Vol. 50, No. 9, pp. 697-700.
77. Stadler, R.; Wolf, W.; Podloucky, R.; Kresse, G.; Furthmüller, J.; Hafner, J. (1996). Ab Initio Calculations of the cohesive, elastic, and dynamical properties of $CoSi_2$ by pseudopotential and all-electron techniques. *Physical Review B*, Vol. 54, No. 3, pp. 1729-1734.
78. Blaha, P.; Schwarz, K.; Madsen, G.K.H.; Kvasnicka, D.; Luitz, J. (2001). Wien2k. *An Augmented Plane Wave+ Local Orbitals Program For Calculating Crystal Properties*.
79. Wimmer, E.; Krakauer, H.; Weinert, M.; Freeman, A.J. (1981). Full-potential self-consistent linearized-augmented-plane-wave method for calculating the electronic structure of molecules and surfaces: O 2 molecule. *Physical Review B*, Vol. 24, No. 2, pp. 864-875.

80. Jamal, M.; Asadabadi, S.J.; Ahmad, I.; Aliabad, H.R. (2014). Elastic constants of cubic crystals. *Computational Materials Science*, Vol. 95, pp. 592-599.

81. Birch, F. (1938). The effect of pressure upon the elastic parameters of isotropic solids, according to Murnaghan's theory of finite strain. *Journal of Applied Physics*, Vol. 9, No. 4, pp.279-288.

82. Kuriyama, K.; Miyamoto, Y.; Okada, M. (1999). Redshift of the longitudinal optical phonon in neutron irradiated GaP. *Journal of applied physics*, Vol. 85, No. 7, pp. 3499-3502.

83. Moss, D.J.; Ghahramani, E.; Sipe, J.E.; Van Driel, H.M. (1986). Empirical tight-binding calculation of dispersion in the linear optical properties of tetrahedral solids. *Physical Review B*, Vol. 34, No. 12, pp. 8758-8770.

84. Al-Douri, Y.; Reshak, A.H. (2011). Calculated optical properties of GaX (X= P, As, Sb) under hydrostatic pressure. *Applied Physics A*, Vol. 104, No. 4, pp. 1159-1167.

85. Lichanot, A.; Causa, M. (1997). Compared electron charge densities for the series of solid phosphide compounds; an ab initio study. *Journal of Physics: Condensed Matter*, Vol. 9, No. 15, pp. 3139-3149.

86. Limpijumnong, S.; Reunchan, P.; Janotti, A.; Van de Walle, C.G. (2008). Carbon-nitrogen molecules in GaAs and GaP. *Physical Review B*, Vol. 77, No. 19, pp. 195209(1-7).

87. Yogurtçu, Y.K.; Miller, A.J.; Saunders, G.A. (1981). Pressure dependence of elastic behaviour and force constants of GaP. *Journal of Physics and Chemistry of Solids*, Vol. 42, No. 1, pp. 49-56.

88. Besson, P.L.J.P.J. (1982). Melting Curve and High Pressure Phases of 4He above 10 GPa. In *High Pressure in Research and Industry: Proceedings [of The] 8th AIRAPT Conference, 19th EHPRG Conference, 17-22 August 1981, Institute of Physical Chemistry, University of Uppsala, Sweden* (Vol. 1, p. 358). Arkitektkopia.

89. Baublitz Jr, M.; Ruoff, A.L. (1982). Diffraction studies of the high pressure phases of GaAs and GaP. *Journal of Applied Physics*, Vol. 53, No. 9, pp. 6179-6185.

90. Froyen, S.; Cohen, M.L. (1982). High pressure phases of III–V semiconductors: A microscopic theory. *Solid State Communications*, Vol. 43, No. 6, pp. 447-450.

91. Garci, A.; Cohen, M.L. (1993). Effect of Ga 3d states on the structural properties of GaAs and GaP. *Physical Review B*, Vol. 47, No. 11, pp. 6751-6754.

92. Ozoliņs, V.; Zunger, A. (1999). Theory of systematic absence of NaCl-Type (β-Sn–Type) high pressure phases in covalent (ionic) semiconductors. *Physical review letters*, Vol. 82, No. 4, pp. 767-770.

93. Singh, R.K.; Singh, S. (1989). Structural phase transition and high-pressure elastic behavior of III-V semiconductors. *Physical Review B*, Vol. 39, No. 1, pp. 671-676.

94. Zhang, S.B.; Cohen, M.L. (1987). High-pressure phases of III-V zinc-blende semiconductors. *Physical Review B*, Vol. *35*, No.14, pp.7604-7610.

95. Donohue, J. (1974). Structures of the Elements. (New York: Wiley)

96. Lai-Yu, L.; Xiang-Rong, C.; Bai-Ru, Y.; Qing-Quan, G. (2006). First-principles calculations for transition phase and thermodynamic properties of GaAs. *Chinese Physics*, Vol. 15, No. 4, pp. 802-806.

97. Mujica, A.; Munoz, A.; Needs, R.J. (1998). Theoretical study of the cinnabar phases in GaAs and GaP. *Physical Review B*, Vol. 57, No. 3, pp. 1344-1347.

98. Arabi, H.; Pourghazi, A.; Ahmadian, F.; Nourbakhsh, Z. (2006). First-principles study of structural and electronic properties of different phases of GaAs. *Physica B: Condensed Matter*, Vol. 373, No. 1, pp.16-22.

99. Hong-Ling, C.; Xiang-Rong, C.; Guang-Fu, J.I.; Dong-Qing, W. (2008). Structures and Phase Transition of GaAs under pressure. *Chinese Physics Letters*, Vol. 25, No. 6, pp. 2169-2172.

100. Albe, K.; Nordlund, K.; Nord, J.; Kuronen, A. (2002). Modeling of compound semiconductors: Analytical bond-order potential for Ga, As, and GaAs. *Physical Review B*, Vol. 66, No. 3, p.035205 (1-14).

101. Kittel, C. (1986). Introduction to Solid State Physics, 6th edn., translated by Y. *Uno, N. Tsuya, A. Morita and J. Yamashita,(Maruzen, Tokyo, 1986)* pp. 124-129.

102. Zunger, A.; Kim, K.; Ozolins, V. (2001). Why are the conventionally-assumed high-pressure crystal structures of ordinary semiconductors unstable? *physica status solidi(b)*, Vol. 223, No. 2, pp. 369-378.

103. Gupta, D.C.; Kulshrestha, S. (2008). Pressure-induced phase transitions and electronic structure of GaAs. *Journal of Physics: Condensed Matter*, Vol. 20, No. 25, p. 255204(1-7).

104. Madelung O. (1982). Semiconductors Physics of Group IV elements and III-V compounds Landolt Bornstein, New Series, Group III Vol.17 part A (Springer-Verlag, Berlin)

105. Kalvoda, S.; Paulus, B.; Fulde, P.; Stoll, H. (1997). Influence of electron correlations on ground-state properties of III-V semiconductors. *Physical Review B*, Vol. 55, No. 7, pp. 4027-4030.

106. Seidl, A., Görling, A., Vogl, P., Majewski, J.A. and Levy, M., 1996. Generalized Kohn-Sham schemes and the band-gap problem. *Physical Review B*, Vol. 53, No. 7, pp. 3764-3774.

107. Nichols, D.N.; Rimai, D.S.; Sladek, R.J. (1980). Elastic anharmonicity of InP: Its relationship to the high pressure transition. *Solid State Communications*, Vol. 36, No. 8, pp. 667-669.

108. Yousaf, M.; Saeed, M.A.; Ahmed, R.; Alsardia, M.M.; Isa, A.R.M.; Shaari, A. (2012). An Improved Study of Electronic Band Structure and Optical Parameters of X-Phosphides (X= B, Al, Ga, In) by Modified Becke—Johnson Potential. *Communications in Theoretical Physics*, Vol. 58, No. 5, p. 777-784.

109. Wyckoff, R.W.G. (1986). Crystal Structures, 2nd edition Krieger Malabar.

110. Ahmed, R.; Hashemifar, S.J.; Akbarzadeh, H. (2008). First-principles study of the structural and electronic properties of III-phosphides. *Physica B: Condensed Matter*, Vol. 403, No. 10, pp. 1876-1881.

111. Mc Mahon, M. I.; Nelmes, R. J.; Wright, N. G.; Allan, D. R. (1993) Proceedings of the Joint Conference on the AIRATP/APS On High-Pressure Science and Technology, June28–July2, edited by S C Schmit, J W Shaner, G A Samaraand , M Ross, (ColoradoSprings, Colorado) p. 629.

112. Hu, C.; Wang, F.; Zheng, Z., (2012). Pressure-induced metallic phase transition and elastic properties of indium phosphide III-V semiconductor. *Journal of Materials Research*, Vol. 27, No. 08, pp. 1105-1111.

113. Mayer, B.; Anton, H.; Bott, E.; Methfessel, M.; Sticht, J.; Harris, J.; Schmidt, P.C., 2003. Ab-initio calculation of the elastic constants and thermal expansion coefficients of Laves phases. *Intermetallics*, Vol. 11, No. 1, pp. 23-32.

114. Jeong, J.; Schlesinger, T.E.; Milnes, A.G.; (1988). X-ray characterization of InxGa1− xAs/GaAs quantum wells. *Journal of crystal growth*, Vol. 87, No. (2-3), pp. 265-275.

115. Christensen, N.E.; Satpathy, S.; Pawlowska, Z. (1987). Bonding and ionicity in semiconductors. *Physical Review B*, Vol. 36, No. 2, pp. 1032-1050.

116. Pedesseau, L.; Even, J.; Bondi, A.; Guo, W.; Richard, S.; Folliot, H.; Labbé, C.; Cornet, C.; Dehaese, O.; Le Corre, A.; Durand, O. (2008). Theoretical study of highly strained InAs material from first-principles modelling: application to an ideal QD. *Journal of Physics D: Applied Physics*, Vol. 41, No. 16, pp. 165505(1-11).

117. Shen, S.G. (1994). Calculation of the elastic properties of semiconductors. *Journal of Physics: Condensed Matter*, Vol. 6, No. 42, pp. 8733-8743.

118. Vohra, Y.K.; Weir, S.T.; Ruoff, A.L. (1985). High-pressure phase transitions and equation of state of the III-V compound InAs up to 27 GPa. *Physical Review B*, Vol. 31, No. 11, pp. 7344-7347.

119. McMahon, M.I.; Nelmes, R.J. (1996). New Structural Systematics in the II–VI, III–V, and Group-IV Semiconductors at High Pressure. *physica status solidi (b)*, Vol. 198, No. 1, pp. 389-402.

120. Mujica, A.; Needs, R.J.; Munoz, A. (1996). High Pressure Stability in III–V and II-VI Binary Compounds and the Cmcm Phase A Theoretical Study. *physica status solidi (b)*, Vol. 198, No. 1, pp. 461-467.

121. Bannikov, V.V.; Shein, I.R.; Ivanovskii, A.L. (2007). Electronic structure, chemical bonding and elastic properties of the first thorium-containing nitride perovskite $TaThN_3$. *physica status solidi (RRL)-Rapid Research Letters*, Vol. 1, No. 3, pp. 89-91.

122. Fu, H.; Li, D.; Peng, F.; Gao, T.; Cheng, X. (2008). Ab initio calculations of elastic constants and thermodynamic properties of NiAl under high pressures. *Computational Materials Science*, Vol. 44, No. 2, pp. 774-778.
123. Pugh, S.F. (1954). XCII. Relations between the elastic moduli and the plastic properties of polycrystalline pure metals. *The London, Edinburgh, and Dublin Philosophical Magazine and Journal of Science*, Vol. 45, No. 367, pp. 823-843.
124. Johnston, L.; Keeler, G.; Rollins, R.; Spicklemire, S. (1996). *The Consortium for Upper-Level Physics Software,* (New York: John Wiley)
125. Anderson, O.L. (1963). A simplified method for calculating the Debye temperature from elastic constants. *Journal of Physics and Chemistry of Solids*, Vol. 24, No. 7, pp. 909-917.
126. Schreiber, E.; Anderson, O.L.; Soga, N. (1973). Elastic constants and their measurements. (McGraw-Hill, New York).
127. Vagelatos, N.; Wehe, D.; King, J.S. (1974). Phonon dispersion and phonon densities of states for ZnS and ZnTe. *The Journal of Chemical Physics*, Vol. 60, No. 9, pp. 3613-3618.
128. Postnikov, A.V.; Pages, O.; Hugel, J. (2005). Lattice dynamics of the mixed semiconductors (Be, Zn) Se from first-principles calculations. *Physical Review B*, Vol. 71, No. 11, pp. 115206(1-10).
129. Casali, R.A.; Christensen, N.E. (1998). Elastic constants and deformation potentials of ZnS and ZnSe under pressure. *Solid state communications*, Vol. 108, No. 1, pp. 793-798.
130. Khenata, R.; Bouhemadou, A.; Sahnoun, M.; Reshak, A.H.; Baltache, H.; Rabah, M. (2006). Elastic, electronic and optical properties of ZnS, ZnSe and ZnTe under pressure. *Computational Materials Science*, Vol. 38, No. 1, pp.29-38.
131. Jamieson, J.C.; Demarest, H.H. (1980). A note on the compression of cubic ZnS. *Journal of Physics and Chemistry of Solids*, Vol. 41, No. 9, pp.963-964.

132. Madelung, O. (1986). Landolt-Bornstein Tables, New Series Vol III/22a edited by Springer.
133. Zhou, Y.; Campbell, A.J.; Heinz, D.L. (1991). Equations of state and optical properties of the high pressure phase of zinc sulfide. *Journal of Physics and Chemistry of Solids*, Vol. 52, No. 6, pp. 821-825.
134. Madelung, O. (1982). Numerical Data and Functional Relationships in Science and Technology, in: New Series, Vol. 17b, Springer-Verlag, Berlin.
135. Nazzal, A.; Qteish, A. (1996). Ab initio pseudopotential study of the structural phase transformations of ZnS under high pressure. *Physical Review B*, Vol. 53, No. 13, pp. 8262-8266.
136. Miao, M.S.; Lambrecht, W.R. (2005). Universal transition state for high-pressure zinc blende to rocksalt phase transitions. *Physical review letters*, Vol. 94, No. 22, pp. 225501(1-4).
137. Cui-E, H.; Li-Li, S.; Zhao-Yi, Z.; Xiang-Rong, C. (2008). Pressure and temperature induced phase transition of ZnS from first-principles calculations. *Chinese Physics Letters*, Vol. 25, No. 2, pp. 675-678.
138. Chen, X.R.; Li, X.F.; Cai, L.C.; Zhu, J. (2006). Pressure induced phase transition in ZnS. *Solid state communications*, Vol. 139, No. 5, pp. 246-249.
139. Lalitha, S.; Karazhanov, S.Z.; Ravindran, P.; Senthilarasu, S.; Sathyamoorthy, R.; Janabergenov, J. (2007). Electronic structure, structural and optical properties of thermally evaporated CdTe thin films. *Physica B: Condensed Matter*, Vol. 387, No. 1, pp. 227-238.
140. Polit, J.; Sheregii, E.M.; Cebulski, J.; Robouch, B.V.; Marcelli, A.; Guidi, M.C.; Piccinini, M.; Kisiel, A.; Zajdel, P.; Burattini, E.; Mycielski, A. (2006). Phonon and vibrational spectra of hydrogenated CdTe. *Journal of applied physics*, Vol. 100, No. 1, pp. 013521(1-10).
141. Ouendadji, S.; Ghemid, S.; Meradji, H.; Hassan, F.E.H. (2011). Theoretical study of structural, electronic, and thermal properties of CdS, CdSe and CdTe compounds. *Computational Materials Science*, Vol. 50, No. 4, pp. 1460-1466.

142. Zerroug, S.; Sahraoui, F.A.; Bouarissa, N. (2007). Structural parameters and pressure coefficients for CdSxTe1-x: FP-LAPW calculations. *The European Physical Journal B*, Vol. 57, No. 1, pp. 9-14.
143. Al-Douri, Y.; Reshak, A.H.; Baaziz, H.; Charifi, Z.; Khenata, R.; Ahmad, S.; Hashim, U. (2010). An ab initio study of the electronic structure and optical properties of CdS 1− xTex alloys. *Solar Energy*, Vol. 84, No. 12, pp. 1979-1984.
144. Strossner, K.; Ves, S.; Dieterich, W.; Gebhardt, W.; Cardona, M. (1985). High pressure X-ray investigations of phase transitions in $Cd_{1-x}Mn_xTe$. *Solid state communications*, Vol. 56, No. 7, pp. 563-565.
145. Smith, T.F.; White, G.K. (1975). The low-temperature thermal expansion and Gruneisen parameters of some tetrahedrally bonded solids. *Journal of Physics C: Solid State Physics*, Vol. 8, No. 13, pp. 2031-2042.
146. Van Camp, P.E.; Van Doren, V.E. (1994). Structural phase transformation and ground state properties of cadmium telluride. *Solid state communications*, Vol. 91, No. 8, pp. 607-610.
147. Sharma, E.; Singh, A.; Sakalle, U.K. (2012). Anharmonic properties of Cadmium Telluride (CdTe). *Int. J. of Engg. Sci. & Mgmt. (IJESM)*. Vol. 2, No. 1, pp. 86-90.
148. Zerroug, S.; Sahraoui, F.A.; Bouarissa, N. (2007). Structural parameters and pressure coefficients for CdSxTe1-x: FP-LAPW calculations. *The European Physical Journal B*, Vol. 57, No. 1, pp. 9-14.
149. Mei, J.R.; Lemos, V. (1984). Photoluminescence on CdSe and CdTe under hydrostatic pressure. *Solid state communications*, Vol. 52, No. 9, pp. 785-788.
150. Nelmes, R.J.; McMahon, M.I.; Wright, N.G.; Allan, D.R. (1995). Phase transitions in CdTe to 28 GPa. *Physical Review B*, Vol. 51, No. 22, pp. 15723-15731.
151. Alfer, S.A.; Skums, V.F. (2001). Electrical resistance of CdSe and CdTe at elevated temperatures and pressures. *Inorganic materials*, Vol. 37, No. 12, pp. 1237-1240.

152. Borg, I.Y.; Smith, D.K. (1967). X-ray diffraction studies on CdTe at high pressure. *Journal of Physics and Chemistry of Solids*, Vol. 28, No.1, pp. 49-53.

153. Lee, B.H. (1970). Pressure Dependence of the Second-Order Elastic Constants of ZnTe and ZnSe. *Journal of Applied Physics*, Vol. 41, No. 7, pp. 2988-2990.

154. McMahon, M.I.; Nelmes, R.J.; Allan, D.R.; Belmonte, S.A.; Bovornratanaraks, T. (1998). Observation of a simple-cubic phase of GaAs with a 16-atom basis (SC16). *Physical review letters*, Vol. 80, No. 25, pp. 5564-5567.

155. Saini, P.K.; Singh, D.; Ahlawat, D.S. (2014). Calculations of the Structural, Elastic and Optical Properties of Znse at ambient and High Pressure. *Chalcogenide Letters*, Vol. 11, No. 9, pp. 405-414.

156. Karzel, H.; Potzel, W.; Kofferlein, M.; Schiessl, W.; Steiner, M.; Hiller, U.; Kalvius, G.M.; Mitchell, D.W.; Das, T.P.; Blaha, P.; Schwarz, K. (1996). Lattice dynamics and hyperfine interactions in ZnO and ZnSe at high external pressures. *Physical Review B*, Vol. 53, No. 17, pp. 11425-11438.

157. Greene, R.G.; Luo, H.; Ruoff, A.L. (1995). High pressure X-ray and Raman study of ZnSe. *Journal of Physics and Chemistry of Solids*, Vol. 56, No. 3, pp. 521-524.

158. Köfferlein, M.; Karzel, H.; Potzel, W.; Schiessl, W.; Steiner, M.; Kalvius, G.M.; Mitchell, D.W.; Das, T.P. (1994). High-pressure phase transition in ZnSe. *Hyperfine Interactions*, Vol. 93, No. 1, pp. 1505-1510.

159. Smelyansky, V.I.; John, S.T. (1995). Theoretical study on the high-pressure phase transformation in ZnSe. *Physical Review B*, Vol. 52, No. 7, pp. 4658-4661.

160. Vegard, L. (1921). Formation of mixed crystals by solid-phase contact. *Journal of Physics*, Vol. 5, No. 5, pp.393-395.

161. Denton, A.R.; Ashcroft, N.W. (1991). Vegard's Law. *Physical. Review. A*, Vol. 43, No. 6, pp. 3161-3164.

162. Jobst, B.; Hommel, D.; Lunz, U.; Gerhard T.; Landwehr G. (1996). E_0 Band-Gap Energy and Lattice Constant of Ternary Zn1−*x*Mg*x*Se as Functions of Composition. *Applied Physics Letters*, Vol. 69, No. 1, pp. 97-100.

163. Hassan, F. El H.; Akbardadeh, H. (2005). First-principles Investigation of BN*x*P1-*x*, BN*x*As1-*x* and BP*x*As1-*x* Ternary Alloys. *Materials Science and Engineering B*, Vol. 121, No. 1-2, pp. 170-177.

164. Al-Douri, Y. (2004). Structural Phase Transition of Boron Nitride Compound. *Solid State Communications*, Vol. 132, No. 7, pp. 465-470.

165. Al-Douri, Y. (2003). Electronic and Positron Properties of Zinc-Blende Structure of GaN, AlN, and Their Alloy Ga1−xAlxN. *Journal of Applied Physics*, Vol. 93, No. 12, pp. 9730-9736.

166. Al-Douri, Y. (2003). Electronic and Optical Properties of Zn*x*Cd1−*x*Se. *Materials Chemistry and Physics*, Vol. 82, No. 1, pp. 49-54.

167. Al-Douri, Y.; Mecabih, S.; Benosman N.; Aourag, H. (2003). Pressure Effect on Electronic and Positron Charge Densitiesof Zn0.5Cd0.5Se. *Physica B*, Vol. 325, No. 1-4, pp. 362-371.

168. Moon, C.Y.; Li, J.; Wei, S.H.; Lim, A.T.L.; Feng, Y.P. (2006). Ordering induced direct and indirect transitions in semiconductor alloys. *Physical Review B*, Vol. 74, No. 20, pp. 205203(1-5)

APPENDIX A

FUNCTIONAL.

A function is a rule for taking a number as an input and giving a number as an output. Likewise a functional is a rule for taking a function as an input and giving a number as output. An example of a functional is the particle number

$$N[\rho(r)] = \int \rho(r) dr \tag{1}$$

The particle number functional, $N[\rho(r)]$, takes a function (the electron density) as its input and gives a number (the number of particles) as its output. Other good examples of functional might be the average temperature during a day.

$$\langle T \rangle [T(t)] = \int_{t=0}^{t=24hr} \frac{T(t)}{24h} dt \tag{2}$$

And the expectation value of the kinetic energy for a quantum system

$$K[\psi(r)] = \int \psi(r)^* \left(-\frac{1}{2} \nabla^2 \right) \psi(r) dr \tag{3}$$

Functionals have their own type of differentiation rule. The functional derivative $\frac{\delta F[\rho(r)]}{\delta \rho(r)}$ of the function $F[\rho(r)]$ is defined as

$$\Delta F[\rho(r)] \equiv \int \frac{\delta F[\rho(r)]}{\delta \rho(r)} \Delta \rho(r) dr \tag{4}$$

where Δ represents an infinitesimally small change (Δ was chosen instead of δ to avoid confusion with the δ's used in the notation for the functional derivative). As an example we know that the particle number N is given as

$$N[\rho(r)] = \int \rho(r) dr \tag{5}$$

So,

$$\Delta N[\rho(r)] = \int ((\rho(r) + \Delta\rho(r)) - \rho(r))dr = \int \Delta\rho(r)dr \quad (6)$$

and

$$\frac{\delta N[\rho(r)]}{\delta\rho(r)} = 1 \quad (7)$$

Likewise the contribution to the energy eigenvalue from the external potential is

$$V_{ne}[\rho(r)] = \int \rho(r)\upsilon(r)dr \quad (8)$$

so,

$$\Delta V_{ne}[\rho(r)] = \int [(\rho(r) + \Delta\rho(r)) - \rho(r)]\upsilon(r)dr = \int \Delta\rho(r)\upsilon(r)dr$$

(9)

$$\frac{\delta V_{ne}[\rho(r)]}{\delta\rho(r)} = \upsilon(r) \quad (10)$$

As we can see from the last example and the definition (4), the functional derivative does not have to be constant with respect to position. Additionally, it may also depend on the function, $\rho(\vec{r})$, at which it is evaluated. For instance if we have a functional

$$A[\rho(r)] = \int f(r)[\rho(r)]^2 dr$$

then,

$$\Delta A[\rho(r)] = \int f(r)\left([\rho(r)]^2 + 2\rho(r)[\Delta\rho(r)] + [\Delta\rho(r)]^2 - [\rho(r)]^2\right)d\vec{r}$$

So the functional becomes,

$$\frac{\delta A}{\delta\rho} = 2\rho(r)f(r)$$

As we saw in the previous section, a density can only be the ground state density of maximum one external potential. If $\rho(r)$ corresponds to the ground state we can therefore unambiguously define the energy functional

$$E[\rho(r)] \equiv \langle \psi \mid \hat{H} \mid \psi \rangle$$

Where ψ denotes the ground state corresponding $\rho(r)$ and $\hat{H}$ is the Hamiltonian yielding this ground state.

APPENDIX B

PROOF OF HOHENBERG AND KOHN THEOREMS

THEOREM 1. The external potential is determined by the electron density and for a given density there will be a single external potential.

Proof:

Let us assume that ρ(r) is the ground state density of a system of electrons. Let us also assume that there are two potentials V_1 and V_2 which produces two different Hamiltonian H_1 and H_2 respectively as

$$H_1 = V_1 + T + V_{ee}$$

and,

$$H_2 = V_2 + T + V_{ee}$$

Again we assume that there are two wave functions ψ_1 and ψ_2 that produce the same density $\rho(r)$. Therefore,

$$E_1 = \langle \psi_1 | H | \psi_1 \rangle \langle \psi_2 | H | \psi_2 \rangle \tag{1}$$

Now, we consider the term,

$$\langle \psi_2 | H_1 | \psi_2 \rangle = \langle \psi_2 | H_2 - H_2 + H_1 | \psi_2 \rangle$$

$$\langle \psi_2 | H_1 | \psi_2 \rangle = \langle \psi_2 | H_2 | \psi_2 \rangle + \langle \psi_2 | H_1 - H_2 | \psi_2 \rangle$$

$$\langle \psi_2 | H_1 | \psi_2 \rangle = E_2 + \langle \psi_2 | V_1 - V_2 | \psi_2 \rangle \tag{2}$$

Thus equation (1) becomes,

$$E_1 < E_2 + \int \rho(r)[V_1 - V_2] d^3 r \tag{3}$$

Similarly,

$$E_2 = \langle \psi_2 \mid H_2 \mid \psi_2 \rangle < \langle \psi_1 \mid H_2 \mid \psi_1 \rangle$$

Considering the term,

$$\langle \psi_1 \mid H_2 \mid \psi_1 \rangle = \langle \psi_1 \mid H_1 - H_1 + H_2 \mid \psi_1 \rangle$$

$$\langle \psi_1 \mid H_2 \mid \psi_1 \rangle = \langle \psi_1 \mid H_1 \mid \psi_1 \rangle + \langle \psi_1 \mid H_2 - H_1 \mid \psi_1 \rangle$$

$$\langle \psi_1 \mid H_2 \mid \psi_1 \rangle = E_1 + \int \rho(r)[V_2 - V_1] d^3 r$$

$$\langle \psi_1 \mid H_2 \mid \psi_1 \rangle = E_1 - \int \rho(r)[V_1 - V_2] d^3 r$$

Thus equation (3) becomes,

$$E_2 < E_1 - \int \rho(r)[V_1 - V_2] d^3 r \tag{4}$$

Adding equation (2) and (4) we get,

$$E_1 + E_2 < E_2 + E_1 \tag{5}$$

This equation is naturally not correct and contradictory to each other. This is due to the fact that we considered two potential V_1 and V_2 for a given potential $\rho(r)$.

Hence we conclude that there cannot be two external potential for a single $\rho(r)$.

Theorem 2. The functional $F_{HK}[\rho] = T[\rho] + V_{ee}[\rho]$ determines the ground state energy if and only if the input density is the true ground state density.

Proof:

Let us assume that $\rho(r)$ is the ground state density for the system of electron. Then the ground state energy functional is

$$E[\rho] = \int \rho(r) V_{ext}(r) d^3 r + F_{HK}[\rho]$$

Here, $F_{HK}[\rho] = T[\rho] + V_{ee}[\rho]$ is the universal functional.

Let us consider a trial density $\tilde{\rho}(r)$ that determines its own $\tilde{V}_{ext}(r)$, the Hamiltonian $\tilde{H}$ and $\tilde{\psi}$.

Let us take $\tilde{\psi}$ as trial function of the Hamiltonian H of the ground state density $\rho(r)$.

Then, $E[\rho] \leq \langle \tilde{\psi} \mid H \mid \tilde{\psi} \rangle$

Now,

$$\langle \tilde{\psi} \mid H \mid \tilde{\psi} \mid \rangle = \langle \tilde{\psi} \mid V_{ext}(r) \mid \tilde{\psi} \rangle + \left\langle \tilde{\psi} \mid -\frac{1}{2}\nabla^2 + V_{ee} \mid \tilde{\psi} \right\rangle$$

$$\langle \tilde{\psi} \mid H \mid \tilde{\psi} \mid \rangle = \int \tilde{\rho} V_{ext}(r) d^3 r + T[\tilde{\rho}] + V_{ee}[\tilde{\rho}]$$

$$\langle \tilde{\psi} \mid H \mid \tilde{\psi} \mid \rangle = \int \tilde{\rho} V_{ext}(r) d^3 + F_{HK}[\tilde{\rho}]$$

$$\langle \tilde{\psi} \mid H \mid \tilde{\psi} \mid \rangle = E[\tilde{\rho}]$$

where, $F_{HK}[\tilde{\rho}] = T[\tilde{\rho}] + V_{ee}[\tilde{\rho}]$

so, $E[\rho] \leq E[\tilde{\rho}]$

Thus, the functional $F_{HK}[\rho]$ delivers the ground state energy if and only if input density is the true ground state density.

APPENDIX C

DEDUCTION OF KOHN SHAM EQUATION

The total energy,

$$E[\rho]=\frac{1}{2}\sum_i\left\langle\phi_i\mid\nabla^2\mid\phi_i\right\rangle+\frac{1}{2}\iint\frac{\rho(r)\rho(r')}{|r-r'|}drdr'+\int\upsilon_{ext}\rho dr+E_{XC}[\rho] \quad (1)$$

Let us apply the variational principle with the constraints that all the integrals,

$$I_K=\int\phi_i^*(r)\phi_i(r)dr=1 \quad (2)$$

For this we follow the following steps:

Step 1:

First term in equation 1

$$-\frac{1}{2}\sum_i\left\langle\phi_i\mid\nabla^2\mid\phi_i\right\rangle$$

The orbital function ϕ_K tem in this summation is

$$-\frac{1}{2}\left\langle\phi_K(r)\mid\nabla^2\mid\phi_K(r)\right\rangle$$

$$=-\frac{1}{2}\int\phi_K^*(r)\nabla^2\phi_K(r)dr$$

$$=\int\phi_K^*(r)\left(-\frac{1}{2}\nabla^2\right)\phi_K(r)dr$$

Second term in equation (1):

$$\frac{1}{2}\iint\frac{\rho(r)\rho(r')}{|r-r'|}drdr'$$

$$=\frac{1}{2}\sum_i \iint \frac{\phi_i^*(r)\phi_i(r)\rho(r')}{|r-r'|}drdr'$$

The orbital function $\phi_K(r)\frac{\rho(r')}{|r-r'|}\phi_K(r)drdr'$

3rd term in the equation (1)

$$\int \upsilon_{ext}(r)\rho(r)dr$$

$$=\sum_i \int \upsilon_{ext}(r)\phi_i^*(r)\phi_i(r)dr$$

The orbital function $\phi_K(r)$ term in this summation is

$$\int \phi_K^*(r)\upsilon_{ext}(r)\phi_K(r)dr$$

Fourth term equation (1) is

$$E_{XC}[\rho]=\int \upsilon_{XC}(r)\rho(r)dr$$

$$= \sum_i \upsilon_{exc}(r)\phi_i^*(r)\phi_i(r)dr$$

The orbital function $\phi_K(r)$ term in the summation is

$$\int \phi_K^*(r)\upsilon_{exc}(r)\phi_K(r)dr$$

Step 2:

By variational principle,

$$\delta[E[\rho]-E_K I_K]=0$$

Where E_K are Lagrange multipliers which is to be determined.

$$\delta E[\rho]-E_K\delta I_K=0$$

Step 3:

$$I_K = \int \phi_K^*(r)\phi_k(r)dr$$

$$I_K + \delta I_K = \int (\phi_K^* + \delta\phi_K^*)(\phi_K + \delta\phi_K)dr$$

$$= I_K + \delta I_K = \int \phi_K^*(r)\phi_K(r)dr + \int \phi_K^*(r)\delta\phi_K(r)dr + \int \delta\phi_K^*(r)\phi_K(r)dr + \int \delta\phi_K^*(r)\delta\phi_K(r)$$

i.e. $\delta I_K = \int \delta\phi_K^*(r)\phi_K(r)dr + \int \phi_K^*(r)\delta\phi_K(r)dr$

Step 4:

Considering the variation in $\phi_K(r)$ and the term containing $\phi_K^*(r)$, we can write,

$\delta E[\rho] - E_K \delta I_K = 0$ as,

$$\int \delta\phi_K(r)\left(-\frac{1}{2}\nabla^2\right)\phi_K(r)dr$$

The term containing $\delta\phi_K^*(r)$ in the second term variation is,

$$\frac{1}{2}\iint \delta\phi_K^*(r)\frac{\rho(r')}{|r-r'|}\phi_K(r)drdr' + \frac{1}{2}\iint \delta\phi_K^*(r')\frac{\rho(r)}{|r-r'|}\phi_K(r')drdr'$$

It can be written as,

$$\int \delta\phi_K^*(r)\frac{\rho(r)}{|r-r'|}\phi_K(r)drdr'$$

The term containing $\delta\phi_K^*(r)$ in the third term variation is,

$$\int \delta\phi_K^*(r)\upsilon_{ext}(r)\phi_K(r)dr$$

The term containing $\delta\phi_K^*(r)$ in the fourth term variation is,

$$\int \delta\phi_K^*(r)\upsilon_{exc}(r)\phi_K(r)dr$$

And the term containing $\delta\phi_K^*(r)$ in the constraint variation is,

$$\delta I_K = \int \delta\phi_K^*(r)\phi_K(r)dr$$

Thus, we can write the equation of variation,

$$\delta E[\rho] - E_K \delta I_K = 0.$$

Hence $\delta\phi_K^*(r)$ can be written as,

$$\int \delta\phi_K^*(r)\left(-\frac{1}{2}\nabla^2\right)\phi_K(r)dr + \iint \delta\phi_K^*(r)\frac{\rho(r')}{|r-r'|}\phi_K(r)drdr' + \int \delta\phi_K^*(r)\upsilon_{exc}(r)\phi_K(r)dr - \int \delta\phi_K^*(r)E_K\phi_K(r)dr = 0$$

$$\int \delta\phi_K^*(r)\left[-\frac{1}{2}\nabla^2 + \int\frac{\rho(r')}{|r-r'|}dr' + \upsilon_{ext}(r) + \upsilon_{exc}(r) + E_K\right]\phi_K(r)dr = 0$$

This implies,

$$\left[-\frac{1}{2}\nabla^2 + \int\frac{\rho(r')}{|r-r'|}dr' + \upsilon_{ext}(r) + \upsilon_{exc}(r) - E_K\right]\phi_K(r) = 0$$

$$\left[-\frac{1}{2}\nabla^2 + \int\frac{\rho(r')}{|r-r'|}dr' + \upsilon_{ext}(r) + \upsilon_{exc}(r)\right]\phi_K(r) = -E_K\phi_K(r)$$

LIST OF PUBLICATIONS

1. Kabita, K.; Maibam, J.; Sharma, B.I.; Singh, R.K.; Thapa, R.K. (2016). First principles phase transition, elastic properties and electronic structure calculations for cadmium telluride under induced pressure: density functional theory, LDA, GGA and modified Becke–Johnson potential. *Materials Research Express*, Vol. 3, No. 1, pp. 015901 (1-11).
2. Kabita, K.; Jameson, M.; Sharma, B.I.; Brojen, R.K.; Thapa, R.K. (2015). A detailed first principle study on the structural, elastic, and electronic properties of indium arsenide (InAs) under induced pressure. *Canadian Journal of Physics*, Vol. 94, No. 3, pp. 254-261.
3. Kabita, K.; Maibam, J.; Sharma, I.; Singh, R.K.; Thapa, R.K. (2015). Elastic Properties and Electronic Structures of Pressure Induced Zinc Sulphide (ZnS): A Density Functional Theory Study. *Advanced Science Letters*, Vol. 21, No. 9, pp. 2906-2910.
4. Kabita, K.; Maibam, J.; Sharma, B.I.; Thapa, R.K.; Singh, R.K. (2015). First principle study on pressure-induced electronic structure and elastic properties of indium phosphide (InP). *Indian Journal of Physics*, Vol. 89, No. 12, pp. 1265-1271.
5. Kabita, K.; Sharma, B. I. (2015). Electronic Structures of GaX (X=P, As) under Induced Pressure: A First Principle Study. *Jounal of Basic and Applied Engineering Research,* Vol. 2, No. 13, pp. 1064-1067.
6. Kabita, K.; Sharma, B. I. (2015). Structural Phase Transition of Indium Arsenide under Induced Pressure: A Density Functional Theory Study. *Journal of Applied and Fundamental Sciences*, Vol. 1, No. 1, pp.7-10.
7. Kabita, K.; Maibam, J.; Sharma, B.I.; Singh, R.K.; Thapa, R.K. (2014). Density functional theory study on pressure induced structural transformation, elastic properties and electronic structure of gallium

arsenide (GaAs). *International Journal of Innovation and Applied Studies*, Vol. 8, No. 1, pp.382-393.

8. Kabita, K.; Maibam, J.; Sharma, B.I.; Thapa, R.K.; Singh, R.K. (2014). Density Functional Theory Study of Electronic Structure, Elastic Properties and Phase Transition of Gallium Phosphide (GaP). *Advanced Science, Engineering and Medicine*, Vol. 6, No. 3, pp.354-358.
9. Kabita, K.; Maibam, J.; Sharma, B.I.; Thapa, R.K.; Singh, R.K. (2013). First Principle Calculation of Pressure-Induced Phase Transition and Band Structure of Gallium Phosphide. *Iraqi Journal of Applied Physics*, Vol. 9 No. 4, pp. 17-20.

LIST OF CONFERENCES, SEMINARS AND WORKSHOPS ATTENDED

1. Presented a paper titled "First principles study on structural, phase transition and electronic structure of Zinc Sulfide (ZnS) within LDA, GGA and mBJ potential" at XXVII IUPAP Conference on Computational Physics CCP 2015, IIT Guwahati.
2. Presented a paper titled "Theoretical study on the B3 phases of ZnSe: Structural and Electronic properties" at International E-Workshop/ Conference on Computational Condensed Matter Physics and Material Science (IWCCMP-2015), IIIITM, Gwalior.
3. Presented a paper titled "Electronic Structures of GaX (X=P, As) Under Induced Pressure: A DFT study" at the International conference on Recent trends in Applied Physical, Chemical Sciences, Mathematical/Statistical and Environmental Dynamics (PCME-2015), at JNU, New Delhi.
4. Presented a paper titled "Electronic properties of B3 phases of GaP at High Pressure: A DFT study" at the National Conference on Current Perspectives on Research on Chemical Sciences (CPRCS-2015), AUS, Silchar.
5. Presented a paper titled "Elastic Properties and Electronic Structures of Pressure induced ZnS: A DFT study" at International E-Workshop/ Conference on Computational Condensed Matter Physics and Material Science (IWCCMP-2014), IIIITM, Gwalior.
6. Presented paper titled "Ab-initio study on the electronic structure of InP" at the National seminar on Frontiers of Research in Physical Sciences, 2014, Karimganj, Assam.
7. Attended workshop on "Microwave: Basics and Applications"2014, at AUS, Silchar.
8. Attended summer school on Materials Simulation Theory and Numerics, 2014, IISER Pune.
9. Attended "Refresher Course in Theoretical Physics" 2013, at AUS, Silchar.

10. Presented paper titled “FP-LAPW investigation of the electronic structure of GaP in zinc-blende structure” 2013, at the National Seminar on Advances in Research in Physical Sciences, Cachar College, Silchar.

First principles phase transition, elastic properties and electronic structure calculations for cadmium telluride under induced pressure: density functional theory, LDA, GGA and modified Becke–Johnson potential

2016 Mater. Res. Express 3 015901

(http://iopscience.iop.org/2053-1591/3/1/015901)

Materials Research Express

PAPER

First principles phase transition, elastic properties and electronic structure calculations for cadmium telluride under induced pressure: density functional theory, LDA, GGA and modified Becke–Johnson potential

RECEIVED
7 September 2015

REVISED
30 November 2015

ACCEPTED FOR PUBLICATION
8 December 2015

PUBLISHED
14 January 2016

Kh Kabita[1], **Jameson Maibam**[1], **B Indrajit Sharma**[1], **R K Brojen Singh**[2] **and R K Thapa**[3]

[1] Department of Physics, Assam University, Silchar-788011, Assam, India
[2] School of Computational and Integrative Sciences, JNU, New Delhi 110067, India
[3] Department of Physics, Mizoram University, Tanhril, Aizawl-796 009, India

E-mail: indraofficial@rediffmail.com

Keywords: DFT, phase transition, elastic properties, electronic structure

Abstract

We report first principles phase transition, elastic properties and electronic structure for cadmium telluride (CdTe) under induced pressure in the light of density functional theory using the local density approximation (LDA), generalised gradient approximation (GGA) and modified Becke–Johnson (mBJ) potential. The structural phase transition of CdTe from a zinc blende (ZB) to a rock salt (RS) structure within the LDA calculation is 2.2 GPa while that within GGA is found to be at 4 GPa pressure with a volume collapse of 20.9%. The elastic constants and parameters (Zener anisotropy factor, Shear modulus, Poisson's ratio, Young's modulus, Kleinmann parameter and Debye's temperature) of CdTe at different pressures of both the phases have been calculated. The band diagram of the CdTe ZB structure shows a direct band gap of 1.46 eV as predicted by mBJ calculation which gives better results in close agreement with experimental results as compared to LDA and GGA. An increase in the band gap of the CdTe ZB phase is predicted under induced pressure while the metallic nature is retained in the CdTe RS phase.

1. Introduction

The II-VI semiconductor compounds have been extensively studied for several decades [1–3]. The study of the high pressure properties of these compound semiconductors has been of much scientific interest in recent years as important information about the electronic and elastic properties of the material can be gained by understanding the strained effects on the bulk compounds [4]. Cadmium telluride (CdTe) is a II-VI compound semiconductor which is being studied for its application in γ-ray detectors, infrared windows, solar cells and other optoelectronic devices [5]. Its high pressure behaviour has attracted much attention in recent years. It is found to occur in zinc blende (ZB) structures and wurtzite structures under ambient conditions and transforms to a rock salt (RS) structure at high pressures [6].

Ab-initio studies of the structural, mechanical and electronic properties of a material have become more precise and systematic due to the development in computer simulations. It helps us to better understand the properties of solids which are difficult to study experimentally. Generally the theoretical investigation of the band structure and electronic properties of compound semiconductors are performed using the local density approximation (LDA), generalised gradient approximation (GGA) and GW [7, 8]. Theoretical calculation within LDA and GGA approximation underestimates the energy band gap. The most appropriate tool for studying the energy band gap is the many perturbation theory within the GW approximation [9] but it is very expensive. In 2009 an alternative method for band gap calculation was given by Tran and Blah [10] which was equally efficient and computationally cheap. The modified Becke–Johnson (mBJ)-GGA potential [11]

minimises the limitation of LDA and GGA and performs the calculation of band gaps precisely similar to the computationally expensive GW calculations.

To date there have been detailed studies on the electronic and elastic properties of CdTe [12–14] but not much has been done at high pressures. In 1993, McMahon and his group found out that with increasing pressure, the ZB structure underwent a transition to a cinnabar structure which was stable for only a short pressure interval and later changed to an RS structure on further increasing pressure [15]. Earlier studies also confirmed the phase transition of CdTe from a ZB to an RS structure at 3.8 GPa pressure [16]. In our previous work we have reported a detailed study on the pressure induced electronic structure and elastic properties of GaP [17, 18] and GaAs [19]. The aim of the present work is to perform first principles calculations for CdTe at different pressures and study the pressure induced phase transition from the ZB to RS phase as well as the effects of pressure in the elastic properties and electronic structures.

2. Computational method

All the calculations reported in this work are performed using the full potential linearized augmented plane wave [20] method under the framework of density functional theory (DFT) [21–23] as implemented in the WIEN2K code [24]. The exchange correlation interaction effects were treated with LDA, the generalized gradient approximation of the Perdew–Burke–Ernzerhof (PBE–GGA) [25] scheme and GGA with the modified Becke–Johnson (mBJ) potential. The use of the mBJ potential along with GGA in electronic structure calculation keeps the band gap in close agreement with the experimental value. In this method, the lattice is divided into non-overlapping spheres (called an atomic or muffin tin (MT) sphere) surrounding each atomic site and an interstitial region. Inside the MT region, the potential is a product of radial function and spherical harmonics and expanded up to order $l = 10$. For the interstitial regions that are outside the MT sphere, the potentials are expanded in plane waves. In the present study the number of k-points used for the integration part for both the ZB and RS structure of CdTe is 8000 k-points with 20*20*20 k mesh which is reduced to 256 irreducible k-points inside the Brillion zone including five high symmetry points W, L, Γ, X and K. Convergence of the basis set is obtained at $R_{MT}K_{max} = 9.0$ where K_{max} gives us the plane wave cut-off. The RMT_{min} used in the calculation is 2.5. The position of the first and second atom in the ZB structure is taken to be (0, 0, 0) and (0.25, 0.25, 0.25) and in the RS structure it is (0, 0, 0) and (0.5, 0.5, 0.5) respectively. The states $4d^{10}5s^2$ and $4d^{10}5s^25p^4$ are considered as a valence electron for Cd and Te respectively. The total energy difference used for succeeding iterations is less than 0.00 001 Ryd per formula unit. The elastic constants have been determined using the stress–strain method with a volume conserving technique [26]. Only a small distortion has been considered in our calculation in order to remain within the elastic domain of the crystal.

3. Results and discussion

3.1. Structural and phase transition

Figure 1 shows the plot of total energy as a function of volume of CdTe for both the ZB and RS phase within LDA and GGA for structure optimization. From the figure, one can see that the ZB structure of CdTe has lower total energy at the equilibrium volume in both the LDA and GGA method thus indicating that the ZB structure is more stable than the RS structure. The equilibrium structural parameters of the different phases of CdTe are obtained by fitting into the Birch–Murnaghan equation [27].

The obtained structural parameters are listed in table 1 along with other theoretical and experimental data. In general the present work agrees well with other experimental and theoretical results and hence is used for further high pressure calculation.

A thermodynamically stable phase is defined as the phase with the lowest Gibb's free energy at a given pressure and temperature. In our calculation we have ignored the entropy contribution as it is basically done at zero temperature. Therefore the structural phase transition is calculated from the equal enthalpy conditions, $H = E + PV$. In figure 2, the calculated enthalpy curves of the ZB and RS phase have been plotted as a function of pressure within both (a) LDA and (b) GGA. One can see from the figures that there is a crossing over of the enthalpy at 2.2 GPa pressure with the LDA calculation and 4.0 GPa pressure with the GGA calculation. It indicates a phase transition between the two phases. The experimental data available for this phase transition of CdTe-ZB to CdTe-RS is 3.0 GPa to 3.9 GPa [36–38]. Thus we observe that the LDA method underestimates the phase transition pressure while the GGA method gives a better result than the LDA and is in close agreement with the experimentally obtained values.

Since the phase transition pressure as determined with the GGA method gives us a better result we calculate the volume collapse for GGA only. Figure 3 shows the normalised volume (Vp/Vo) as a function of pressure. It is seen that during the phase transition, the normalised volume of the ZB and RS phase is 0.90 and 0.69 respectively

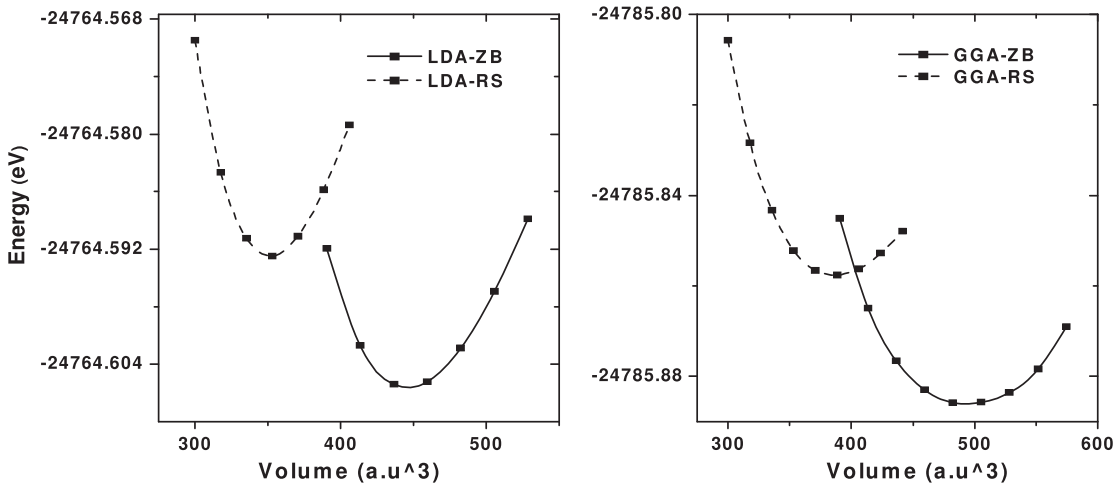

Figure 1. Total energy as a function of the volume of CdTe for ZB and RS structures within LDA and GGA.

Table 1. Experimental and calculated ground state structural parameters of CdTe.

		Zinc blende (ZB) strucutre			Rock salt (RS) structure		
		a_0 (A^0)	B_0 (GPa)	$B^/$	a_0 (A^0)	B_0 (GPa)	$B^/$
Present work	LDA	6.42	47.67	5.05	5.92	63.82	5.01
	GGA	6.65	25.28	8.35	6.11	48.24	4.99
Experimental work		6.53[a], 6.49[b]	42[g], 45[h]	6.4[g]	—	—	—
Other calculation		6.63[c], 6.62[d], 6.58[e]	33.8[c], 39.0[d], 36.6[e]	5.26[c], 5.14[c], 4.6[d]	6.11[d], 5.94[d], 5.9[f]	56.0[d], 66.4[f]	4.3[d], 5.1[i], 4.67[j]

[a] Reference [28],
[b] Reference [29],
[c] Reference [30],
[d] Reference [31],
[e] Reference [32],
[f] Reference [14],
[g] Reference [33],
[h] Reference [34],
[i] Reference [13],
[j] Reference [35].

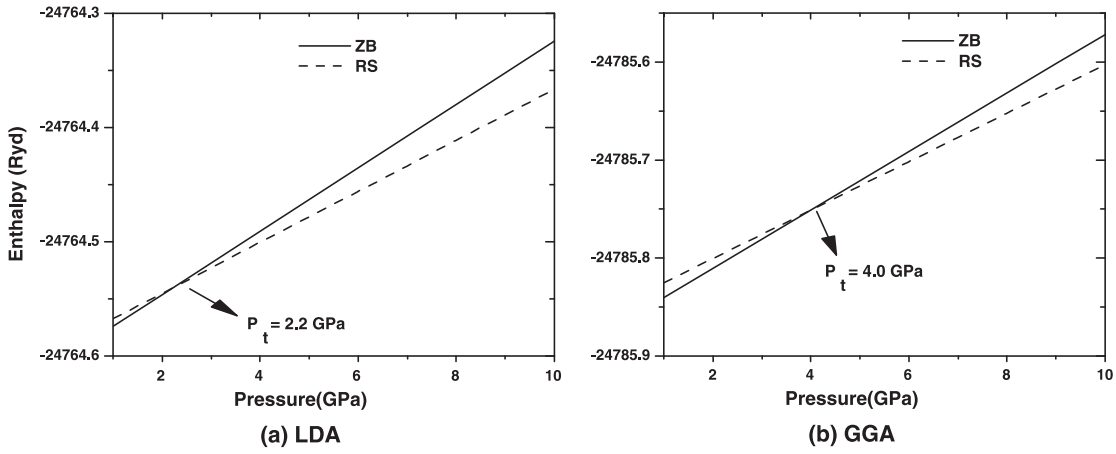

Figure 2. Enthalpy as a function of pressure for the ZB and RS phase of CdTe within (a) LDA and (b) GGA.

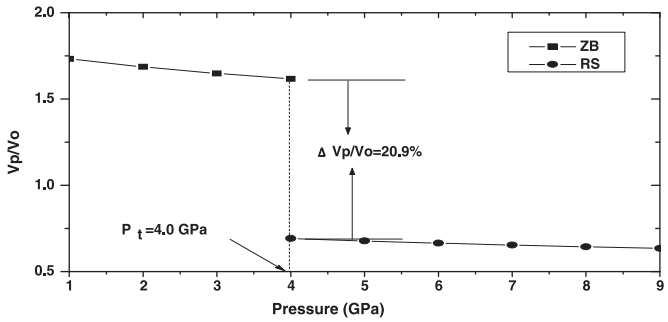

Figure 3. Normalised volume versus pressure for ZB and RS structures of CdTe within GGA.

Table 2. Phase transition pressure and volume collapse of CdTe.

	Present calculation	Expt. results	Theoretical results
Phase transition pressure (P_t) (GPa)	4.0	3.9[a], 3.8[b], 3.8[c], 3.8[d]	4.0[e], 3.9[f]
V_p/V_0	0.90	0.92[d]	0.93[b], 0.90[e]
Volume collapse (%)	20.9	—	19.0[b], 19.0[e]

[a] Reference [37],
[b] Reference [36],
[c] Reference [38],
[d] Reference [39],
[e] Reference [3],
[f] Reference [31].

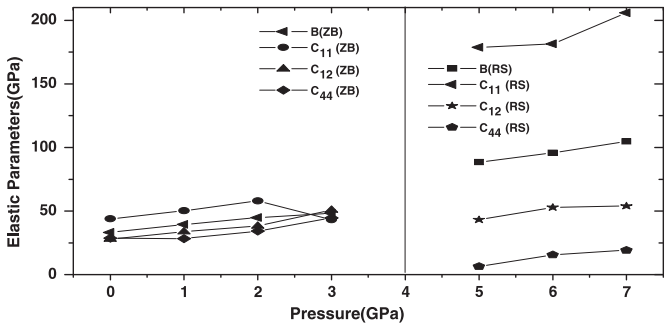

Figure 4. Elastic parameters versus pressure for the ZB and RS phase of CdTe.

with a volume reduction of 20.9% indicating that the CdTe-ZB phase is more compressible than the CdTe-RS phase. A comparison of the present results of the phase transition and volume collapse within the GGA with other experimental and theoretical results is given in table 2. It is observed that the present results of phase transition within GGA are in good agreement with other experimental and theoretical results.

3.2. Elastic properties

The elastic constants provide us with important information about the structural stability, binding characteristics and many mechanical properties of a material. For a cubic crystal the mechanical stability conditions: $(C_{11} + 2C_{12}) > 0$; C_{11}-$C_{12} > 0$; $C_{44} > 0$; $C_{11} > 0$ should be satisfied. In the present study the elastic constants are calculated within the GGA only as it has already been shown that it gives us better results than calculation within the LDA. The elastic constants of CdTe-ZB under induced pressure ranging from 0 GPa to 3 GPa pressure and for CdTe-RS at various pressures from 5 GPa to 7 GPa pressure are calculated and shown in figure 4.

In figure 4, one can clearly see that there is a linear variation in the bulk modulus as well as the elastic constants up to 2 GPa pressure in the ZB phase and 5 GPa to 7 GPa pressure in the RS phase. It is seen that at around 3 GPa pressure, the stability condition of the CdTe-ZB phase is not satisfied indicating that the structural transformation from ZB to RS starts at around 3 GPa pressure and is completed at 4 GPa pressure. Since the

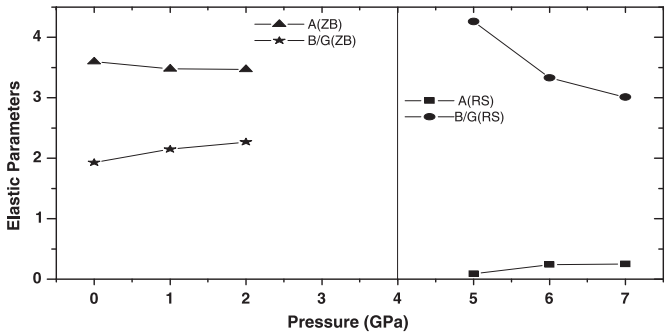

Figure 5. Elastic parameters (Zener anisotropy factor and B/G ratio) versus pressure for the ZB and RS phase of CdTe.

stability conditions are not satisfied from 3 GPa pressure and structural transition occurs at 4 GPa pressure, we perform further calculations of the elastic parameters like the Zener anisotropic factor (A), B/G ratio, Poisson's ratio (υ), Kleinmann parameter (ζ), Youngs modulus (Y), and Debye's temperature (θ_D) to determine the mechanical and thermal behaviour of CdTe in both the phases from 0 GPa to 2 GPa pressure for the CdTe-ZB phase and 5 GPa to 7 GPa pressure for the CdTe-RS phase.

The Zener anisotropy factor (A) gives us an insight into the elastic isotropy of a material. A material is said to be elastically isotropic with uniform deformation along all directions when $A = 1$. For $A > 1$, it is stiffest along <111> body diagonal and when $A < 1$, it is stiffest along <100> cube axes. In terms of elastic constants it is expressed as:

$$A = \frac{2C_{44}}{C_{11} - C_{12}} \tag{1}$$

Our calculation shows that for the CdTe-ZB phase, the value of A decreases from 3.60 to 3.46 while it increases from 0.09 to 0.25 in the RS phase with increasing pressure. It indicates that CdTe is not an elastically isotropic material in the ZB phase; it is stiffest along <111> body diagonal while it is stiffest along <100> cube axis in the RS phase. The ductility or brittleness of a material is determined by the ratio of bulk and shear modulus, B/G as proposed by Pugh [40]. If the shear modulus (G) is low we know that it has a low resistance to shear and hence is ductile, while if a material has low bulk modulus, it means the resistance fracture is low and hence is brittle. We know that the critical value which separates the ductility and brittleness of a material is 1.75. A material is said to be ductile if $B/G > 1.75$ and brittle if $B/G < 1.75$. In our calculation, we find that the B/G ratio for CdTe-ZB ranges from 1.93 to 2.15 with an increase in pressure which indicates the ductile nature at high pressure. For CdTe-RS, it is seen that after the transition pressure, the B/G ratio decreases from 4.26 to 3.01 with an increase in pressure but is greater than 1.75. Hence we can conclude that both CdTe-ZB and CdTe-RS maintain their ductile nature even at high pressures. The Zener anisotropy factor and B/G ratio as a function of pressure are shown in figure 5.

The Poisson's ratio (υ) of a material gives us information about the characteristics of bonding forces. For covalent materials, υ is 0.1, whereas for ionic materials, $\upsilon = 0.25$ [41]. It is given by the relation:

$$\upsilon = \frac{1}{2}\left(\frac{B - \left(\frac{2}{3}\right)G}{B + \left(\frac{1}{3}\right)G}\right) \tag{2}$$

where

$$G = \frac{G_V + G_R}{2} \tag{3}$$

is the isotropic shear modulus, G_v is the Voigt's shear modulus and G_R is the Reuss's shear modulus and can be expressed as:

$$G_V = \frac{C_{11} - C_{12} + 3C_{44}}{5} \tag{4}$$

and

$$\frac{5}{G_R} = \frac{4}{C_{11} - C_{12}} + \frac{3}{C_{44}} \tag{5}$$

In the present calculation, the value of υ increases from 0.27 to 0.30 in the ZB phase and decreases from 0.39 to 0.35 in the RS phase indicating higher ionic contribution in intra-atomic bonding with increasing pressure in both the phases. The lower and upper limits of υ in central force solids have been reported to be 0.25 and 0.5 respectively [42]. Thus the present result also indicates that inter atomic forces tend to be more central as pressure increases.

The relative ease of bond bending against the bond stretching is indicated by ζ (Kleimann parameter) and is calculated using the relation:

$$\zeta = \frac{C_{11} + 8C_{12}}{7C_{11} + 2C_{12}} \tag{6}$$

It also implies resistance against bond bending or bond angle distortion. In a system, minimizing bond bending leads to $\zeta = 0$ and minimizing bond stretching leads to $\zeta = 1$.

In the present study, as the pressure increases, ζ does not vary much and remains around 0.75 for CdTe-ZB and 0.41 for CdTe-RS indicating shrinkage in bond-stretching in both phases.

The Young's modulus (Y) determines the stiffness of a material and is given by

$$Y = \frac{9GB}{G + 3B} \tag{7}$$

Also, from the bulk modulus (B) and the isotropic shear modulus (G), the longitudinal elastic wave velocity (v_l) and the transverse elastic wave velocity (v_t) are calculated as follows:

$$v_l = \sqrt{\frac{3B + 4G}{3\rho}} \tag{8}$$

$$v_t = \sqrt{\frac{G}{\rho}} \tag{9}$$

Now, the average sound velocity (v_m) is given by

$$v_m = \left[\frac{1}{3}\left(\frac{2}{v_t^3} + \frac{1}{v_l^3}\right)\right]^{-(1/3)} \tag{10}$$

Using the average sound velocity υ_m, the Debye's temperature θ_D is calculated from the elastic constants data as given by:

$$\theta_D = \frac{h}{k}\left[\frac{3n}{4\pi}\left(\frac{N_A\rho}{M}\right)\right]^{1/3} v_m \tag{11}$$

where h is the Plank's constant, k is the Boltzmann constant, N_A is the Avogadro's number, n is the number of atoms per formula unit, M is the molecular mass per formula unit, $\rho\,(=M/V)$ is the density.

In the present calculation for CdTe-ZB, the value of Y increases from 44.08 GPa to 54.15 GPa while in CdTe-RS it increases from 57.65 GPa to 93.84 GPa. Hence CdTe becomes stiffer with an increase in pressure in both phases. The Debye's temperature thus calculated shows variation from 181 K to 194 K for the ZB structure while in the RS phase it is found to increase from 209 K to 247 K indicating better thermal conductivity under pressure.

3.3. Electronic structures

Under ambient pressure CdTe crystallizes in the ZB structure and the RS structure is stable at high pressures. We have therefore studied the electronic structure of CdTe at 0 GPa pressure only for the ZB phase and the electronic structure of the RS phase is studied only at high pressures. The energy band diagram of CdTe-ZB at 0 GPa pressure calculated using LDA, GGA and mBJ-GGA are shown in figure 6. From the figure one can see clearly that the conduction band minimum and the valance band maximum are located at the middle of the brillouin zone, Γ point indicating the band gap is a direct band gap. However the band gap calculated using the LDA method and GGA method in figure 6 are 0.51 eV and 0.56 eV respectively which are lower than the experimentally reported 1.44 eV [43]. Thus the LDA and GGA method underestimate the energy band gap. The mBJ-GGA calculation of the band gap in figure 6 shows 1.46 eV that reasonably agrees with the experimentally reported value of 1.44 eV with a mere difference of about 1.4%. One of the reasons for the mere difference is that the present calculation is performed in the light of DFT at absolute temperature whereas the reported

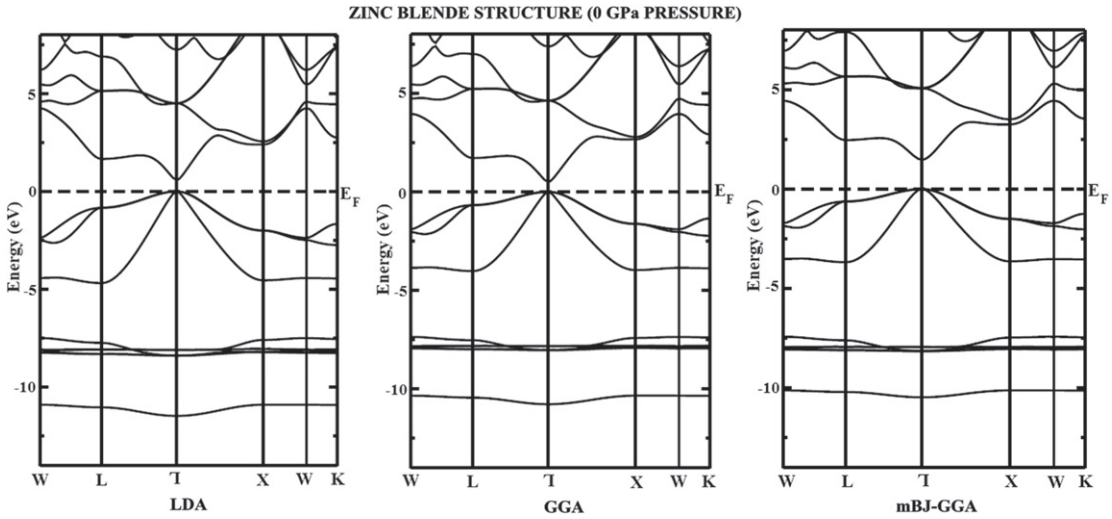

Figure 6. Band structure of CdTe-ZB at 0 GPa pressure within LDA, GGA and mBJ-GGA.

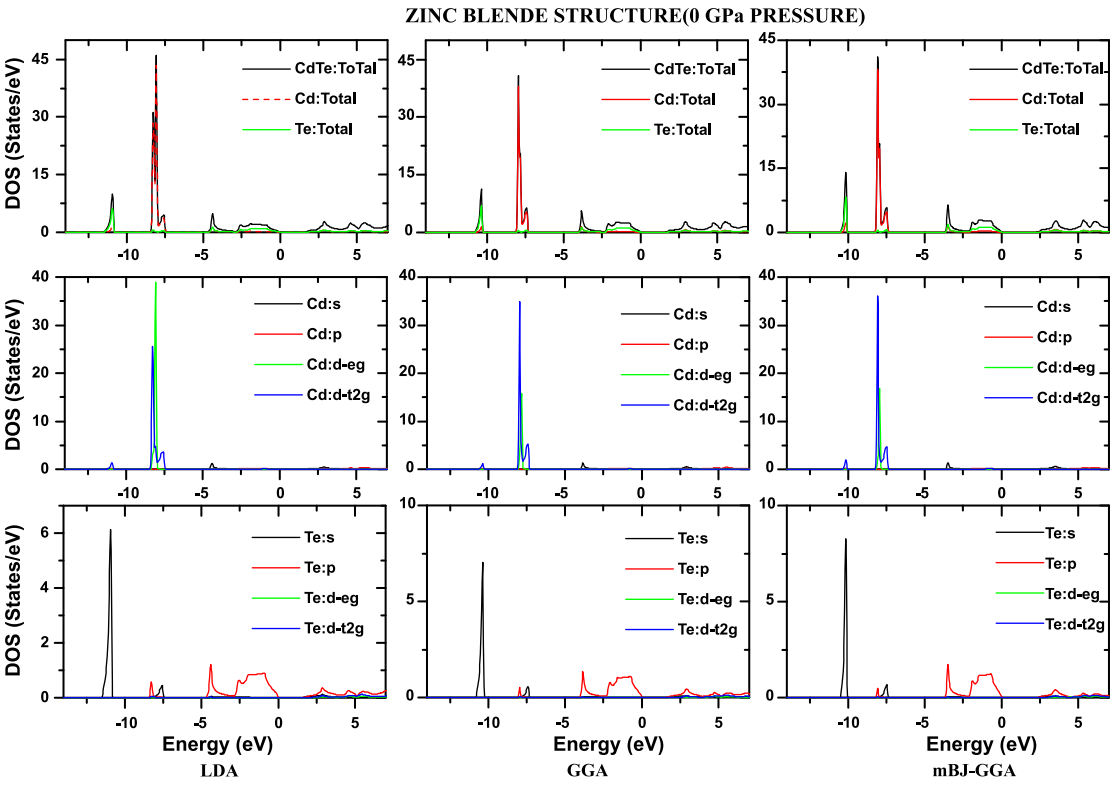

Figure 7. Total and partial DOS of CdTe-ZB at 0 GPa pressure within LDA, GGA and mBJ-GGA.

experimental value is at room temperature. Also the gap between the first and second lowest band in the band diagrams obtained using the three approximations is found to decrease following the trend LDA $>$ GGA $>$ mBJ and more importantly the gap between the lowest band and the valence band increases as LDA $<$ GGA $<$ mBJ. To better understand the electronic structure of CdTe, the total and partial DOS within the LDA, GGA and mBJ have also been studied and are shown in figure 7. Firstly, within the LDA calculation, the presence of the two lowest bands is indicated with the first lowest band mainly contributed with 6.10 eV of s-state (Te-atom) with little contribution of 1.31 eV from the d-t2g-state (Cd-atom) while the second lowest band shows a higher contribution of 39.04 eV of the d-eg- state (Cd atom) with 25.27 eV of the d-eg-state (Cd atom). One interesting fact about the contribution of the state within the LDA, GGA and mBJ is that in the first lowest band, the contribution trend of the s-state (Te atom) follows the trend LDA $<$ GGA $<$ mBJ. Similarly in

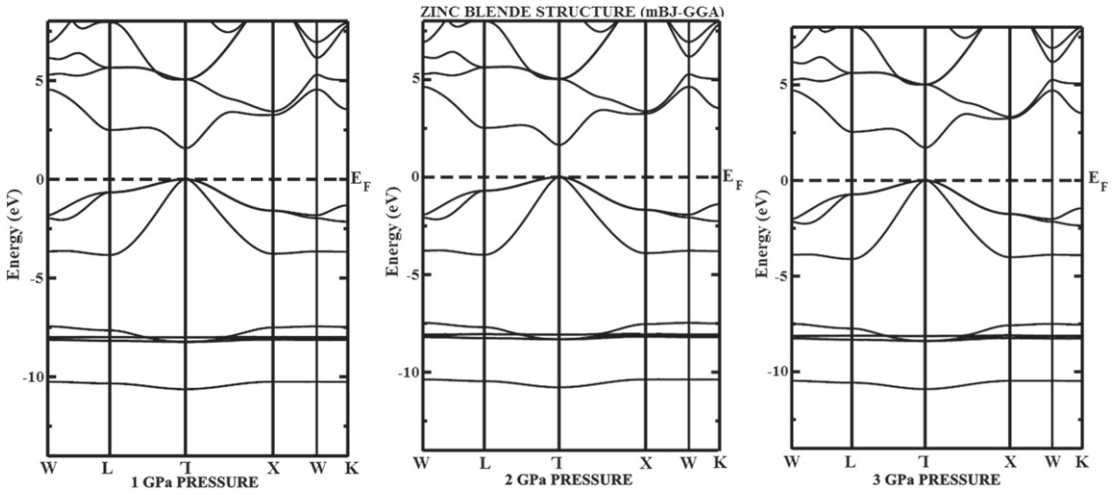

Figure 8. Energy band diagram of the CdTe ZB structure at 1 GPa, 2 GPa and 3 GPa pressure.

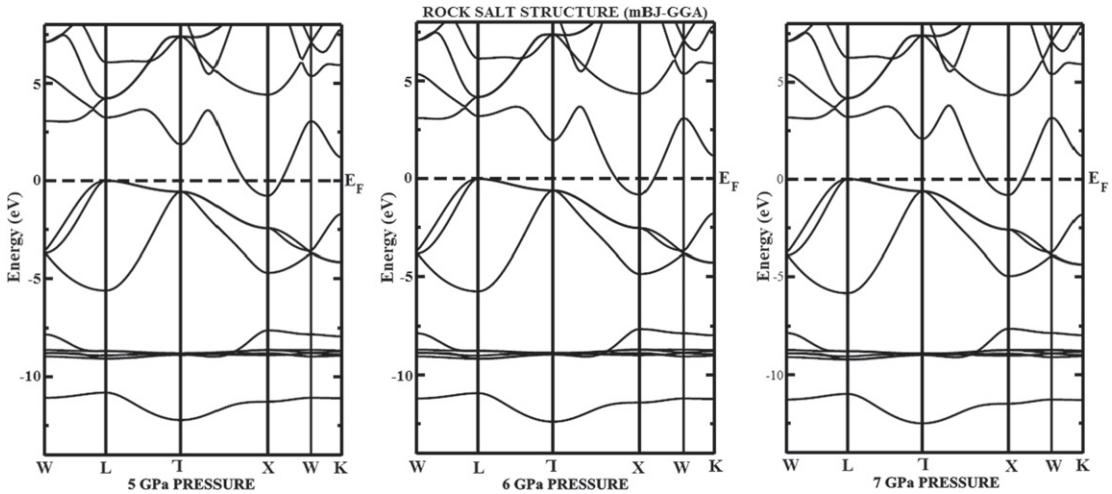

Figure 9. Energy band diagram of the CdTe RS structure at 5 GPa, 6 GPa and 7 GPa pressure.

the second lowest band the contribution trend of the d-eg state (Cd atom) is LDA $>$ GGA $>$ mBJ and for the d-t2g state (Cd atom) is LDA $<$ GGA $<$ mBJ. The valance band study of DOS within the LDA shows a contribution of 1.38 eV of the s-state (Cd atom) and 1.28 eV of the s-state (Te atom). GGA calculation shows an equal contribution of about 1.39 eV of the s-state (Cd atom) and s-state (Te atom) but within mBJ the contribution of the s-state (Te atom) is 1.78 eV while that of the s-state (Cd atom) is 1.46. Therefore the overall contribution trend of the states in the valance band within the three methods is found as LDA $<$ GGA $<$ mBJ. Thus the effective results within the mBJ calculation are due to the proper treatment of the electronic states.

The energy band diagram of CdTe-ZB at different pressures from 1 GPa pressure to 3 GPa is shown in figures 8(a)–(c) and from 5 GPa pressure to 7 GPa of CdTe-RS is also shown in figures 9(a)–(c). The band diagram under induced pressure of CdTe-ZB in figure 8 shows that as the pressure increases to 1 GPa, 2 GPa and 3 GPa, the energy gap between Γ and X increases to 2.42 eV $<$ 2.45 eV $<$ 2 .47 eV while the gap between Γ and L decreases from 3.21 eV $>$ 3.18 eV $>$ 3.16 eV respectively towards the Fermi level. On the other hand the band diagram under pressure 5 GPa, 6 GPa, 7 GPa of CdTe-RS in figures 9(a)–(c) clearly indicates the conduction band crosses towards the valance band confirming the transition from the direct band gap nature to metallic at higher pressure.

For detailed analysis on the band structure of CdTe, the total DOS plots for both the ZB and RS structures are also studied at different pressures. Figures 10 and 11 show the total DOS plots of CdTe-ZB at 1 GPa, 2 GPa and 3 GPa pressure and CdTe-RS at 5 GPa, 6 GPa and 7 GPa pressure. In figure 10 the contribution of the Te atom and Cd atom in the lowest band and the contribution of the Cd atom in the valance band decreases with

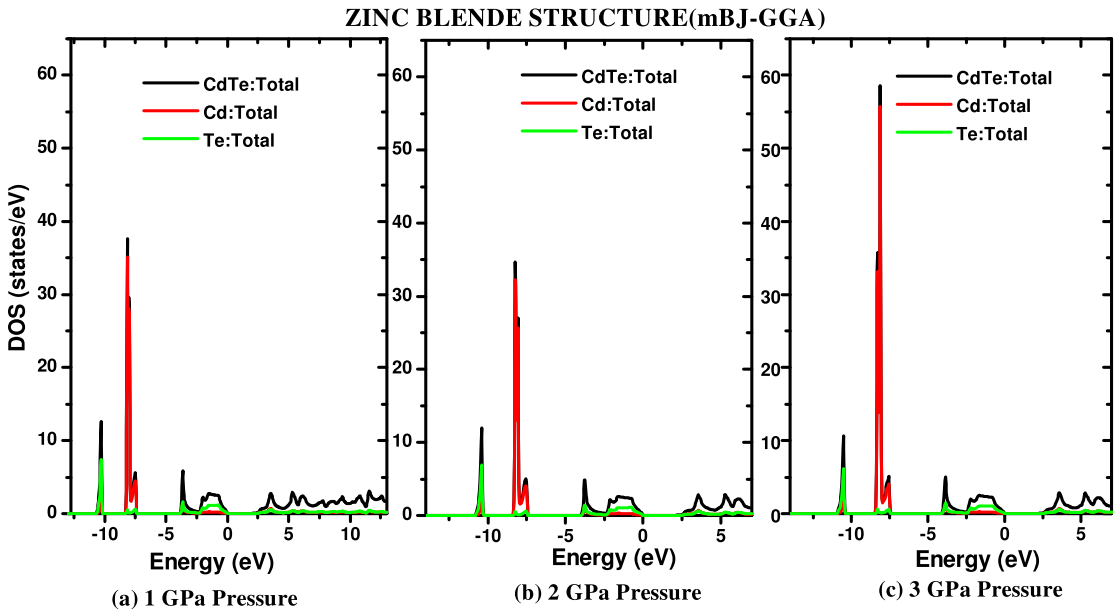

Figure 10. Total DOS of the CdTe-ZB structure at (a) 1 GPa pressure, (b) 2 GPa pressure and (c) 3 GPa pressure.

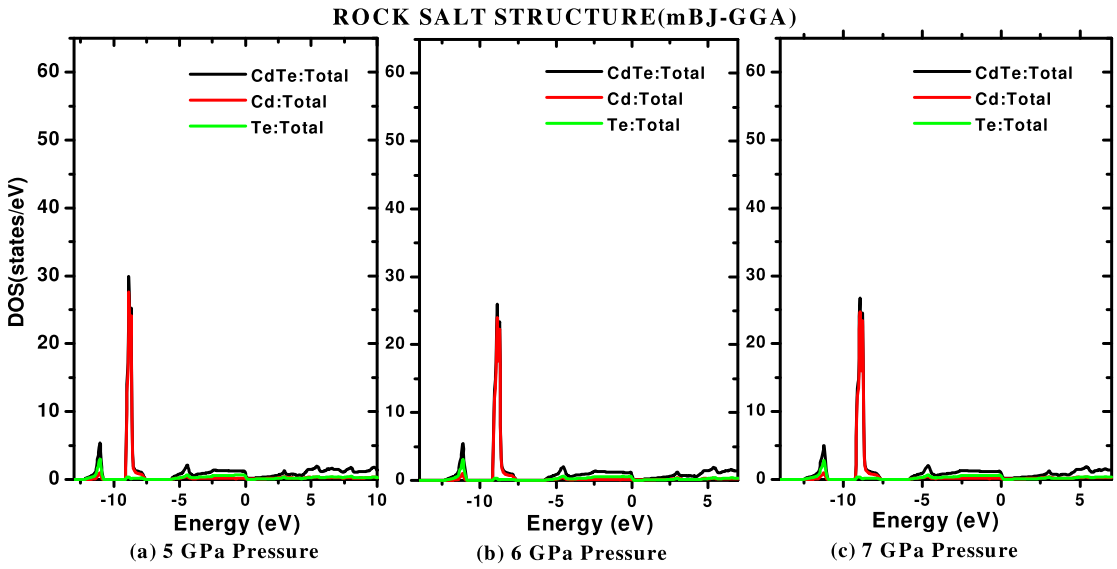

Figure 11. Total DOS of the CdTe-RS structure at (a) 5 GPa pressure, (b) 6 GPa pressure and (c) 7 GPa pressure.

pressure. But at 3 GPa, pressure around the structural transition starts and the contribution of the Cd atom in the lowest band suddenly increases. However in the DOS of CdTe-RS as shown in figure 11, it is clear that there is crossing over of the conduction band in the valance band indicating a metallic character.

Thus to conclude, the variation of the direct energy band gap of CdTe-ZB with pressure is shown in figure 12. It is clearly seen that as the pressure increases the band gap of CdTe-ZB increases linearly. This may be due to the fact that with an increase in pressure the unit cell in the lattice is compressed leading to smaller normalised volume and larger binding energy which would therefore result in an increasing band gap with increasing pressure. However in the case of CdTe-RS there is no prominent change in the metallic nature of the band structure with increasing pressure. Thus we conclude that the variation in pressure does not much affect the band gap of CdTe-RS and only affects the CdTe-ZB structure.

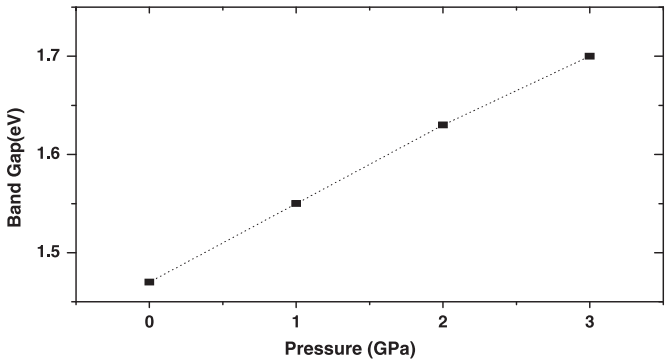

Figure 12. Variation of the direct band gap of CdTe-ZB with pressure.

4. Summary and conclusions

The structural properties of CdTe in both the ZB and RS phases are studied within the LDA and GGA. The structural phase transition of CdTe from the ZB structure to the RS structure within the LDA is found to occur at 2.2 GPa pressure while calculation within the GGA shows a phase transition at 4 GPa pressure with a volume collapse of 20.9%. The GGA calculation shows close agreement with other experimental and theoretical results. The elastic constants for both the structures are calculated at different pressures and found to show a linear increase with pressure. The elastic parameters such as the Zener anisotropy factor, Shear modulus, Poisson's ratio, Young's modulus, Kleinmann parameter and Debye's temperature are also calculated and it is found that both the ZB and RS phase maintain their ductile nature even at high pressures. Shrinkage in bond-stretching and the stiffness of CdTe are observed in both the phases with an increase in pressure while the ZB phase shows a poor thermal conductivity at high pressures. The band diagram of CdTe-ZB at 0 GPa pressure within the LDA, GGA underestimate the band gap while the mBJ method shows a direct band gap of 1.46 eV and is found to be in close agreement with the experimental value. The direct band gaps of CdTe-ZB show a linear increase while the metallic nature is found to be retained in CdTe-RS under induced pressure. Thus we conclude that the mBJ-GGA is an efficient theoretical technique for the calculation of band structures and will be a successful tool for the engineering of compound semiconductors. The present study will stimulate experimental studies of high pressures and shed new light on high pressure applications of optoelectronic devices.

References

[1] Mujica A, Rubio A, Munoz A and Needs R J 2003 *Rev. Mod. Phys.* **75** 863
[2] Shimojo F *et al* 2004 *Phys. Rev.* B **70** 184111
[3] Miao M S and Lambrecht W R L 2005 *Phys. Rev. Lett.* **94** 225501
[4] Nelmes R J and McMahon M I 1998 *Semicond. Semimetals* **54** 145
[5] Wei S and Zhang S B 2000 *Phys. Rev.* B **62** 6944
[6] Deligoz E, Colakoglu K and Ciftci Y 2006 *Physica* B **373** 124
[7] Aulbur W G, Städele M and Görling A 2000 *Phys. Rev.* B **62** 7121
[8] Shishkin M, Marsman M and Kresse G 2007 *Phys. Rev. Lett.* **99** 246403
[9] Aryasetiawan F and Gunnarsson O 1998 *Rep. Prog. Phys.* **61** 237
[10] Tran F and Blaha P 2009 *Phys. Rev. Lett.* **102** 226401
[11] Perdew J P, Burke S and Ernzerhof M 1996 *Phys. Rev. Let.* **77** 3865
[12] McMahon M I, Nelmes R J, Wright N G and Allan D R 1993 *Phys. Rev.* B **48** 16246
[13] Benkhettou N, Rached D and Rabah M 2006 *Czech. J. Phys.* **56** 409
[14] Sharma E, Singh A and Sakalle U K 2012 *Int. J. of Engg. Sci. & Mgmt.* (*IJESM*) **2** 186
[15] Nelmes R J, McMahon M I, Wright N G and Allan D R 1993 *Phys. Rev.* B **48** 1314
[16] Edwards L and Drickamer H G 1961 *Phys. Rev.* **122** 1149
[17] Kabita K, Maibam J, Indrajit Sharma B, Thapa Singh R K and Brojen R K 2014 *Adv. Sci. Engg. Med.* **6** 354
[18] Kabita K, Maibam J, Indrajit Sharma B, Thapa Singh R K and Brojen R K 2014 *Iraqi J Appl. Phys.* **9** 17
[19] Kabita K, Maibam J, Indrajit Sharma B, Thapa Singh R K and Brojen R K 2014 *Int. J. Innovation and Appl. Stds.* **8** 382
[20] Wimmer E, Krakauer H, Weinert M and Freeman A J 1981 *Phys. Rev.* B **24** 864
[21] Hohenberg P and Kohn W 1964 *Phys. Rev. 3B* **136** 864
[22] Kohn W and Sham L J 1965 *Phys. Rev. 4A* **140** 1133
[23] Cottenier S 2002 *Density Functional Theory and the Family of (L)APW-methods: a step-by-step Introduction* (Belgium: Insti-tuut voor Kern-en Stralingsfysica, K U Leuven)
[24] Blaha P, Schwarz K, Madsen G K H, Kvasnicka D and Luitz J 2001 *WIEN2k An Augmented Plane Wave + Local Orbitals Program for Calculating Crystal Properties* (Austria: Karlheinz Schwarz, Techn. Universitat Wien)
[25] Becke D and Johnson E R 2006 *J. Chem. Phys.* **124** 221101
[26] Birch F 1947 *Phys. Rev.* **71** 809

[27] Birch F J 1938 *J. Appl. Phys.* **9** 279
[28] Lalitha S, Karazhanov S Z, Ravindran P, Senthilarasu S, Sathyamoorthy R and Janabergenov J 2006 *Physica* B **387** 227
[29] Polit J *et al* 2006 *J. Appl. Phys.* **100** 013521
[30] Ouendadji S, Ghemid S, Meradji H and Hassan F E H 2011 *Comput. Mater. Sci.* **50** 1460
[31] Zerroug S, Sahraoui F A and Bouarissa N 2007 *Eur. Phys. J.* B **57** 9
[32] Al-Douri Y, Reshak A H, Baaziz H, Charifi Z, Khenata R, Ahmad S and Hashim U 2010 *Sol. Energy* **84** 1979
[33] Strössner K, Ves S, Dieterich W, Gebhardt W and Cardona M 1985 *Solid State Commun.* **56** 563
[34] Smith T F and White G K 1975 *J. Phys. C Solid state Phys.* **8** 2031
[35] Van Camp P E and Van Doren V E 1994 *Solid State Commun.* **91** 607
[36] Mei J R and Lemos V 1984 *Solid State Commun.* **52** 785
[37] Nelmes R J, McMahon M I, Wright N G and Allan D R 1995 *Phys. Rev.* B **51** 15723
[38] Al'fer S A and Skums V F 2001 *Inorg. Mater.* **37** 1237
[39] Borg Y I and Smith D K 1967 *J. Phys. Chem. Sol.* **28** 49
[40] Pugh S F 1954 *Phil. Mag.* **45** 823
[41] Bannikov V 2, Shein I R and Ivanovskii A L 2007 *Phys. Status. Solidi. Rapid. Res. Lett.* **3** 89
[42] Fu H *et al* 2008 *Comput. Mater. Sci.* **44** 774
[43] Kittel C 1986 *Introduction to Solid State Physics* 6th edn (New York: John Wiley) p185

Volume 94

2016

An NRC Research Press Journal

Une revue de NRC Research Press

www.nrcresearchpress.com

Canadian Journal of Physics

Revue canadienne de physique

In cooperation with the Canadian Association of Physicists

Avec le concours de l'Association canadienne des physiciens et physiciennes

NRC Research Press

NRC Research Press

ARTICLE

A detailed first principle study on the structural, elastic, and electronic properties of indium arsenide (InAs) under induced pressure

Kh. Kabita, M. Jameson, B.I. Sharma, R.K. Brojen, and R.K. Thapa

Abstract: An ab initio calculation of the structural, elastic, and electronic properties of indium arsenide (InAs) under induced pressure is investigated using density functional theory with modified Becke–Johnson potential within the generalised gradient approximation of the Perdew–Burke–Ernzerhof scheme. The lattice parameters are found to be in good agreement with experimental and other theoretical data. The pressure-induced structural phase transition of InAs zinc blende to rock salt structure is found to occur at 4.7 GPa pressure with a 17.2% of volume collapse. The elastic properties of both the zinc blende and rock salt structures at different pressures are studied. The electronic band structures at different pressures for both the structures are investigated using the total and partial density of states. The energy band gap of the InAs zinc blende phase is increased with increasing pressure while in rock salt the phase the conduction band crosses towards the valence band and thus shows metallic behaviour.

Key words: density functional theory (DFT), modified Becke–Johnson (mBJ) potential, density of states (DOS), energy band diagram, elastic properties, phase transition.

Résumé : Nous présentons un calcul ab initio des propriétés structurelles, élastiques et électroniques de l'arséniure d'indium (InAs) sous pression, à l'aide de la théorie de la fonctionnelle de densité avec un potentiel modifié de Becke–Johnson, à l'intérieur de l'approximation du gradient généralisé du schéma de Perdew–Burke–Ernzerhof. Nous trouvons que les paramètres du réseau sont en bon accord avec les données expérimentales et d'autres résultats théoriques. Nous trouvons que la transition de phase de InAs induite par la pression, de la phase blende de zinc à sel gemme se produit à 4.7 GPa, avec diminution de volume de 17.2 %. Nous étudions les propriétés élastiques des structures blende de zinc et sel gemme en utilisant les densités d'état, totale et partielle. La bande en énergie interdite du blende de zinc croît avec l'augmentation de pression, alors que dans la phase sel gemme la bande de conduction traverse vers la bande de valence et montre ainsi de meilleures propriétés métalliques. [Traduit par la Rédaction]

Mots-clés : théorie de la fonctionnelle de densité, diagramme de la bande d'énergie, densité d'états, propriétés élastiques, transition de phase.

PACS Nos.: 71.15.Mb, 71.20.-b;71.20.Nr.

1. Introduction

The technological importance of group III–V compound semiconductors has increased over the past years because of its electronic and mechanical properties and has received considerable interest from experimentalist and theorists [1–3]. To understand, the structural phase transition of a material and the influence of band structure parameters on the electronic properties of semiconductors, their study under induced pressure is found to be an effective tool. Also, the study of elastic constants at different pressures plays an important role in mechanical stability, strength, phase transition, and a material response to various conditions [4, 5]. One of the interesting phenomena that may occur under applied pressure is a sudden change in the arrangement of the atoms (i.e., structural phase transition). Indium arsenide is an important group III–V compound semiconductor having high electron mobility and narrow energy band gap. It is widely used in construction of infrared detectors and diode lasers [6]. It crystallizes in cubic zinc blende (ZB) structure under ambient conditions. At high pressure it is found to undergo structural phase transition to rock salt (RS) structure. The pressure-induced phase transition to metallic state was first reported by Minomura and Drickamer [7] at 8.46 GPa pressure from high pressure resistivity measurements. Pitt and Vyas [8] in 1973 reported the phase transition from the ZB to RS through resistivity measurements. In 2014, Wang et al. [9] also studied its electronic transport properties using the non-equilibrium Green's function combined with density functional theory. Although there have been extensive studies on structural, mechanical, and electronic properties of InAs, the experimental and theoretical study of these properties under high pressure is still very scarce. In our previous study we extensively studied the pressure-induced structural, mechanical, and electronic properties of GaP [10, 11] and GaAs [12]. The main aim of this work is to present a detailed study of the behaviour of the elastic and electronic properties of InAs in ZB and RS phases under pressure.

2. Computational methods

All theoretical calculations of InAs are performed based on the WIEN2K code [13] using the full potential linearized augmented plane wave (FP-LAPW) [14] method with modified Becke–Johnson potential [15] under the framework of density functional theory

Received 29 April 2015. Accepted 2 November 2015.

Kh. Kabita, M. Jameson, and B.I. Sharma. Department of Physics, Assam University, Silchar-788011, Assam, India.
R.K. Brojen. School of Computational and Integrative Sciences, JNU, New Delhi 110067, India.
R.K. Thapa. Department of Physics, Mizoram University, Tanhril, Aizawl-796 009, India.
Corresponding author: B.I. Sharma (email: indraofficial@rediffmail.com).

[16–18]. The generalized gradient approximation of the Perdew–Burke–Ernzerhof scheme [19] is used for treating the exchange correlation interaction effects. In this method, the lattice is divided into non-overlapping spheres (called atomic or muffin tin sphere) surrounding each atomic site and an interstitial region. Inside the muffin tin region, the potential is a product of radial function and spherical harmonics and is expanded up to order $l = 10$. For the interstitial regions that are outside the muffin tin spheres, the potentials are expanded in plane waves. The number of k-points used for the integration part is 8000k-points, which is reduced to 256 irreducible k-points inside the Brillion zone, including five high symmetry points W, L, Γ, X, and K. Convergence of the basis set is obtained at $R_{MT}K_{max} = 9.0$ where K_{max} gives us the plane wave cut-off. The elastic constants have been determined using the stress–strain method with volume conserving technique [20]. In our calculation only a small distortion has been considered to remain within the elastic domain of the crystal.

3. Results and discussion

3.1. Structural properties

The stability structure of InAs is obtained from the ground state structures of ZB and RS structures of InAs. The energy as a function of the primitive cell volume of ZB and RS phases is shown in Fig. 1. From Fig. 1, one can clearly see that the InAs-ZB structure is more stable than the RS structure. The equilibrium lattice parameters of InAs crystal in ZB and RS structures are obtained by fitting the resultant curve to the Birch–Murnaghan equation [21]. The calculated structural parameters are compared with other results [22–27] and are given in Table 1, and the results are found to be in good agreement with other results and hence are used for further calculations.

3.2. Phase transition and elastic properties

The pressure-induced phase transition of InAs-ZB to InAs-RS phase at zero temperature is investigated from the equal enthalpy conditions, $H = E + PV$. Figure 2 shows the enthalpy as a function of pressure of both the InAs-ZB and InAs-RS structures. It is clearly seen that the phase transition of InAs-ZB to InAs-RS is found to occur at 4.7 GPa pressure. The normalised volumes (V_p/V_o) of the crystals in ZB and RS phases are found to be 0.924 and 0.752, respectively, during the phase transition with a volume collapse of 17.2% indicating that the ZB phase is more compressible than the RS phase, as given in Fig. 3. Our calculated results of phase transition and volume collapse are compared with other experimental and theoretical results [8, 26–29] and are shown in Table 2. The present calculation of phase transition is found to be small as compared to the reported experimental results. The reasoning for the difference may be because the present calculation is done at absolute zero temperature.

The elastic constants of a material give us important information about the nature of the force operating in the solids and are the basic parameters that are used for studying the elastic properties of a material. Because the phase transition pressure is 4.7 GPa, elastic constants are calculated for the lattice corresponding to pressure ranging from 0 to 4 GPa of the ZB phase and 5 to 9 GPa of the RS phase. The results for our calculation are shown in Fig. 4. Our obtained results are found to satisfy the mechanical stability conditions: $(C_{11} + 2C_{12}) > 0$; $C_{11}C_{12} > 0$; $C_{44} > 0$; $C_{11} > 0$ of ZB and RS structures. Also in Fig. 4, one can clearly see that there is a linear variation of elastic constants with pressure up to 4 GPa of ZB phase and 5 to 9 GPa of RS phase, which indicates the stability of the ZB and RS phases before and after the transition pressure 4.7 GPa.

Fig. 1. Total energy as a function of primitive cell volume of InAs in ZB and RS phases.

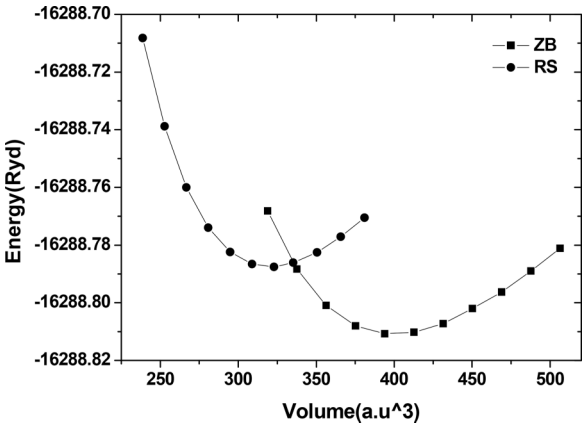

Table 1. Lattice constant, a_0 (Å); bulk modulus, B (GPa); and pressure derivative of bulk modulus, B' of ZB and RS structure of InAs at zero pressure.

Structure		a_0 (Å)	B_0 (GPa)	B'_0
ZB	Present work	6.18	49.48	4.78
	Expt. results	6.058[a]	59.2±5[e]	6.8±2[e]
	Theo. results	6.10[b], 6.08[c]	55.51[c], 50.4[d]	—
RS	Present work	5.74	62.98	4.84
	Expt. results	5.5005[e], 5.514[f]	40.6±14[e]	7.3±1[e]
	Theo. results	5.65[c]	—	—

[a][21].
[b][22].
[c][23].
[d][24].
[e][25].
[f][26].

Fig. 2. Enthalpy variation of InAs in ZB and RS structure as a function of pressure.

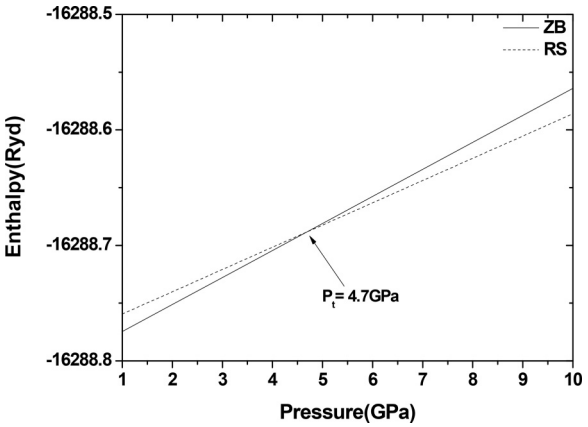

In light of these observations, the elastic parameters, such as Zener anisotropic factor (A), Poisson's ratio (υ), Kleinmann parameter (ζ), Young's modulus (Y), and Debye's temperature (θ_D), are calculated for both the InAs-ZB and InAs-RS phases to determine the mechanical and thermal behaviour at high pressure from the relation given by Mayer et al. [30].

The Zener anisotropy factor of a material determines the isotropy of that material. A material is said to be elastically isotropic with uniform deformation along all directions when $A = 1$. For

Fig. 3. Phase transition between ZB and RS structure of InAs at 4.7 GPa pressure.

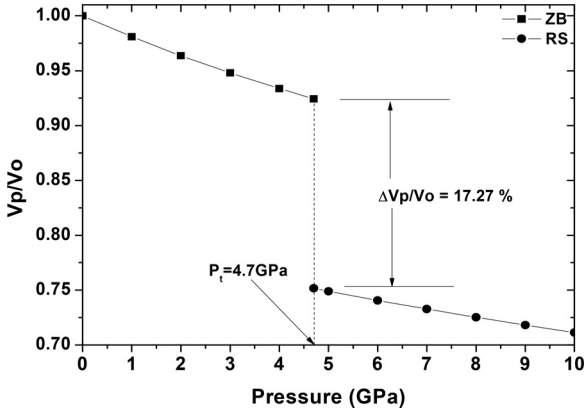

Table 2. Phase transition pressure P_t (GPa) and volume collapse of InAs.

	Present calculation	Expt. results	Theo. results
Transition pressure, P_t (GPa)	4.7	7[a], 6.9±0.2[c]	3.9[d], 4.0[e]
Volume collapse (%)	17.2	17.0±0.2[a], 18.8[b]	17.0[f]

[a][25].
[b][26].
[c][8].
[d][28].
[e][29].

Fig. 4. Elastic constants (C_{11}, C_{12}, C_{44}) as a function of pressure of InAs-ZB and InAs-RS phases.

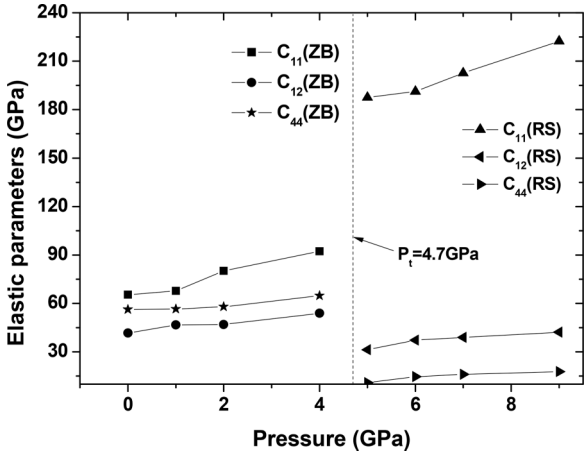

$A > 1$, it is stiffest along ⟨111⟩ body diagonal and when $A < 1$, it is stiffest along ⟨100⟩ cube axes.

In terms of elastic constants it is expressed as

$$A = \frac{2C_{44}}{C_{11} - C_{12}} \tag{1}$$

In our calculation, the value of A decreases from 5.35 to 3.37 in the ZB phase while in the RS phase it increases from 0.18 to 0.2 with pressure. Thus we find that A is stiffest along ⟨111⟩ body diagonal in the ZB phase and after transition to RS phase it becomes stiffest along ⟨100⟩ cube axes. Poisson's ratio (υ) gives us

Fig. 5. Elastic parameters (Zener anisotropy factor, Poisson's ratio, Kleinmann parameter, and B/G ratio) as a function of pressure of InAs in (*a*) ZB phase and (*b*) RS phase.

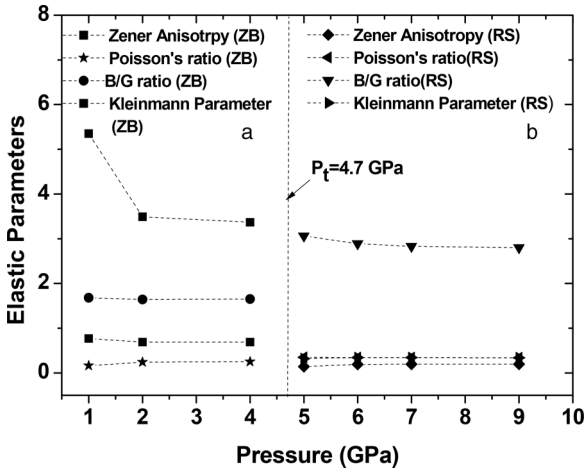

Fig. 6. Elastic parameters (Debye's temperature and Young's modulus) as a function of pressure of InAs in (*a*) ZB phase and (*b*) RS phase.

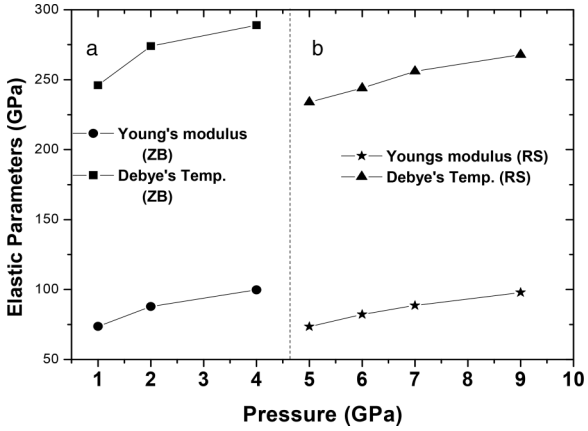

information about the characteristics of bonding forces. It is given by the relation

$$\upsilon = \frac{1}{2}\left[\frac{B - (2/3)G}{B + (1/3)G}\right] \tag{2}$$

where

$$G = \frac{G_V + G_R}{2} \tag{3}$$

is the isotropic shear modulus, G_V is Voigt's shear modulus, and G_R is the Reuss's shear modulus and can be expressed as

$$G_V = \frac{C_{11} - C_{12} + 3C_{44}}{5} \tag{4}$$

and

$$\frac{5}{G_R} = \frac{4}{(C_{11} - C_{12})} + \frac{3}{C_{44}} \tag{5}$$

Fig. 7. Energy band diagram of InAs at zero pressure in (*a*) ZB structure and (*b*) RS structure.

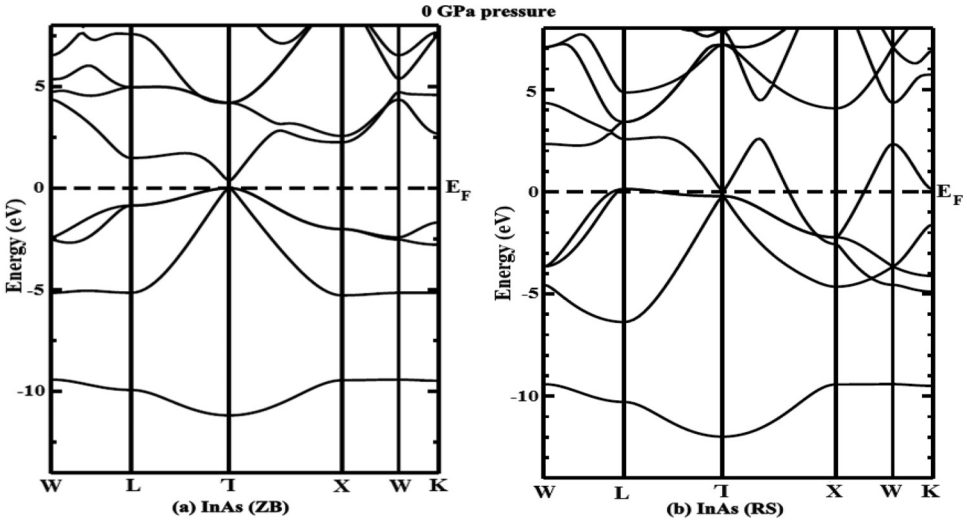

Fig. 8. DOS of InAs: (*a*) total DOS of InAs-ZB; (*b*) In (indium atom) partial DOS in InAs-ZB; (*c*) As (arsenic atom) partial DOS in InAs-ZB; (*d*) total DOS of InAs-RS; (*e*) In (indium atom) partial DOS in InAs-RS; and (*f*) As (arsenic atom) partial DOS in InAs-RS.

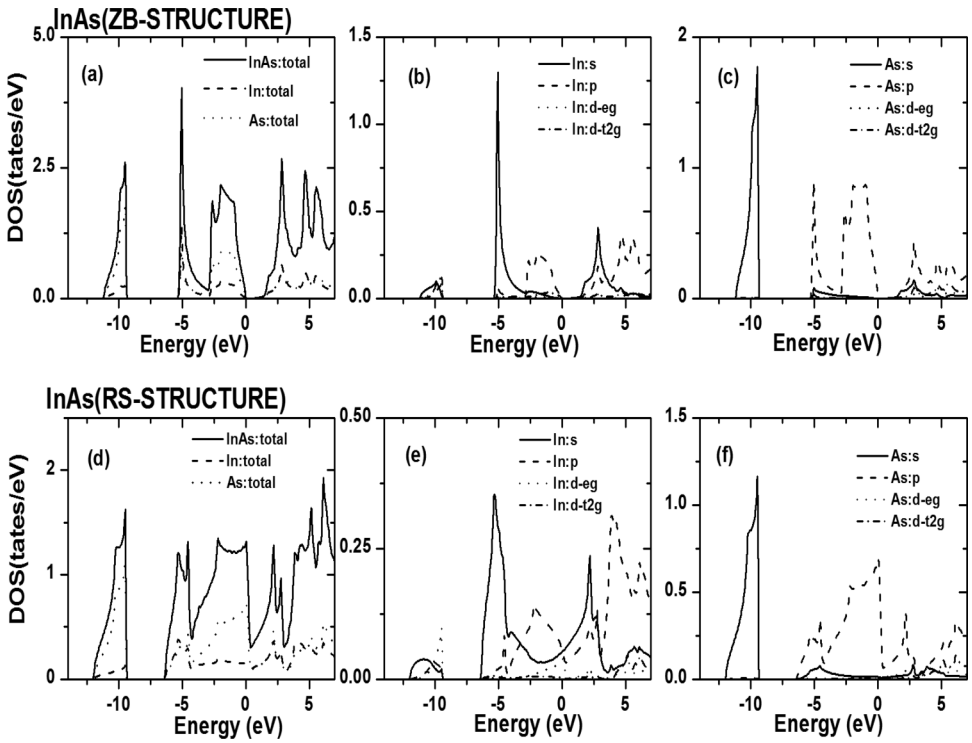

For covalent materials, the value of Poisson's ratio (υ) is 0.1, whereas for ionic materials $\upsilon = 0.25$ [31]. The lower and upper limits of υ in central force solids have been reported to be 0.25 and 0.5, respectively [32]. Our results for Poisson's ratio show that as pressure increases, the value of υ increases from 0.16 to 0.25 in the ZB phase while it remains around 0.34 in the RS phase indicating that with increasing pressure the ionic contribution to the interatomic bonding becomes dominant. It also indicates that with increasing pressure interatomic forces tend to be more central.

The relative ease of bond bending against the bond stretching is indicated by ζ (Kleimann parameter) and is calculated using the relation

$$\zeta = \frac{C_{11} + 8C_{12}}{7C_{11} + 2C_{12}} \tag{6}$$

It also implies resistance against bond bending or bond angle distortion. In a system, minimizing bond bending leads to $\zeta = 0$ and minimizing bond stretching leads to $\zeta = 1$.

In the present study, ζ of the ZB phase is found to vary from 0.77 to 0.69 with pressure while in the RS phase it is found to increase from 0.31 to 0.34 showing shrinkage in bond stretching in the ZB phase and shrinkage in bond bending in the RS phase.

Fig. 9. Energy band diagram of InAs-ZB structure: (*a*) 1 GPa pressure; (*b*) 2 GPa pressure; (*c*) 3 GPa pressure; and (*d*) 4 GPa pressure.

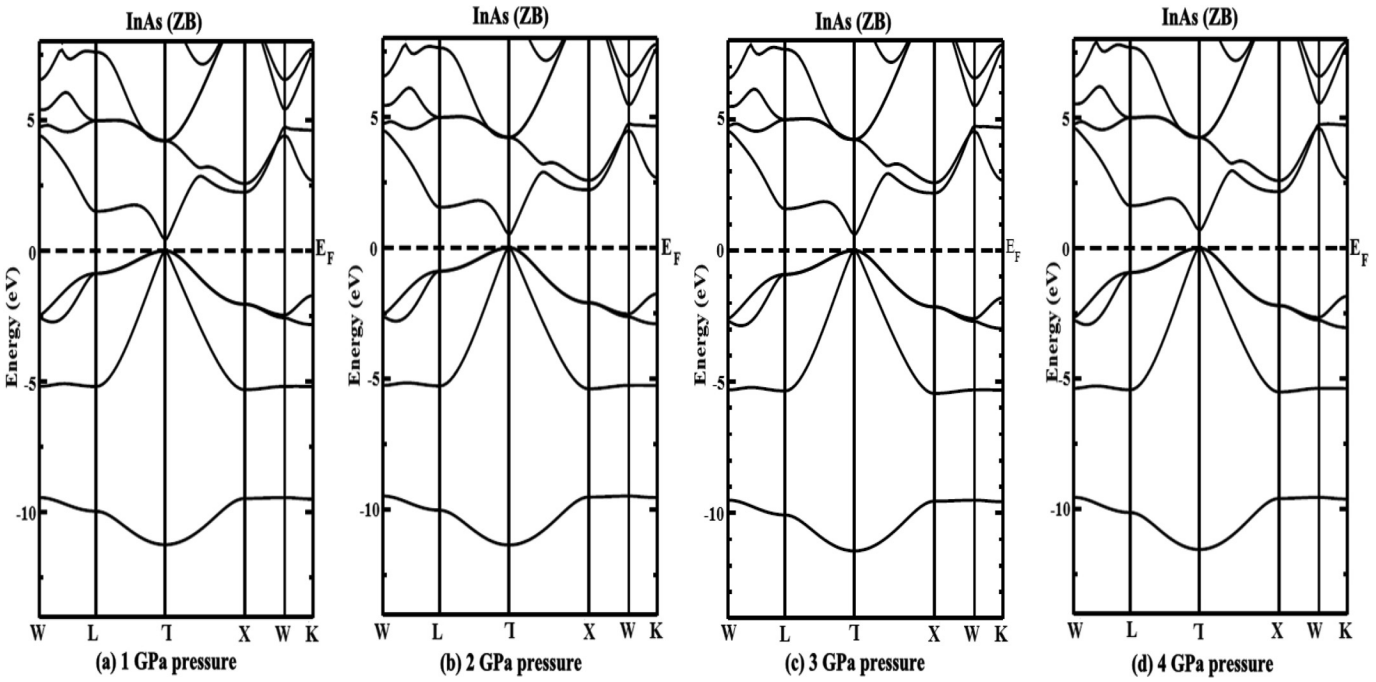

The ductile and brittle behaviour of a material can be understood from the ratio of the bulk and shear moduli (B/G) [33]. If the shear modulus (G) is low we know that the material has a low resistance to shear and hence is ductile, while if a material has low bulk modulus, it means the resistance to fracture is low and hence the material is brittle. We know that the critical value, which separates the ductility and brittleness of a material, is 1.75. A material is said to be ductile if $B/G > 1.75$ and brittle if $B/G < 1.75$. In our calculation, the B/G ratio of InAs-ZB remains around 0.64 with increase in pressure, which shows that InAs-ZB retains its brittle nature even at high pressure, but in the case of InAs-RS it is greater than 1.75 and decreases with increasing pressure. Hence we conclude that the ZB phase of InAs is brittle in nature and becomes ductile after it undergoes a structural phase transition to the RS phase. The elastic parameters as a function of pressure of both the InAs-ZB and InAs-RS are given in Fig. 5.

The stiffness of a material is given by Y (Young's modulus)

$$Y = \frac{9GB}{G + 3B} \tag{7}$$

Also, from the bulk modulus (B) and the isotropic shear modulus (G), the longitudinal elastic wave velocity (v_l) and the transverse elastic wave velocity (v_t) are calculated as follows:

$$v_l = \sqrt{\frac{3B + 4G}{3\rho}} \tag{8}$$

$$v_t = \sqrt{\frac{G}{\rho}} \tag{9}$$

Now, the average sound velocity (v_m) is given by

$$v_m = \left[\frac{1}{3}\left(\frac{2}{v_t^3} + \frac{1}{v_l^3}\right)\right]^{(-1/3)} \tag{10}$$

Fig. 10. Variation of band gap with pressure of InAs-ZB structure.

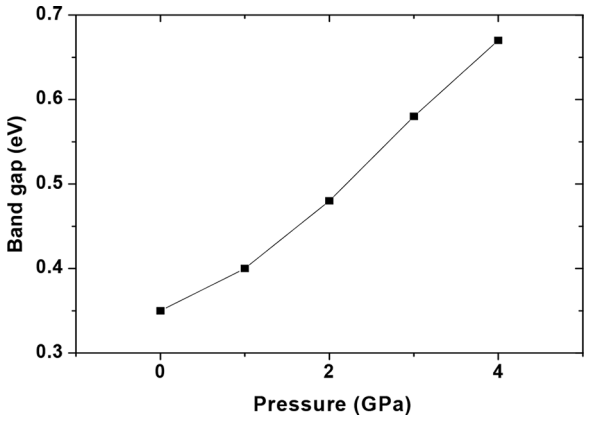

Using the average sound velocity, v_m, the Debye temperature θ_D is calculated from the elastic constants data as given by

$$\theta_D = \frac{h}{k}\left[\frac{3n}{4\pi}\left(\frac{N_A\rho}{M}\right)\right]^{1/3} v_m \tag{11}$$

where h is Plank's constant, k is the Boltzmann's constant, N_A is Avogadro's number, n is the number of atoms per formula unit, M is the molecular mass per formula unit, and ρ (= M/V) is the density.

Our calculated results of Young's modulus and Debye's temperature are given in Fig. 6. We find a linear increase in Y from 73.62 to 99.72 GPa in the InAs-ZB phase with increasing pressure while in the InAs-RS phase the value of Y increases from 73.53 to 97.84 GPa. Hence InAs becomes more rigid with increasing pressure. The value of Debye's temperature is also found to increase from 246 to 290 K for the InAs-ZB phase and 234 to 268 K in InAs-RS, indicating a stiffer lattice and better thermal conductivity in both phases.

Fig. 11. Energy band diagram of InAs-RS structure: (*a*) 5 GPa pressure; (*b*) 6 GPa pressure; (*c*) 7 GPa pressure; and (*d*) 9 GPa pressure.

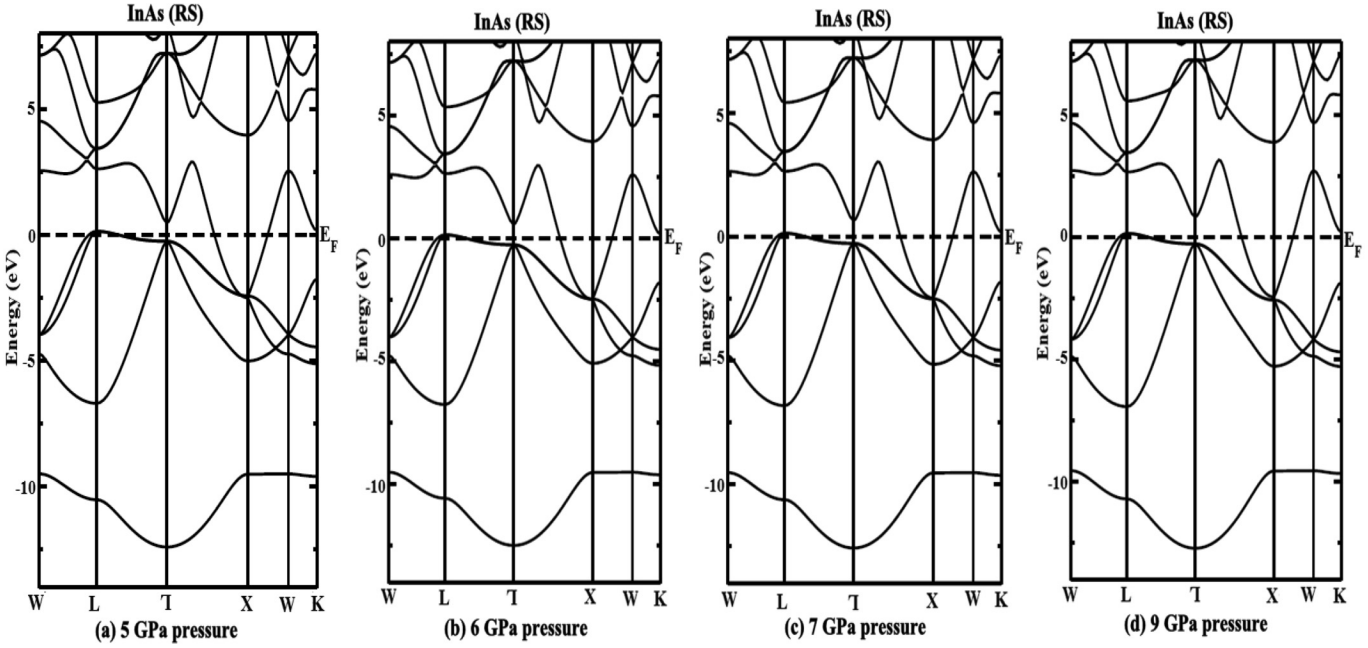

Fig. 12. Total DOS of InAs-ZB under pressure: (*a*) 1 GPa pressure; (*b*) 2 GPa pressure; (*c*) 3 GPa pressure; and (*d*) 4 GPa pressure.

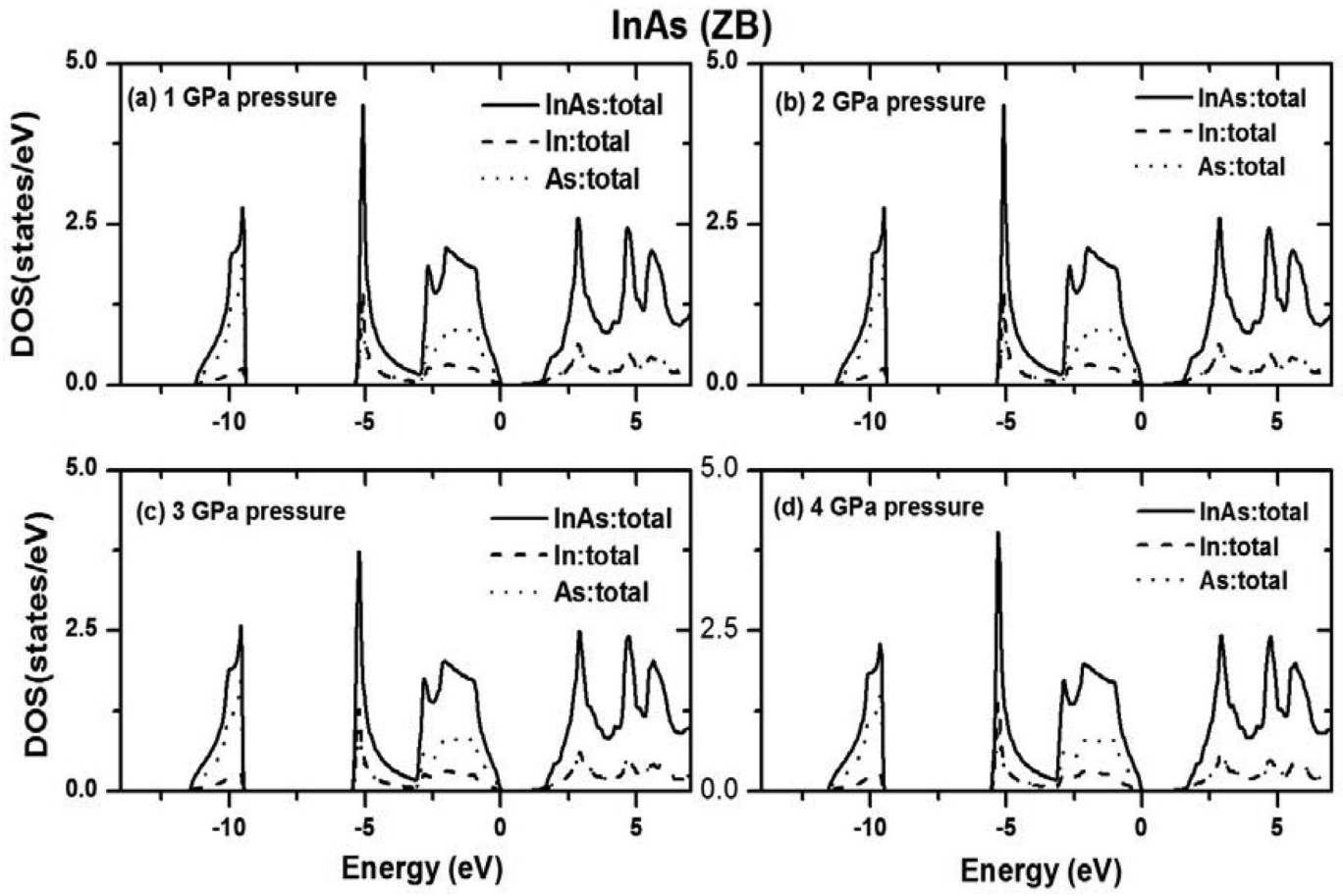

Fig. 13. Total DOS of InAs-RS under pressure: (*a*) 5 GPa pressure; (*b*) 6 GPa pressure; (*c*) 7 GPa pressure; and (*d*) 9 GPa pressure.

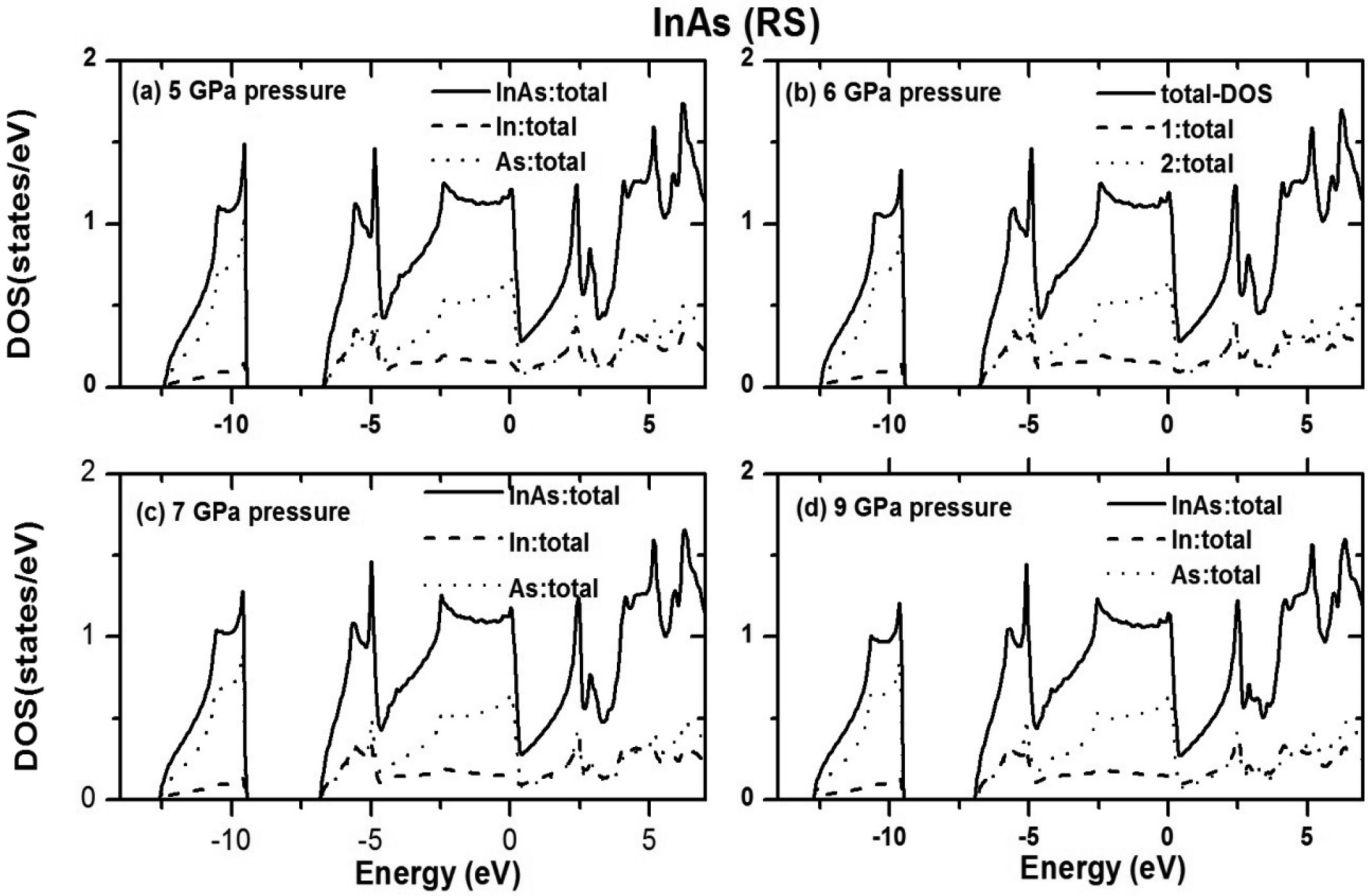

3.3. Electronic structure

Figures 7*a* and 7*b* show the energy band diagrams of InAs-ZB and InAs-RS, respectively, at zero pressure. In Fig. 7*a*, it is observed that the conduction band minimum and the valance band maximum are located at the middle of the Brillioun zone, Γ point. Therefore InAs-ZB structure is a direct band gap semiconductor with an energy band gap of 0.35 eV, which is in good agreement with the experimental value of 0.43 eV [34]. The energy band diagram of InAs-RS as given in Fig. 7*b* shows a prominent difference in the band diagram as compared to that of InAs-ZB. It is interesting to note that there is a crossover of the conduction band towards the valence band, thus indicating the metallic nature of InAs-RS structure. In other words, InAs crystallized in RS structure has a tendency to exhibit metallic nature under high induced pressure above 4.7 GPa. The total and partial DOS plots of InAs-ZB and InAs-RS are shown in Figs. 8*a*–8*c* and 8*d*–8*f*, respectively. From the DOS plots of InAs-ZB, one can see that the lowest band is mainly contributed by the As-s state. The valance band is found to be mainly contributed by the In-s state with significant contribution from the As-p state and In-p state with little contribution from the In-d state. A strong hybridisation is found to occur between the In and As atoms. In the same pattern, the DOS plots of InAs-RS indicate that the lowest band is mainly dominated by the As-s state and the valance band is mainly contributed by As-p and In-p orbitals.

The energy band diagram of InAs-ZB structure under induced pressures 1, 2, 3, and 4 GPa are shown in Figs. 9*a*, 9*b*, 9*c*, and 9*d*, respectively. From these figures, one can observe that there is increase in the band gap with increasing pressure. Figure 10 shows the variation in band gap of InAs-ZB with increasing pressure. This variation could be explained based on DOS diagrams under pressure; the energy eigenvalue corresponding to s, p, and d orbital lies in the higher region with increasing pressure. In the same way, energy band diagrams of InAs-RS structure under induced pressures 5, 6, 7, and 9 GPa are shown in Figs. 11*a*, 11*b*, 11*c*, and 11*d*, respectively. Interestingly, it is seen that there is still crossover of the conduction band towards the valance band under pressure and thus the metallic nature remains. The total density of states of InAs-ZB and InAs-RS under induced pressures are shown in Figs. 12*a*–12*d* and Figs. 13*a*–13*d*, respectively. In Fig. 12, if one sees it systematically, it is found that the band separation near the Fermi line increases with increasing pressure. This is consistent with the observation for band gap in band structure. Similarly in Fig. 13, one observes the continuation of band across the Fermi line indicating metallic character, which is the prominent observation in the band structure of InAs-RS structure. One of the reasons for the metallic nature is band broadening with increase in pressure and the overlap of filled valance band and conduction band.

4. Conclusion

The phase transition under induced pressure of InAs–ZB to RS structure occurs at 4.7 GPa pressure with a volume collapse of 17.2% indicating that the ZB phase is more compressible than the RS phase. The elastic constants of both the phases are found to satisfy the stability conditions and undergo a linear variation with increase in pressure. The elastic parameters are also calculated for both ZB and RS phases. With increase in pressure, InAs-ZB is stiffest along ⟨111⟩ body diagonal while it becomes stiffest along ⟨100⟩ cube axes in InAs-RS. The ionic contribution to interatomic bond-

ing is also dominant as the pressure increases. The ZB phase of InAs is found to be brittle in nature and becomes ductile after it undergoes a structural phase transition to RS phase. It is also found that with increasing pressure both InAs-ZB and InAs-RS showed stiffer lattice and better thermal conductivity. The InAs-ZB phase is found to be a direct band gap semiconductor with an energy band gap of 0.35 eV while the InAs-RS phase exhibits metallic properties. The band gap under induced pressure of InAS-ZB is found to increase, while in the case of InAs-RS there is crossover of atomic orbitals across the Fermi level and hence it exhibits a metallic nature. The total DOS of the InAs-ZB phase shows that the band gap increases because of the energy eigenvalue corresponding to s, p, and d orbitals lies in the higher region with increasing pressure while in the case of the InAs-RS phase there is a broadening of conduction band width with increase in pressure resulting in crossover of conduction orbital towards the valence band. The prominent contribution in the total DOS near the Fermi level of InAs comes from the atomic In-s orbital, As-p, and In-p orbitals in both the phases.

References

1. A. Rashid, H. Javad, A. Hadi, A. Maqsood, and Fazal-e-Aleem. Comput. Mater. Sci. **39**, 580 (2006). doi:10.1016/j.commatsci.2006.08.014.
2. S. Anantathanasarn, Y. Barbarin, N.I. Cade, P.J. van Veldhoven, E.A.J.M. Bente, Y.S. Oei, H. Kamada, M.K. Smit, and R. Nötzel. Mater. Sci. Eng. B, **147**, 124 (2008). doi:10.1016/j.mseb.2007.08.027.
3. J.M Besson, J.P. Itié, A. Polian, G. Weil, J.L. Mansot, and J. Gonzales. Phys. Rev. B, **44**, 4214 (1991). doi:10.1103/PhysRevB.44.4214.
4. S.Q. Wang and H.Q. Ye. Phys. Stat. Sol. (b), **240**, 45 (2003). doi:10.1002/pssb.200301861.
5. A. Mujica, A. Rubio, A. Muñoz, and R.J. Needs. Rev. Mod. Phys. **75**, 863 (2003). doi:10.1103/RevModPhys.75.863.
6. D.R. Lide. 1998. Handbook of chemistry and physics. CRC Press, Boca Raton, Fla. 87th ed.
7. S. Minomura and H.G. Drickamer. J. Phys. Chem. Solids, **23**, 451 (1962). doi:10.1016/0022-3697(62)90085-9.
8. G.D Pitt and M.K.R. Vyas. J. Phys. C: Solid State Phys. **6**, 274 (1973). doi:10.1088/0022-3719/6/2/009.
9. Q. Wang, J. Zhang, R. Li, Y. Xu, X. Miao, and D. Zhang. J. Appl. Phys. **115**, 233712 (2014). doi:10.1063/1.4885039.
10. Kh. Kabita, M. Jameson, B. Indrajit Sharma, R.K. Thapa, and R.K. Brojen Singh. Adv. Sci. Eng. Med. **6**, 354 (2014). doi:10.1166/asem.2014.1483.
11. Kh. Kabita, M. Jameson, B. Indrajit Sharma, R.K. Thapa, and R.K. Brojen Singh. Iraqi J. Appl. Phys. **9**, 17 (2014).
12. Kh. Kabita, J. Maibam, B. Indrajit Sharma, R K. Brojen Singh, and R.K. Thapa. Int. J. Innovation Appl. Stud. **8**, 382 (2014).
13. P. Blaha, K. Schwarz, G.K.H. Madsen, D. Kvasnicka, and J. Luitz. 2001. WIEN2k an augmented plane wave + local orbitals program for calculating crystal properties. Karlheinz Schwarz, Techn. Universitat Wien, Austria.
14. E. Wimmer, H. Krakauer, M. Weinert, and A.J. Freeman. Phys. Rev. B, **24**, 864 (1981). doi:10.1103/PhysRevB.24.864.
15. A.D. Becke and E.R. Johnson. J. Chem. Phys. **124**, 221101 (2006). doi:10.1063/1.2213970. PMID:16784253.
16. P. Hohenberg and W. Kohn. Phys. Rev. **136**, B864 (1964). doi:10.1103/PhysRev.136.B864.
17. W. Kohn and L.J. Sham. Phys. Rev. **140**, A1133 (1965). doi:10.1103/PhysRev.140.A1133.
18. S. Cottenier. 2002. Density functional theory and the family of LAPW-methods: a step- by-step Introduction. Insti-tuut voor Kern-en Stralingsfysica, K.U.Leuven, Belgium.
19. J.P. Perdew, K. Burke, and M. Ernzerhof. Phys. Rev. Lett. **77**, 3865 (1996). doi:10.1103/PhysRevLett.77.3865.
20. F. Birch. Phys. Rev. **71**, 809 (1947). doi:10.1103/PhysRev.71.809.
21. F. Birch. J. Appl. Phys. **9**, 279 (1938). doi:10.1063/1.1710417.
22. J. Jeong, T.E. Schlesinger, and A.G. Milnes. J. Cryst. Growth, **87**, 265 (1988). doi:10.1016/0022-0248(88)90174-1.
23. N.E. Christensen, S. Satpathy, and Z. Pawlowska. Phys. Rev. B, **36**, 1032 (1987). doi:10.1103/PhysRevB.36.1032.
24. L. Pedesseau, J. Even, A. Bondi, et al. J. Phys. D: Appl. Phys. **41**, 165505(1-8) (2008). doi:10.1088/0022-3727/41/16/165505.
25. S.G. Shen. J. Phys. Condens. Matter, **6**, 8733 (1994). doi:10.1088/0953-8984/6/42/006.
26. Y.K. Vohra, S.T. Weir, and A.L. Ruoff. Phys. Rev. B, **31**, 7344 (1985). doi:10.1103/PhysRevB.31.734.
27. J.C. Jamieson. Science, **139**, 845 (1963). doi:10.1126/science.139.3557.845. PMID:17798195.
28. M.I. McMahon and R.J. Nelmes. Phys. Status Solidi (b), **198**, 389 (1996). doi:10.1002/pssb.2221980151.
29. A. Mujica, R.J. Needs, and A. Muñoz. Phys. Status Solidi (b), **198**, 461 (1996). doi:10.1002/pssb.2221980160.
30. B. Mayer, H. Anton, E. Bott, M. Methfessel, J. Sticht, J. Harris, and P.C. Schmidt. Intermetallics, **11**, 23 (2003). doi:10.1016/S0966-9795(02)00127-9.
31. V.V. Bannikov, I.R. Shein, and A.L. Ivanovskii. Phys. Status Solidi RRL, **1**, A89 (2007). doi:10.1002/pssr.200600116.
32. H. Fu, D. Li, F. Peng, T. Gao, and X.L. Cheng. Comput. Mater Sci. **44**, 774 (2008). doi:10.1016/j.commatsci.2008.05.026.
33. S.F. Pugh. Philos. Mag. **45**, 823 (1954). doi:10.1080/14786440808520496.
34. C. Kittel. 1986. Introduction to solid state physics. John Wiley, New York. 6th ed. pp. 185.

Advanced Science Letters
Vol. 21, 2906-2910, 2015

Elastic Properties and Electronic Structures of Pressure Induced Zinc Sulphide (ZnS): A Density Functional Theory Study

Kh. Kabita[1], Jameson Maibam[1], B. Indrajit Sharma[1]*, R.K. Thapa[2] and R. K. Brojen Singh[3]

[1]*Department of Physics, Assam University, Silchar-788011, Assam, India.*
[2]*Department of Physics, Mizoram University, Tanhril, Aizawl-796 009*
[3] *School of Computational and Integrative Sciences, JNU, New Delhi 110067, India.*

A self-consistent ab-initio investigation on the pressure induced elastic properties and electronic structure of ZnS in zinc-blende (ZB) and rock-salt (RS) structure is performed using the full potential linearized augmented plane wave (FP-LAPW) method with modified Becke-Johnson (mBJ) potential under the framework of Density Functional Theory (DFT). A phase transition from the four-fold ZB structure to six-fold RS structure is found occurring at 17.6 GPa pressure with a volume collapse of 12.8%. The obtained results are compared and found to be in consistent with other experimental and theoretical results. The elastic constants and elastic parameters are calculated at different pressures. We find a linear dependence between the elastic constants and pressure in both ZB and RS structure except in C_{44} of the RS structure. The energy band diagrams of both the structures under induced pressure are also studied. The ZB structure is found to be a direct band gap semiconductor while the RS structure is found to be an indirect band gap semiconductor.

Keywords: Density Functional Theory (DFT), Density of states (DOS), Energy band structure, Elastic properties, Phase transition.

1. INTRODUCTION

In recent years, the interest in study of II-VI compound semiconductors has considerably increased because of its developments in the field of optoelectronics and scientific applications. A number of theoretical and experimental studies have been performed for better understanding of the structural and electronic properties of the II-VI compounds [1, 2, 3]. ZnS is a II-VI compound semiconductor having wide band gap which is of great importance due to its potential applications in many optoelectronic devices such as light emitting diodes (LED) and laser diodes (LD) [4, 5]. It is found to crystallize in zinc-blende (ZB) and wurzite (WZ) structure under ambient pressure conditions. In various studies, a phase transition from four-fold co-ordinated zinc-blende (ZB) to six-fold co-ordinated rock-salt (RS) has been reported at elevated pressure [6, 7, 8].

The developments in the computer simulations have resulted in the ab-initio study of the structural, mechanical and electronic properties more systematic and precise. It helps us in better understanding and estimation of the properties of solids under induced pressure which are difficult to study experimentally. The band gap and the elastic constants play a fundamental role in understanding the electrical, optical and mechanical properties of a material. Therefore the study of the band gap and elastic constant at various pressures are important for proper understanding of these properties. Even though there have been many studies on the phase transition and electronic structure of ZnS, there has been very few study on the pressure-induced elastic properties and band structure of ZnS. In our previous studies we have presented a detailed study on the structural, electronic and elastic properties of GaP [9, 10] under induced pressure. The present

*Author to whom correspondence should be addressed.

 1936-6612/2015/21/2906/005 doi: 10.1166/asl.2015.6347

paper is a continuation of our first principle study of the compound semiconductors and a detailed study of the electronic structures of ZnS in both the ZB and RS phases under induced-pressure has been presented. The paper has been organised as follows. After this introduction, the methods used in our calculation are described in section 2. In section 3 the results of our study are given and discussed in detailed. The conclusion of our study is given in section 4.

2. COMPUTATIONAL METHOD

The first principle study of ZnS calculation is performed using the first principle full potential linearised augmented plane wave (FP-LAPW) [11] method within the generalised gradient approximation (GGA) of Perdew-Burke-Ernzerhof (PBE-GGA) [12] with modified Becke-Johnson (mBJ) [13] potential under the framework of density functional theory (DFT) [14,15,16]. This method is used as it is one of the most accurate methods in electronic structure calculation of crystals. In this method, the lattice is divided into non-overlapping atomic spheres surrounding each atomic sites and an interstitial region [17]. Inside the muffin tin (MT) region, the potential is a product of radial function and spherical harmonics and expanded up to order l = 10. For the interstitial regions that are outside the muffin tin spheres, the potentials are expanded in plane waves. 8000 k-points are used for the integration part which reduces to 256 irreducible k-points inside the Brillouin zone. Convergence is obtained at $R_{MT}K_{max}$ = 9.0 where R_{MT} is the atomic sphere radii and K_{max} gives the plane wave cut-off. All calculations are performed with the equilibrium lattice constants which are determined from the plot of the total energy against the unit cell volume by fitting to the Birch-Murnaghan equation of states [18]. The overall calculation is done with WIEN2K [19].

3. RESULTS AND DISCUSSION

3.1. Phase Transition and Elastic Properties

The phase transition of a material plays an important role in understanding the structural, mechanical and physical properties of a material under pressure. For determination of the zero temperature pressure induced phase transition of ZnS-ZB phase to ZnS-RS phase the usual condition of equal enthalpies i.e. H=E+PV is used. The transition pressure from the ZB phase to the RS phase is calculated at the precise point where the enthalpies of the two phases are equal. The enthalpy as a function of energy is shown in figure 1. The phase transition from ZB to RS structure is found to occur at 17.6 GPa pressure which agrees well with the experimental value of 18.1 GPa pressure [20] and other theoretical results of 17.5 GPa and 17.4 GPa pressures [21, 22] respectively. There is a volume collapse of 12.8% at the transition pressure indicating ZB phase is more compressible than the RS phase.

Elasticity describes the response of a compound to a very small loading which causes reversible deformation. The anisotropic features, binding characteristics and structural stability of a material can be determined from study of the pressure dependence of elastic constants. For a cubic crystal, the mechanical stability conditions are: $(C_{11}+2C_{12}) > 0$; $C_{11}C_{12} > 0$; $C_{44} > 0$; $C_{11} > 0$. The elastic constants with increase in pressure for both the structures are shown in figure 2. It is found that the mechanical stability conditions are satisfied when the pressure is below the transition pressure in the ZB phase and above the transition pressure in the RS structure.

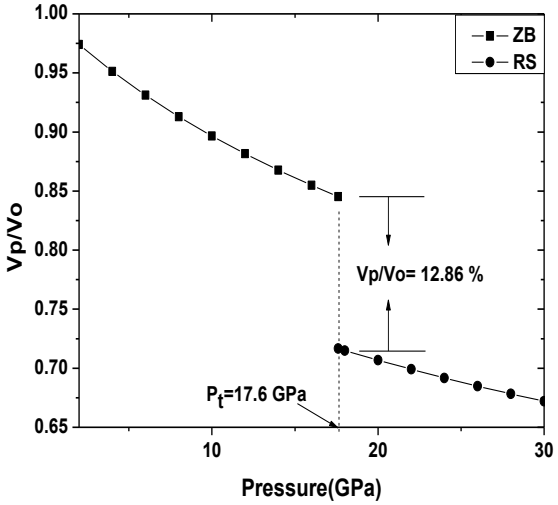

Figure 1. Phase transition of ZnS in zinc blende structure to rock salt structure.

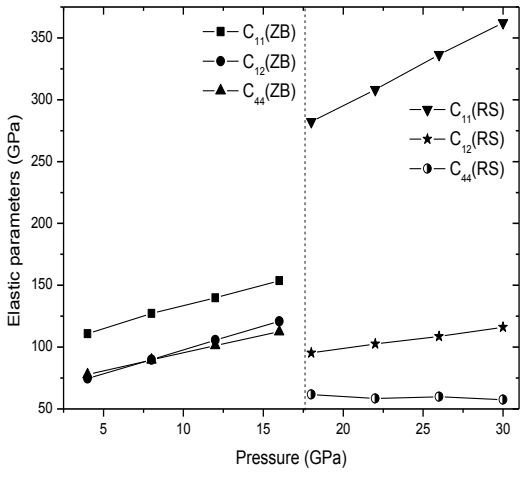

Figure 2. Elastic constants (C_{11}, C_{12}, C_{44}) as a function of pressure for ZnS-ZB and ZnS-RS structure.

A linear relationship between the elastic constants (C_{11}, C_{12}, C_{44}) and pressure can be seen in both the phases

except for C_{44} in RS structure. Also C_{11} is found to be more sensitive to change in pressure than C_{12} and C_{44}.

In the light of these observations, the elastic parameters, Zener anisotropic factor (A), Poisson's ratio (υ), Kleinmann parameter (ζ), Youngs modulus (Y), and Debye's temperature (θ_D) are calculated to determine the mechanical and thermal behaviour ZnS in both the structures. Figure 3(a), 3(b), 4(a) and 4(b) shows the calculated elastic parameters of ZnS with variation in pressure from 0 to 16 GPa pressure for ZB phase and from 18 GPa to 30 GPa pressure for RS phase. Poisson's ratio (υ) gives us information about the characteristics of bonding forces. The value of poisson's ratio (υ) is 0.1 for covalent materials, whereas for ionic materials, υ = 0.25 [23]. In our calculation, the value of υ varies from 0.28 to 0.32 in the ZB phase and from 0.29 to 0.32 in the RS phase indicating higher ionic contribution in intra-atomic bonding with increasing pressure. The lower and upper limits for υ in central force solids have been reported to be 0.25 and 0.5 respectively [24]. Thus our values also indicates that, inter atomic forces tends to be more central as pressure increases. The relative ease of bond bending against the bond stretching is indicated by ζ (Kleimann parameter). It also implies resistance against bond bending or bond angle distortion. In a system, minimizing bond bending leads to ζ = 0 and minimizing bond stretching leads to ζ =1. In the present study, as the pressure increases, ζ for the ZB phase is found to vary from 0.76 to 0.85 and 0.47 to 0.48 for the RS phase, indicating shrinkage in bond-stretching.

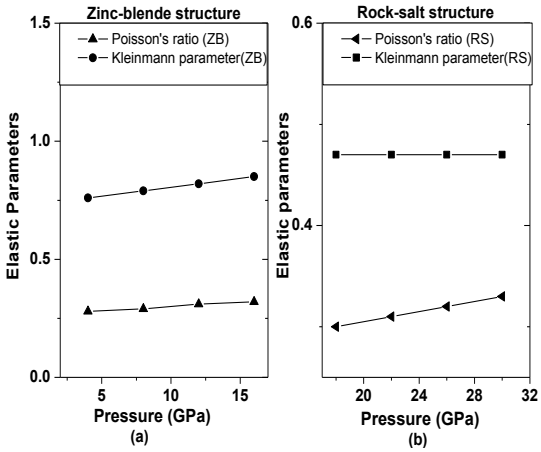

Figure 3. Elastic parameters (Poisson's ratio and Kleinmann parameter) as a function of pressure for ZnS in (a) ZB phase and (b) RS phase.

The stiffness of a material is given by Y (Young's modulus). A linear increase in Y with increase in pressure is found in both phases of ZnS and hence ZnS becomes more rigid with increase in pressure. The value of Debye's temperature is also found to vary from 401K to 437K for the ZB phase and from 493K to 509K for the RS phase indicating stiffer lattice and better thermal conductivity.

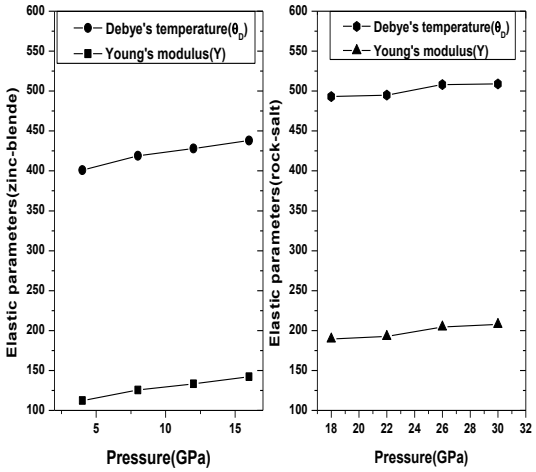

Figure 4. Elastic parameters (Debye's temperature and Young's modulus) as a function of pressure for ZnS in (a) ZB phase and (b) RS phase.

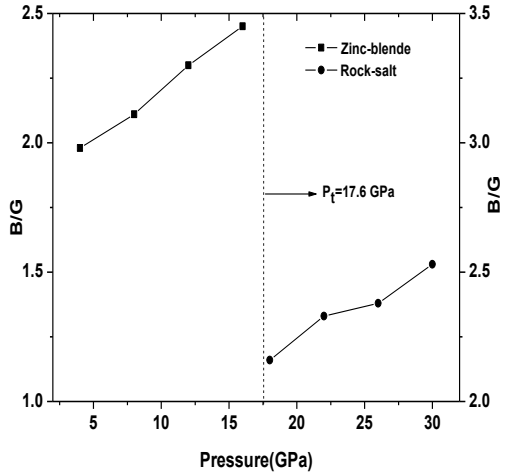

Figure 5. B/G ratio as a function of pressure for ZB and RS phase

The ductility or brittleness of a material is determined by the ratio between the bulk and shear modulus, B/G as proposed by Pugh [25]. A material is found to be brittle if B/G < 1.75 and ductile if B/G > 1.75. The B/G ratio of our present study varies from 1.91 to 2.45 for ZB phase and 2.16 to 2.53 for RS phase with increase in pressure as shown in figure 5. Therefore ZnS structure is found to be ductile and even with increase in pressure ductility is retained.

3.2. Electronic Properties

The energy band diagram of ZnS- ZB structure at 0 GPa pressure has been presented in many studies and found to be a direct band gap semiconductor. In our study we have found out the energy band gap of ZnS at different pressures. The variation in the energy band gap with pressure is shown in figure 6. Figure 7(a), 7(b), 7(c) and

7(d) shows the energy band diagram of ZnS- ZB structure at different pressures. The direct band gap of ZnS-structure is found to increase with pressure which is due to the fact that the energy eigenvalues corresponding to s, p, and d orbital's lies in the higher region with increasing pressure.

The energy band diagram of ZnS-RS structure at different pressures are shown in figure 8(a), 8(b), 8(c) and 8(d). The ZnS-RS structure is found to be an indirect band gap semiconductor. In this case, variations of band gap under pressures are not observed prominently. Thus we conclude that the band gap of RS structure of ZnS is not much affected by pressure.

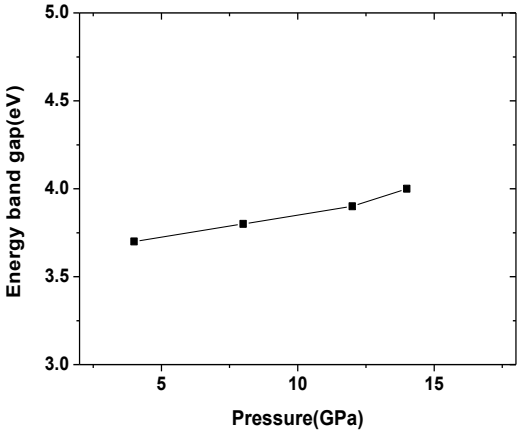

Figure 6. Variation of energy band gap of ZnS-ZB structure with pressure.

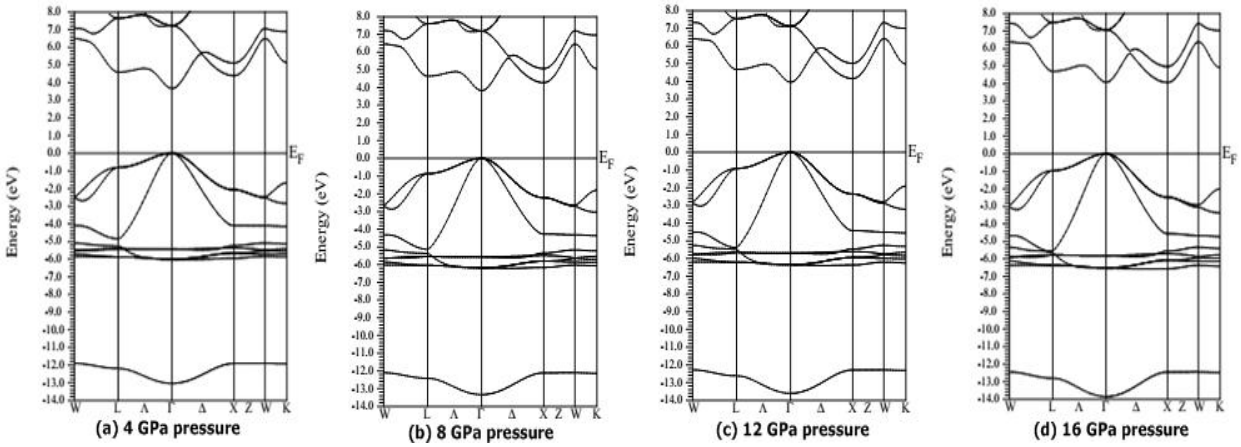

Figure 7. Energy band diagram of ZnS-ZB-structure at (a) 4 GPa pressure, (b) 8 GPa pressure, (c) 12 GPa pressure and (d) 16 GPa pressure.

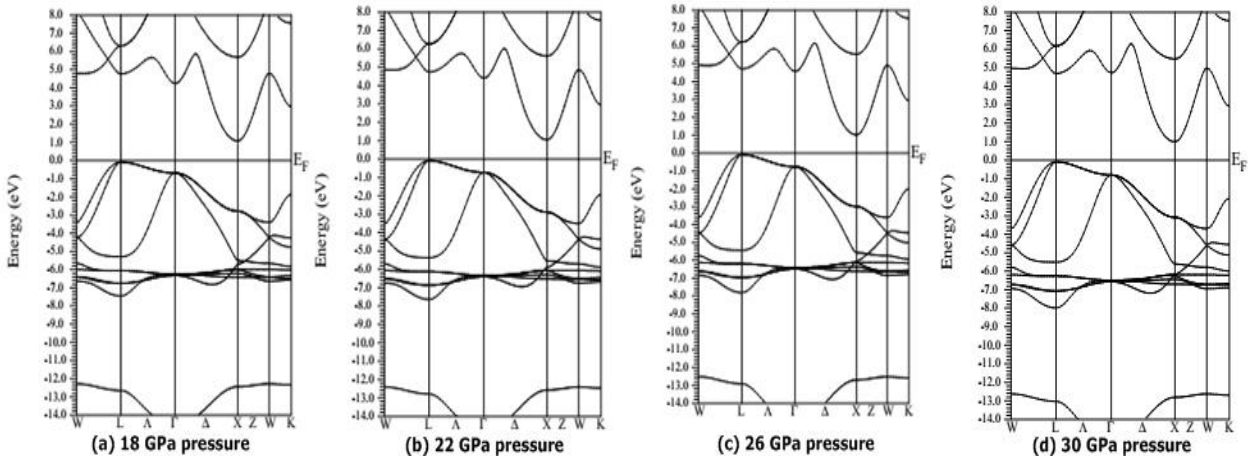

Figure 8. Energy band diagram of ZnS-RS-structure at (a) 18 GPa pressure, (b) 22 GPa pressure, (c) 26 GPa pressure and (d) 30 GPa pressure.

4. CONCLUSIONS

The phase transition of ZnS-zinc blende phase to rock salt phase is found to occur at 17.6 GPa pressure with a volume collapse of 12.86% indicating that zinc blende structure is more compressible than the rock salt structure. The values of elastic constants for both the structures are satisfied for mechanical stability conditions. A linear relationship between the elastic constants and induced pressures is observed in both the phases. In the electronic structure, the zinc blende structure of ZnS is found to be a direct band gap semiconductor with a band gap of 3.49 eV at ambient pressure and increases with pressure whereas rock salt structure is found as indirect band gap having not much variation in band gap with pressure.

REFERENCES

1. C.S. Wang and B.M. Klein, *Phys. Rev. B* **24,** 3393-3416 (1981).
2. Y. N. Xu and W. Y. Ching, *Phys. Rev. B* **48**, 4335-4351 (1993).
3. P. Schrer, P. Kruger and J. Pollmann, *Phys. Rev. B* **47,** 6971-6980 (1993).
4. E. Bellotti, K. F. Brennan, R. Wang and P. P. Ruden, *J. Appl. Phys.* **82,** 2961-2964 (1997).
5. S. Q. Wang, Appl. *Phys. Lett.* **88**, 061902(1)-061902(3) (2006).
6. S. Desgreniers, L. Beaulieu, and I. Lepage, *Phys. Rev. B* **61**, 8726 –8733 (2000).
7. S. K. Gupta, S. Kumar and S. Auluck, *Opt. Commun.* **284 (1),** 20-26 2011.
8. Z. Li, B. Lui, S. Yu, J. Wang, Q. Li, B. Zou, T. Cui, Z. Liu, Z. Chen and J. Lui J. *Phys. Chem. C* **115** 357-361 (2011).
9. Kh. Kabita, Maibam Jameson, B. Indrajit Sharma, R. K. Thapa Singh and R. K. Brojen *Adv. Sci. Eng. Med.* **6** 354-358 (2014)
10. Kh. Kabita, Maibam Jameson, B. Indrajit Sharma, R. K. Thapa Singh, R. K. Brojen *Iraqi J Appl. Phys.* **9** 17-20 (2014).
11. E. Wimmer, H. Krakauer, M. Weinert and A. J. Freeman, *Phys. Rev. B* **24,** 864-875 (1981).
12. J. P. Perdew, K. Burke and M. Ernzerhof *Phys. Rev. Lett.* **77,** 3865-3868 (1996).
13. A. D. Becke and E. R. Johnson, *J. Chem. Phys.* **124,** 221101-221104 (2006).
14. P. Hohenberg and W. Kohn, *Phy. Rev.3B* **136,** 864-871 (1964).
15. W. Kohn and L. J. Sham, *Phys. Rev. 4A* **140,** 1133-1138 (1965).
16. S. Cottenier, *"Density Functional Theory and the family of (L)APW-methods: a step-by-step Introduction"* Belgium, Insti-tuut voor Kern-en Stralingsfysica, K.U.Leuven ISBN 90-807215-1-4. (2002).
17. O. K. Andersen *Phys. Rev. B.* **12,** 3060-3083 (1975).
18. F. Birch, *Phys. Rev.* **71,** 809-824 (1947).
19. P. Blaha, K. Schwarz, G. K. H. Madsen, D. Kvasnicka and J. Luitz, *"An anaugmented plane wave + local orbitals program for calculating crystal properties*",*Wien2k. Techn. Universitat* (Wien, Austria) ISBN 3-9501031-1-2. (2001)
20. A. Nazzal and A. Qteish, *Phys. Rev. B* **53** 8262-8266 (1996).
21. R. Chen, X. F. Li, L. C. Cai and J. Zhu, *Solid State Comm.* 139 246-249 (2006).
22. C.E. Hu, L.L. Sun, Z.Y. Zeng and X.R. Chen, *Chin. Phys. Letters* **25**, 675-678 (2008).
23. V. V. Bannikov, I. R. Shein and A. L. Ivanovskii *Phys. Status. Solidi. Rapid. Res. Lett.* **3** 89-100 (2007)
24. H. Fu, D. Li, F Peng et al. *Comput. Mater. Sci.* **44** 774-778 (2008)
25. S. F. Pugh *Phil. Mag.* **45** 823-843 (1954).

Received: 8 April 2015. Accepted: 22 May 2015.

First principle study on pressure-induced electronic structure and elastic properties of indium phosphide (InP)

K. Kabita, J. Maibam, B. I. Sharma, R. K. Thapa & R. K. Brojen Singh

Indian Journal of Physics

ISSN 0973-1458
Volume 89
Number 12

Indian J Phys (2015) 89:1265-1271
DOI 10.1007/s12648-015-0701-0

Springer

Indian J Phys (December 2015) 89(12):1265–1271
DOI 10.1007/s12648-015-0701-0

ORIGINAL PAPER

First principle study on pressure-induced electronic structure and elastic properties of indium phosphide (InP)

K Kabita[1], J Maibam[1], B I Sharma[1]*, R K Thapa[2] and R K Brojen Singh[3]

[1]Department of Physics, Assam University, Silchar 788011, Assam, India

[2]Department of Physics, Mizoram University, Tanhril, Aizawl 796 009, India

[3]School of Computational and Integrative Sciences, JNU, New Delhi 110067, India

Received: 22 January 2015 / Accepted: 02 April 2015 / Published online: 26 May 2015

Abstract: The structural, elastic and electronic properties of indium phosphide in zinc-blende and rock-salt structure under various pressures are studied using the first principle calculation based on the density functional theory with modified Becke–Johnson potential. The pressure-induced structural phase transition from zinc blende to rock salt is observed at 9.3 GPa pressure with 16.4 % volume collapse, indicating that zinc-blende structure is more compressible as compared to rock-salt structure. The elastic constants and elastic parameters such as Zener anisotropic factor, Kleinmann parameter, Poisson's ratio, isotropic shear modulus, Young's modulus and Debye's temperature under different pressures are obtained and show a linear relation with pressure. The electronic band structures at different pressures are investigated using the total and partial density of states. The calculated results are found to be in good agreement with other theoretical and experimental results.

Keywords: Density functional theory; Energy band diagram; Elastic properties; Phase transition

PACS Nos.: 71.15.Mb; 71.20.−b; 71.20.Nr

1. Introduction

The study of compound semiconductors exhibiting new crystal phases under pressure has led to an increase interest in the study of high-pressure behaviour of III–V compound semiconductors [1, 2]. The studies of structural properties, phase diagram and high-pressure phases of III–V compounds have aroused considerable scientific interest in the past decades due to its technological importance. In recent years many theoretical and experimental studies on the electronic and structural properties as well as the phase transition of group III–V compound semiconductors have been undertaken [3–7]. Indium phosphide (InP) is an important III–V compound semiconductor, which has been intensively studied for their technological importance and has become a very promising material for opto-electronic devices, solar cells, high-performance computing and communications [8–10]. The study of the effect of pressure in materials has recently become of much interest in solid-state physics. The energy band gap and elastic constants of a semiconductor play crucial role in the study of material properties. Therefore, in order to gain better understanding of material properties, the studies of the changes in the energy band gap and elastic constants of semiconductor compounds under externally induced pressure are very important.

In the literature, the semiconductor-to-metallic phase transition from zinc-blende (ZB) to rock-salt (RS) structure of InP is found to occur between 8.5 and 13.3 GPa pressures [11–14]. The phase stability of group III phosphide has been studied by Arbouche et al. [15], who have found the phase transition of InP occurring at about 7.35 GPa pressure. Branicio et al. [16] have studied the high-pressure phases of InP and found the phase transition from ZB to RS occurring at 10.2 GPa pressure. Although there have been many studies on the structural and electronic properties of InP, the high-pressure study on the electronic structures and elastic properties of InP is still very rare. The experimental study of these quantities at high pressure is very

*Corresponding author, E-mail: indraofficial@rediffmail.com

difficult and therefore, many theoretical calculations are usually used. GW [17] is a method, which is commonly used for the calculation of the electronic structures but also very expensive in terms of computational cost and time of calculation. For calculation of systems, which are not complex systems of heavy atom, LDA and GGA methods are good enough for the electronic structure calculations but results in underestimation of the band gaps. In our previous studies, we have extensively studied the pressure-induced phase transition, structural, electronic and elastic properties of GaP [18, 19]. In the present paper, we have performed the pressure-induced phase transition from the fourfold coordinated ZB structure to sixfold coordinated RS structure of InP using the full potential linearized augmented plane wave (FP-LAPW) method with modified Becke–Johnson (mBJ) potential under the framework of density functional theory (DFT) with main emphasis on the study of the variation in elastic constants, elastic parameters, band gap and density of states (DOS) with increasing pressure.

2. Theoretical and computational method

The calculations of InP are performed using the FP-LAPW [20] method with mBJ potential [21] under the framework of DFT [22–24]. The exchange–correlation interaction effects are treated within the generalized gradient approximation of Perdew–Burke–Ernzerhof (PBE-GGA) scheme [25] as implemented in the WIEN2k code [26]. In this method, the lattice is divided into non-overlapping spheres (called atomic or muffin tin sphere) surrounding each atomic sites and an interstitial region. Inside the muffin tin (MT) region, the potential is a product of radial function and spherical harmonics and expanded up to order of $l = 10$. For the interstitial regions that are outside the muffin tin spheres, the potentials are expanded in plane waves. The number of k-points used for the integration part is 8000, which is reduced to 256 irreducible k-points inside the Brillouin zone including five high-symmetry points W, L, Γ, X and K. Convergence of the basis set is obtained at $R_{MT}K_{max} = 9.0$, where K_{max} gives us the plane-wave cut-off. The elastic constants have been determined using the stress–strain method with volume-conserving technique [27]. In our calculations, only small lattice distortions have been considered in order to remain within the elastic domain of the crystal.

3. Results and discussion

3.1. Structural properties

The static equilibrium properties of the crystal structure of ZB and RS of InP are obtained by minimization of the total energy with respect to the unit cell volumes per molecule and fitting it to the Birch–Murnaghan equation [28]. The calculated structural parameters are compared with other results and are given in Table 1. Our results are found to be in good agreement with other experimental results of Paul [29] with lattice constant 5.9 Å and 5.87 Å by Madelung [30] along with the theoretical results of Mujica and Needs [31] with lattice constant of 5.94 Å, bulk modulus of 68 GPa and 4.9 derivative of bulk modulus. There are also other references reporting lattice constants as 5.87 Å, 5.95 Å, bulk modulus as 65.5, 72, 68, 71, 60 GPa and derivative of bulk modulus as 4.59, 4.67, 4.41 [32–38]. For the InP-RS structure, there are not much available data on the structural parameters. Hence, the results of our structural data for both the ZB and RS structure are used for further elastic and electronic structure calculations.

Table 1 Lattice constant 'a(Å)', bulk modulus 'B(GPa)' and pressure derivative of bulk modulus (B′) of ZB and RS structure of InP at zero pressure

	a(Å)	B(GPa)	B′
ZB structure			
Present work	5.97	60.5	4.64
Expt. results	5.90[a], 5.87[b]	65.5[d], 72[e]	4.59[c],
Theoretical results	5.94[b], 5.95[c]	68[b], 71[f], 60 [g]	4.9[b], 4.41 [g], 4.67 [h]
RS structure			
Present work	5.54	74.78	4.76
Expt. results	5.71[b], 5.24[b]		
Theoretical results			

[a] Ref [30], [b] Ref [32], [c] Ref [33], [d] Ref [34], [e] Ref [38], [f] Ref [39], [g] Ref [37], [h] Ref [36]

3.2. Phase transition and elastic properties

The usual conditions for equal enthalpy, i.e. the pressure at which, the enthalpy $H = E + PV$ is same for both the structures, are used to obtain the zero-temperature pressure-induced phase transition. The ZB–RS phase transition of InP is found to occur at 9.3 GPa pressure with a volume collapse of 16.4 %, indicating that the ZB phase is more compressible than the RS phase. Our calculated results of phase transition are compared with other experimental results of 9.5 GPa by Menoni et al. [14], 9.8 GPa pressure by Mc Mahon [39] and 10.3 GPa transition pressure and 14.9 volume collapse by Madelung [30] and theoretical results of transition pressure as 7.3, 7.5, 8.5, 10.2, 11.0 GPa and volume collapse as 18, 15, 17 % by different group of researchers [15, 16, 40–43] as shown in Table 2. We find

Table 2 Phase transition pressure 'P_t(GPa)' and volume collapse of InP

	Present calculation	Expt. results	Theoretical results
Transition pressure (P_t) (GPa)	9 .3	9.5[a], 10.3 ± 0.2[b], 9.8[c]	7.3[d], 7.5[e], 8.5[f], 11.0 [g]
Volume collapse (%)	16.45	14.9[b]	18[f], 15 [g], 17 [h]

[a] Ref [14], [b] Ref [32], [c] Ref [40], [d] Ref [15], [e] Ref [41], [f] Ref [42], [g] Ref [43], [h] Ref [44]

that our results are closer to the experimental data than other theoretical results. Hence, the DFT calculation using the mBJ potential gives us more accurate results than other theoretical studies.

The elastic constant plays an important role in the study of the relationship between crystal structure and bonding. The mechanical stability condition of a crystal at high pressure can be understood from the pressure dependence of the elastic constants. For a cubic crystal, the Born mechanical stability conditions are as follows: $(C_{11} + 2C_{12}) > 0$; $C_{11}C_{12} > 0$; $C_{44} > 0$; $C_{11} > 0$. In the present study, the elastic constants (C_{11}, C_{12}, C_{44}) are computed using the volume-conserving technique [27] for a lattice volume corresponding to pressure ranging from 0 to 8 GPa pressure for the ZB and 10 GPa pressure to 16 GPa pressure for RS phase and found to satisfy the stability conditions. The Zener anisotropic factor (A), Poisson's ratio (υ), Kleinmann parameter (ζ), Young's modulus (Y) and Debye's temperature (θ_D) are important elastic parameters, which determine the mechanical and thermal behaviour of a material. In our study we have calculated these parameters for both the structures using the relation given by Mayer et al. [44]. The elastic isotropy of a material is determined by the Zener anisotropic factor (A). For $A = 1$, the material is elastically isotropic and deform uniformly along all directions of the body. If $A > 1$, it is stiffest along <111> body diagonals and when $A < 1$, it is stiffest along <100> cube axes. It is expressed as:

$$A = \frac{2C_{44}}{C_{11} - C_{12}} \tag{1}$$

Kleinmann parameter (ζ) describes the relative position of the cation and anion sub-lattices and is given by the relation:

$$\zeta = \frac{C_{11} + 8C_{12}}{7C_{11} + 2C_{12}} \tag{2}$$

The Poisson's ratio (υ) provides a sharp criterion for differentiating the brittleness and ductility in solids. It gives us the stability of crystal against shear and is calculated using the relation,

$$\upsilon = \frac{1}{2}\left(\frac{B - (2/3)G}{B + (1/3)G}\right) \tag{3}$$

where B is the Bulk modulus and G is the isotropic shear modulus given by

$$G = \frac{G_V + G_R}{2} \tag{4}$$

where G_v is the Voigt's shear modulus corresponding to the upper bound of G values and G_R is the Reuss's shear modulus corresponding to the lower bound of G values. G_v and G_R can be expressed as:

$$G_V = \frac{C_{11} - C_{12} + 3C_{44}}{5} \tag{5}$$

$$G_R = \frac{5(C_{11} - C_{12})C_{44}}{4C_{44} + 3(C_{11} - C_{12})} \tag{6}$$

The Young's modulus is determined to measure the stiffness of the solid and is given by:

$$Y = \frac{9GB}{G + 3B} \tag{7}$$

Debye's temperature gives us explicit information about lattice vibrations and is also an important parameter determining the thermal characteristics of a material. It is calculated using the average sound velocity (υ_m) given by the relation [45]:

$$\theta_D = \frac{h}{k}\left[\frac{3n}{4\pi}\left(\frac{N_A\rho}{M}\right)\right]^{1/3}\upsilon_m \tag{8}$$

where h is the Plank's constant, k is the Boltzmann constant, N_A is the Avogadro's number, n is the number of atoms per formula unit, M is the molecular mass per formula unit, ρ is the density and υ_m is given by [46]:

$$\upsilon_m = \left[\frac{1}{3}\left(\frac{2}{\upsilon_t^3} + \frac{1}{\upsilon_l^3}\right)\right]^{-(1/3)} \tag{9}$$

where υ_t and υ_l are the transverse and longitudinal velocities, respectively, which are obtained from Navier's equation as [47]:

$$\upsilon_l = \sqrt{\frac{3B + 4G}{3\rho}} \tag{10}$$

$$\upsilon_t = \sqrt{\frac{G}{\rho}} \tag{11}$$

The calculated elastic parameters of InP with variation of pressure from 0 GPa pressure up to 8 GPa of ZB phase and

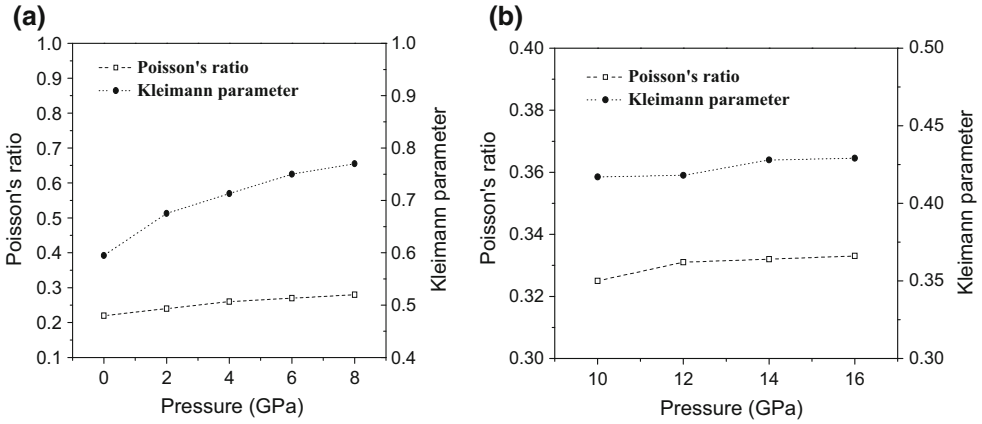

Fig. 1 Elastic parameters (Poisson's ratio and Kleinmann parameter) as a function of pressure of InP in: (**a**) ZB phase and (**b**) RS phase

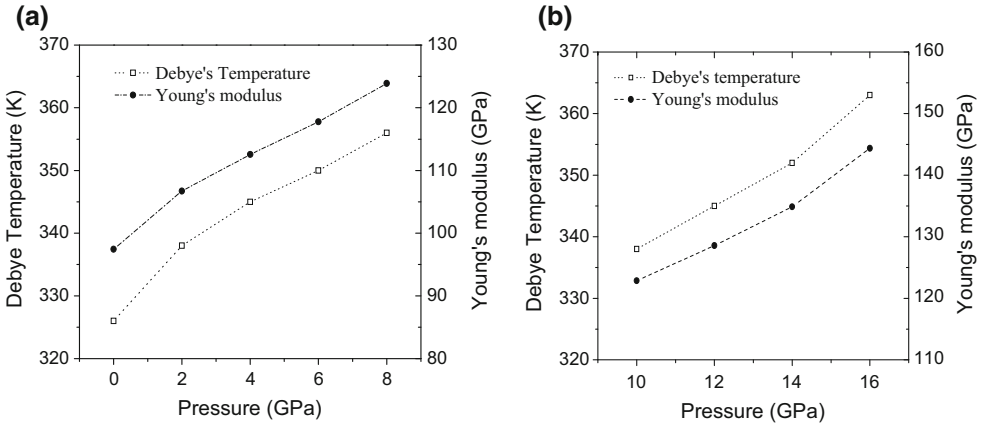

Fig. 2 Elastic parameters (Debye's temperature and Young's modulus) as a function of pressure of InP in: (**a**) ZB phase and (**b**) RS phase

from 10 to 16 GPa pressure of RS phase are shown in Figs. 1(a), 1(b) and 2(a), 2(b). A consistent pattern of linear increase in elastic parameters with increase in pressure can be observed from these figures. The parameter A (Zener anisotropic factor) shows a variation from 3.16 to 4.77 and 0.35 to 0.36 with increase in pressure of ZB and RS phase, respectively, showing the degree of elastic anisotropy. The degree of directionality of the covalent bonds is given by the Poisson's ratio (υ). For covalent materials, $\upsilon = 0.1$, whereas for ionic materials, $\upsilon = 0.25$ [48]. Our calculations show that with increase in pressure, the value of υ varies from 0.22 to 0.28 of the ZB phase and from 0.32 to 0.33 of the RS phase, showing that with increase in pressure, the ionic contribution to inter-atomic bonding becomes dominant. It has been reported [49] that for central force solids the lower and upper limits for υ are 0.25 and 0.5, respectively. Our values also indicate that as pressure increases, inter-atomic forces tend to be more central. ζ (Kleinmann parameter) quantifies internal strain and thus indicates the relative ease of bond bending against the bond stretching. It also implies resistance against bond bending or bond angle distortion. In a system, minimizing bond bending leads to $\zeta = 0$ and minimizing bond stretching leads to $\zeta = 1$. In the present study, as the pressure increases, ζ of the ZB phase is found to vary from 0.59 to 0.77 and 0.41 to 0.42 of the RS phase, indicating the shrinkage in bond stretching. The larger the value of Y (Young's modulus), the stiffer is the material. Our results show a linear increase in Y with increase in pressure and hence, InP becomes more rigid with increase in pressure in both the phases. With increase in pressure, the value of Debye's temperature is also found to vary from 326 to 357 K of the ZB phase and from 338 to 363 K of the RS phase, indicating stiffer lattice and better thermal conductivity. The empirical malleability measure of a material is determined by the value of B/G ratio [50]. A material is found to be brittle if $B/G < 1.75$ and ductile if $B/G > 1.75$. The B/G ratio of present study varies from 1.52 to 1.94 of ZB phase and 2.5 to 2.6 of RS phase with increase in pressure as shown in Fig. 3. Therefore, InP structure is found to be brittle and with increase in pressure it tends to become ductile.

3.3. Electronic structures and density of states

The energy band diagram of the ZB structure of InP at 0 GPa pressure has been reported in many papers and found to be a direct band gap semiconductor [5, 7, 16]. The

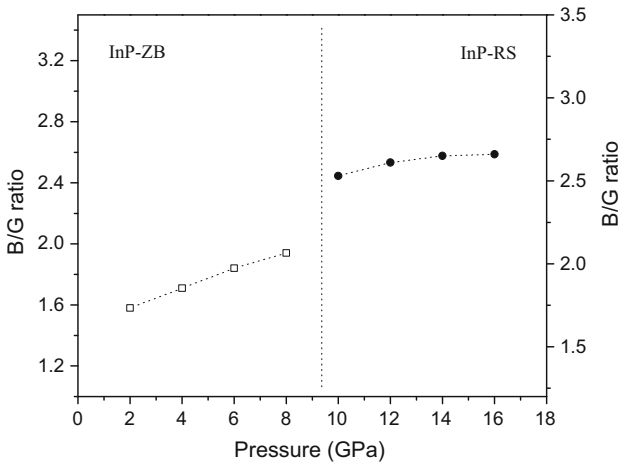

Fig. 3 B/G ratio as a function of pressure of InP-ZB and InP-RS phase

results of our energy band diagram show a direct energy band gap of 1.31 eV, which is in good agreement with the experimental value of 1.42 eV [38] and better than other LDA results of 0.62 eV and GGA results of 0.85 eV [38], and in case of InP-RS structure metallic nature is found to occur. The partial DOS plots of InP-ZB are shown in Fig. 4(a), 4(b) and for InP-RS structure in Fig. 4(c), 4(d) respectively. In the partial DOS plot of InP-ZB the three prominent peaks could be seen in valence band. The first peak from the left is dominated by the *P–p* state with a significant contribution from the In-d state. The second peak is mainly dominated by the In-s state with significant contribution from the *P–p* state and small contribution from the In-p state and In-d state. In case of the RS structure, the first peak is mainly dominated by the *P-s* state with little contribution from the In-*d* state and In-*p* state and the second peak is found to be mainly contributed by the *P–p* state with a mere contribution from the In-*s* state. We therefore find that the highest contribution towards the total density of states near the Fermi level of the ZB structure is In-s state and of RS structure is the *P–p* state. In our study the energy band gaps of InP at various pressures have also been calculated. Figure 5(a)–5(d) show the energy band diagrams of InP-ZB structure at different pressures. The variation in energy band gap of InP-ZB with increase in pressure is also shown in Fig. 6. We find that there is a linear increase in the band gap of InP-ZB as the pressure increases, which may due to

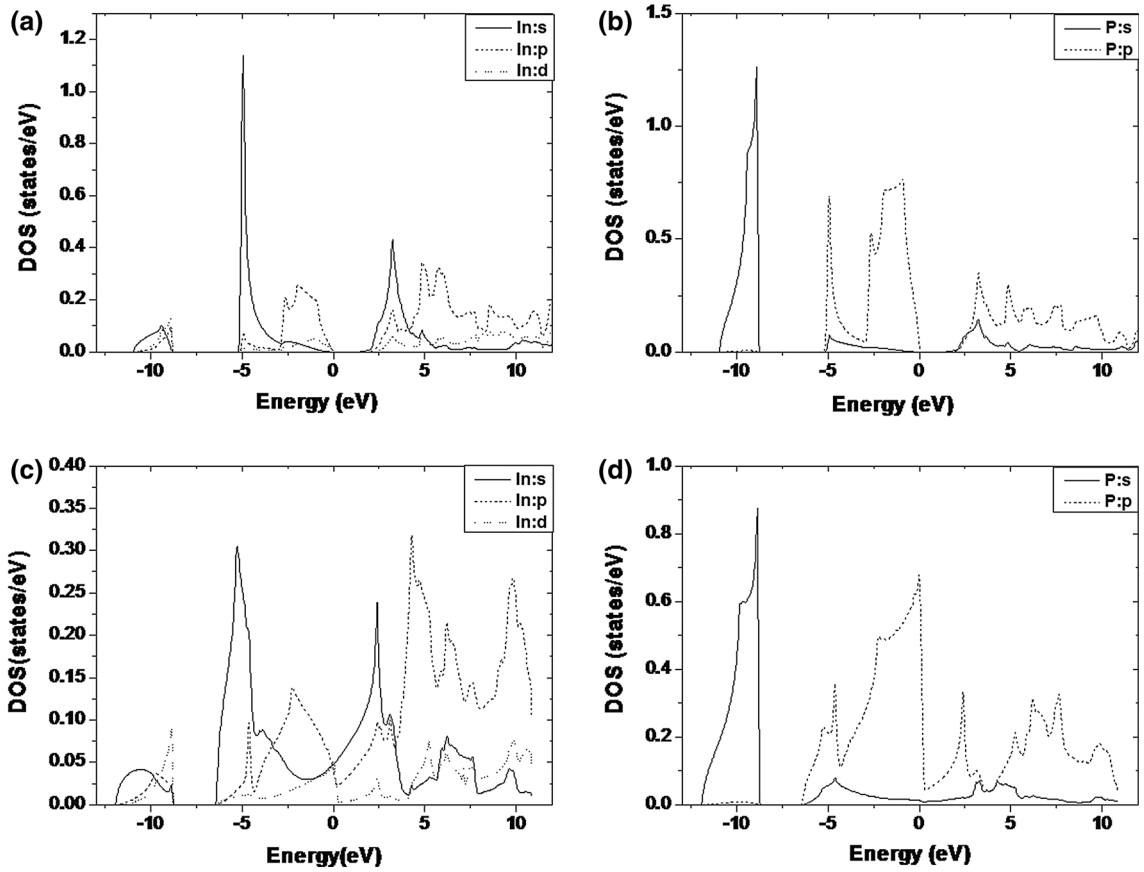

Fig. 4 DOS of InP: (**a**) In partial DOS of InP-ZB (**b**) P partial DOS of InP-ZB (**c**) In partial DOS of InP-RS (**d**) P partial DOS of InP-RS

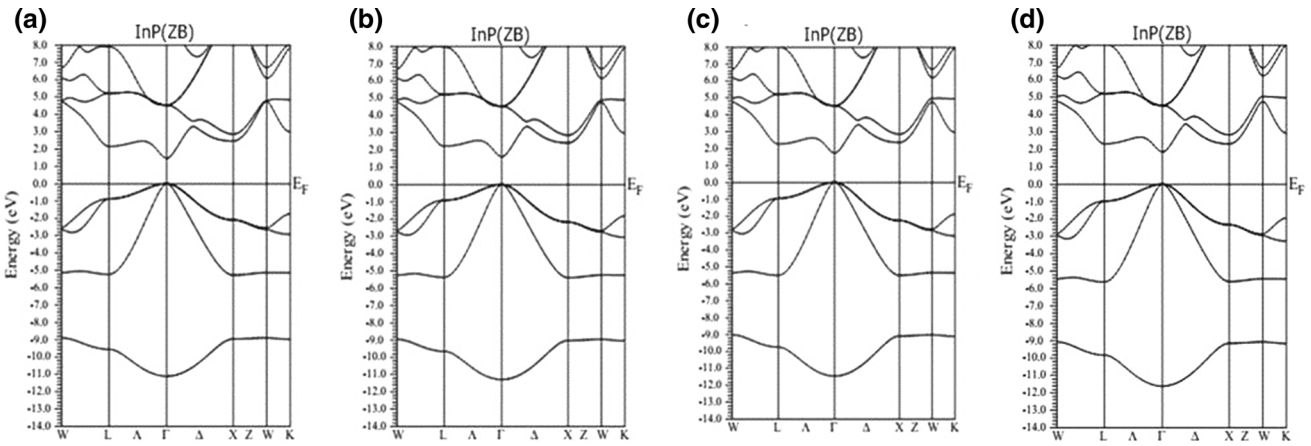

Fig. 5 Energy band diagram of InP-ZB structure: (**a**) 2 GPa pressure, (**b**) 4 GPa pressure, (**c**) 6 GPa pressure and (**d**) 8 GPa pressure

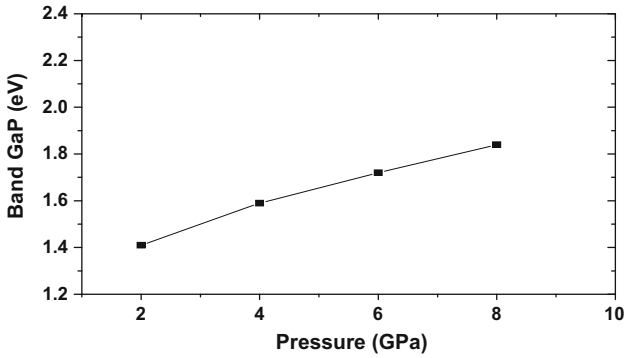

Fig. 6 Pressure versus band gap of InP-ZB structure at different pressures

presence of the energy eigenvalues corresponding to *s*, *p* and *d* orbitals in the higher region with increasing pressure. In Fig. 7(a)–7(d), the energy band diagrams under various pressures of the RS structure are presented and observed that the crossing over of conduction band towards the valence band does not change and hence, the metallic nature is retained even at higher pressures. Our result concludes that the energy band gap of the RS phase of InP is not much affected by the variation in pressure.

4. Conclusions

The structural properties of both InP-ZB and InP-RS are studied and found to be in good agreement with other experimental and theoretical results. The phase transition from the ZB structure to RS structure of InP is found to occur at 9.3 GPa pressure with a volume collapse of 16.45 %, indicating that InP-ZB structure is more compressible than the InP-RS structure. The elastic constants of InP at various pressures of both the structures are obtained and the corresponding elastic parameters are calculated. In both the ZB and RS structures, the values of elastic

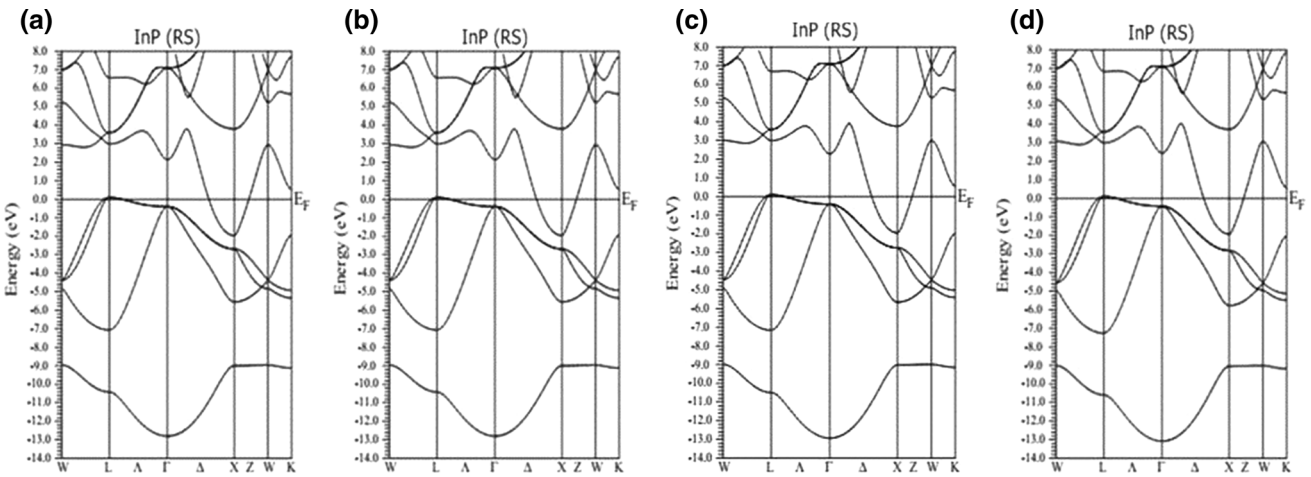

Fig. 7 Energy band diagram of InP-RS structure: (**a**) 2 GPa pressure, (**b**) 4 GPa pressure, (**c**) 6 GPa pressure and (**d**) 8 GPa pressure

constants as well as the elastic parameters are found to have a linear relation with increase in pressure. The Poisson's ratio calculation shows dominance in the ionic contribution to the inter-atomic bonding with increase in pressure. Shrinkage in bond stretching with increase in pressure is also found from the study of Kleinmann parameter. The study of the Debye's temperature shows stiffer lattice and better thermal conductivity with pressure. The InP-ZB structure is found to be a direct band gap semiconductor with an energy band gap of 1.31 eV, while the InP-RS structure is found to be metallic. The total density of states of InP is obtained and we find that in the ZB structure, In-*s* state has the highest contribution towards the total density of states near the Fermi level, whereas in RS structure, *P–p* state has the highest contribution. It is found that in the InP-ZB structure the band gap increases with increasing pressure, whereas in the InP-RS structure there is no much variation in band gap with increase in pressure. Hence, our results conclude that there are substantial changes in the elastic parameters of both InP-ZB and InP-RS structures and energy band gap of InP-ZB phase, but no prominent change is observed in the electronic structure of InP-RS phase with variation in pressure.

References

[1] Y K Vohra, S T Weir and A L Ruoff *Phys. Rev. B* **31** 7344 (1981)
[2] S Schilling and R N Shelton *Phys. of Solids Under Pressure* (New York: North-Holland) (1981)
[3] J M Besson, J P Itie, A Polian, G Weil, J L Mansot and J Gonzales *Phys. Rev. B* **44** 4214 (1991)
[4] M Jameson, B Indrajit Sharma, R Bhattacharjee, R K Thapa and R K Brojen *Physica B* **406** 4041 (2011)
[5] A Mujica, A Rubio, A Munoz and R J Needs *Rev. Mod. Phys.* **75** 912 (2003)
[6] J Sjakste, N Vast and V Tyuterev *Phys. Rev. Lett*. **99** 236405 (2007)
[7] E S Kadantsev arXiv:1005.0615vl [*cond-mat.mtrl-sci*] (2010)
[8] L Sukit, P Reunchan, A Janotti and G V W Chris *Phys. Rev. B* **77** 195209 (2008)
[9] L Lin, G T Woods and T A Callcott *Phys. Rev. B* **63** 235107 (2001)
[10] J G Díaz, G W Bryant, W Jaskólski and M Zielinski *Phys. Rev. B* **75** 245433 (2007)
[11] S Minomura and H G Drickamer *J. Phys. Chem. Solids* **23** 451 (1962)
[12] J C Jamieson *Science* **139** 845 (1963)
[13] T Soma, J Satoh and H Matsuo *Solid State Commun*. **42** 889 (1982)
[14] C S Menoni and I L Spain *Phys. Rev. B* **35** 7520 (1987)
[15] O Arbouche, B Belgoumene, B Soudinia, Y Azzaz, H Bendaoud and K Amara *Comput. Mater. Sci.* **47** 685 (2010)
[16] P S Branicio, J P Rino and F Shimojo *Appl. Phys. Lett*. **88** 161919 (2006)
[17] G Onida, L Reining and A Rubio *Rev. Mod. Phys*. **74** 601 (2012)
[18] K. Kabita, M Jameson, B Indrajit Sharma, R K Thapa Singh and R K Brojen *Adv. Sci. Eng. Med.* **6** 354 (2014)
[19] K. Kabita, M Jameson, B Indrajit Sharma, R K Thapa Singh and R K Brojen *Iraqi. J. Appl. Phys.* **9** 17 (2014)
[20] E Wimmer, H Krakauer, M Weinert and A J Freeman *Phys. Rev. B* **24** 864 (1981)
[21] A D Becke and E R Johnson *J. Chem. Phys*. **124** 221101 (2006)
[22] P Hohenberg and W Kohn *Phys. Rev*. **136** 864 (1964)
[23] W Kohn and L J Sham *Phys. Rev.* **140** 1133 (1965)
[24] S Cottenier *Density Functional Theory and the family of (L)APW-methods: a step-by-step Introduction* (Belgium: Instituut voor Kern-en Stralingsfysica, K. U. Leuven) ISBN 90-807215-1-4 (2002)
[25] J P Perdew, S Burke and M Ernzerhof *Phys. Rev. Lett.* **77** 3865 (1996)
[26] P Blaha, K Schwarz, G K H Madsen, D Kvasnicka and J Luitz WIEN2k *An Augmented Plane Wave + Local Orbitals Program for Calculating Crystal Properties* (Austria: Karlheinz Schwarz, Techn. Universitat Wien) ISBN 3-9501031-1-2 (2001)
[27] F Birch *Phys. Rev.* **71** 809 (1947)
[28] F Birch, *J. Appl. Phys*. **9** 279 (1938)
[29] W Paul *J. App. Phys.* **32** 2082 (1961)
[30] O Madelung *Semiconductors Physics of Group IV elements and III-V compounds* Landolt-Bornstein, New Series, Group III vol. 17 part A (Berlin: Springer-Verlag) (1982)
[31] A Mujica and R J Needs *Phys. Rev. B* **55** 9659 (1997)
[32] S Kalvoda, B Paulus, P Flude and H Stoll *Phys. Rev. B* **7** 4027 (1997)
[33] A Seidl, A Gorling, P Vogl, J A Majewski and M Levy *Phys. Rev. B* **53** 3764 (1996)
[34] D Nichols, D Rimia and R Sladek *Solid State Commun.* **36** 667 (1980)
[35] R Trommer, H Muller, M Cardona and P Vogl *Phys. Rev. B* **21** 4878 (1980)
[36] M Yousaf, M A Saeed, R Ahmed, MM Alsardia, A R M Isa and A Shaari *Commun. Theor. Phys*. **58** 777 (2012)
[37] R W G Wyckoff, *Crystal Structures* 2nd edn. (Malabar: Krieger) (1986)
[38] R Ahmed, F Aleem, S J Hashemifar and H Ak-barzadeh *Phys. B* **403** 1876 (2008)
[39] M I Mc Mahon, R J Nelmes, N G Wright and D R Allan *Proceedings of the Joint Conference on the AIRATP/APS On High-Pressure Science and Technology*, June 28–July 2 (eds.) S C Schmit, J W Shaner, G A Samara and M Ross (Colorado: ColoradoSprings) p 629 (1993)
[40] I Lukacevic, D Kirin, P K Jha and S K Gupta *Phys. Status Solidi B* **247** 273 (2010)
[41] H Chenghua, F Wang and Z Zheng *J. Mater. Res*. **27**, 1105 (2012)
[42] R K Singh and S Singh *Phys. Rev. B* **39** 671 (1989)
[43] S B Zhang and M L Cohen *Phys. Rev. B* **35** 7604 (1987)
[44] B Mayer et al. *Intermetallics* **11** 23 (2003)
[45] L Johnston, G Keeler, R Rollins and S Spicklemire *The Consortium for Upper-Level Physics Software*, (New York: John Wiley) (1996)
[46] I Anderson *J. Phys. Chem. Solids* **24** 909 (1963)
[47] E Schreiber, O L Anderson and N Soga *Elastic constants and their measurements.* (New York: McGraw-Hill) (1973)
[48] V V Bannikov, I R Shein and A L Ivanovskii *Phys. Status. Solidi. Rapid. Res. Lett.* **3** 89 (2007)
[49] H Fu et al. *Comput. Mater. Sci.* **44** 774 (2008)
[50] S F Pugh *Phil. Mag.* **45** 833 (1954)

Journal of Basic and Applied Engineering Research
Print ISSN: 2350-0077; Online ISSN: 2350-0255; Volume 2, Number 13; April-June, 2015 pp. 1064-1067

http://www.krishisanskriti.org/jbaer.html

Electronic Structures of GaX(X=P, As) under Induced Pressure: A First Principle Study

Kh. Kabita[1] and B. Indrajit Sharma[2]*

1,2*Department of Physics, Assam University, Silchar-788011, Assam,* ***India***
E-mal: [2]indraofficial@rediffmail.com

Abstract—*A first principle study on the electronic structures of GaX (X=P, As) under induced pressure is performed using the modified-becke Johnson potential under the framework of Density Functional Theory. In the present calculation, GaP undergoes a phase transition from B3 to B1 phase at 21.9 GPa pressure with a volume collapse of 14.11% while GaAs undergoes a transition from B3 to B1 phase at 10.7 GPa pressure with a volume collapse of 14.2% indicating that B3 phase of both the compounds is more compressible than the B1 phase. The energy band diagram of GaP-B3 phase and GaAs-B3 phase show an indirect band gap of 2.33eV and a direct band gap of 1.3eV respectively while B1 phase for both the compounds show metallic nature which is in good agreement with other theoretical and experimental studies. Under induced pressure the indirect band gap of GaP-B3 phase and direct band gap of GaAs-B3 phase increases while in the B1 phase, the metallic nature of GaP and GaAs is retained and does not vary with pressure.*

1. INTRODUCTION

The development in the field of optoelectronic devices and scientific applications of III-V compound semiconductors has led to its extensive study in recent years [1-3]. GaX (X=P, As) is a III-V compound semiconductor which is being considered of great technological importance due to its potential application in many optoelectronic devices such as light emitting diodes (LED) and laser diodes (LD)[4,5]. The study of the electronic and structural properties helps us in characterizing, understanding and predicting the mechanical properties of a material. Therefore the variation in the energy band gap under induced pressure help us for better understanding of these properties under extreme conditions of pressure.

In literature it has been reported that GaP and GaAs crystallizes in zinc-blende (B3) structure under ambient pressure conditions. In various studies it is reported that when pressure is applied the volume decreases and a structural phase transition to rock salt (B1) structure is found to occur [6-8].

The ab-inito study of the structural and electronic properties of a material has become more systematic and precise with the developments in the computer simulation. It helps us in better understanding and estimation of the properties of a material under induced pressure which are difficult to study experimentally. Even though there have been many studies on the phase transition and electronic properties of GaP and GaAs, there have been few studies on the effect of pressure on the electronic structure of these compounds. The present paper is mainly focused on the study of the variation in the energy band gap under induced pressure in both B3 and B1 phases using the WIEN2K code based on DFT. The paper has been organized as follows. After this introduction, the methods used in our calculation are described in section 2. In section 3 the results of our study are given and discussed in detailed. The conclusion of our study is given in section 4.

2. COMPUTATIONAL METHODS

The first principle study of GaX(X=P,As) calculation is performed using the first principle full potential linearized augmented plane wave (FP-LAPW) [9] method within the generalized gradient approximation (GGA) of Perdew-Burke-Ernzerhof (PBE-GGA) [10] with modified Becke-Johnson (mBJ) [11] potential under the framework of density functional theory (DFT) [12-14]. This method is used as it is one of the most accurate methods in electronic structure calculation of crystals. In this method, the lattice is divided into non-overlapping atomic spheres surrounding each atomic sites and an interstitial region [15]. Inside the muffin tin (MT) region, the potential is a product of radial function and spherical harmonics and expanded up to order l = 10. For the interstitial regions that are outside the muffin tin spheres, the potentials are expanded in plane waves. 8000 k-points are used for the integration part which reduces to 256 irreducible k-points inside the Brillouin zone. Convergence is obtained at $R_{MT}K_{max}$ = 9.0 where R_{MT} is the atomic sphere radii and K_{max} gives the plane wave cut-off. The position of the first and second atom of the B3 and B1 structures of GaP is taken to be (0,0,0), (0.25,0.25,0.25) and (0,0,0), (0.5,0.5,0.5) respectively. $3d^{10}4s^24p^1$, $3s^23p^3$ and $3d^{10}4s^24p^3$ states are respectively considered as the valence electrons for Ga, P and As respectively. All calculations are performed with the equilibrium lattice constants which are determined from the plot of the total energy against the unit cell volume by fitting to the Birch-Murnaghan equation of states [16]. The overall calculation is done with WIEN2K [17].

3. RESULTS AND DISCUSSION

The ground state lattice parameter for GaP and GaAs in both B3 and B1 phase are obtained by the structure optimization. A series of different lattice constant are used to calculate the total energy and the corresponding primitive cell volume. The energy versus unit cell volume curves for both GaP and GaAs are shown in Fig. 1(a) and Fig. 1(b). We can clearly see that in both the figures the B3 phase is more stable than the B1 phase which is in good agreement with other theoretical and experimental results.

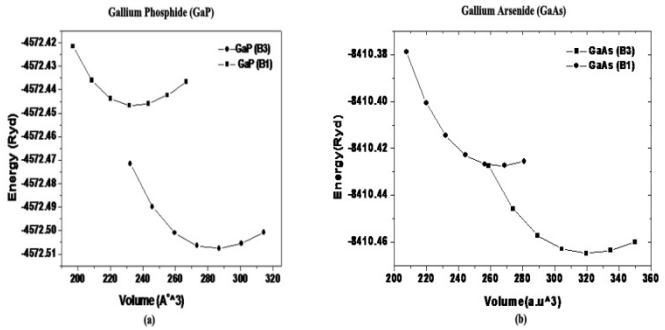

Fig. 1: Total energy verses unit cell volume for B3 and B1 phases of (a) GaP and (b) GaAs.

The phase transition is important for understanding the structural, mechanical and physical properties of a material under pressure. The phase transformation of four-fold coordinated structure (B3) of GaX (X=P, As) to a more denser six fold coordinated structure (B1) under pressure is calculated using the condition of equal enthalpies i.e. the H=E+PV. The structural phase transition from B3 to B1 phase for GaP and GaAs are shown in Fig. 2(a) and Fig. 2(b).

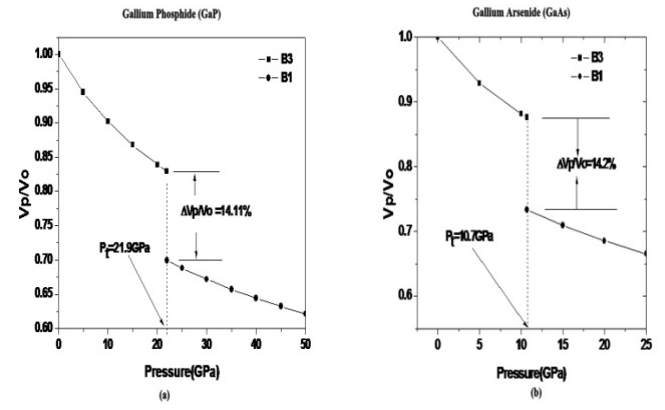

Fig. 2: Phase transition from B3 to B1 phase for (a) GaP and (b) GaAs.

We find that the structural phase transition for GaP-B3 to GaP-B1 occurs at 21.9 GPa pressure with a volume collapse of 14.11% while GaAs undergoes a structural phase transition from B3 to B1 phase at 10.7 GPa pressure with a volume collapse of 14.2% indicating that in both GaP and GaAs, the B3 phase is more compressible than the B1 phase. The energy band diagram of GaP and GaAs has already been reported in many theoretical and experimental studies [18-20]. In the present study we find that GaP-B3 phase is an indirect band gap semiconductor with a band gap of 2.3eV while GaP-B1 phase is metallic. Also GaAs-B3 phase is a direct band gap semiconductor with a band gap of 1.3eV while GaAs-B1 phase shows metallic nature. Therefore we find that our results for both B1 and B3 phases of GaP and GaAs are in close agreement with previous reported data. We have also calculated the energy band gap of GaX(X=P, As) at different pressures for both B1 phase and B3 phase.

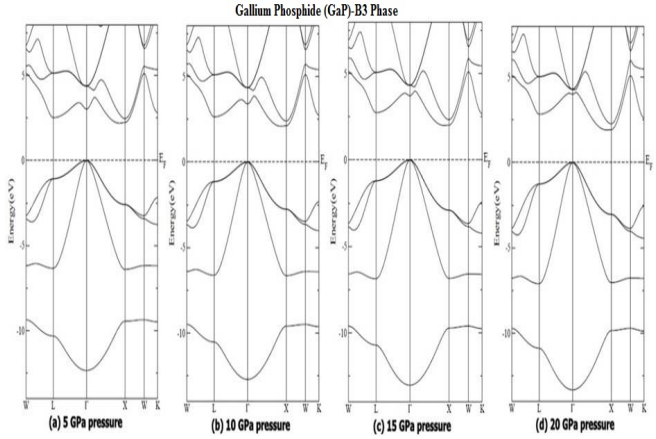

Fig. 3: Energy band diagram of B3-phase of GaAs in (a) 5 GPa pressure (b) 10 GPa pressure (c) 15 GPa pressure and (d) 20 GPa pressure.

Fig. 3(a), 3(b), 3(c) and 3(d) shows the energy band diagram of B3 phase of GaP at different pressures. One interesting thing that we find from the band structure diagrams in Fig. 4 is that as the pressure increases to 5 GPa, 10 GPa 15 GPa and 20 GPa, the gap between the Γ-L increases while the gap between Γ-X decreases towards the fermi level indicating possibilities of crossing over of the conduction band towards the valance band. The variation in the energy band gap with pressure for B3 phase of GaP is also shown in Fig. 6 for clear analysis of the changes between Γ-X and Γ-L with pressure. The energy band diagram of B1 phase of GaP at different pressures after the phase transition is also shown in Fig. 5(a), 5(b), 5(c) and 5(d). From the Fig. we can clearly see crossing over of the conduction band towards the valance band hence confirming the transition from direct band gap nature to metallic at higher pressure.

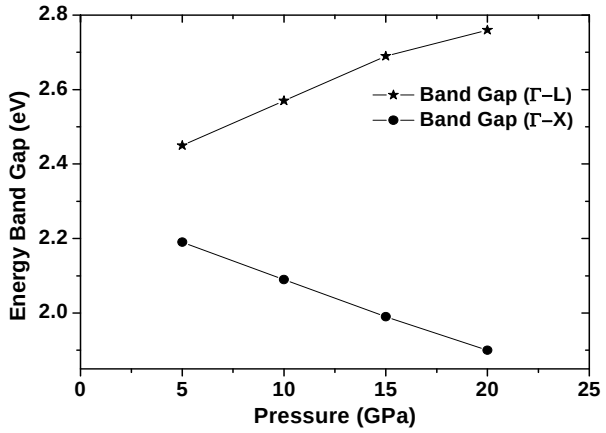

Fig. 4: Variation of Energy band gaps of GaP-B3 phase with pressure.

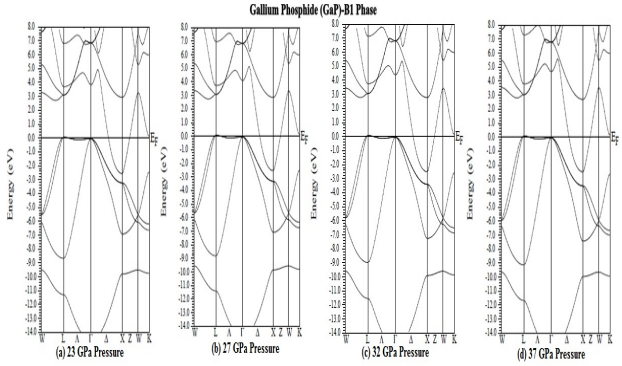

Fig. 5: Energy band diagram of B1-phase of GaP in (a) 23 GPa pressure (b) 27 GPa pressure (c) 32 GPa pressure and (d) 37 GPa pressure.

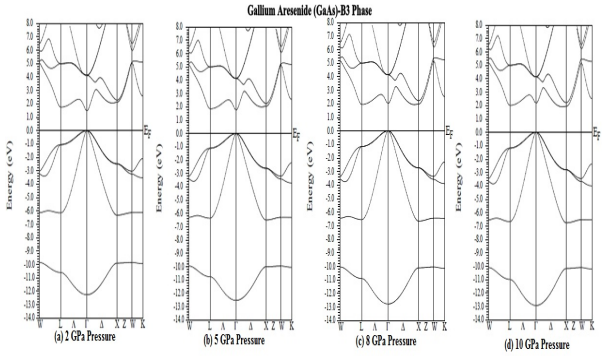

Fig. 6: Energy band diagram of B3-phase of GaAs in (a) 2 GPa pressure (b) 5 GPa pressure (c) 8 GPa pressure and (d) 10 GPa pressure.

In Fig. 6(a), 6(b), 6(c) and 6(d), the energy band diagrams of GaAs-B3 phase at different pressures are given. From the figures we find that the gap between the Γ point increases as the pressure increases but if we closely study the energy band diagram we find that the gap at the X point decreases which indicates possibility of crossing over at higher pressure as in case of GaP. The variation of gap at the Γ point and X point with increase in pressure is given in Fig. 7.

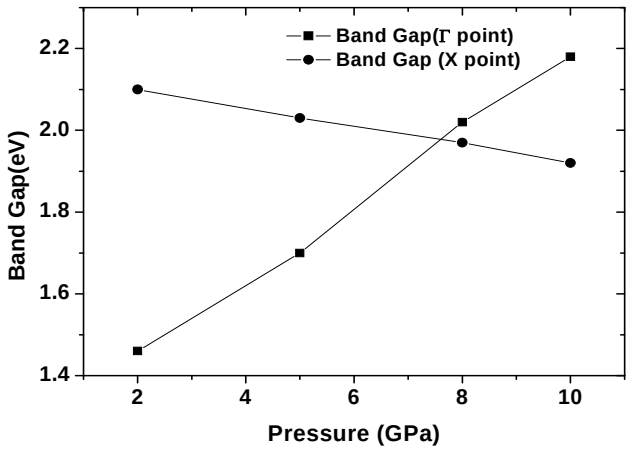

Fig. 7: Variation of Energy band gaps of GaAs-B3 phase with pressure.

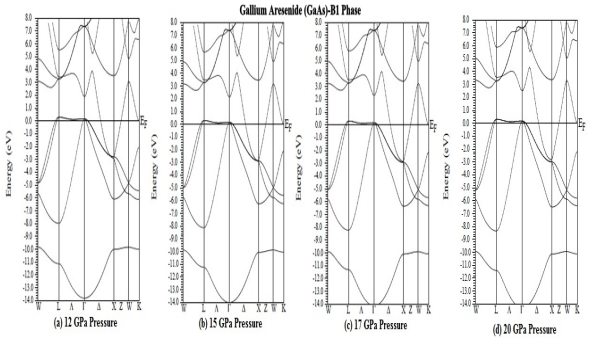

Fig. 8: Energy band diagram of B1-phase of GaAs in (a) 12 GPa pressure (b) 15 GPa pressure (c) 17 GPa pressure and (d) 20 GPa pressure.

Fig. 8(a), 8(b), 8(c) and 8(d) shows the energy band diagram of the B1 phase of GaAs. From the Fig. we find that the metallic nature is retained even at high pressure without much variation. Hence we conclude that the energy band gap of both GaP and GaAs in B3 phase is affected by pressure while the energy band gaps of B1 phase is not much affected by pressure.

4. CONCLUSIONS

The structural properties of GaX (X=P, As) in both B3 and B1 structure are studied and B3 phase is found to be more stable than the B1 phase. A structural phase transition from B3 to B1 is found to occur at 21.9 GPa pressure with a volume collapse

of 14.11% in GaP while GaAs undergoes a structural transition from B3 to B1 phase at 10.7 GPa pressure with a volume collapse of 14.2% indicating that B3 phase of both the compounds is more compressible than the B1 phase. The energy band diagram shows that GaP-B3 is an indirect band gap semiconductor with a band gap of 2.3 eV while GaAs-B3 is a direct band gap semiconductor with a band gap of 1.3 eV. The B1 phase of both the compounds is also found to be metallic which are found to be in good agreement with other experimental and theoretical studies. The energy band gaps for GaP-B3 phase between the Γ-L points, increased while the gap between the Γ-X points decreased under induced pressure. Also GaAs-B3 phase showed an increase in gap at the Γ point and decrease at X point under induced pressure. However the metallic behavior of GaP-B1 and GaAs-B1 phase do not show any change under induced pressure. Thus we conclude that the B3 phase of both GaP and GaAs are affected by pressure while the B1 phase is not affected by pressure.

REFERENCES

[1] Bouhemadou, A., Khenata, R., Kharoubi, M., Seddik, T., Reshak, A. H., and Al-Douri, Y., *Comp. Mater. Sci.*, 45, 2009, pp. 474-479.

[2] Arbouche, O., Belgoum`ene, B., Soudini, B., Azzaz, Y., Bendaoud, H., and Amara, K., *Comp. Mater. Sci*., 47, 2010, pp. 685-692.

[3] Sukit, L., Reunchan, P., Janotti, A., and Chris, G. V. W., *Phys. Rev. B*, 77, 2008, 195209-1952015.

[4] Jiao, Z. Y., Ma, S. H., and Guo, Y. L., *Comp. Theor. Chem*., 970, 2011, 79-87.

[5] Smith, F. W., Le, H. Q., Diadiuk, V., Hollis, M. A. Calawa, A. R., Gupta, S., Frankel, M., Dykaar, D. R., Mourou, G. A., and Hsiang, T. Y., *Appl. Phys. Lett.*, 54, 1989, 890-892.

[6] Durandurdu, M., and Darbold, D. A., *Phys. Rev* B, 66, 2002, 045209(1)-045209(5).

[7] Al-Douri, Y., Mecabih, S., Benosman, N., and Aourag, H., *Physica B*, 325, 2003, pp. 362-371.

[8] Mujica, A., and Needs, R. J., *J. Phys. Condens. Matter*, 8, 1996, L237-L243.

[9] Wimmer, E., Krakauer, H., Weinert, M., and Freeman, A. J., *Phys. Rev. B* 24**,** 1981, pp. 864-875

[10] Perdew, J. P., Burke, K., and Ernzerhof, M., *Phys. Rev. Lett*. 77, 1996, pp. 3865-3868.

[11] Becke, A. D., and Johnson, E. R., *J. Chem. Phys.* 124, 2006, pp. 221101-221104.

[12] Hohenberg , P., and Kohn, W., *Phy. Rev.3B*, 136, 1964, pp. 864-871.

[13] Kohn, W., and Sham, L. J., *Phys. Rev. 4A* 140, 1965, pp. 1133-1138.

[14] Cottenier, S., *"Density Functional Theory and the family of (L)APW-methods: a step-by-step Introduction"* Belgium, Instituut voor Kern-en Stralingsfysica, K.U.Leuven ISBN 90-807215-1-4, 2002.

[15] Andersen, O. K., *Phys. Rev. B*. 12, 1975, pp. 3060-3083.

[16] Birch, F., *Phys. Rev.* 71, 1947, pp. 809-824.

[17] Blaha, P., K. Schwarz, Madsen, G. K. H., Kvasnicka, D., and Luitz, J., *"An anaugmented plane wave + local orbitals program for calculating crystal properties*",*Wien2k. Techn. Universitat* (Wien, Austria) ISBN 3-9501031-1-2. 2001.

[18] Al-Douri, Y., Ali Hussain, R., *Applied Phys.A*, 2011, pp. 1159-1167.

[19] C. Kittel, Introduction to Solid State Physics 6th Ed. (New York: John Wiley) 1986, pp.185.

[20] Madelung, O., *Landolt-Börnstein, Semiconductor, Physics of II-IV and I-VII Compounds, Semimagnetic Semiconductors, New Series, Group III,* V. 17 (Springer: Berlin

STRUCTURAL PHASE TRANSITION OF INDIUM ARSENIDE UNDER INDUCED PRESSURE: A DENSITY FUNCTIONAL THEORY STUDY

Kh. Kabita[1], B. Indrajit Sharma*[1], Jameson Maibam[1], R. K. Brojen Singh[2] and R.K. Thapa[3]
[1]*Department of Physics, Assam University, Silchar-788011, Assam, India.*
[2] *School of Computational and Integrative Sciences, JNU, New Delhi 110067, India.*
[3]*Department of Physics, Mizoram University, Tanhril, Aizawl-796 00, India.*
*For correspondence. (indraofficial@rediffmail.com)

Abstract: We have carried out the first-principles calculations to show phase transition of binary compound semiconductor Indium Arsenide under induced pressure in the light of density functional theory with the generalised gradient approximation of Perdew-Burke-Ernzerhof as exchange correlation potential. The calculated lattice parameters are found to be in good agreement with other theoretical and experimental data. The pressure induced phase transition from zinc-blende to rock salt structure is found to occur at 4.7 GPa pressure with a 17.27% of volume collapse.

Keywords: Density Functional Theory (DFT); energy band diagram; elastic properties; phase transition

PACS: 71.15.Mb, 71.20.-b, 71.20.Nr

1. Introduction:

The technological importance of group III-V compound semiconductors have increased over the past years due to its electronic and mechanical properties and have received considerable interest from experimentalist and theorists. To understand, the structural phase transition of a material and the influence of band structure parameters on the electronic properties of semi-conductors, the study under induced pressure is found to be an effective tool. Also the study of elastic constants at different pressure plays an important role in mechanical stability, strength, phase transition and a material response to various conditions. One of the interesting phenomena that may occur under applied pressure is a sudden change in the arrangement of the atoms i.e. structural phase transition. Indium Arsenide (InAs) is an important group III-V compound semiconductor having high electron mobility and narrow energy band gap. It is widely used in construction of infrared detectors and diode lasers [1]. It crystallizes in cubic zinc-blende (ZB) structure under ambient conditions. At high pressure it is found to undergo structural phase transition to rock-salt (RS) structure. The pressure-induced phase transition to metallic state was first reported by Minomura and Drickamer at 8.46 GPa pressure from high pressure resistivity measurements [2]. Pitt and Vyas reported the phase transition from the Zinc-blende (ZB) to Rock-salt (RS) through resistivity measurements [3]. Although there have been extensive studies on structural, mechanical and electronic properties of InAs, the experimental and theoretical study of these properties under high pressure is still very scarce. The main aim of this work is to present a detailed study of the structural changes of InAs in ZB to RS phase under induced pressure. The paper is organised as follows. The theoretical and computational method is described in section 2. In section 3, the results and discussion of our study is given and our conclusions are summarized in section 4.

2. Theoretical and Computational Method:

All theoretical calculations of InAs is performed based on the WIEN2K code [4] using the full potential linearized augmented plane wave (FP-LAPW) [5] method with modified Becke-Johnson (mBJ) potential [6] under the framework of Density Functional Theory (DFT) [7,8,9]. The generalized gradient approximation (GGA) of Perdew-Burke-Ernzerhof scheme is used for treating the exchange correlation interaction effects [10]. In this method, the lattice is divided into non-overlapping spheres (called atomic or muffin tin sphere) surrounding each atomic sites and an interstitial region. Inside the muffin tin (MT) region, the potential is a product of radial function and spherical harmonics and expanded up to order l = 10. For the interstitial regions that are outside the muffin tin spheres, the potentials are expanded in plane waves. The number of k-points used

for the integration part is 8000 k-points which is reduced to 256 irreducible k-points inside the Brillion zone including five high symmetry points W, L, Γ, X and K. Convergence of the basis set is obtained at $R_{MT}K_{max}$ = 9.0 where K_{max} gives us the plane wave cut-off.

3. Results and Discussion:

The energy as a function of the primitive cell volume for ZB and RS phase is shown in figure 1. From the figure, one can clearly see that the InAs-ZB structure is more stable than the RS structure. The equilibrium lattice parameters of the InAs crystal in zinc-blende and rock-salt structure is obtained by fitting the resultant curve to the Birch-Murnaghan equation [11]. The calculated structural parameters are compared with other results [12,13,14,15,16] and are given in table 1. Our results are found to be in good agreement with other results and hence are used for further calculations.

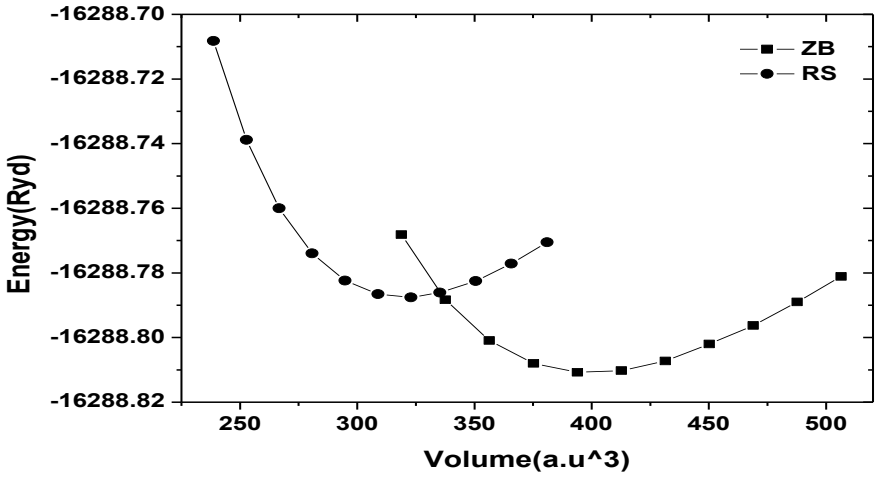

Figure 1. Total energy as a function of primitive cell volume of InAs in ZB and RS phases.

Table 1. Lattice constants, bulk modulus and pressure derivative of bulk modulus of InAs-ZB and InAs-RS at zero pressure.

Structure		a(A^0)	B(GPa)	B/
ZB	Present work	6.188	49.48	4.78
	References	6.058[a], 6.10[b], 6.08[c]	55.51[c], 59.2±5[d]	6.8±2[d]
RS	Present work	5.748	62.98,	4.84
	References	5.65[c], 5.5005[d], 5.514[e]	40.6±14[d]	7.3±1[d]

Ref.12[a], Ref.13[b], , Ref.14[c] , Ref.15[d] , Ref.16[e]

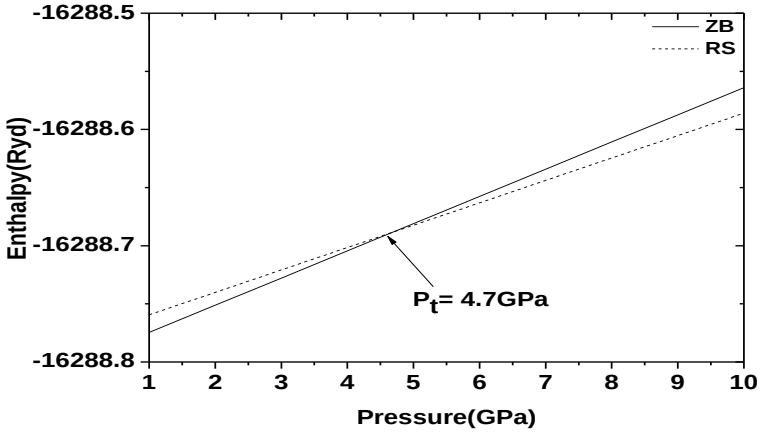

Figure 2. Enthalpy variation of InAs in ZB and RS structures as a function of pressure.

The pressure induced phase transition of InAs-ZB to InAs-RS phase is investigated from a series of ground state optimisation at various pressures. After optimisation, the enthalpy, H = E + PV is used to obtain the pressure induced phase transition. Figure 2 shows the enthalpy as a function of pressure of both the InAs-ZB and InAs-RS structure. It is clearly seen that the phase transition of InAs-ZB structure to InAs-RS structure is found to occur at 4.7 GPa pressure.

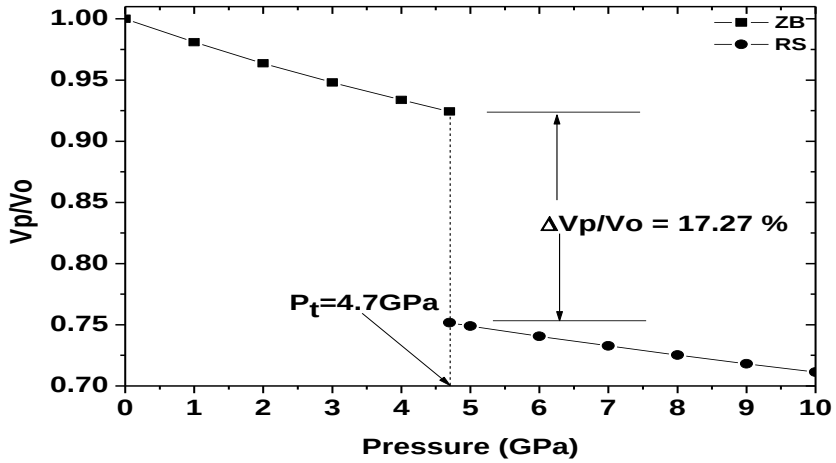

Figure 3. Phase transition between ZB and RS structure of InAs at 4.7 GPa pressure.

Table 2. Phase transition pressure and volume collapse comparisons with other experimental and theoretical data:

	Present calculation	Expt. results	Theoretical results
Transition pressure (P_t) (GPa)	4.7	7[a] , 6.9±0.2[c]	3.9[d], 4.0[e], 6.0[f],
Volume collapse (%)	17.2	17.0±0.2[a], 18.8[b]	17.0[g], 24.0[h]

Ref.15[a], Ref.16[b], Ref.17[c], Ref.18[d], Ref.19[e], Ref.20[g], Ref.21[h]

The normalised volume (V_p/V_o) of the crystal in ZB phase and RS phase is also found to be 0.924 and 0.752 respectively during the phase transition with a volume collapse of 17.2% indicating that ZB phase is more compressible than the RS phase as given in figure 3. Our calculated results of phase transition and volume collapse are compared with other experimental and theoretical results [17,18,19,20,21] and are shown in table 2. We find that our results are closer to the experimental data than other theoretical results.

4. Conclusions:

The calculated optimised structural parameter of Indium Arsenide in both zinc-blende and rock salt structure phase are compared with other theoretical end experimental results and are found to be in good agreement. The phase transition of InAs-ZB structure to InAs-RS structure under induced pressure is found to occur at 4.7 GPa pressure. The normalized volume of the crystal in ZB phase and RS phase is also found to be 0.924 and 0.752 respectively during the phase transition with a volume collapse of 17.2% indicating that ZB phase is more compressible than the RS phase.

References:

[1] D. R. Lide, Handbook of Chemistry and Physics (87 ed.), Boca Raton, CRC Press, pp 4–61, 1998.
[2] S. Minomura, H. G. Drickamer, J. Phys. Chem Solids, 23, 451, 1962.
[3] G. D. Pitt and M. K. R. Vyas, J. Phys. C: Solid State Phys., 6, 274, 1973.
[4] P. Blaha, K. Schwarz, G. K. H. Madsen, D. Kvasnicka and J. Luitz, WIEN2k An Augmented Plane Wave + Local Orbitals Program for Calculating Crystal Properties (Austria : Karlheinz Schwarz, Techn. Universitat Wien), ISBN3- 9501031-1-2, 2001.
[5] E. Wimmer, H. Krakauer, M. Weinert and A. J. Freeman, Phys. Rev. B, 24, 864, 1981.
[6] A. D. Becke and E. R. Johnson, J. Chem. Phys., 124, 221101, 2006.
[7] P. Hohenberg and W. Kohn, Phys. Rev., 136 (3B), 864, 1964.
[8] W. Kohn and L. J. Sham, Phys. Rev., 140 (4A), 1133, 1965.
[9] S. Cottenier, Density Functional Theory and the family of (L)APW-methods: a step-by-step Introduction (Belgium: Insti-tuut voor Kern-en Stralingsfysica, K.U.Leuven), ISBN 90-807215-1-4, 2002.
[10] J. P. Perdew, S. Burke and M. Ernzerhof, Phys. Rev. Let., 77**,** 3865, 1996.
[11] F. Birch, Phys. Rev., 71, 809, 1947.
[12] G. Giesecke, H. Pfister, Acta Crystallogr , 11, 369, 1958.
[13] N. E. Christensen, S. Satpathy, Z. Pawlowska, Phys. Rev. B, 36, 1032. 1987.
[14] L. Pedesseau, J. Even, A. Bondi, W. Guo, S. Richard, H. Folliot, C. Labbe, C. Cornet, O. Dehaese, A. Le Corre, O. Durand and S. Loualiche, J. Phys. D: Appl. Phys., 41, 165505, 2008.
[15] Y. K. Vohra, S. T. Weir and A. L. Ruoff, Phys. Rev. B, 31, 7344, 1987.
[16] J. C. Jamieson, Science, 139, 845, 1963.
[17] S. K. Tewksbury, "Semiconductor Materials", Microelectronic System Research Center, Department Of Electrical And Computer Engineering, West Virginia University, Morgantown, WV 26506 (304), pp 293-6371, 1995.
[18] M. I. McMahon and R. J. Nelmes, Phys. Status Solidi (b), 198, 389, 1996.
[19] A. Mujica, R. J. Needs and A. Muñoz, Phys. Status Solidi (b), 198, 461, 1996.
[20] S. B. Zhang and M. L. Cohen, Phys. Rev. B, 35, 7604, 1987.
[21] R. K. Singh and Sadhna Singh, Phys. Rev. B, 39, 671. 1989.

International Journal of Innovation and Applied Studies
ISSN 2028-9324 Vol. 8 No. 1 Sep. 2014, pp. 382-393

http://www.ijias.issr-journals.org/

Density functional theory study on pressure induced structural transformation, elastic properties and electronic structure of gallium arsenide (GaAs)

Kh. Kabita[1], Jameson Maibam[1], B. Indrajit Sharma[1], R. K. Brojen Singh[2], and R. K. Thapa[3]

[1]Department of Physics,
Assam University, Silchar-788011,
Assam, India

[2]School of Computational and Integrative Sciences,
JNU, New Delhi 110067, India

[3]Department of Physics,
Mizoram University,
Tanhril, Aizawl-796 009, India

ABSTRACT: The structural phase transformation under induced pressure of the GaAs- zinc blende (ZB) phase to rock salt (RS) phase, elastic properties and electronic structure of the stable (ZB) phase are studied under the framework of the density functional theory (DFT). When pressure is increased up to 10.7 GPa, transition from the GaAs-ZB to GaAs-RS structure occurs and the dependence of volume decrease of ZB to RS structure at the transition pressure is 14.11%. The elastic parameters such as elastic constants C_{11}, C_{12}, C_{33}, Zener anisotropic factor (A), Kleinmann parameter (ζ), Poisson's ratio (υ), Youngs modulus (Y) and energy band gap of GaAs-ZB structure shows a systematic variation with increase in pressure upto transition pressure. The results are found to be in consistent with other experimental and theoretical results.

KEYWORDS: Density Functional Theory (DFT); Energy band structure; Elastic properties; Phase transition.

1 INTRODUCTION

Gallium arsenide (GaAs) is a group III-V binary compound semiconductor utilized in the electronics and telecommunications industries and in the military science [1, 2]. Gallium arsenide chips are found in products such as night vision telescopes, discrete microwave circuitry, and room temperature lasers. It is superior semiconductors to silicon for optoelectronic devices due to its ability to handle signals at higher frequencies, at the same time generate lower noise [3, 4]. It is the most technologically important compound semiconductor material which has been intensively investigated in recent years. The study of electronic and structural properties helps us to understand, characterize and predict the mechanical properties of materials in the surroundings under extreme conditions. This study plays an important role in physical condensed matter [5]. With technological development, study of structural properties, phase diagram and high pressure phases of GaAs has aroused considerable scientific interest in the past decades. Froyen and Cohen [6] first reported the structural phase of GaAs in 1983. The structural transformation in GaAs was also investigated by Besson *et al* [7] and Weir *et al* [8] using the single-crystal x-ray absorption spectroscopy and elastic neutron scattering. Studies on electronic structures, high-pressure properties have been reported by various groups [9-12]. In literature, works on the phase transformation, band structure, density of states (DOS) and elastic properties with variation of pressure is still rare. To the best of our knowledge none of the papers in open literature has considered the variation of energy band gap and elastic properties from the induced pressure perspective and investigated the behavior of the same with the available experimental data. The present paper is mainly focused on study of the phase transition from the zinc-blende to rocksalt structure, band structure

Corresponding Author: B. Indrajit Sharma

and elastic properties of GaAs with increasing pressure using WEIN2K code based on DFT. This paper is organised as follows: Section 2 describes the theoretical and computational method used in this study. The results are discussed in section 3 and conclusions are given in section 4.

2 THEORETICAL AND COMPUTATIONAL METHOD

The calculation of GaAs has been performed with modified Becke-Johnson (mBJ) [13] exchange potential using full-potential linearised augmented plane wave (FP-LAPW) method [14] within the framework of density functional theory (DFT) [15, 16, 17] with Perdew-Bruke-Ernzerhof-Generalized Gradient Approximation (PBE-GGA) for the exchange correlation potential [18] as implemented in the WIEN2K code [19]. Within DFT formalism, the total energy can be expressed as a functional of density of electron system, ρ and can be written by the following functional,

$$E[\rho] = T_o[\rho] + V_H[\rho] + V_{xc}[\rho] + V_{ext}[\rho] \quad (1)$$

where, $T_o[\rho]$ is the kinetic energy of a non-interacting electron system, $V_H[\rho]$ and $V_{XC}[\rho]$ are the Hartree and exchange-correlation contributions to the energy and V_{ext} [ρ] is the energy due to the external potential of the system. Thus the corresponding Hamiltonian called the Kohn-Sham Hamiltonian is

$$\begin{aligned}\hat{H}_{KS} &= \hat{T}_o + \hat{V}_H + \hat{V}_{XC} + \hat{V}_{ext} \\ &= -\frac{\hbar^2}{2m_e}\vec{\nabla}^2{}_i + \frac{e^2}{4\pi\varepsilon_o}\int\frac{\rho(\vec{r}^{\,/})}{|\vec{r}-\vec{r}^{\,/}|}d\vec{r}^{\,/} + V_{XC} + V_{ext}\end{aligned} \quad (2)$$

The exact density of N electron system can be expressed in ground state by:

$$\rho(\vec{r}) = \sum_{i=1}^{N} \phi_i(\vec{r}) * \phi_i(\vec{r})$$

where the single particle wave functions $\phi_i(r)$ are the N lowest energy solutions of the Kohn Sham equation: $\hat{H}_{ks}\phi_i = \phi_i\phi_i$ of the N electron system.

These equations can be solved self consistently in an iterative process. In this method, the lattice is divided into non-overlapping spheres (called atomic or muffin tin sphere) surrounding each atomic sites and an interstitial region [20]. Inside the muffin tin (MT) region, the potential is a product of radial function and spherical harmonics and expanded up to order l = 10. For the interstitial regions that are outside the muffin tin spheres, the potentials are expanded in plane waves. 8000 k-points are used for the integration procedure as we find that above 8000 k-points the energy remains same and this 8000 k-points reduces to 256 irreducible k-points inside the Brillion zone including five high symmetry points W, L, Γ, X and K. Convergence is obtained at $R_{MT}K_{max}$ = 9.0 where R_{MT} is the atomic sphere radii and K_{max} gives the plane wave cut-off. The calculations are performed with the equilibrium lattice constants which are determined from the plot of the total energy against the unit cell volume by fitting to the Birch-Murnaghan equation of states [21].

3 RESULTS AND DISCUSSION

3.1 STRUCTURAL PROPERTIES

The total energy curve as a function of unit cell volume for GaAs in zinc-blende and rocksalt structure is shown in figure 1. It is clearly seen that ZB structure of GaAs is more stable than the RS structure which is in good agreement with previous results [22, 23, 24]. The obtained zero pressure equilibrium lattice constant (a_0) for GaAs-ZB structure is found as 5.74 A^o. This lattice constant corresponding to the optimized structure is slightly larger than experimental values as given in table 1. It has an error of about 1.8% which is quite acceptable under the 2% error and is used for further calculation. Thus the agreement between our result and other available theoretical and experimental data [25, 26, 27, 28, 29, 30] is well good indicating that our calculation can proceed for further study.

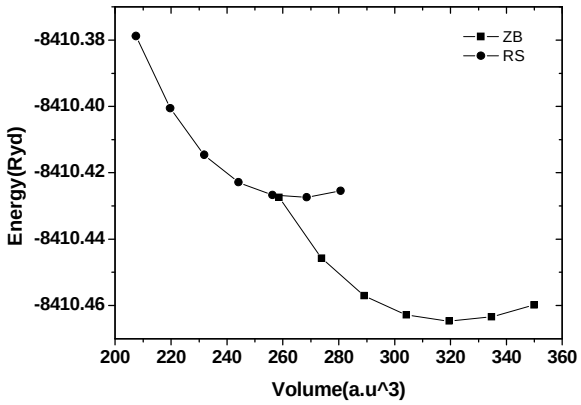

Fig.1. Energy versus volume for ZB and RS structure of GaAs.

Table 1. Lattice Constants, Bulk Modulus And Pressure Derivative Of Bulk Modulus Of ZB And RS Structure Of Gaas At Zero Pressure.

Structure		A_0 [A^0]	B_0 [Gpa]	B_0'
ZB	Present Work	5.74	61.08	4.86
	References	5.65[a], 5.64[b],5.59[c]	60.4[d],74.7[a]	4.8[e],4.71[c],4.56[f]
RS	Present Work	5.39	71.10	4.90
	References	5.32[g],5.31[h],5.28[i]	73.54[c],69.95[i]	4.05[c],4.77[g],4.87[i]

Ref[a] [22], Ref[25][B], Ref[26][C], Ref[27][D], Ref[28][E], Ref[29][F], Ref[23][G], Ref[24][H], Ref[30][I],

3.2 PHASE TRANSITION AND ELASTIC PROPERTIES

The zero temperature pressure induced phase transition between the GaAs-ZB structure and GaAs-RS structure has been determined using the usual condition of equal enthalpies i.e. H = E + PV. The enthalpy as a function of energy is shown in figure 2. The phase transition from ZB to RS structure is found to occur at a pressure of 10.7 GPa which is close to the experimental values [31, 32] and other theoretical results as shown in table 2.

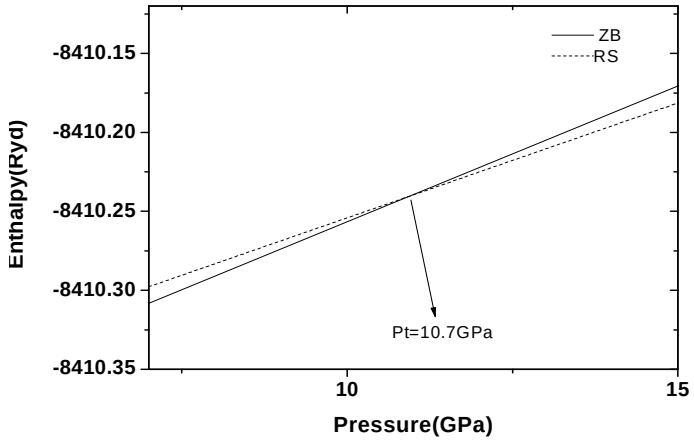

Fig.2. Enthalpy as a function of pressure.

Table 2. Transition pressure from ZB to RS in GaAs.

ZB-RS	Pressure [GPa]
Present work	10.7
Ref [7]	12±1.5
Ref [30]	10.5
Ref [31]	11.8
Ref [32]	12.3

To understand the volume collapse at the transition, the unit cell volume at different pressures (V_P) are normalised by dividing with volume at zero pressure (V_O). The normalised volume (Vp/Vo) of ZB and RS structure of GaAs at different pressure is shown in figure 3. With increase in pressure the relative volume is found to decrease for the two structures. During phase transition, the normalised volume of ZB phase is found to be occurring at 0.876 and for RS phase at 0.734. It is clearly seen that volume collapse occurs at 14.2% indicating that the ZB phase is more compressible than the RS phase.

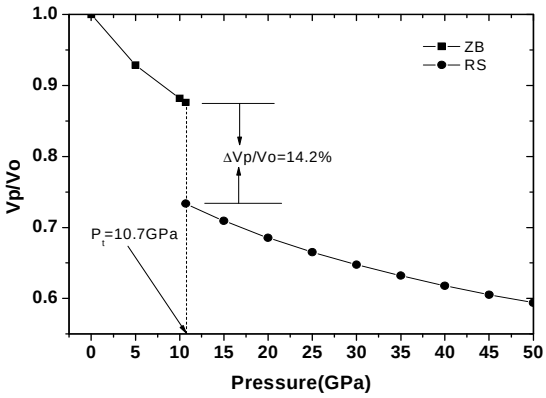

Fig. 3. Phase transition between ZB and RS structure of GaAs at 10.7 GPa pressure.

Since the transition pressure occurs at 10.7 GPa, the three independent observable elastic constants are obtained from 0 to 10 GPa pressure for ZB phase and 12 GPa to 25 GPa pressure for RS phase and is shown in figure 4. Figure 4 shows the linear increase in C_{11}, C_{12}, C_{44} value with increase in pressure for ZB phase. Also these values satisfy the mechanical stability conditions: $(C_{11}+2C_{12}) > 0$; $C_{11}C_{12} > 0$; $C_{44} > 0$; $C_{11} > 0$. In case of RS phase after transition pressure, even though there is a little variation in C_{44} value with linear increase in C_{11}, C_{12} values, and the stability conditions are found to be satisfied.

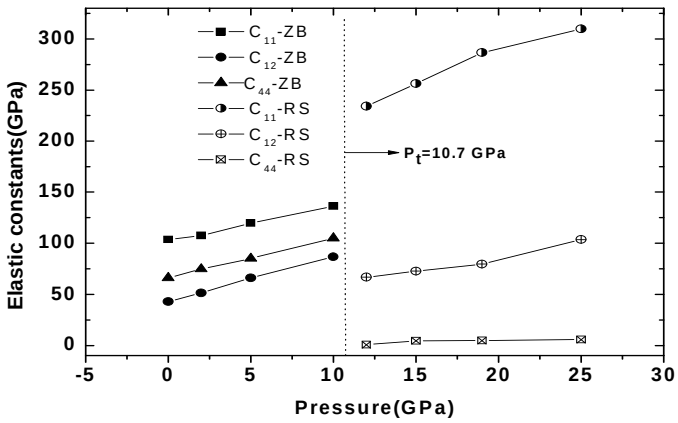

Fig. 4. Elastic constants (C_{11}, C_{12}, C_{44}) as a function of pressure for GaAs-ZB and GaAs-RS structure.

In this light of observations, we are confined our calculation for the elastic parameters on ZB structure up to a higher pressure of 10 GPa. The Zener anisotropic factor (A), Poisson's ratio (υ), Kleinmann parameter (ζ), Youngs modulus (Y), and Debye's temperature (θ_D) are important elastic parameters which determine the mechanical and thermal behaviour of a material.

The Zener anisotropic factor (A), Poisson's ratio (υ), Kleinmann parameter (ζ), Youngs modulus (Y) are calculated using the relation given by Mayer *et. al* [33]. The Zener anisotropy factor gives us an insight on the elastic isotropy of the material. For an elastically isotropic material, A = 1. If A > 1, it is stiffest along <111> plane body diagonals and when A < 1, it is stiffest along <100> cube axes. It is expressed as:

$$A = \frac{2C_{44}}{C_{11} - C_{12}} \tag{3}$$

Kleinmann parameter describes the relative position of the cation and anion sub-lattices and is given by the relation:

$$\zeta = \frac{C_{11} + 8C_{12}}{7C_{11} + 2C_{12}} \tag{4}$$

The Poisson's ratio gives us the stability of crystal against shear and provides a sharp criterion for differentiating the brittleness and ductility in solids and it is calculated using the relation,

$$\upsilon = \frac{1}{2}\left(\frac{B - (2/3)G}{B + (1/3)G}\right) \tag{5}$$

The Young's modulus is determined to measure the stiffness of the solid and is given by:

$$Y = \frac{9GB}{G + 3B} \tag{6}$$

where, $G = \frac{G_V + G_R}{2}$ is the isotropic shear modulus , G_v is the Voigt's shear modulus corresponding to the upper bound of G values, and G_R is the Reuss's shear modulus corresponding to the lower bound of G values. G_v and G_R can be expressed as

$$G_V = \frac{C_{11} - C_{12} + 3C_{44}}{5} \tag{7}$$

$$G_R = \frac{5(C_{11} - C_{12})C_{44}}{4C_{44} + 3(C_{11} - C_{12})} \tag{8}$$

Debye's temperature is an important parameter which determines the thermal characteristics of a material. Debye's temperature also gives us explicit information about lattice vibrations. It is calculated using the average sound velocity (υ_m) given by the common relation [34]

$$\theta_D = \frac{h}{k}\left[\frac{3n}{4\pi}\left(\frac{N_A\rho}{M}\right)\right]^{1/3}\upsilon_m \tag{9}$$

Where *h* is the Plank's constant, *k* is the Boltzmann constant, N_A is the Avogadro's number, *n* is the number of atoms per formula unit, *M* is the molecular mass per formula unit, *ρ* is the density and υ_m is given by [35]

$$\upsilon_m = \left[\frac{1}{3}\left(\frac{2}{\upsilon_t^3} + \frac{1}{\upsilon_l^3}\right)\right]^{-(1/3)} \tag{10}$$

where υ_t and υ_l are the transverse and longitudinal velocities respectively, which are obtained from Navier's equation [36] as

$$\upsilon_t = \sqrt{\frac{3B+4G}{3\rho}} \tag{11}$$

$$\upsilon_l = \sqrt{\frac{G}{\rho}} \tag{12}$$

The calculated elastic parameters for ZB phase with variation of pressure up to 10 GPa are shown in figure 5(a) and figure 5(b). A consistent pattern of linear increase in elastic parameters with increase in pressure can be observed from these figures.

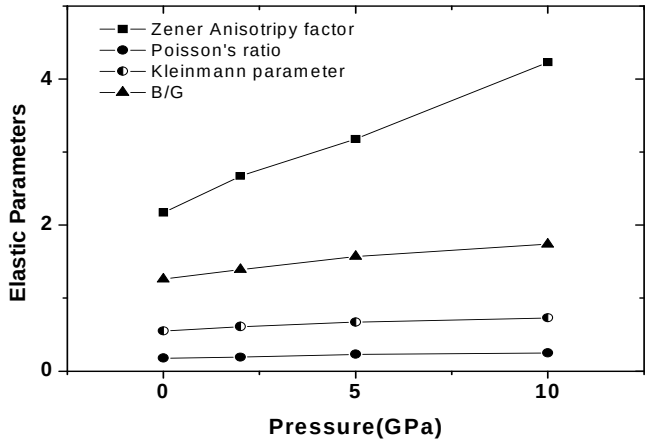

Fig. 5a. Elastic parameters (Zener anisotropic factor, Poisson's ratio, Kleinmann parameter and B/G ratio) as a function of pressure.

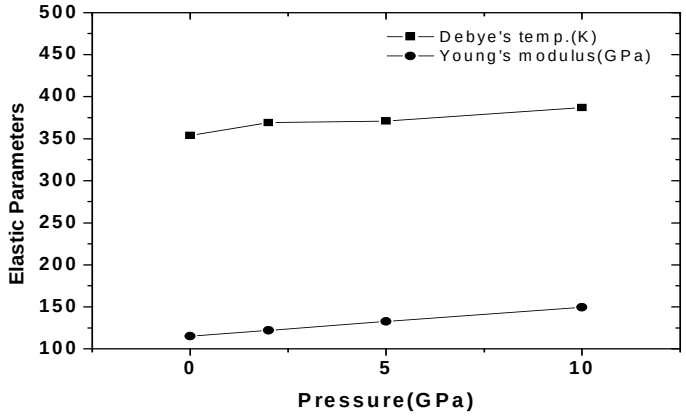

Fig. 5b. Debye's temperature and Young's modulus as a function of pressure.

The Kleimann parameter quantifies internal strain and thus indicates the relative ease of bond bending against the bond stretching. It also implies resistance against bond bending or bond angle distortion. In a system, minimizing bond bending leads to Kleinmann parameter, ζ = 0 and minimizing bond stretching leads to ζ =1. In the present study, the parameter ζ is found to be 0.55 to 0.73 with the variation of pressure, indicating the shrinkage in bond-stretching. Also the value of the Zener anisotropic factor varies from 2.17 to 4.23 with increase in pressure showing the degree of elastic anisotropy. The empirical malleability measure of a material is determined by the value of B/G [37]. A material is found to be brittle if B/G < 1.75 and ductile if B/G > 1.75. B/G value of the present studies varies from 1.26 to 1.74 with increase in pressure and hence it is found that GaAs-ZB structure is brittle and with increase in pressure it tends to become ductile. The larger the value of Young's modulus, the stiffer is the material and since the value of Y varies from 114.96 GPa to 149.456 GPa as pressure

increases, we find that GaAs-ZB pahse becomes more rigid. Poisson's ratio gives us the degree of directionality of the covalent bonds. For covalent materials, υ = 0.1, whereas for ionic materials, υ = 0.25 [38]. Our calculations show that with increase in pressure the value of υ varies from 0.18 to 0.25 showing that with increase in pressure the ionic contribution to inter atomic bonding becomes dominant. Fu *et al* [39] reported that for central force solids the lower and upper limits for υ are 0.25 and 0.5 respectively. Our values also indicates that as pressure increases, inter atomic forces tends to be more central. The value of Debye's temperature is also found to vary from 354K to 387K suggesting that with increasing pressure the Debye's temperature also increases indicating stiffer lattice and better thermal conductivity.

3.3 BAND STRUCTURE AND DENSITY OF STATES

The energy band diagram of GaAs-ZB structure and GaAs-RS structure at zero pressure and zero temperature is calculated using mBJ as it gives us more accurate results closer to the experimental values and the results are given in figure 6(a) and figure 6(b) respectively. From figure 6(a) we observed that the conduction band minimum as well as the valance band maximum is located at the middle of the Brillioun zone, Γ point. From these observations we can conclude that the band gap of GaAs-ZB structure is direct band gap with an energy band gap of 1.3eV while the experimental value is 1.4 eV. Again from figure 6(b) we find that the conduction band crosses the Fermi level and lies within the valance band making the GaAs-RS structure metallic in nature. The reason for the metallic nature in the RS structure is due to broadening of the band with increase in pressure and overlapping of the filled valance band and conduction band.

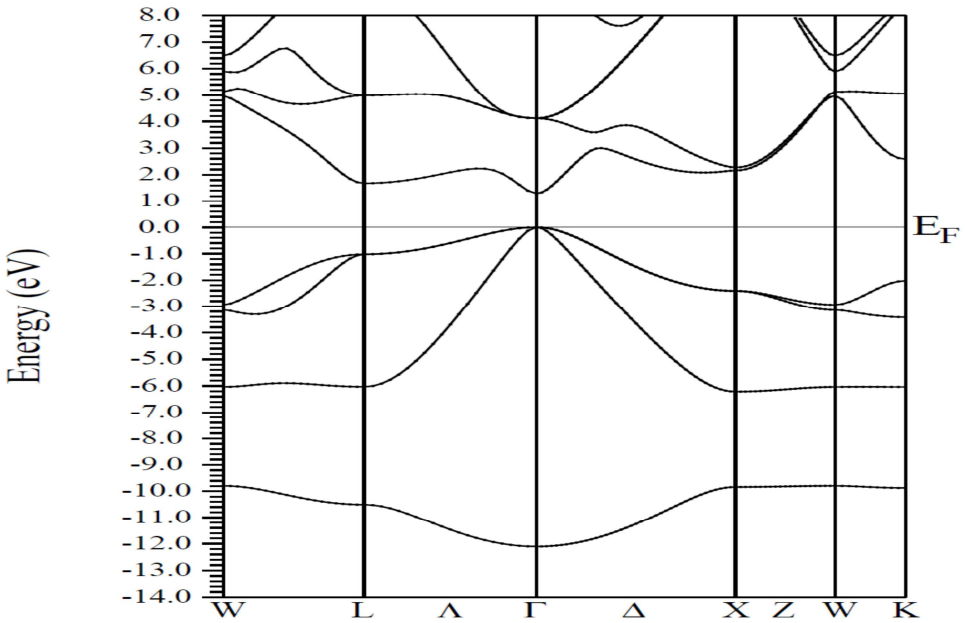

Fig. 6a. Band structure of GaAS-ZB structure.

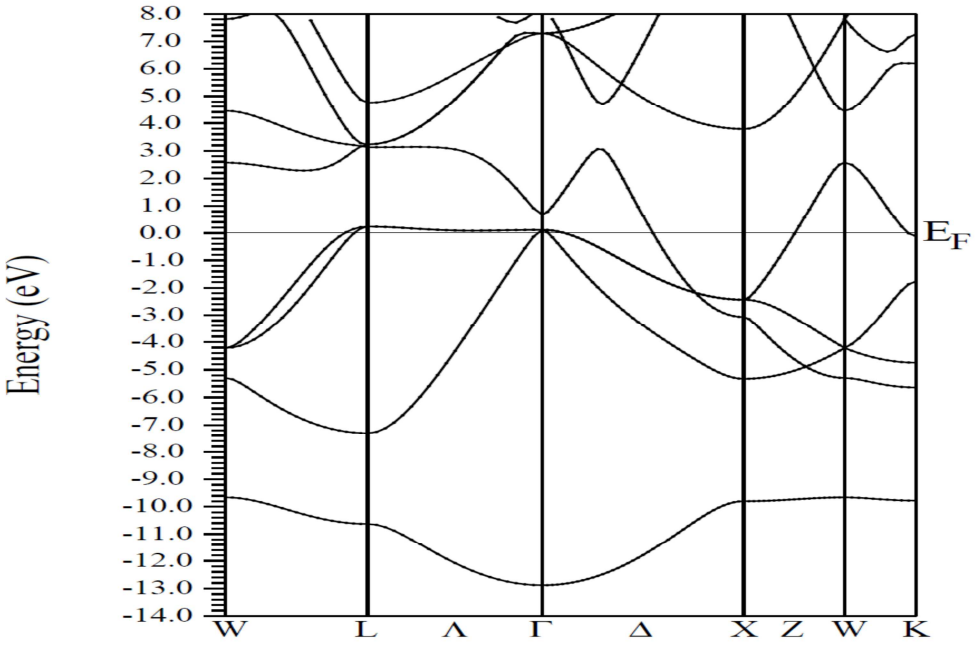

Fig. 6b. Band structure of GaAs-RS structure.

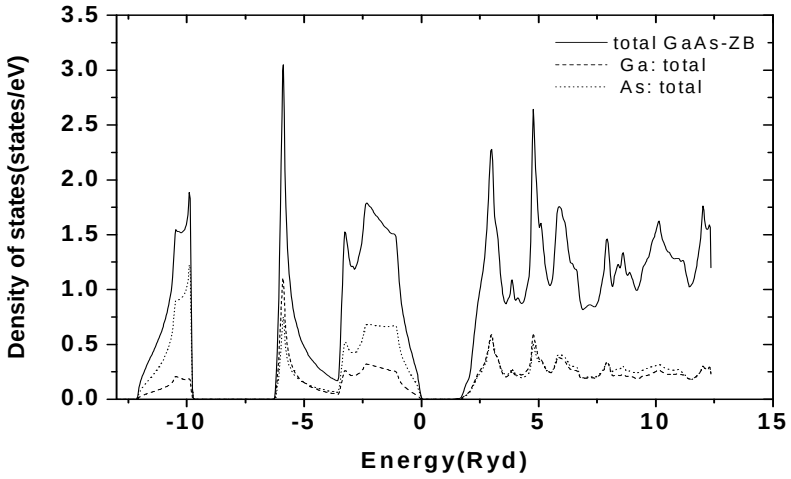

Fig. 7a. Total DOS of GaAs -ZB structure.

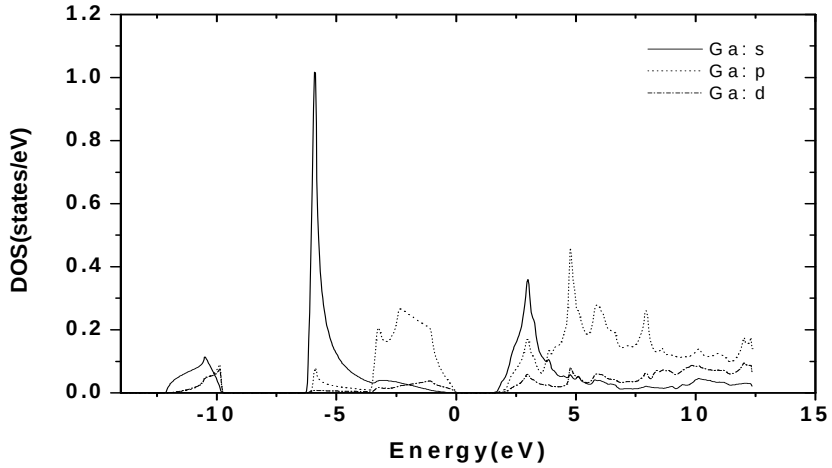

Fig. 7b. Partial DOS of Ga atom in GaAs-ZB structure.

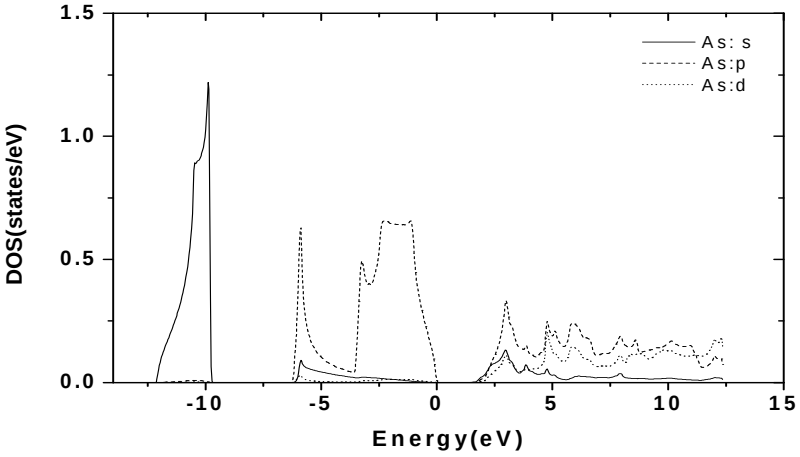

Fig. 7c . Partial density of As atom in GaAs-ZB structure.

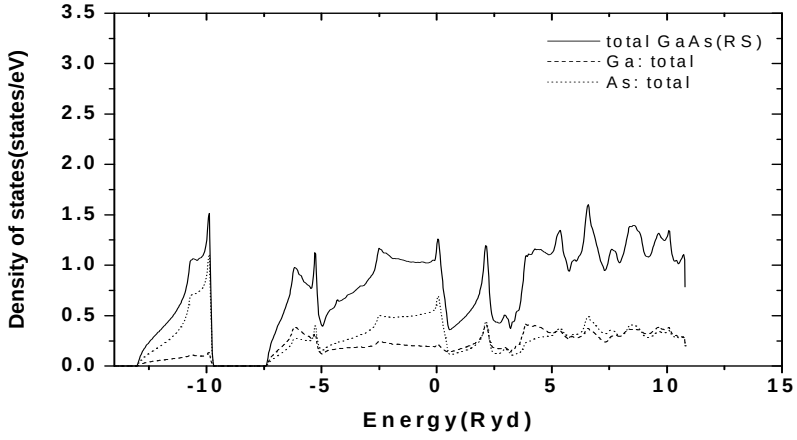

Fig. 8a. Total DOS of GaAs-RS structure.

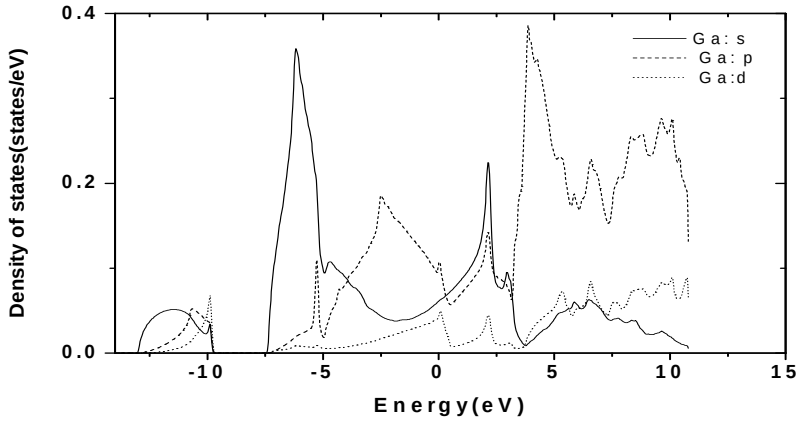

Fig. 8b. Partial DOS of Ga atom in GaAs-RS structure.

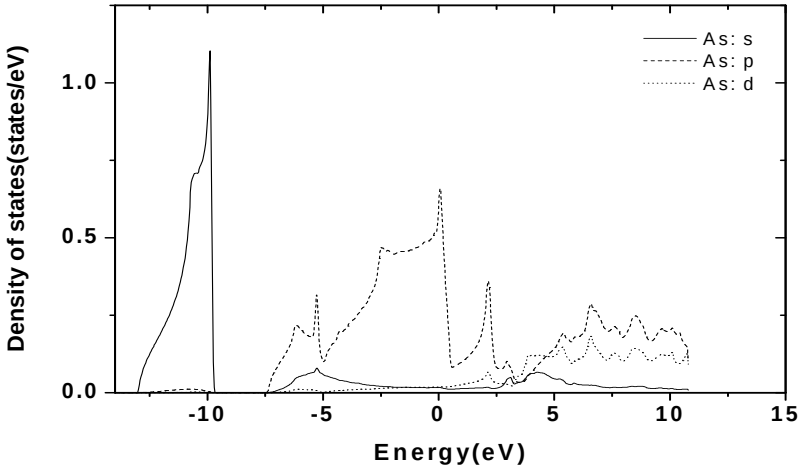

Fig. 8c. Partial DOS of As atom in GaAs-RS structure.

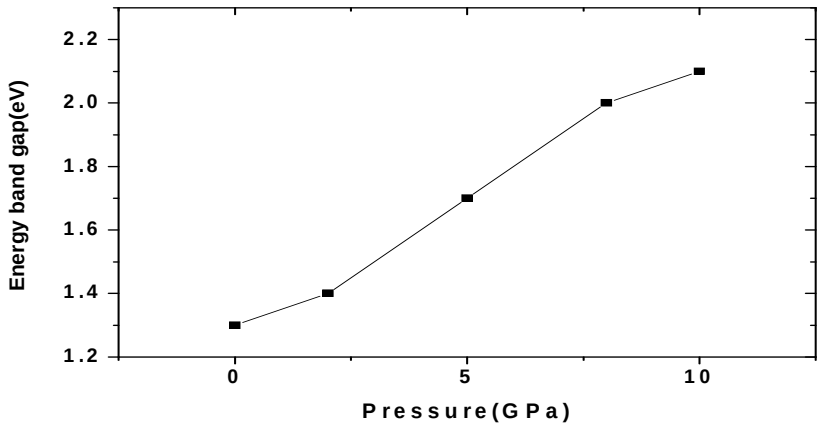

Fig. 9. Variation of energy band gap with pressure in GaAs ZB structure.

Figure 7(a,b,c) shows the total and partial DOS of GaAs in ZB phase and figure 8(a,b,c) shows the same in RS phase. From the partial DOS as shown in figure 7(b) and figure 7(c), one can observe that the lowest band appears in energy band diagram of ZB phase is mainly contributed from s-non metal (As atom) orbital and the valance band is mainly contributed by the s-metal (Ga atom) orbital and p-non metal (As atom) orbital with little contribution from the p-metal (Ga atom) orbital. The contribution of the s, p orbital of metal and non-metal in DOS in the lowest and valence band is found to decrease with increase in pressure. Similar behaviour is observed in partial DOS of GaAs-RS structure in figure 8(b) and figure 8(c) as the lowest band is mainly contributed by the s-non metal orbital while the valence band is mainly contributed by the p-non metal orbital and s- metal orbital with little contribution from the p-metal and d-metal orbital. An important observation in the energy band diagram of GaAs-RS structure is the crossing of the conduction band towards valence band and hence results in metalic nature. It is interesting to see the variation of band gap with pressure for the direct band gap in GaAs-ZB phase. These variations of the energy band gap with increase in pressure is shown in figure 9 and observe that with increase in pressure the band gap also increases. The resaon is that the energy eigenvalues corresponding to s, p, and d orbital's lies in the higher region with increasing pressure.

4 CONCLUSION

In this paper we present a detailed study of pressure induced structural transformation, elastic properties and electronic structure of GaAs. The phase transition from ZB to RS structure is obtained at 10.7 GPa and ZB structure is found to be more stable. During the phase transition, the relative volume of ZB structure occurs at 0.876 and the RS structure at 0.734 and volume collapses at 14.2% indicating that ZB structure of GaAs is more compressible as compared to RS structure. The calculated equilibrium lattice parameter, bulk modulus, pressure derivative of the bulk modulus and elastic constants are found to be in good agreement with the other experimental and theoretical studies. The elastic constants satisfy the mechanical stability condition from 0 to 10 GPa pressure for ZB structure and 12 GPa to 25 Gpa pressure for RS structure. The elastic parameters for the stable GaAs-ZB phase such as Zener anisotropic factor, Kleinmann parameter, Poisson's ratio and Youngs modulus show a systematic variation with increase in pressure up to 10 GPa pressure before transition. The GaAs-ZB structure is found to be direct band gap semiconductor of 1.3 eV and the band gap increases with increase in pressure.

REFERENCES

[1] A. L. Robinson, "GaAs readied for high speed microcircuit", *Science*, vol. 219, pp. 275-277, 1983.

[2] R. J. Harrison, "Gallium arsenide: state of the art reviews", *Occup. Med*., vol. 1, pp. 49-58, 1986.

[3] F. W. Smith, H. Q. Le, V. Diadiuk, M. A. Hollis, A. R. Calawa, S. Gupta, M. Frankel, D. R. Dykaar, G. A. Mourou and T. Y. Hsiang, "Picosecond GaAs based photoconductive optoelectronic detectors", *Appl. Phys. Lett*., vol. 54, no. 10, pp. 890-892, 1989.

[4] D. K. W. Lam and R. Macdonald, "GaAs optoelectronic mixer operation at 4.5 GHz", *IEEE Trans. Electron Devices*", vol. 31, pp. 1766-1768, 1984.

[5] E. Wachowicz and A. Kiejna, "Bulk and surface properties of hexagonal-close-packed Be and Mg", *J. Phys. Condens. Matter*., vol. 13, pp. 10767-10776, 2001.

[6] S. Froyen and M. L. Cohen, "Structural properties of III-V zinc-blende semiconductors under pressure", *Phys. Rev. B*, vol. 28, pp. 3258-3265, 1983.

[7] J. M. Besson, J. P. Itie, A. Polian, G. Weil, J. L. Mansot and J. Gonzales, "High pressure phase transition and phase diagram of gallium arsenide", *Phy. Rev. B*, vol. 44, pp. 4214-4234, 1991.

[8] S. T. Weir, Y. K. Vohra, C. A. Vanderborgh and L. A. Rouff, " Structural phase transitions in GaAs to 108 GPa", *Phys. Rev. B*, vol. 39, pp. 1280-1285, 1989.

[9] J. R. Chelikowsky, "High-pressure phase transitions in diamond and zinc-blende semiconductors", *Phys. Rev. B*, vol. 35, pp. 1174-1180, 1987.

[10] Kh. Kabita, M. Jameson, B. Indrajit Sharma, R. K. Thapa Singh, R. K. Brojen, "First principle calculation of pressure induced phase transition and band structure of Gallium phosphide", *Iraqi J Appl. Phys*., vol. 9, pp. 17-20, 2014.

[11] M. Durandurdu and D. A. Darbold, "Ab initio simulation of high pressure phases of GaAs", *Phys. Rev. B*, vol. 66, pp. 045209(1) – 045209(5), 2002.

[12] A. Mujica and R. J. Needs, "The Cmcm structure as a stable phase of binary compounds : application to GaAs-II", *J. Phys. Condens. Matter*., vol. 8, pp. L237 –L243, 1996.

[13] A. D. Becke and E. R. Johnson, "A simple effective potential for exchange", *J. Chem. Phys*., vol. 124, pp. 221101-221104, 2006.
[14] E. Wimmer, H. Krakauer, M. Weinert and A. J. Freeman, "Full-potential self-consistent linearized-augmented-plane-wave method for calculating the electronic structure of molecules and surfaces: O_2 molecule", *Phys.Rev. B*, vol. 24, pp. 864 -875, 1981.
[15] P. Hohenberg and W. Kohn, "Inhomogeneous electron gas", *Phy. Rev. B*, vol. 136, no. 3, pp. B864-B871, 1964.
[16] W. Kohn and L. J. Sham, "Self-Consistent Equations Including Exchange and Correlation Effects", *Phys. Rev*., vol. 140, no. 4A, pp. 1133-1138, 1965.
[17] S. Cottenier, *Density Functional Theory and the family of (L) APW-methods: a step-by-step introduction*, Belgium, ISBN 90-807215-1-4, 2002.
[18] J. P. Perdew, K. Burke and M. Ernzerhof, "Generalized Gradient Approximation Made simple", *Phys. Rev. Lett*., vol. 77, pp. 3865-3868, 1996.
[19] P. Blaha, K. Schwarz, G. K. H. Madsen, D. Kvasnicka and J. Luitz, *Wien2k. Techn. Universitat*, Wien, Austria, ISBN 3-9501031-1-2, 2001.
[20] O. K. Andersen, "Linear methods in band theory", *Phys. Rev. B*, vol. 12, pp. 3060-3083, 1975.
[21] F. Birch, "Finite Elastic Strain of Cubic Crystals", *Phys. Rev*., vol. 71, pp. 809-824, 1947.
[22] O. Madelung, M. Schulz, H. Weiss (Eds.), *Physics of II–VI and I–VII Compounds*, Landolt-Börnstein, Vol. 17b, Springer, Berlin, 1982.
[23] K. Albe, L. Nordlund, J. Nord and A. Korunen, "Modelling of compound semiconductors: Analytical bond-order potential for Ga, As and GaAs", *Phys. Rev. B*, vol. 66, pp. 035205(1)-035205(14), 2002.
[24] L. Y. Lu, X. R. Chen, B. R. Yu and Q. Q. Gou, "First-principles calculations for transition phase and thermodynamic properties of GaAs", *Chin. Phys*., vol. 15, no. 4, pp. 802-806, 2006.
[25] Cui Hong-Ling, Chen Xiang-Rong, J. I. Guang- Fu, "Structures and Phase Transition of GaAs under pressure", *Chin. Phys. Lett*., vol. 25, no. 6, pp. 2169-2172, 2008.
[26] A. Mujica, R. J. Needs and A. Munoz, "First-principles pseudopotential study of the phase stability of the III-V semiconductors GaAs and A1As" , *Phys. Rev. B*, vol. 52, no. 12, pp. 8881-8892, 1995.
[27] S. Lee, J. Kang and M. Kang, "Structural properties of semiconductors in the generalized gradient approximation", *Journal of the Korean Physical Society*, vol. 31, no. 5, pp. 811-814, 1997.
[28] R. Smith, "A semi-empirical many-body interatomic potential for modelling dynamical processes in gallium arsenide", *Nuclear Inst. and Methods in Physics Research B,* vol. 67, no. 1-4, pp. 335-339, 1992.
[29] D. Dunslan, *Properties of GaAs*, edited by M. R. Brozel and. G. E. Stillmann, Inspec, London, 1996.
[30] D. C. Gupta and Subhra Kulshrestha, "Pressure induced phase transitions and electronic structure of GaAs", *J. Phys. Condens. Matter*, vol. 20, pp. 255204(1)- 225204(7), 2008.
[31] A. Gracia and M. L. Cohen, "Effect of Ga 3*d* states on the structural properties of GaAs and GaP", *Phys. Rev. B*, vol. 47, pp. 6751-6754, 1993.
[32] J. Cai, N. Chen and H. Wang, "Atomistic study of the pressure-induced phase-transition mechanism in GaAs by Möbius inversion potentials", *J. Phys. Chem. Solids*, vol. 68, no. 3, pp. 445-457, 2007.
[33] B. Mayer, H. Anton, E. Bott, M. Methfessel, J. Sticht, J. Harris, P. C. Schmidt, "Ab-initio calculation of the elastic constants and thermal expansion coefficients of Laves phases", *Intermetallics*, vol. 11, no. 1, pp. 23-32, 2003.
[34] L. Johnston, G. Keeler, R. Rollins and S. Spicklemire, *Solid State Physics Simulations, The Consortium for Upper-Level Physics Software*, New York, John Wiley, 1996.
[35] O. L. Anderson, "A simplified method for calculating the Debye temperature from elastic constants", *J. Phys. Chem. Solids*, vol. 24, pp. 909-917, 1963.
[36] E. Schreiber, O. L. Anderson and N. Soga, *Elastic constants and their measurements*, New York, McGraw-Hill, 1973.
[37] S. F. Pugh, "Relations between the elastic moduli and the plastic properties of polycrystalline pure metals", *Philosophical Magazine*, vol. 45, pp. 823-843, 1954.
[38] V. V. Bannikov, I. R. Shein and A. L. Ivanovskii, "Electronic structure, chemical bonding and elastic properties of the first thorium containing nitride perovskite $TaThN_3$", *Phys Status Solidi Rapid Res. Lett*., vol. 3, pp. 89-91, 2007.
[39] H. Fu, D. Li, F. Peng , T. Gao, X. Cheng, "Ab initio calculations of elastic constants and thermodynamic properties of NiAl under high pressures", *Computational Material Science*, vol. 44, pp. 774-778, 2008.

AMERICAN SCIENTIFIC PUBLISHERS

Advanced Science, Engineering and Medicine
Vol. 6, pp. 354-358, 2014
(www.aspbs.com/asem)

ARTICLE

Density Functional Theory Study of Electronic Structure, Elastic Properties and Phase Transition of Gallium Phosphide (GaP)

Kh. Kabita[1], Jameson Maibam[1], B. Indrajit Sharma[1,*], R. K. Thapa[2], and R. K. Brojen Singh[3]

[1]*Department of Physics, Assam University, Silchar 788011, Assam, India*
[2]*Department of Physics, Mizoram University, Aizawl 796001, Mizoram, India*
[3]*School of Computational and Integrative Sciences, JNU, New Delhi 110067, India*

Using the first principle full-potential linearized augmented plane wave (FP-LAPW) method the electronic structure, elastic properties of GaP in zinc-blende (ZB) structure and its phase transition to rock-salt (RS) structure under different pressures are studied. The phase transition from ZB to RS structure is found to occur at a pressure of 21.9 GPa. It exhibits a 14.11% volume decrease of ZB to RS structure at the transition pressure. The energy band diagram of GaP ZB structure shows an indirect band gap of 2.33 eV. The partial density of states (DOS) shows the main contributions of *s*, *p*, and *p*, *d* atomic orbital states of non-metal *P* and metal Ga atom in the band diagram.

KEYWORDS: ELASTIC PROPERTIES; ELECTRONIC STRUCTURE; GALLIUM PHOSPHIDE (GAP); PHASE TRANSITION.

1. INTRODUCTION

Gallium phosphide is an important group III–V binary compound semiconductor. In quantum and optoelectronic devices, it is often used as a substrate.[1] It is a popular semiconductor material and is considered to be of wide-band gap and hence making it a good candidate for room-temperature device applications such as top junction solar cells in multi junction solar cell system. GaP is used as a substrate in low-cost red, orange, and green light-emitting diodes (LEDs) with low to medium brightness since the 1960s. It has a relatively short life at higher current and its lifetime is sensitive to temperature. Because of its many uses, the investigation of its physical properties has become of great interest. In 1983, Froyen and Cohen calculated the electronic band structure of GaP using the psedopotential total energy approach.[2] Many other groups have also calculated the electronic structure of GaP using different methods like the semi empirical pseudopotential, the tight binding method and full potential method.[3–6] Although there are more theoretical and experimental papers on GaP, to the best of our knowledge, there are not much paper on the study of electronic structure, elastic properties and phase transition. In this present work we have investigated the electronic structure, elastic properties as well as its phase transition from ZB to RS structure of GaP using the FP-LAPW method based on density functional theory (DFT). In this method the exchange-correlation potential was calculated with Generalised Gradient approximation (GGA) using the Perdew–Burke–Ernzerhof (PBE-GGA) scheme.[7] The paper is organised into the following sections, in Section 2 we briefly describe the computational technique used in the calculation of the electronic structure of GaP. In Section 3 we compare our results with the previous theoretical and experimental results. The conclusion of our work is given in Section 4.

*Author to whom correspondence should be addressed.
Email: indraofficial@rediffmail.com
Received: 9 September 2013
Accepted: 29 September 2013

2. COMPUTATIONAL METHOD

Within the formalism of DFT,[8–10] the total energy is expressed as a functional of density of the electron system, ρ as

$$E[\rho] = T_0[\rho] + V_H[\rho] + V_{xc}[\rho] + V_{ext}[\rho]$$

where, $T_0[\rho]$ is the kinetic energy of a non-interacting electron system, $V_H[\rho]$ and $V_{XC}[\rho]$ are the Hartree and exchange-correlation contributions to the energy and $V_{ext}[\rho]$ is the energy due to the external potential of the system. Thus the corresponding Hamiltonian called the Kohn-Sham Hamiltonian is

$$\hat{H}_{KS} = \hat{T}_0 + \hat{V}_H + \hat{V}_{XC} + \hat{V}_{ext}$$
$$= -\frac{\hbar^2}{2m_e}\vec{\nabla}_i^2 + \frac{e^2}{4\pi\varepsilon_0}\int \frac{\rho(\vec{r}')}{|\vec{r}-\vec{r}'|}d\vec{r}' + V_{XC} + V_{ext}$$

The exact density of N electron system can be expressed in ground state by, $\rho(\vec{r}) = \sum_{i=1}^{N} \Phi_i(\vec{r}) * \Phi_i(\vec{r})$ where the single particle wave functions $\Phi_i(r)$ are the N lowest energy solutions of the Kohn Sham equation: $\hat{H}_{ks}\Phi_i = \epsilon_i\Phi_i$ of the N electron system. This equation can be solved self consistently in an iterative process. DFT calculation is performed using the first principle FP-LAPW method as well as GGA as implemented in WIEN2K.[10–12] This method is used as it is one of the most accurate methods in electronic structure calculation of crystals. In this method, the lattice is divided into non-overlapping spheres (called atomic or muffin tin sphere) surrounding each atomic sites and an interstitial region.[13] Inside the muffin tin (MT) region, the potential is a product of radial function and spherical harmonics and expanded up to order $l = 10$. For the interstitial regions that are outside the muffin tin spheres, the potentials are expanded in plane waves. 8000 k-points are used as we find that above 8000 k-points the energy remains same for the integration part which reduces to 256 irreducible k-points inside the Brillion zone. Convergence is obtained at $R_{MT}K_{max} = 9.0$ where R_{MT} is the atomic sphere radii and K_{max} gives the plane wave cut-off.

3. RESULTS AND DISCUSSION

3.1. Structural Properties

The first important step in calculating the total energy of the system is to generate the optimized structure. So, the number of optimized k points used in the Brillouin zone is essential. Figure 1(a) shows the variation of k-points with energy per unit cell structure of GaP. One can see a lot of energy variations at different k values. It is observed that at around 7500 k-points onwards there is no much variation of energy. Thus taking 8000 k-points is well good enough for further calculations. In literature, there are two phases of GaP such as ZB and RS and shows phase transition under pressure.[14] Figure 1(b) shows the two curves of total energy as a function of primitive cell volume of ZB and RS structures of GaP to make a sense of more stable structure. A series of different lattice constants are used to calculate the total energy and the corresponding unit cell volume. From the figure one can see that the ZB structure of GaP is more stable in comparison to the RS structure which is in agreement with the other's previous work.[1, 14] The two curves are fitted with Birch-Murnaghan equation of state.[15] The obtained equilibrium lattice parameter (a_0), bulk modulus (B_0), and pressure derivative of the bulk modulus (B') are listed in Table I. These values are compared with the previous theoretical and experimental results as published by other groups.[14–21] It shows that our results are reasonably in agreement with the previous reported data.

3.2. Phase Transition and Elastic Properties

The phase transition pressure at absolute temperature is found out from the equal enthalpy condition i.e., the pressure at which the enthalpies of both ZB and RS structure

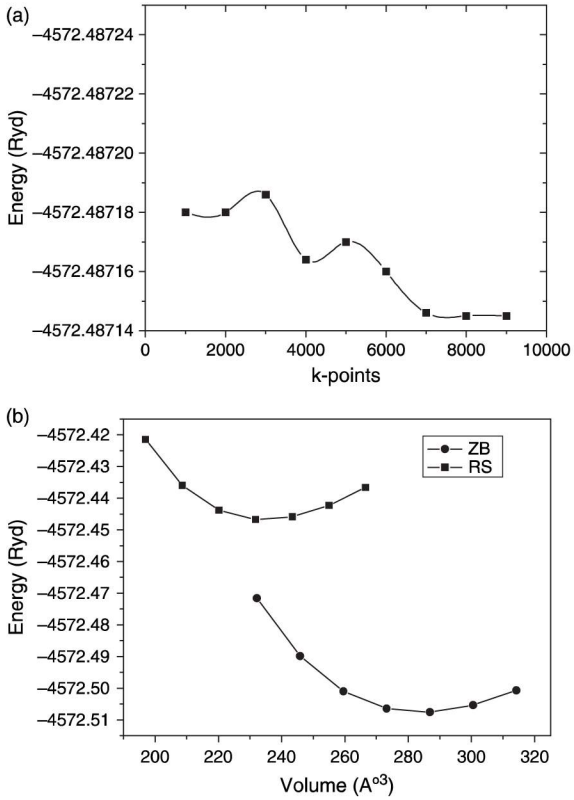

Fig. 1. (a) Total energy per unit cell of GaP verses number of k-points. (b) Total energy verses unit cell volume of GaP-ZB and RS structures.

is same. In Figure 2 the enthalpy as a function of pressure is shown. It is observed that the phase transition from the ZB to RS structure occurred at a pressure of 21.9 GPa which is in good agreement with the other's experimental and theoretical results as shown in Table II. Figure 3 shows the variation of normalised volume (V_p/V_o) with respect to equilibrium volume (V_o) with pressure of both the phases. It is observed that the normalised volumes of both the phases are found to decrease with increase in pressure. During the phase transition, V_p/V_o of ZB phase is found to occur at 0.8293 and of the RS phase at 0.6882. It clearly shows the volume collapses at 14.11%

Table I. Equilibrium lattice constant (a_0), bulk modulus (B_0), pressure derivative (B_0') of GaP ZB and RS structures.

Structure	a_0 (Å)	B_0 (GPa)	B_0'
ZB			
Present work	5.523	77.708	4.347
References	5.512;[a] 5.411;[b] 5.50;[c] 5.386[d]	76.0;[a] 90.0;[b] 77.21;[c] 86.8[d]	4.59;[a] 4.50;[b] 4.88;[c] 4.00[d]
RS			
Present work	5.181	88.342	4.814
References	5.165;[e] 5.160[f]	87.3;[e] 87.59[f]	3.78;[e] 4.54[f]

Notes: [a]Ref. [16]; [b]Ref. [17]; [c]Ref. [20]; [d]Ref. [19]; [e]Ref. [14]; [f]Ref. [1].

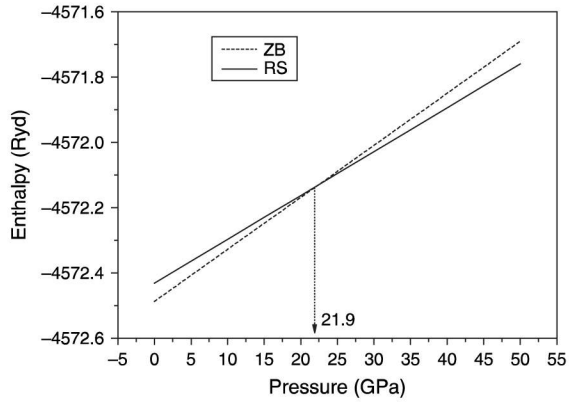

Fig. 2. Enthalpy per unit cell of GaP-ZB and RS structures as a function of pressure.

Table II. Transition pressure for ZB to RS structure of GaP under pressure.

ZB–RS	Pressure (GPa)
Present work	21.9
Ref. [14]	21.9
Ref. [24]	24 ± 0.3
Ref. [25]	22.0
Ref. [26]	21.5 ± 0.8

indicating that RS phase of GaP is more compressible as compare to ZB phase. Hence the elastic constants C_{11}, C_{12}, C_{44} of GaP ZB structure are calculated for the lattice volume corresponding to the pressure ranging from 0 GPa to 21.9 GPa using the stress–strain method.[22] For computing the elastic constants C_{ij}, the volume conserving technique is used.[23] The results are listed in Table III.

The results clearly show the mechanical stability conditions: $(C_{11}+2C_{12}) > 0$; $C_{11}C_{12} > 0$; $C_{44} > 0$ are satisfied and hence the stable GaP ZB structure can exists up to higher pressure of 22.3 GaP. The other elastic parameters

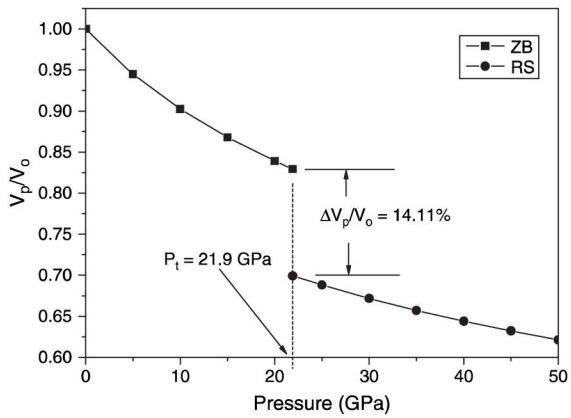

Fig. 3. Normalised volume under pressure verses pressure of GaP-ZB and RS structures.

Table III. Calculated elastic constants C_{11}, C_{12}, C_{44} of GaP ZB structure.

Structure:	P (GPa)	C_{11} (GPa)	C_{12} (GPa)	C_{44} (GPa)
Zinc-blende	0	124.1; 123.5;[e] 137.5[g]	54.9; 50.9;[e] 59.4[g]	84.1; 70.9;[e] 72.2[g]
	5	147.864	72.587	100.640
	10	171.107	90.325	117.443
	15	183.915	112.007	130.246
	20	201.757	130.358	144.158
	22.3	206.420	139.969	150.128

Notes: [e]Ref. [14]; [g]Ref. [27].

Table IV. Calculated values of density ρ, Zener anisotropy factor A, Poisson's ratio υ, Kleinman parameter ζ, Youngs modulus Y and Deby's temperature Θ_D of GaP ZB structure.

ρ (kg/m^3)	A	υ	ζ	Y (GPa)	G (GPa)	Θ_D (K)
3969.3279	2.43	0.197	0.567	141.069	58.9017	458.82

such as Zener Anisotropy factor A, Poisson's ratio υ, and Young's modulus Y are calculated at zero pressure lattice volume by using the relations given by Mayer et al.[28,29]

$$A = 2C_{44}/(C_{11}-C_{12})$$

$$\upsilon = (1/2)[B-(2/3)G]/[B+(1/3)G]$$

$$Y = 9GB/(G+3B)$$

where $G = (G_V + G_R)/2$ is the isotropic shear modulus,

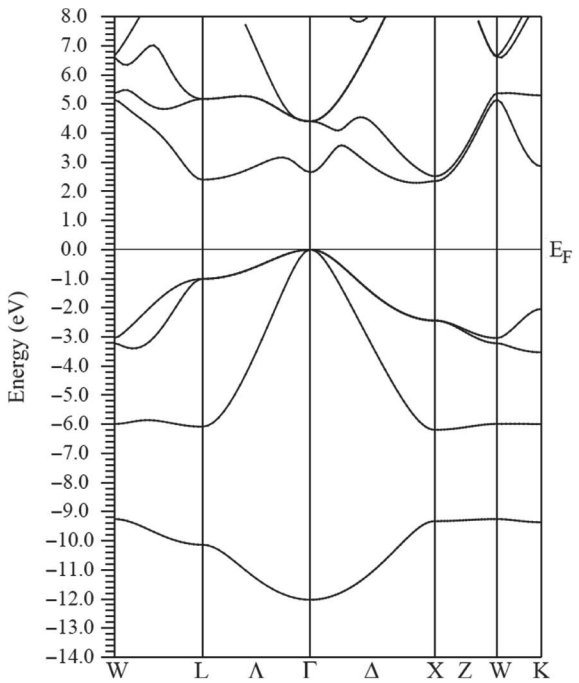

Fig. 4. Energy band diagram of GaP ZB structure.

G_v is the Voigt's shear modulus and G_R is the Reuss's shear modulus and can be expressed as:

$$G_V = (C_{11} + C_{12} + 3C_{44})/5 \text{ and}$$
$$5/G_R = 4/(C_{11} - C_{12}) + 3/C_{44}$$

It is well understood that the relative positions of the cation and anion sub-lattices under volume conserving strain distortions, for which the positions are fixed by symmetry is described by the kleinman parameter ζ given by:

$$\zeta = (C_{11} + 8C_{12})/(7C_{11} + 2C_{12})$$

Also, from the bulk modulus and the isotropic shear modulus, the longitudinal elastic wave velocity (v_l) and the transverse elastic wave velocity (v_t) are calculated as follows:

$$v_l = [(3B + 4G)/3\rho]^{1/2} \text{ and } v_t = (G/\rho)^{1/2}$$

Now, the average sound velocity (v_m) is given by

$$v_m = [(1/3)\{2/v_t^3 + 1/v_l^3\}]^{-1/3}$$

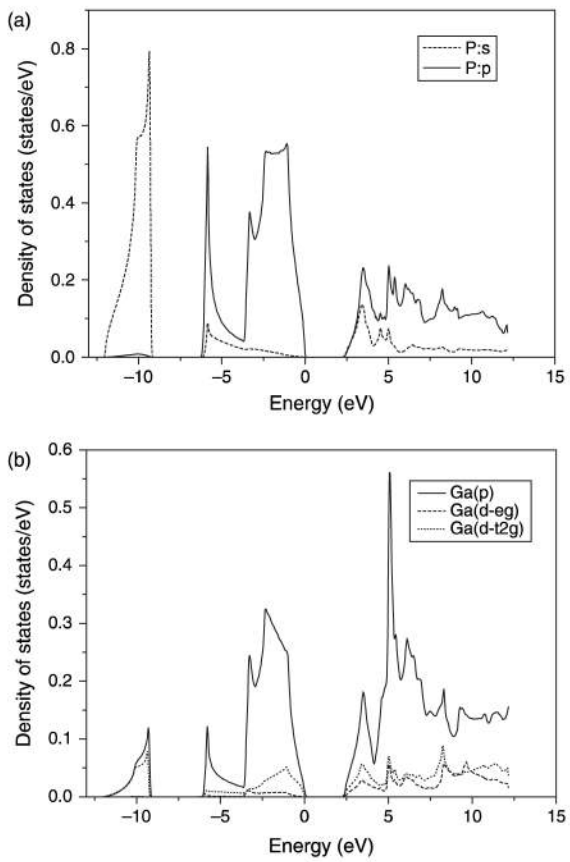

Fig. 5. (a) Partial DOS of P (s, p) in GaP ZB structure. (b) Partial DOS of Ga (p, d) in GaP ZB structure.

Using the average sound velocity v_m, the Debye's temperature θ_D is calculated from the elastic constants data as given by:

$$\theta_D = (h/k)[(3n\rho N_A)/(4\pi M)]^{1/3} V_m$$

where h is the Plank's constant, k is the Boltzmans constant, N_A is the Avogadro's number, n is the number of atoms per formula unit, M is the molecular mass per formula unit, ρ ($= M/V$) is the density. Thus computed elastic parameters are listed in Table IV.

3.3. Band Structure and Density of States

Figure 4 shows the band diagram of GaP ZB structure. In this band diagram, one can observe that the valance band maximum occurs at the Γ point and the minimum conduction band occurs at L point. Hence GaP is found to be an indirect band gap material with the band gap of 2.33 eV which is in quite agreement with the theoretical and experimental values of 2.09 eV–2.74 eV as reported by other groups.[5, 20, 21, 30] Figures 5(a) and (b) shows the partial DOS of the non metal P atom and metal Ga atom in GaP respectively. From the partial DOS as shown in Figures 5(a) and (b), one can observe that the lowest band appears in energy band diagram (in Fig. 4) is mainly contributed from 2s-non metal (P atom). This band is distributed in a width of approximately 3 eV. Above this band, there lies valence band of width of approximately 6 eV. This valence band is contributed together from the 2p non-metal orbital, and 2s, 2p metal orbital with a little contribution from d metal orbital.

4. CONCLUSION

In this paper we present a detailed study of electronic structure and elastic properties of GaP along with its phase transition from ZB to RS structure under pressure using the full-potential linearized augmented plane wave method. The exchange correlation potential was calculated within the generalized gradient approximation using the Perdew–Burke–Ernzerhof (PBE-GGA) scheme. The phase transition from ZB to RS structure is found to occur at 21.9 GPa and GaP ZB phase is more stable. At the transition, the volume collapses at 14.11% indicating the RS phase of GaP is more compressible as compare to ZB phase. The band diagram of GaP in ZB structure exhibits an indirect band gap of 2.33 eV. The partial DOS shows the main contributions from s, p orbital of non metal P atom and p, d orbital of metal Ga atom in the band diagram of GaP. The calculated equilibrium lattice parameter, bulk modulus and pressure derivative of the bulk modulus are found to be in good agreement with the other experimental and theoretical studies. Also using the stress–strain method, the elastic parameters such as Zener anisotropy factor, Poisson's ratio, Kleinman parameter, Young's modulus and Deby's temperature Θ_D are found to be 2.43, 0.197, 0.567, 141.0693 GPa and 458.82 K respectively.

References and Notes

1. L. Sukit, P. Reunchan, A. Janotti, and G. V. W. Chris, *Phys. Rev. B* 77, 195209 **(2008)**.
2. S. Froyen and M. R. Cohen, *Phys. Rev. B* 28, 3258 **(1983)**.
3. Y. Al-Douri and H. Aourag, *Physica B* 324, 173 **(2002)**.
4. Y. Al-Douri, S. Mecabih, N. Benosman, and H. Aourag, *Physica B* 325, 362 **(2003)**.
5. M. Rabah, Y. Al-Douri, M. Sehil, and D. Rached, *Mater. Chem. Phys.* 80, 34 **(2003)**.
6. A. H. Reshak, *Eur. Phys. J. B* 47, 503 **(2005)**.
7. J. P. Perdew, S. Burke, and M. Ernzerhof, *Phys. Rev. Lett.* 77, 3865 **(1996)**.
8. P. Hohenberg and W. Kohn, *Phys. Rev. B* 136, 64 **(1964)**.
9. W. Kohn and L. J. Sham, *Phys. Rev. A* 140, 1133 **(1965)**.
10. S. Cottenier, Density functional theory and the family of (L) APW-methods: A step-by-step introduction (Belgium, Insti-tuut voor Kern-en Stralingsfysica, K. U. Leuven ISBN 90-807215-1-4) **(2002)**.
11. E. Wimmer, H. Krakauer, M. Weinert, and A. J. Freeman, *Phys. Rev. B* 24, 864 **(1981)**.
12. P. Blaha, K. Schwarz, G. K. H. Madsen, D. Kvasnicka, and J. Luitz, Wien2k.Techn.Universitat, Wien, Austria, ISBN 3-9501031-1-2 **(2001)**.
13. O. K. Andersen, *Phys. Rev. B* 12, 3060 **(1975)**.
14. L. Liu, J. J. Wei , X. Y. An, X. M. Wang, H. N. Liu, W. D. Wu, *Chin. Phys. B* 20, 106201 **(2011)**.
15. F. Birch, *Phys. Rev.* 71, 809 **(1947)**.
16. R. Rashid Ahmed, F. Aleem, S. J. Hashemifar, and H. Akbarzadeh, *Physicab. Conden. Matter.* 403, 1876 **(2008)**.
17. A. Mujica, R.J. Needs, *Phys. Rev. B* 55, 9659 **(1997)**.
18. B. Bouhafs, H. Aourag, and M. J. Cartier, *Phys: Conden Matter.* 12, 5655 **(2000)**.
19. S. B. Zhang and M. L. Cohen, *Phys. Rev. B* 35, 7604 **(1987)**.
20. Y. Al-Douri and A. H. Reshak, *Applied Phys. A* 104, 1159 **(2011)**.
21. N. Bouarissa, H. Baazis, and Z. Charifi, *Phys. Status Solidi (b). Basic Solid State Phys.* 231, 403 **(2002)**.
22. F. Birch, *J. Appl. Phys.* 9, 279 **(1938)**.
23. D. C. Wallace, Thermodynamics of Crystals, Wiley, New York **(1972)**.
24. J. P. Pinceaux, J. M Besson, A. Rimsky, and G. Weil (eds.), High pressure in research and industry, *Proceedings of the 8th AIRAPT Conference*, Institute of Physical Chemistry, University of Uppsala, Sweden, August **(1981)**.
25. A. J. Miller, G. A. Saunders, and Y. K. Yogurtcu, *Philos. Mag. A* 43, 1447 **(1981)**.
26. M. Baublitz and A. L. Ruoff, *J. Appl. Phys.* 53, 6179 **(1982)**.
27. D. Gehrlich and M. Wolf, High Pressure Science and Technology, Pergamon, Oxford **(1980)**.
28. H. Mayer, E. Anton, M. Bott, J. Methfessel, J. Sticht, and P. C. Schmidt, *Intermetallics* 11, 23 **(2003)**.
29. M. Jamseson, B. I. Sharma, R. Bhattacharjee, R. K. Thapa, and R. K. B. Singh, *Physica B* 406, 4041 **(2011)**.
30. S. K. Tewksbury, Semiconductor materials, edited by C. J. Whitaker, Microelectronic System Research Center, West Virginia University **(2005)**.

ARTICLE

Kh. Kabita [1]
Jameson Maibam [1]
B. Indrajit Sharma [1*]
R.K. Brojen Singh [2]
R. K. Thapa [3]

[1]Department of Physics, Assam University, Silchar-788011, Assam, INDIA
[2]School of Computational and Integrative Sciences, JNU, New Delhi, INDIA
[3]Department of Physics, Mizoram University, Aizawl, Mizoram, INDIA
** Corresponding author: indraofficial@rediffmail.com*

First Principle Calculation of Pressure-Induced Phase Transition and Band Structure of Gallium Phosphide

A first principle study of the electronic, structural and phase transition of the III-V binary compound semiconductor gallium phosphide (GaP) is performed under the framework of density functional theory (DFT). Structural transformation from the zinc-blende (ZB) to rocksalt (RS) structure is observed at a pressure of about 21.9 GPa and the dependence of the volume decrease of ZB to RS structure at the transition pressure is 14.11% . The variation of the energy band gap, elastic constants and debye's temperature with pressure are also obtained successfully. Our results are found to be in consistent with other experimental and theoretical results.

Keywords: Density Functional Theory, Density of states (DOS), Band structure, Phase transition
Received: 27 November 2013, **Revised:** 8 December 2013, **Accepted:** 15 December 2013

1. Introduction

Gallium phosphide is an important III-V compound semiconductor which has increasingly attracted attention theoretically and experimentally and can be used advantageously in a variety of technological areas. It is also considered to be of wide-band gap and hence making it a good candidate for room-temperature device applications such as top junction solar cells and multi junction solar cell system. The variation of band gap of GaP with pressure is important for the identification of some of the luminescent processes and for a better understanding of their origin. In recent years the study of the structural properties, phase diagram and effect of pressure has aroused considerable scientific interest. Two phases of GaP such as zinc-blende (ZB) and rock-salt (RS) has been found with phase transition taking place under pressure [1]. The ZB to RS structure phase transition has been found to occur around 18.8 GPa with unstable RS structure [2]. Using the density functional theory (DFT) Rashid et al. [3] have studied the structural and electronic properties of GaP and compared the lattice parameters, bulk modulus, pressure derivative of the bulk modulus with earlier data. A. Mujica and R. J. Needs [4] found that the simple cubic phase of GaP should be stable between 14.7 GPa and 20.3 GPa. The High-pressure properties of the zinc-blende structure have been determined by Raman scattering, ultrasonic measurements, fundamental absorption, and refractive-index measurements [5-7]. Even though GaP has been well known for a long time, calculations on the elastic properties and pressure variation of GaP are still very rare. In the present work, the phase transformation from zinc-blende to rocksalt structure along with the electronic structure, density of states (DOS), change in band gap, and variation in mechanical properties is studied for better understanding of the semiconductor.

2. Computational Method

The calculation of GaP was performed within the framework of density functional theory (DFT) using the full potential linearised augmented plane wave (FP-LAPW) method [8]. The exchange-correlation effects are treated within the generalised gradient approximation of Perdew-Burke-Ernzerhof (PBE-GGA) scheme [9] as implemented in wien2k code [8,10,11]. This method is used as it is one of the most accurate methods in electronic structure calculation of crystals. In this method, the lattice is divided into non-overlapping atomic spheres surrounding each atomic sites and an interstitial region [12]. Inside the muffin tin (MT) region, the potential is a product of radial function and spherical harmonics and expanded up to order l = 10. For the interstitial regions that are outside the muffin tin spheres, the potentials are expanded in plane waves. 8000 k-points are used for the integration part which reduces to 256 irreducible k-points inside the Brillion zone. Convergence is obtained at $R_{MT}K_{max}$ =9.0 where R_{MT} is the atomic sphere radii and K_{max} gives the plane wave cut-off.

3. Results and Discussion

3.1 Structural properties

The ground state lattice parameter of ZB and RS structure of GaP are obtained by optimisation of the structures. The total energy and the corresponding primitive cell volume are calculated by setting a series of different lattice constants for both the structures and the energy versus volume curves are shown in figure 1. From figure 1 it is clearly seen

that the ZB structure of GaP is more stable as compared to RS structure which is in good agreement with other previous results [1,4]. The zero pressure, lattice constant a_o, bulk modulus B_o, pressure derivative of the bulk modulus $B_o^{/}$ are obtained by fitting the calculated energy-volume points to the Birch-Murnaghan equation of states [13] and the obtained results are listed in table 1. It shows that our results are reasonably in agreement with the previous reported data [1, 4, 14-16].

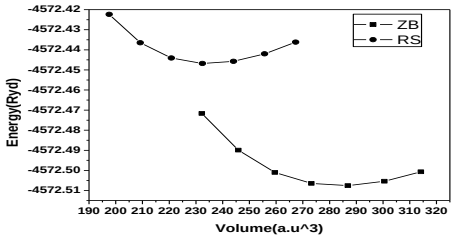

Fig. (1) Energy versus volume for different structure of GaP

Table (1) Lattice constants a_o, bulk modulus B_o, and pressure derivative of bulk modulus $B_o^{/}$ for ZB and RS structures of GaP at zero pressure

Structure		a_0 (A^0)	B_0 (GPa)	$B_0^{/}$
ZB	Present work	5.523	77.709	4.347
	References	5.411[a]; 5.50[b]; 5.386[c]	90.0[a]; 7.21[b] ; 86.8[c]	4.50[a];4.88[b]; 4.00[c]
RS	Present work	5.181	88.303	4.84
	References	5.165[d]; 5.160[e]	87.3[d]; 87.59[e]	3.78[d]; 4.54[e]

[a]Ref. [4]; [b]Ref. [14]; [c]Ref. [15]; [d]Ref. [1]; [e]Ref. [16].

3.2 Phase transition and Elastic properties

For the determination of phase transition pressure at zero temperature, the usual condition of equal enthalpies i.e. H=E+PV is used. The enthalpy as a function of pressure is shown in figure 2. The phase transition of GaP from ZB to RS is found to occur at 21.9 GPa pressure. The obtained transition pressure is found to be in good agreement with other experimental and theoretical results which are shown in table 2. In figure 3, the normalised volume (Vp/Vo) of ZB and RS of GaP at different pressure is shown. The relative volume is found to decrease as pressure increases for the two structures. During the phase transition, V_p/V_o of ZB phase is found to occur at 0.8293 and the RS phase at 0.6882. It clearly shows that the volume collapses at 14.11% indicating that ZB phase of GaP is more compressible as compare to RS phase. Hence the elastic constants C_{11}, C_{12}, C_{44} of GaP-ZB structure are calculated for the lattice volume corresponding to the pressure ranging from 0 GPa to 21.9 using the stress-strain method [20].

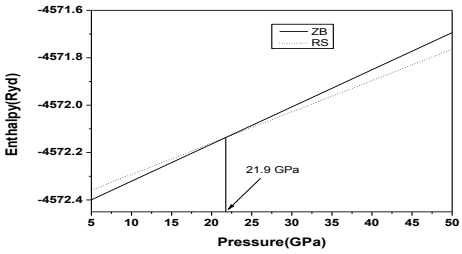

Fig. (2) Enthalpy as a function of pressure

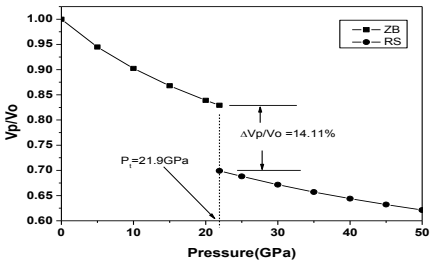

Fig. (3) Phase transition between ZB and RS structure of GaP at 21.9 GPa

For computing the elastic constants C_{ij}, the volume conserving technique is used [21]. The results are shown in figure 4. The results clearly show the mechanical stability conditions: $(C_{11}+2C_{12})>0$; $C_{11}C_{12}>0$; $C_{44}>0$ are satisfied and hence the stable GaP-ZB structure can exists up to higher pressure of 21.9 GaP. Using the calculated elastic constants (C_{11}, C_{12}, C_{44}), the Debye's temperatures of the ZB phase at different pressures are obtained. Form figure 4 and figure 5, it is also observed that the elastic constants as well as the Debye's temperature increases with increasing pressure.

Table (2) Transition pressure from ZB to RS in GaP

ZB - RS	Pressure (GPa)
Present work	21.9
Ref.1	21.9
Ref.17	24±0.3
Ref.7	22.0
Ref.18	21.5±0.8
Ref.19	21.7

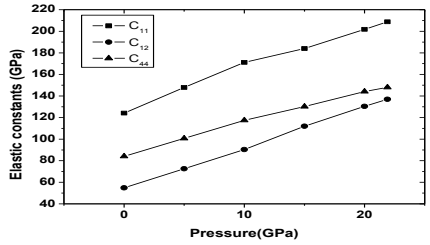

Fig. (4) Elastic constants (C_{11},C_{12},C_{44}) as a function of pressure

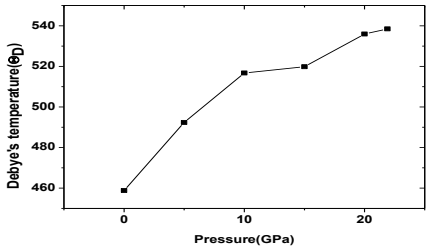

Fig. (5) Debye's temperature as a function of pressure

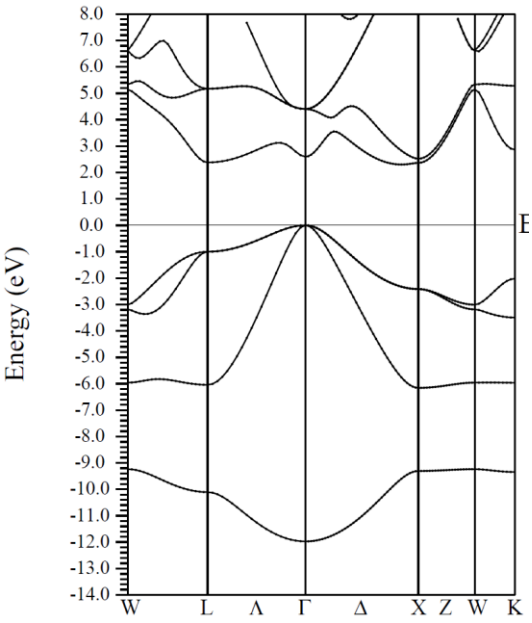

Fig. (6) Energy band diagram of GaP ZB structure at zero pressure

3.3 Band structure and Density of states

The energy band diagram of GaP-ZB at zero pressure is shown in figure 6 and the partial DOS of Ga and P in GaP-ZB are shown in figure 7 (a) and 7 (b) respectively. In the band diagram, one can observe that the valance band maximum occurs at the Γ point and the minimum conduction band occurs at L point. Hence GaP-ZB is found to be an indirect band gap semiconductor material of 2.3 eV. From the partial DOS one can observe that the lowest band appears in energy band diagram is mainly contributed from s-non metal (P atom) orbital and the valance band is mainly contributed by the s-metal (Ga- atom) orbital and p-non metal orbital with little contribution from the p-metal orbital. The contribution of the s, p orbitals of metal and non-metal in Density of States (DOS) in the lowest and valence band is found to decrease with increase in pressure. The variation of band gap of GaP-ZB structure under pressure ranging from 0 GPa to 21.9 GPa is shown in figure 8 and observed that there is increase in band gap with increase of pressure.

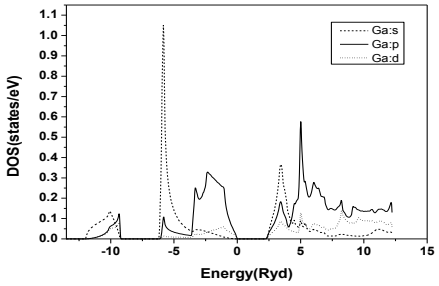

(a)

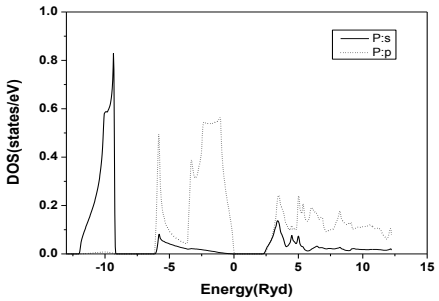

(b)

Fig. (7) (a) Partial DOS of Ga in GaP, (b) Partial DOS of P in GaP

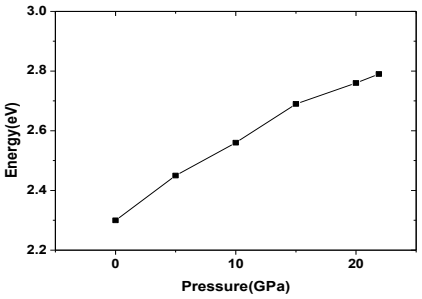

Fig. (8) Pressure versus energy band gap in GaP

4. Conclusion

In this paper we present a detailed study of pressure induced phase transition and electronic structure of GaP from ZB to RS structure. The phase transition from ZB to RS structure is obtained at 21.9 GPa and ZB phase is found to be more stable. During the phase transition, the relative volume of ZB phase is occured at 0.8293 and the RS phase at

0.6882 and volume collapses at 14.11% indicating that ZB phase of GaP is more compressible as compare to RS phase. The calculated equilibrium lattice parameter, bulk modulus and pressure derivative of the bulk modulus are found to be in good agreement with the other experimental and theoretical studies. The Debye's temperature calculated from the elastic constants is increased with increase in pressure. GaP-ZB phase is found to be an indirect band gap semiconductor material of 2.3eV and band gap increases with increase in pressure. The partial DOS shows the main contributions from s, p orbital of non metal-P atom and p, d orbital of metal-Ga atom in the band diagram of GaP.

References

[1] L. Lui et al., *Chinese Physics B*, 20(10) (2011) 106201-106206.
[2] A. Garcia, and M. L. Cohen, *Phys. Rev. B*, 47 (1993) 6751-6754.
[3] A.R. Rashid et al., *Physica B: Condens. Matter*, 403 (2008) 1876-1881.
[4] A. Mujica and R. J. Needs, *Phys. Rev. B*, 55 (1997) 9659-9670.
[5] J.P. Itie et al., *Phys. Rev. B*, 40 (1989) 9709–9714.
[6] A. Bernard, Weinstein and G.J. Piermarini, *Phys. Rev. B*, 12 (1975) 1172–1186.
[7] A.J. Miller, G.A. Saunders and Y.K. Yogurtcu, *Philos. Mag. A*, 43 (1981) 1447-1471.
[8] E. Wimmer et al., *Phys. Rev. B*, 24 (1981) 864-875.
[9] J.P. Perdew, K. Burke and M. Ernzerhof, *Phys. Rev. Lett*., 77 (1996) 3865-3868.
[10] P. Blaha et al., Techn. Universitat, Wien, Austria, ISBN 3-9501031-1-2, (2001).
[11] S. Cottenier, "Density Functional Theory and the family of (L) APW-methods: a step-by-step Introduction" (Belgium, Instituut voor Kern-en Stralingsfysica, K. U. Leuven., ISBN 90-807215-1-4, (2002).
[12] O.K. Andersen, *Phys. Rev. B*, 12 (1975) 3060-3083.
[13] F. Birch, *Phys. Rev*., 71 (1947) 809-824.
[14] Y. Al-Douri, and A.H. Reshak, *Applied Physics A*, 104 (2011) 1159-1167.
[15] S.B. Zhang and M.L. Cohen, *Phys. Rev. B*, 35 (1987) 7604-7610.
[16] L. Sukit et al., *Phys. Rev. B*, 77 (2008) 195209-1952015.
[17] J.P. Pinceaux et al., "High pressure in research and industry", Proc. of the 8th AIRAPT Conf.; August 17-22; Institute of Physical Chemistry, University of Uppsala, Sweden, (1981).
[18] M. Baublitz and A.L Ruoff, *J. Appl. Phys*. 53 (1982) 6179-6186.
[19] J. Sjakste, N. Vast and V. Tyuterev, *Phys. Rev. Lett*. 99 (2007) 236405-236409.
[20] F Birch, *J. Appl. Phys*., 9 (1938) 279-288.
[21] D.C. Wallace, **"Thermodynamics of Crystals"**, Wiley, New York, (1972).